

AD-A130 043

NUMERICAL SIMULATION OF SPACECRAFT CHARGING PHENOMENA  
AT HIGH ALTITUDE..(U) YORK UNIV DOWNSVIEW (ONTARIO)  
CENTRE FOR RESEARCH IN EXPERIME..

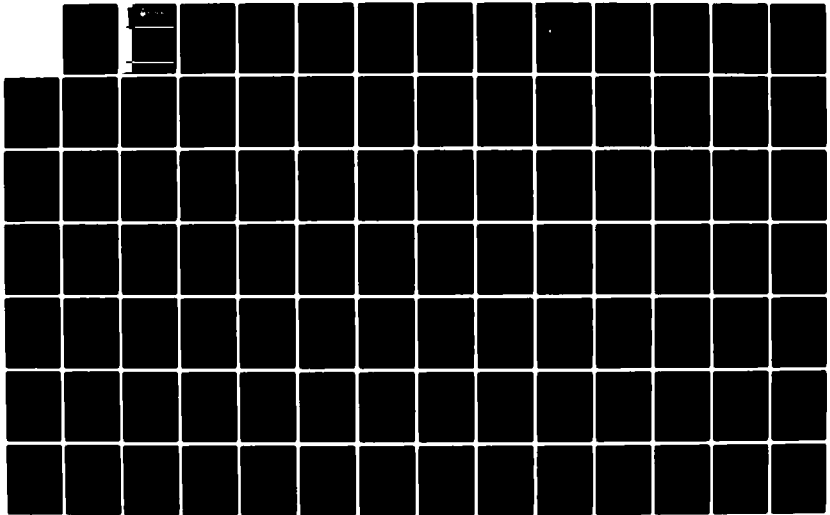
1/2

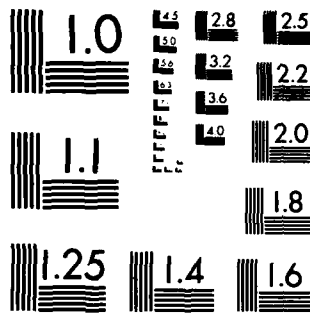
UNCLASSIFIED

J G LAFRAMBOISE ET AL. 10 AUG 82

F/G 22/2

NL





MICROCOPY RESOLUTION TEST CHART  
NATIONAL BUREAU OF STANDARDS-1963-A

10

ADA130049



YORK  
UNIVERSITY



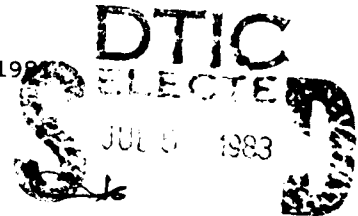
NUMERICAL SIMULATION OF SPACECRAFT CHARGING  
PHENOMENA AT HIGH ALTITUDE

J.G. Laframboise, M. Kamitsuma, S.M.L. Prokopenko,  
Jen-Shih Chang, and R. Godard

Physics Department and Centre for Research in Experimental Space Science  
York University  
Toronto, Canada M3J 1P3  
10 August 1982

Approved for public release;  
distribution unlimited.

FINAL REPORT  
1 March 1976 through 31 August 1982  
Grant AFOSR-76-2962



A

Prepared for  
Air Force Office of Scientific Research (AFSC)  
Bolling Air Force Base, D.C., U.S.A. 20332

83 07 01 023

Unclassified

SECURITY CLASSIFICATION OF THIS PAGE (When Data Entered)

REPORT DOCUMENTATION PAGE		READ INSTRUCTIONS BEFORE COMPLETING FORM
1. REPORT NUMBER <b>AFOSR-TR- 83-0549</b>	2. GOVT ACCESSION NO. <b>AD-A130043</b>	3. RECIPIENT'S CATALOG NUMBER
4. TITLE (and Subtitle) NUMERICAL SIMULATION OF SPACECRAFT CHARGING PHENOMENA AT HIGH ALTITUDE		5. TYPE OF REPORT & PERIOD COVERED Final Report 1 March 1976 - 31 August 1981
		6. PERFORMING ORG. REPORT NUMBER
7. AUTHOR(s) J.G. Laframboise, M. Kamitsuma, S.M.L. Prokopenko, Jen-Shih Chang, and R. Godard		8. CONTRACT OR GRANT NUMBER(s) AFOSR-76-2962
9. PERFORMING ORGANIZATION NAME AND ADDRESS York University, Toronto, Canada M3J 1P3		10. PROGRAM ELEMENT, PROJECT, TASK AREA & WORK UNIT NUMBERS 61102F 2311/A1
11. CONTROLLING OFFICE NAME AND ADDRESS Air Force Office of Scientific Research (AFSC) Bolling Air Force Base, D.C., U.S.A. 20332 Monitor/H. Radoski/NP		12. REPORT DATE 10 August 1982
		13. NUMBER OF PAGES
14. MONITORING AGENCY NAME & ADDRESS (if different from Controlling Office)		15. SECURITY CLASS. (of this report) Unclassified
		15a. DECLASSIFICATION/DOWNGRADING SCHEDULE
15. DISTRIBUTION STATEMENT (of this Report) Approved for public release; distribution unlimited.		
17. DISTRIBUTION STATEMENT (of the abstract entered in Block 20, if different from Report)		
18. SUPPLEMENTARY NOTES		
19. KEY WORDS (Continue on reverse side if necessary and identify by block number) Numerical Simulation, Spacecraft Charging, Spacecraft - Environment Interactions		
20. ABSTRACT (Continue on reverse side if necessary and identify by block number) This report describes work done under grant AFOSR-76-2962. This work has included the development of computer programs for simulating spacecraft charging at three levels of complexity: LOCHG, a relatively simple local-charging calculation; CYLVIA, a two-dimensional simulation program for treating cylindrical spacecraft cross-sections, and XYCIC, a simulation program for the treatment of a larger variety of two-dimensional geometries. This work has also included studies of two physical phenomena which are fundamental to an improved understanding of spacecraft charging: the "threshold temperature" effect (over)		

DD FORM 1473  
1 JAN 73

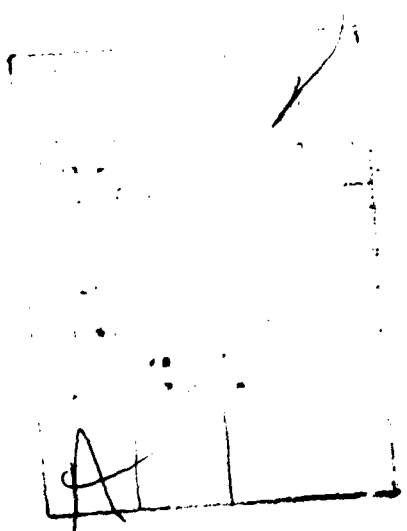
Unclassified

SECURITY CLASSIFICATION OF THIS PAGE (When Data Entered)

Unclassified

SECURITY CLASSIFICATION OF THIS PAGE(When Data Entered)

and the "barrier" effect. Also included is a derivation of two results which appear likely to be of use in future simulation studies: an analytic expression for photoelectron currents on surfaces with variable illumination in electric fields, and a perturbation technique for calculating space-charge density and flux along particle orbits.



DTIC  
COPY  
REQUESTED  
2

Unclassified

SECURITY CLASSIFICATION OF THIS PAGE(When Data Entered)

NUMERICAL SIMULATION OF SPACECRAFT CHARGING

PHENOMENA AT HIGH ALTITUDE

J.G. Laframboise, M. Kamitsuma, S.M.L. Prokopenko,  
Jen-Shih Chang, and R. Godard

Physics Department and Centre for Research in Experimental Space Science

York University

Toronto, Canada M3J 1P3

10 August 1982

Final Report

1 March 1976 through 31 August 1981

Grant AFOSR-76-2962

AIR FORCE OFFICE OF SCIENTIFIC RESEARCH (AFSC)  
NOTICE OF TRANSMITTAL TO DTIC  
This technical report has been reviewed and is  
approved for distribution under DTIC AFR 190-12.  
Distribution is unlimited.

MATTHEW J. KENNER  
Chief, Technical Information Division

Prepared for

Air Force Office of Scientific Research (AFSC)  
Bolling Air Force Base, D.C., U.S.A. 20332

TABLE OF CONTENTS		PAGE
Acknowledgments		iii
Abstract		iv
1. Introduction		1
2. LOCHG: a local-charging calculation		4
2.1 Introduction		4
2.2 Theory		6
2.3 Results and discussion: shaded cavities and multiple floating potentials		12
2.4 Prediction of ion drift effects on spacecraft floating potentials		18
2.4.1 Introduction		18
2.4.2 Theory of local ion collection on a unipotential sphere		20
2.4.3 Results and discussion		22
3. Multiple floating potentials, and the "threshold material temperature for high-voltage charging".		24
3.1 Introduction		24
3.2 The threshold-temperature property		26
3.3 Calculation of threshold temperatures; discussion		30
4. CYLVIA: a two-dimensional charging simulation for cylindrical spacecraft cross-sections with angle-dependence.		34
4.1 Introduction; the quasistatic iteration method		34
4.2 Use of approximate space-charge density expressions		35
4.3 Approximate inclusion of finite-cylinder-length (three-dimensional) effects in Poisson's equation		37
4.4 Orbit integration and current calculations		39
4.5 Results and discussion		43
4.6 The barrier effect		46
5. XYCIC: a simulation for general planar-symmetric (two-dimensional) spacecraft geometries		50
5.1 Introduction		50
5.2 Preliminary results		51
6. An analytic calculation of surface photocurrents		53
6.1 Introduction		53
6.2 Theory		53
6.3 Comparison with a numerical result from CYLVIA.		57
7. Flux and Density Calculation for Collisionless Particle Orbits		59
References		66
Tables		73
Figures		75

Appendix A:	Listing of LOCHG	A1
Appendix B:	Listing of threshold temperatures program	B1
Appendix C:	Listing of CYLVIA	C1
Appendix D:	Listing of Plotting program used with CYLVIA	D1
Appendix E:	Listing of XYCIC	E1




## ACKNOWLEDGMENTS

We are indebted to H.I. Cohen, L.W. Parker, and A.D. Stauffer for valuable discussions, and to M. Mandell for providing unpublished data used in Fig. 4.7 and discussed in Sec. 4.5. One of us (J.G. Laframboise) wishes to acknowledge the contributions of co-authors to specific sections of this Report, as follows: M. Kamitsuma (Secs. 3, 4, 5, and 6.3; Appendices B, D, and E), S.M.L. Prokopenko (Secs. 2 and 4; Appendices A, C, and D), Jen-Shih Chang (Sec. 2), and R. Godard (Secs. 2, 4, and 6.3; Appendices C and D). We wish to thank the computer center of Air Force Geophysics Laboratory for the provision of computer time, and the Department of Computer Services of York University for the use of its facilities. Special thanks are due to S. Bredesen of AFGL for much assistance with computing arrangements. We are grateful to the National Center for Atmospheric Research for the provision of computer software.

This work was supported by the U.S. Air Force Office of Scientific Research under grant number AFOSR-76-2962.

## ABSTRACT

This report describes work done under grant AFOSR-76-2962. This work has included the development of computer programs for simulating spacecraft charging at three levels of complexity: LOCHG, a relatively simple local-charging calculation; CYLVIA, a two-dimensional simulation program for treating cylindrical spacecraft cross-sections, and XYCIC, a simulation program for the treatment of a larger variety of two-dimensional geometries. This work has also included studies of two physical phenomena which are fundamental to an improved understanding of spacecraft charging: the "threshold temperature" effect and the "barrier" effect. Also included is a derivation of two results which appear likely to be of use in future simulation studies: an analytic expression for photoelectron currents on surfaces with variable illumination in electric fields, and a perturbation technique for calculating space-charge density and flux along particle orbits.



## 1. INTRODUCTION

The performance of many satellites in geostationary orbit has been degraded by anomalous events which include frequent spurious spacecraft commands and in some cases permanent damage [Rosen, 1975; McPherson and Schober, 1976]. These events invariably appear to involve electrical discharges caused by differential charging of spacecraft surfaces to large relative potentials. The latter condition is known to result from the large average energies (up to a few keV) of the charged-particle environment at geostationary-orbit altitude, particularly in disturbed magnetospheric conditions. In order to be able to design spacecraft in future which do not suffer from such difficulties, it is important to be able to make reliable predictions of them on proposed spacecraft configurations. The ability to make such predictions requires improved understanding of the plasma sheath which connects a spacecraft with its environment in such conditions. This sheath is more complex in many ways than those which usually surround lower-altitude spacecraft because at geostationary-orbit altitude, the fluxes of incident electrons, secondary and backscattered electrons, and photoelectrons can all have comparable magnitudes and usually vary by large amounts over the surface of a spacecraft, and the relative weakness of space-charge shielding (large Debye length) means that electric fields due to charging of one part of a spacecraft surface can readily extend around the spacecraft to other parts, including those on its other sides, exerting strong influences on charged-particle collection by them and hence on their charging.

Because of the magnitude of the spacecraft-charging problem, a joint USAF-NASA programme was commenced during the 1970-1980 decade to study it, including the launching of the P78-2 (SCATHA) satellite, which was specifically devoted to the study of the high-altitude charging process, and also including theoretical work on the nature of the spacecraft-environment interface problem: this work was to be closely coordinated with analysis of SCATHA observations.

The work described in this report is part of this theoretical effort.

This work has been conducted using a number of different approaches. In Sec. 2, we describe a relatively simple local-current-balance calculation of charging which formed the first phase of it, and led to the discovery that floating potentials (voltages) of many spacecraft surface materials can have more than one possible value in certain, frequently-occurring, space environments; the possibility that this might occur had been earlier predicted by Whipple (1965). Attempts to gain further understanding of the conditions in which this might occur led to the realization that this was one of several closely-related phenomena which could all be explained in terms of a newly-defined property of spacecraft surface materials, the threshold material temperature for high-voltage charging (Sec. 3). We present herein a table of these threshold temperatures, calculated for a variety of spacecraft surface materials. A second phase of our effort was the development of a more elaborate, two-dimensional spacecraft charging simulation program called CYLVIA, which treats the regions around circular spacecraft cross-sections (Sec. 4). We have also begun development of another two-dimensional simulation program, called XYCIC (Sec. 5), which treats a wider class of two-dimensional geometries than does CYLVIA. The effort to develop CYLVIA, together with efforts by other workers (Sec. 4.6), led gradually to an understanding of the importance of the barrier effect, an example of which is presented in Sec. 4.6.

A related phase of our work has been an effort to develop efficient numerical techniques, and analytical replacements for some numerical procedures, which will be of general use not only in our own simulation programs but also in other spacecraft-charging simulations. To this end, we have developed an analytic expression for the electric current produced by photoelectron migration on a surface with spatially-varying illumination in an electric field (Sec. 6), and a perturbation technique for calculating current

density and space-charge density carried by collisionless charged-particle orbits (Sec. 7).

Listings of computer programs developed as part of this work appear in Appendices A-E.

## 2. LOCHG: A LOCAL-CHARGING CALCULATION

### 2.1 INTRODUCTION

In order for high-voltage differential charging of a spacecraft to occur, some of its surfaces must charge to large (usually negative) potentials (voltages) relative to space. The amount of such "absolute" charging, for the surface at the largest potential, is generally simpler to estimate than are the differential potentials between this surface and others. On the sunlit side of a spacecraft, photoelectron emission tends to compensate for incident electron fluxes. Sunlit-side surface potentials therefore are generally less negative than shaded-side potentials, and may be slightly positive if photoemission flux  $>$  ambient random electron flux. Therefore, an approximate upper bound on differential charging magnitudes can be obtained by simply calculating floating potentials of electrically-isolated shaded surfaces, relative to space potential. In the present work, we have attempted to obtain upper bounds on these floating potentials, which in cases of interest are usually highly negative, because these bounds constitute "worst cases" for design purposes, and also because unlike more exact calculations, they can be obtained from simple current-balance calculations. Furthermore, it is sufficient to consider local current balance only, because this corresponds to an electrically-isolated surface element, which is also a "worst case" for differential charging. To calculate these bounds, we have constructed a computer program called LOCHG (LOCAL CHARGING), which extends a previous calculation by Knott [1972], of the floating potential of a spherically-symmetric geostationary-altitude satellite in eclipse. A listing of LOCHG appears in Appendix A. To investigate geometrical effects, we have replaced Knott's use of the Mott-Smith and Langmuir [1926] orbit-limited current expression for collection of Maxwellian ions by a unipotential sphere, by the corresponding expression for an infinite cylinder;

both expressions have been shown [Laframboise and Parker, 1973] to be upper bounds for collisionless ion collection as a function of local surface potential, for three- and two-dimensional collectors, respectively, regardless of collector shape, sheath potential, or potential of other parts of the collector. This replacement causes a large decrease in ion collection and a correspondingly large increase in negative shaded-side floating potentials (Sec. 2.3). Another important ion-current restriction may be caused by "effective-potential barrier" or "angular-momentum selection" effects [Bernstein and Rabinowitz, 1959; Laframboise, 1966; Laframboise and Parker, 1973], in which the presence of less-negative sunlit-side potentials produces dipole and higher moments in the sheath potential [Fahleson, 1973], causing steepening and contraction of the potential well surrounding the shaded side (Fig. 2.1). A similar steepening effect will also occur if an isolated shaded surface element is surrounded by adjacent shaded surfaces which for any reason have less-negative potentials (Fig. 2.2). The most extreme possibility would be a potential profile which was equal to space potential almost to the spacecraft surface, then fell discontinuously to surface potential. This limit would correspond to a "planar sheath" situation in which the ion collection on any shaded convex surface would be given by just the ion random flux. This amounts to a further ion-current restriction which produces even larger increases in negative shaded-side floating potentials (Sec. 2.3). This situation corresponds to a velocity-space cutoff boundary for incident ions which is "one-dimensional"; the cutoff boundaries corresponding to spherical and infinite cylindrical collectors are, respectively, "three-dimensional" and "two-dimensional" (Sec. 2.2) [Laframboise and Parker, 1973].

We also show (Sec. 2.3) that if shaded cavities containing isolated surfaces exist on a spacecraft, negative potentials on such surfaces may surpass even these predictions. In some cases, more than one possible floating potential results from the calculation. This has several implications (Sec. 2.3), including the possibility

(a) of "bifurcation phenomena" in which adjacent isolated surfaces of the same material may arrive at different floating potentials as a result of differences in their charging histories (b) that large and relatively sudden changes in surface potentials may result from gradual changes in ambient velocity distributions (c) that such changes may also result from relatively gradual changes in beam emission currents in a beam experiment. In Sec. 2.4 we calculate effects of ion drift motion on floating potentials.

We have also modified Knott's calculation in another way, by including currents due to electron backscattering (Sec. 2.2). These currents will tend to decrease net electron collection, thereby making floating potentials less negative than otherwise (Sec. 2.3). A process not included by either Knott or ourselves is secondary electron emission due to ion impacts; this will also tend to make floating potentials less negative. Ion-produced secondaries have been included in a calculation by DeForest [1972] of the floating potential of a shaded aluminum surface. However, no direct comparison is possible between his result and ours (Sec. 2.3) because we have used different ambient velocity distributions than his.

## 2.2 THEORY

The ambient electron energy distributions used in the present work are a model quiet-time spectrum (Knott [1972], Figure 1) and a model disturbed spectrum (Knott [1972], Figure 2b) based on measurements by Shield and Frank [1970] and DeForest and McIlwain [1971], respectively. Both of these distributions, and also the ambient ion distribution, are assumed isotropic. The disturbed spectrum was chosen from the three used by Knott because it has a higher average electron energy ( $\sim 4$  keV) than the others. In using it, we have changed it as follows: in the energy ranges  $0.5 \text{ keV} \leq E \leq 10 \text{ keV}$  and  $10 \text{ keV} \leq E \leq 40 \text{ keV}$ , we have replaced Knott's differential energy spectrum by  $\sqrt{2} \times 10^8 E^{-1/2}$  and  $\sqrt{2} \times 10^9 E^{-3/2}$  electrons/cm<sup>2</sup> sec steradian keV, respectively, where E is



energy. These relations are simpler than those indicated by Knott, and they also bring the model spectrum into closer agreement with the data on which it is based. We therefore believe that they may have been the ones actually used by Knott, and that the corresponding parts of Figure 2b in his paper may be incorrectly plotted. For any spacecraft surface having a negative potential  $\phi_s < 0$ , or for a three-dimensional (e.g. spherical) surface having  $\phi_s > 0$ , the orbit-limited flux (particle current density)  $J_e$  of ambient electrons is given by [Laframboise and Parker, 1973]:

$$\begin{aligned}
 J_e &= \int f v_n d^3 \vec{v} \\
 &= \int_{E=\max(0, -e\phi_s)}^{E=\infty} \int_{\theta=0}^{\theta=\pi/2} \int_{\psi=0}^{\psi=2\pi} f(E) (v \cos \theta) (v^2 \sin \theta dv d\theta d\psi) \\
 &= \int_{\max(0, -e\phi_s)}^{\infty} (1 + e\phi_s/E) (dJ_{e0}/dE) dE \quad (2.1)
 \end{aligned}$$

where  $e$  is magnitude of unit electronic charge,  $\phi_s$  is local surface potential,  $dJ_{e0}/dE$  is the ambient energy-differential flux incident on one side of an arbitrarily oriented surface element,  $v_n$  is the inward velocity component normal to the same surface element,  $(v, \theta, \psi)$  are spherical coordinates in velocity space with  $v_n$  as polar axis, and  $E = \frac{1}{2}m_e v^2 - e\phi$ .  $dJ_{e0}/dE$  is  $\pi$  times the energy-differential flux per steradian used by Knott [1972], and is given in terms of the ambient electron velocity distribution  $f = d^3 N_{\infty} / d^3 \vec{v}$  by the relation  $dJ_{e0}/dE = 2\pi f E / m_e^2$ , where  $m_e$  is electron mass and  $N_{\infty}$  is ambient ion or electron number density. Since  $f$  is isotropic,  $f \equiv f(E)$ . The factor  $(1 + e\phi_s/E)$  in (2.1), which appears to have been neglected by Knott, leads to a divergent integration in (2.1) if  $\phi_s > 0$ , unless  $dJ_{e0}/dE \rightarrow 0$  as  $E \rightarrow 0$ , i.e.  $f(E)$  remains finite as  $E \rightarrow 0$ . This implies that the differential fluxes in Knott's Figures 1-3 must approach zero linearly with  $E$  at  $E$  values smaller than those shown in these Figures. In the present work we have introduced a linear rise in  $dJ_{e0}/dE$  from 0 to 1 eV. We have also introduced a sharp upper cutoff at 50 keV in the quiet-time spectrum, also in order to avoid a divergent integration when calculating average energy for use in backscattering calculations (see below). The resulting values of  $N_{\infty}$  are  $5.43 \text{ cm}^{-3}$  and  $5.39 \text{ cm}^{-3}$  for the quiet-time

and disturbed spectra, respectively. These values are consistent with those quoted by Knott [1972] for the corresponding spectra. The resulting values of the average ambient electron energy  $\bar{E}$  are 0.176 keV and 4.17 keV, respectively. The incorporation of these changes has a relatively minor influence on Knott's results [Prokopenko and Laframboise, 1977, Table 1].

In order to obtain the orbit-limited electron flux expression for an arbitrary cylindrical collector, the lower integration limit in (2.1) must be replaced by the two-dimensional velocity-space cutoff boundary  $E_1 = \max(0, -e\phi_s)$ , where  $E_1$  is the total energy of transverse motion  $\frac{1}{2}m_e(v_x^2 + v_y^2) - e\phi$ , and we have chosen a  $z$  coordinate perpendicular to the cylinder cross-section. If  $\phi_s > 0$ , this complicates the integration in (2.1), which may then be done in either of two ways. The first [Laframboise and Parker, 1973, Eq. (6)] is to convert (2.1) into an integration using cylindrical coordinates in velocity space. A more convenient method [Mott-Smith and Langmuir, 1926; Polychronopoulos, 1973] is as follows. We choose rectangular coordinates  $(v_n, v_t, v_z)$  in velocity space, such that  $v_n$  is the velocity component in the inward normal direction at the collector surface. Then  $v_t$  and  $v_z$  become tangential coordinates, with  $v_t$  in the plane of the cylinder cross-section. We then transform to spherical coordinates  $(v, \theta, \psi)$  with  $v_z$  as polar axis. Then:  $v_z = v \cos \theta$ ,  $v_n = v \sin \theta \cos \psi$ , and  $v_t = v \sin \theta \sin \psi$ . The condition  $E_1 \geq 0$  is equivalent to  $\sin \theta \geq [e\phi_s / (E + e\phi_s)]^{1/2}$ . For  $\phi_s > 0$ , Eq. (2.1) is then replaced by:

$$\begin{aligned}
 J_e &= \int f v_n d^3 \vec{v} \\
 &= 2 \int_{E=0}^{E=\infty} \int_{\psi=-\pi/2}^{\psi=\pi/2} \int_{\theta=\text{Arc sin}[e\phi_s / (E + e\phi_s)]^{1/2}}^{\theta=\pi/2} f(E) (v \sin \theta \cos \psi) (v^2 \sin \theta dv d\theta d\psi) \\
 &= \int_0^{\infty} \frac{2}{\pi} \left[ \text{Arc sin} \left( \frac{E}{E + e\phi_s} \right)^{1/2} + \frac{(Ee\phi_s)^{1/2}}{E + e\phi_s} \right] \left( 1 + \frac{e\phi_s}{E} \right) \frac{dJ_{e0}}{dE} dE \quad (2.2)
 \end{aligned}$$

In comparison with Eq. (2.1), we see that the integrand in (2.2) contains an extra, energy-dependent weighting factor, which arises from integration of  $v_n$  over the fractional solid angle over which ambient electrons can reach the collector at each energy.

A similar procedure is advantageous in obtaining the one-dimensional (Sec. 2.1) orbit-limited flux expression. In this case, the lower limit in (2.1) must be replaced by:  $E_n = \max(0, -e\phi_s)$ , where  $E_n = \frac{1}{2}m_e v_n^2 - e\phi$ . This time we transform  $(v_n, v_t, v_z)$  to spherical coordinates  $(v, \theta, \psi)$  with  $v_n$  as polar axis. The condition  $E_n \geq 0$  is equivalent to  $\cos \theta \geq [e\phi_s / (E + e\phi_s)]^{1/2}$ . For  $\phi_s > 0$ , Eq. (2.1) is now replaced by:

$$J_e = \int_{E=0}^{E=\infty} \int_{\theta=0}^{\theta=\text{Arc cos}[e\phi_s / (E+e\phi_s)]^{1/2}} f(E) (v \cos \theta) (2\pi v^2 \sin \theta dv d\theta) \\ = \int_0^{\infty} \frac{dJ_{e0}}{dE} dE \quad (2.3)$$

independently of collector potential, as expected.

The corresponding expressions for ion flux  $J_i$  are simpler because the ions are assumed to be Maxwellian. Corresponding to the three-, two-, and one-dimensional velocity-space cutoffs described above, we obtain, respectively [Mott-Smith and Langmuir, 1926; Laframboise and Parker, 1973], for ion-attracting surface potentials  $\chi_{is} > 0$ :

$$J_i = J_{i0} \begin{cases} (1 + \chi_{is}) & (2.4) \\ [2(\chi_{is}/\pi)^{1/2} + \exp(\chi_{is}) \text{erfc}(\chi_{is}^{1/2})] & (2.5) \\ (1) & (2.6) \end{cases}$$

where  $\chi_{is} = -e\phi_s / kT_i$ ,  $k$  is Boltzmann's constant,  $T_i$  is ion temperature and  $J_{i0}$  is the ion random flux  $N_{\infty} (kT_i / 2\pi m_i)^{1/2}$ . For ion-retarding surface potentials  $\chi_{is} < 0$ , we obtain:

$$J_i = J_{i0} \exp(\chi_{is}). \quad (2.7)$$

We have assumed, following Knott [1972], that  $T_i = 1$  keV, and that the random ion-to-electron flux ratio  $J_{io}/J_{eo} = 0.025$ . Making these two assumptions simultaneously causes ambient charge neutrality to be violated in general. Large apparent violations of charge neutrality are frequently observed in measurements made by particle energy analyzers. Such discrepancies are believed to result from failure to measure particles outside the energy ranges of these analyzers, especially at energies of a few volts or less [DeForest and McIlwain, 1971]. Our calculations therefore neglect any current contributions which may be made by such particles.

For the secondary electron fractional yield  $\delta(E)$ , we have used, following Knott [1972], the relation of Sternglass [1954a]:

$$\delta(E) = 7.4 \delta_{\max} (E/E_{\max}) \exp[-2(E/E_{\max})^2]. \quad (2.8)$$

We have used values of  $\delta_{\max}$  and  $E_{\max}$  from Gibbons [1966], Hachenberg and Brauer [1959], and Willis and Skinner [1973].

The process of electron backscattering, which was not included in Knott's calculations, becomes important at incident electron kinetic energies larger than those for which secondary emission is dominant. For the backscattered electron fractional yield  $\eta$ , we have fitted the results of Sternglass [1954b] and Palluel [1947] with a relation of the form:

$$\eta(E) = A - B \exp(-CE) \quad (2.9)$$

where the coefficients  $A$ ,  $B$ , and  $C$  are functions of the atomic number  $Z$  of the surface material. We have evaluated  $A$ ,  $B$  and  $C$  for each surface material considered (Sec. 2.3) by substituting Sternglass' and Palluel's values of  $\eta$  at 0, 1 and 16 keV, into Eq. (2.9). For compound surface materials, we have used an atomic number given by a weighted average of those of each constituent. There exist more recent measurements of  $\eta$  [Thomas and Pattinson, 1970; Darlington and Cosslett, 1972] which give generally larger values than those of Sternglass or Palluel, especially for electrons having near-tangential incidence.

Increased values of  $\delta$  have also been measured for electrons having non-normal incidence [Allen, 1939; Dekker, 1958]. In a separate calculation (Sec. 3), we have included angle-of-incidence effects on  $\eta$  and  $\delta$ , but here we have ignored these. We have therefore underestimated both  $\delta$  and  $\eta$ , and our predicted floating potentials in Sec. 2.3 will therefore be somewhat more negative than more realistic corresponding values.

When  $\phi_s > 0$ , not all secondary and backscattered electrons will escape. To calculate flux escaping, we assume [Sternglass, 1954b; Chung and Everhart, 1974] that both secondary and backscattered electrons are emitted with Maxwellian velocity distributions having thermal energies  $E_{\text{sec}} = kT_{\text{sec}} = 3 \text{ eV}$ , and  $E_{\text{scat}} = kT_{\text{scat}} = (0.45 + 2 \times 10^{-3}Z) \overline{(E + e\phi_s)}$  eV, respectively, regardless of the form of the incident velocity distribution. Here,  $\overline{(E + e\phi_s)}$  is the average incident electron kinetic energy. We further assume that escape of emitted electrons is orbit-limited, i.e. that no barriers of effective potential [Bernstein and Rabinowitz, 1959; Laframboise, 1966; Laframboise and Parker, 1973] or negative barriers of electric potential exist on the shaded side. {Fahleson [1973] has pointed out that such a barrier is likely to exist on the sunlit side independently of any space-charge effects, if substantial shaded-sunlit differences exist in  $\phi_s$ . Such a barrier would cause most electrons emitted from the sunlit side to be recaptured, driving sunlit-side potential just negative enough to almost destroy the barrier [Sec. 4.5]; [Katz et al, 1979, Figs. 17-21]}. The expressions for the escaping secondary and backscattered fluxes  $J_{\text{sec}}$  and  $J_{\text{scat}}$  therefore are:

$$J_{\text{sec}} = \int_{-e\phi_s}^{\infty} \delta(E + e\phi_s) (1 + e\phi_s/E) (dJ_{e0}/dE) dE \quad (2.10)$$

$$J_{\text{scat}} = \int_{-e\phi_s}^{\infty} \eta(E + e\phi_s) (1 + e\phi_s/E) (dJ_{e0}/dE) dE \quad (2.11)$$

if  $\phi_s < 0$ . If  $\phi_s > 0$ , the three-, two-, and one-dimensional cases must be considered separately. We define  $\chi_{\text{sec}} = e\phi_s/kT_{\text{sec}}$  and  $\chi_{\text{scat}} = e\phi_s/kT_{\text{scat}}$ . For brevity, we consider only the secondary fluxes; the corresponding results for backscattered fluxes may be obtained by replacing  $\delta$  by  $\eta$  and  $\chi_{\text{sec}}$  by  $\chi_{\text{scat}}$  throughout. If  $J_s$  is the emitted flux of secondaries,

then their velocity distribution at the surface is  $f_s = (J_s/2\pi) (m_e/kT_{sec})^{-2} \exp(-\frac{1}{2}m_e v^2/kT_{sec})$ . In the three-dimensional case, the cutoff condition for their escape is  $E = \frac{1}{2}m_e v^2 - e\phi_s > 0$ . We redefine  $v_n$  as velocity component in the outward normal direction, and we use spherical coordinates as defined in connection with (2.3). We obtain, for the escaping secondary flux:

$$\begin{aligned} J_{sec} &= \int f_s v_n d^3\vec{v} \\ &= \frac{J_s \left( \frac{m_e}{kT_{sec}} \right)^2 \int_{E=0}^{\infty} \int_{\theta=0}^{\frac{\pi}{2}} \exp(-\frac{1}{2}m_e v^2/kT_{sec}) (v \cos \theta) (2\pi v^2 \sin \theta dv d\theta) \\ &= (1 + \chi_{sec}) \exp(-\chi_{sec}) \int_0^{\infty} \delta(E + e\phi_s) (1 + e\phi_s/E) (dJ_{eo}/dE) dE. \quad (2.12) \end{aligned}$$

The factor  $(1 + \chi_{sec})$  is noteworthy, because it is specific to three-dimensional, as opposed to planar, sheath geometry. In the two-dimensional case, the cutoff condition for escape is  $\frac{1}{2}m_e (v_n^2 + v_t^2) - e\phi_s > 0$ , and the integral for  $J_s$  contains the extra weighting factor which appears in Eq. (2.2). It is convenient to use spherical coordinates as defined in connection with (2.2). We obtain:

$$\begin{aligned} J_{sec} &= \left[ 2(\chi_{sec}/\pi)^{\frac{1}{2}} + \exp(\chi_{sec}) \operatorname{erfc}(\chi_{sec}^{\frac{1}{2}}) \right] \exp(-\chi_{sec}) \\ &\quad \times \int_0^{\infty} \frac{2}{\pi} \left[ \operatorname{Arc} \sin\left(\frac{E}{E + e\phi_s}\right)^{\frac{1}{2}} + \frac{(Ee\phi_s)^{\frac{1}{2}}}{E + e\phi_s} \right] \left(1 + \frac{e\phi_s}{E}\right) \delta(E + e\phi_s) \frac{dJ_{eo}}{dE} dE. \quad (2.13) \end{aligned}$$

In the one-dimensional case, the escape condition is  $\frac{1}{2}m_e v_n^2 - e\phi_s > 0$ , and we again use spherical coordinates as defined in connection with (2.3). We obtain:

$$J_{sec} = \exp(-\chi_{sec}) \int_0^{\infty} \delta(E + e\phi_s) (dJ_{eo}/dE) dE. \quad (2.14)$$

The floating potential(s) of an isolated shaded surface element is (are) now given by the zero(s) of the function:

$$J_{net} = J_i - J_e + J_{sec} + J_{scat}. \quad (2.15)$$

### 2.3 RESULTS AND DISCUSSION: SHADED CAVITIES AND MULTIPLE FLOATING POTENTIALS

Table 1 shows floating potential values obtained using the program LOCHG, which performs numerical solution of the equation  $J_{net} = 0$ , where  $J_{net}$  is given by Eq. (2.15). An important feature of Table 1 is the very

large floating potentials which are evident in disturbed conditions in the presence of the two- and one-dimensional velocity-space cutoffs. The dramatic differences among these results are evidence that spacecraft geometry and sheath potential shape are important influences in determining floating potentials. As floating potential becomes more negative, it also becomes more sensitive to the presence of small amounts of high-energy electrons. This means that if a spacecraft should encounter conditions that are "more disturbed" than those given by Knott's spectrum 2b, the values in Table 1 most likely to be significantly exceeded are those for the one-dimensional cutoff. This implies that for design purposes in which worst-case information is desired, it is important to do calculations with the "most disturbed" electron spectra available. In obtaining these results, we have made no attempt to calculate the charging times involved.

Also evident in Table 1 are situations in which the current-voltage characteristic of the surface has three roots. For these to occur, it is necessary that  $\delta_{\max}$  be substantially greater than one, and that the ambient electron spectrum be at least slightly non-Maxwellian (Sec. 3). The latter requirement arises because if the incident electrons are Maxwellian and ion-produced secondaries are ignored, the ratio of total secondary emission current to incident electron current will then be independent of  $\phi_s$  for  $\phi_s < 0$ , and the total secondary emission will therefore be a monotonic function of  $\phi_s$  for  $\phi_s < 0$ . (An exception to this, in which a triple-root situation occurs with Maxwellian ambient electrons, has been found by Meyer-Vernet (1982), but this exception applies only when  $T_e < T_{\text{sec}}$ , a condition which is not applicable here; see also Sec. 3). The centre root never represents a possible floating potential, because it is "unstable" in the sense that a small change in surface potential would cause a net current collection of a sign which would drive the surface potential away from this root to one on either side. Various consequences of such a situation are discussed later in this Section. A similar phenomenon in electronic image storage devices has been discussed by Kazan and Knoll [1968, pp. 17-19].

In comparison with the results of Knott [1972], Table 1 includes the further addition of backscattered electron flux (Sec. 2.2). In most cases, the effect is a moderate reduction of negative floating potentials. In some cases, the reduction is large, as in the case of a gold surface

exposed to the "quiet" spectrum. In several other cases, all associated with the quiet spectrum, backscattering changes a multiple-root to a single-root situation [Prokopenko and Laframboise, 1977]. As indicated in Sec. 2.2, we have probably underestimated secondary and backscattered fluxes caused by electron impacts, and we have also (Sec. 2.1) ignored secondary electron emission caused by ion impacts. Both of these effects would tend to further reduce negative potentials. For ion-produced secondaries, fractional yields at energies from 5 to 50 keV are generally of order unity to several times unity for metallic surfaces [Cousinie et al, 1959; Ray and Barnett, 1971; Baragiola et al, 1979] so substantial reductions due to this cause can be expected whenever ion collection plays an important role in total current balance. In comparison with the results of Table 1, potentials reaching  $-19kV$  on the ATS 6 spacecraft in eclipse have been observed (E.C. Whipple, Jr., private communication).

Figures 2.3 - 2.7 show current-voltage characteristics for some of the situations in Table 1. Figure 2.3 shows a "typical" single-root situation in which secondary and backscatter contributions do not change the general shape of the net current curve. Figure 2.4 shows the above-mentioned case of gold exposed to the quiet spectrum, in which the backscatter contribution changes a large predicted negative floating potential to a much smaller value. Figure 2.5 shows a triple-root situation. Figure 2.6 shows the disappearance of a triple-root situation because of backscatter. In Fig. 2.7, secondary electron current is sufficient by itself to prohibit a negative floating potential.

We now examine situations which may arise in the case of spacecraft which have shaded cavities containing electrically-isolated interior surfaces. Figure 2.8 shows an idealization of such a spacecraft. We wish to show that the effects of surface concavity may cause ion collection to be reduced more than net electron collection at an interior point such as B, relative to an exterior point A; such a situation would result in floating potentials more negative than those of Table 1. To demonstrate this possibility, we first note that in the presence of an isotropic ambient plasma, incident fluxes to any surface depend only [Laframboise and Parker, 1973] on the locations, in velocity space, of



the cutoff boundaries inside of which the orbits of ambient particles can connect "from infinity" to the surface. Figure 2.8 shows a set of the associated "cutoff orbits". We see from Fig. 2.8 that the included angle between cutoff orbits has been reduced in going from A to B for ions but not for electrons, for which orbits tangential to the surface are shown as reaching both A and B and the range of allowable directions remains  $180^\circ$ . Accordingly, the incident ion current contribution for the energy shown will also be reduced, but the electron contribution will not. This picture is invalid for higher-energy electrons at B, whose orbits are straighter and will have a greater tendency to connect back to the interior surfaces of the cavity. Even though such higher-energy orbits will generally have lower populations than lower-energy orbits, it is not clear whether the relative current reduction at B will be greater for ions or for electrons. Therefore, this argument demonstrates only the possibility that the bounds in Table 1 will be exceeded. On the other hand, this possibility will be enhanced by the effects of secondary and backscattered electrons, which will tend to be recaptured inside any cavity, rather than escaping into space, thus tending to increase net electron collection and driving floating potentials more negative. This effect will be strongest for backscattered electrons because their higher emission energies will cause them to have straighter orbits. The detailed numerical simulation required to draw firm conclusions remains to be done. An additional feature of cavities is their generally higher outgassing pressures, which will increase any tendencies for arcing to occur. More negative floating potentials may also result if the ambient electron distribution contains beam-like constituents [DeForest, 1977] which happen to be directed into a cavity. Severe arcing problems are known to have occurred between electronic components mounted inside a cavity at one end of the DSCS spacecraft.

Finally, we discuss some further implications of the multiple-root results shown in Table 1 and Fig. 2.5. We first consider a situation involving a shaded, isolated spacecraft surface whose external conditions change with time, as in the case of time-varying ambient distributions,

in such a way as to produce an evolution from a multiple-root to a single-root situation. If a spacecraft surface were floating at a potential corresponding to a root which disappeared, a large and relatively sudden change in surface potential would occur, even if external changes were gradual. In many situations, rapid redistribution of potentials on other parts of the spacecraft would result. In order to examine this situation in more detail, we illustrate it schematically in Fig. 2.9.

In Fig. 2.9a, the current-voltage curve at an earlier time  $t_1$  has three roots. The two roots furthest apart,  $\phi_{1a}$  and  $\phi_{1b}$ , correspond to stable floating surface potentials; these are typically from one to ten kilovolts apart. As a result of a changing environment, this curve evolves continuously into the one shown for the later time  $t_2$ , which has only the single root  $\phi_2$ . If the surface happened to be floating at the voltage  $\phi_{1a}$  at time  $t_1$ , then a sudden positive change in surface voltage, toward the voltage  $\phi_2$ , would occur as soon as the two left-hand roots disappeared.

In Fig. 2.9b, a spacecraft surface floating at the more positive root (at  $\phi_{1b}$ ) would undergo a sudden negative change in voltage, toward  $\phi_2$ , as soon as the two right-hand roots disappeared. Sudden voltage changes have been observed both on the SCATHA (P78-2) satellite and in numerical simulations (Sec. 3.1; Schnuelle et al, 1981; Stannard et al, 1982).

Similar sudden changes could occur on a spacecraft which was emitting a changing ion or electron gun current, if an increase or decrease in gun current were to provide enough net current to a surface to cause it to change from one stable floating potential to another. Again, such a change would be relatively sudden even if beam current changes were gradual.

A different effect could arise if the situation evolved in reverse fashion, so that  $t_2$  were now the earlier time. Consider a spacecraft whose rotation carries a number of independently-floating surface panels from sunlight into shade, one after another. Suppose the situation evolves as in Fig. 2.9b. A surface already in the shade when the environment changed would go from voltage  $\phi_2$  to  $\phi_{1a}$ . However, a surface which was

still in the sun, and whose photoemission current held its voltage close to  $\phi_{1b}$ , would go to  $\phi_{1b}$  when it entered the shade. As a result, two adjacent surfaces made of the same material could easily come to quite different voltages in the same environment, with a resulting danger of arcing between them.

In Sec. 3, we examine in detail the conditions in which multiple roots can occur.

## 2.4 PREDICTION OF ION DRIFT EFFECTS ON SPACECRAFT FLOATING POTENTIALS

### 2.4.1 INTRODUCTION

The plasma environment of high-altitude spacecraft has been observed to involve ion velocity anisotropies which sometimes become comparable to ion mean thermal speeds. These anisotropies are varied in nature, but a qualitative estimate of their effects on spacecraft charging may be obtained by considering the effects of a relatively simple anisotropy, namely the addition of a drift to a Maxwellian velocity distribution. Such drifts may cause an electrically-isolated spacecraft surface to float at a substantially increased negative potential if it is simultaneously shaded and downstream relative to the drift direction. In this Section, we present a calculation of upper and lower bounds on such potentials for a spherical spacecraft, based on the fact that ion collection on the spacecraft at its downstream point is bounded above by the corresponding current which would be collected if the spacecraft were an equipotential (i.e. were more attractive for ions elsewhere on its surface than it is in reality) and bounded below by the corresponding result for a sphere at space potential. The results show that (1) the ion speed ratio at which drift effects become "important" (i.e. change the floating potential by at least 10%) can be as low as 0.1, and may be decreased if the ambient electrons are non-Maxwellian; (2) the effects of ion speed ratio increase with increasing ion-to-electron temperature ratio; (3) negative floating potentials for drifting Maxwellian ion velocity distributions with speed ratio unity are typically about twice as large as the corresponding potentials for nondrifting conditions. We now examine the effects of ion drift in detail.

If a spacecraft is exposed to ambient ions whose drift velocity  $U$  is comparable to or larger than their most probable thermal speed [ion speed ratio  $S_i = U / (2kT_i/m_i)^{1/2} \gtrsim 1$ , where  $k$  is Boltzmann's constant and  $m_i$  and  $T_i$  are ion mass and assumed ion temperature], a large decrease in ion flux  $J_i$  to downstream surfaces will occur. Unless such surfaces are able to expel surplus incident electron fluxes, e.g. by photoemission,

## 2.4 PREDICTION OF ION DRIFT EFFECTS ON SPACECRAFT FLOATING POTENTIALS

### 2.4.1 INTRODUCTION

The plasma environment of high-altitude spacecraft has been observed to involve ion velocity anisotropies which sometimes become comparable to ion mean thermal speeds. These anisotropies are varied in nature, but a qualitative estimate of their effects on spacecraft charging may be obtained by considering the effects of a relatively simple anisotropy, namely the addition of a drift to a Maxwellian velocity distribution. Such drifts may cause an electrically-isolated spacecraft surface to float at a substantially increased negative potential if it is simultaneously shaded and downstream relative to the drift direction. In this Section, we present a calculation of upper and lower bounds on such potentials for a spherical spacecraft, based on the fact that ion collection on the spacecraft at its downstream point is bounded above by the corresponding current which would be collected if the spacecraft were an equipotential (i.e. were more attractive for ions elsewhere on its surface than it is in reality) and bounded below by the corresponding result for a sphere at space potential. The results show that (1) the ion speed ratio at which drift effects become "important" (i.e. change the floating potential by at least 10%) can be as low as 0.1, and may be decreased if the ambient electrons are non-Maxwellian; (2) the effects of ion speed ratio increase with increasing ion-to-electron temperature ratio; (3) negative floating potentials for drifting Maxwellian ion velocity distributions with speed ratio unity are typically about twice as large as the corresponding potentials for nondrifting conditions. We now examine the effects of ion drift in detail.

If a spacecraft is exposed to ambient ions whose drift velocity  $U$  is comparable to or larger than their most probable thermal speed [ion speed ratio  $S_i = U / (2kT_i/m_i)^{1/2} \gtrsim 1$ , where  $k$  is Boltzmann's constant and  $m_i$  and  $T_i$  are ion mass and assumed ion temperature], a large decrease in ion flux  $J_i$  to downstream surfaces will occur. Unless such surfaces are able to expel surplus incident electron fluxes, e.g. by photoemission,

their floating potentials will become substantially more negative as a result. If the ambient electron temperature  $T_e$  is simultaneously large, or more generally the ambient electron energy distribution has a significant high-energy component, then large absolute increases in negative floating potentials will occur, with correspondingly increased arcing hazards. Even if  $T_e$  is relatively small, such effects may influence surface potentials enough to disturb particle and field measurements.  $S_i$  values of order unity may be reached in the Earth's outer magnetosphere (Mauk 1975; DeForest 1977, Figs. 6 and 8); larger values are likely in the outer Jovian magnetosphere and magnetosheath (Goldstein and Divine 1977), and in the solar wind (Dessler 1967; Axford 1968; Manka 1973). In both outer magnetospheres, electron distributions having substantial high-energy components have been observed (DeForest and McIlwain 1971; Goldstein and Divine 1977).

A calculation of ion drift effects on the floating potential of the lunar surface has been done by Manka (1973), using a local-current-balance formulation. Parker (1978) has done exact numerical calculations of floating surface potentials for nonconductive finite cylindrical objects, including photoemission due to illumination of one end and ion drift parallel to the axis of symmetry.

In this Section we have done an approximate calculation of ion drift effects on the floating potential of a shaded, downstream, electrically-isolated surface element on a spherical spacecraft (Fig. 2.10), using a local-current-balance formulation which yields upper and lower bounds on such potentials. This formulation is an adaptation of that of Secs. 2.1 to 2.3. The basis of the calculation is as follows: if one compares, on one hand, a situation wherein the entire spacecraft is at the same potential as the surface element in question, with, on the other hand, a more realistic situation wherein the rest of the spacecraft is at a less negative potential (Fig. 2.11), then in the latter case, the potential well surrounding the surface element will be steeper and less spatially extended, and the ion collection will in general be

decreased. When  $S_i \neq 0$ , this argument is subject to qualifications not present in the nondrifting case, for which it is rigorously true in a wide range of conditions (Laframboise and Parker 1973; Laframboise and Godard 1974). In particular, one can envision hypothetical asymmetric sheath potentials which would cause a high-speed-ratio ambient ion distribution to be focused onto the downstream point. We exclude such cases in what follows.

The most extreme example of steepening would be a potential profile which was equal to space potential almost to the spacecraft surface, then fell discontinuously to surface potential. In this limit, the surface element in question would collect just the downstream space-potential current corresponding to the given ion speed ratio. The downstream-point current-density values corresponding to a unipotential sphere at, respectively, the potential of the surface element and space potential may therefore be regarded as upper and lower bounds on the actual current collection at that potential, the upper bound being subject to the above-mentioned qualifications. The resulting values of local floating surface potential may correspondingly be regarded as upper and lower bounds on more realistic values of this quantity. The above-mentioned upper and lower bounds on current correspond, respectively, to the "three-dimensional" and "one-dimensional" velocity-space cutoffs considered in Secs. 2.1 to 2.3 for nondrifting situations.

#### 2.4.2 THEORY OF LOCAL ION COLLECTION ON A UNIPOTENTIAL SPHERE

We assume a collisionless plasma with a drifting Maxwellian ion velocity distribution and negligible magnetic field, containing a fully charge-absorbing, unipotential, spherical electrode. We assume that Debye length  $\lambda_D \gg$  electrode radius  $r_s$ . In the resulting spherically-symmetric Laplace potential  $\phi(r) = \phi_s r_s / r$ , the nondimensional ion current density at the electrode surface is (Godard 1975, p. 31)

$$j_i = \int_{\max(0, \chi_s)}^{\infty} \int_0^{\pi - \chi_s} \exp(-\beta - 2S_i \beta^2 \cos \mu \cos \theta - S_i^2) I_0(2S_i \beta^2 \sin \mu \sin \theta) d\Omega d\beta \quad (2.16)$$

where  $\chi_s = q\phi_s/kT$ ,  $\beta = E/kT$ ,  $\Omega = L^2/(2mr_s^2kT)$ ,  $j = J/[N_\infty q(kT/2\pi m)^{1/2}]$ ,

$I_0$  is the modified Bessel function of zero order,  $N_\infty$  is number density far from the electrode,  $\mu$  is angular surface position coordinate measured from the upstream direction,  $\theta$  is change in direction of the radius vector of a particle as it moves from infinity to radial distance  $r_s$ , and  $\theta$  is related to particle energy  $E$ , angular momentum  $L$ , charge  $q$  and the potential profile  $\phi(r)$  by the following expression (Goldstein 1950, Ch. 3):

$$\theta = \int_{r_s}^{\infty} Ldr / \{r^2 [2mE - 2mq\phi(r) - L^2/r^2]\}^{1/2} \quad (2.17)$$

We have computed  $j_i$  by integrating Eq. (2.16) numerically. For the given Laplace potential, Eq. (2.17) can be integrated analytically. We obtain:

$$\theta = \sin^{-1} [(2\Omega + \chi_s) / (\chi_s^2 + 4\Omega)^{1/2}] - \sin^{-1} [\chi_s / (\chi_s^2 + 4\Omega)^{1/2}] \quad (2.18)$$

For space potential ( $\chi_s = 0$ ), Eq. (2.16) can be integrated analytically. The result is (Tsien 1946)

$$j_i = \pi^{1/2} S_i \cos \mu [1 + \operatorname{erf}(S_i \cos \mu)] + \exp(-S_i^2 \cos^2 \mu) \quad (2.19)$$

Figure 2.12 shows results obtained for the ion current density  $j_{i\pi}$  at the downstream point  $\mu = \pi$ , as a function of  $S_i$ , with  $\chi_s$  as a parameter, where  $\chi_s = e\phi_s/kT_i \leq 0$  and  $e \equiv q_i$ . As expected,  $j_{i\pi}$  decreases with increasing  $S_i$  and increases with increasing  $|\chi_s|$ . In Figure 2.13 the same results are graphed logarithmically as functions of  $\chi_s$ . Figure 2.13 shows that these results may be approximated with an error  $\lesssim 5\%$  by power-law relations of the form

$$j_{i\pi}(\chi_s) = j_{i\pi}(\chi_s = 0) + A_\pi |\chi_s|^{\alpha_\pi}; \quad \chi_s \leq 0 \quad (2.20)$$

The resulting  $S_i$  dependence of the coefficients  $A_\pi$ ,  $\alpha_\pi$  and  $B_\pi \equiv j_{i\pi}(\chi_s = 0)$  is shown in Fig. 2.14.



### 2.4.3 RESULTS AND DISCUSSION

Upper and lower bounds on negative downstream-point floating potentials for a shaded, isolated surface element, obtained by numerical solution of the equation  $J_i + J_e = 0$ , are shown in Fig. 2.15 for various ion-to-electron temperature ratios  $\epsilon = T_i/T_e$ . Here we have assumed that ambient electrons are Maxwellian, and that  $J_i$  is given alternatively by Eq. (2.20) with Fig. 2.14 and by Eq. (2.19), yielding upper and lower bounds on ion current, corresponding respectively to "three-dimensional" and "one-dimensional" ion velocity-space cutoffs (Sec. 2.4.1). We have also assumed that secondary, backscattered, and photoemitted electron currents are zero. The lower-bound results are subject to the qualifications noted in Sec. 2.4.1. The dashed lines in Fig. 2.15 represent floating potentials for the nondrifting case  $S_i = 0$ . At ion speed ratios larger than those shown, the situation becomes complicated by electron speed ratio effects, especially at larger values of  $\epsilon$ . In Fig. 2.15 we see that at larger values of  $\epsilon$ , effects of  $S_i$  become important at smaller  $S_i$  values.

In Fig. 2.16, upper and lower bounds are shown which are similar to those of Fig. 2.15, except that instead of Maxwellian electron velocity distributions, we have used the "quiet" and "disturbed" electron distributions measured by Shield and Frank (1970) and DeForest and McIlwain (1971) respectively in the Earth's outer magnetosphere, and approximated by Knott (1972), as described in Sec. 2.2; see also Prokopenko and Laframboise (1977) and Laframboise and Prokopenko (1978). The ion temperatures used are 111.6 eV and 2.43 keV, respectively. These values were obtained by integrating the electron velocity distributions to find  $N_{e\infty}$ , equating  $N_{i\infty}$  to the result, then assuming that the ions were Maxwellian and that the ratio of ion to electron random fluxes was 0.025. This procedure differs from that used by Knott (1972) and in Secs. 2.1 - 2.3 in which an ion-to-electron random flux ratio of 0.025 and an ion temperature of 1 keV were assumed simultaneously, thereby violating ambient charge neutrality in general. The corresponding electron mean energies are 270 eV and 8.78 keV. The method used for calculating electron currents is described in Sec. 2.2. We see that  $S_i$  effects become important at smaller  $S_i$  values in "quiet" magnetospheric conditions. The ratio of ion to electron mean energies implied by the

above data is also larger in "quiet" conditions, corresponding to the dependence of  $S_i$  effects on  $\epsilon$  noted in Fig. 2.15. The "quiet" and "disturbed" distributions also differ substantially in shape (Knott, 1972, Figs. 1 and 2b). The onset of "significant" drift effects (i.e. floating potential changes  $\approx 10\%$ ) is seen to occur at  $S_i$  values as low as 0.1, depending on conditions. It occurs at lower  $S_i$  values in the presence of the "quiet" distribution than in any of the other cases shown in Figs. 2.15 and 2.16. In Figs. 2.15 and 2.16, negative floating potentials for  $S_i = 1$  are in most cases about twice as large as the corresponding potentials for nondrifting situations.

### 3. MULTIPLE FLOATING POTENTIALS, AND THE "THRESHOLD MATERIAL TEMPERATURE FOR HIGH-VOLTAGE CHARGING"

#### 3.1 INTRODUCTION

The high-voltage charging behaviour of spacecraft surfaces, especially in outer-magnetospheric plasma conditions, displays a variety of unexpectedly complex features.

These features are most evident in the absence of photoemission (as on shaded surfaces of a spacecraft). One of them is the existence of multiple roots (zeros) in the current-voltage characteristic of various spacecraft materials exposed to certain kinds of ambient plasma environments. An example of such a current-voltage characteristic was shown in Fig. 2.5. In this illustration, only the right- and left-hand roots, which are located at +1.9 and -4100 volts, respectively, represent stable floating surface potentials, because the centre root is an unstable one, in the sense that any voltage excursion from the indicated value (-500V) would result in a net current of a sign which would cause the voltage excursion to increase, ultimately driving the voltage to the right- or left-hand roots.

The possibility of such triple-root situations was first proposed by Whipple (1965, pp. 4-7). Prokopenko and Laframboise (1977, 1980) calculated current-voltage characteristics of various surface materials in outer-magnetospheric (including geostationary-orbit) plasma environments, and found numerous examples in which triple-root characteristics were actually obtained. Sanders and Inouye (1979) did calculations to examine the ranges of conditions in which such characteristics would occur. Besse (1981) examined the mechanisms underlying them. Meyer-Vernet (1982) showed that they may also occur on dust grains in space, such as those in Saturn's rings. It is now generally recognized that in triple-root situations, the stable floating potential near space potential is the result primarily of a current balance between incident "primary" electrons and emitted (secondary and backscattered) electrons,

with incident ion current making only a minor contribution, while at the more negative stable potential, the current balance is primarily between incident ion and electron currents, even though in this case also, both of these may be substantially modified by secondary or backscattered electron emission.

Another feature of the high-voltage charging phenomenon is the occurrence of "sensitivity" effects in the numerical prediction of spacecraft potentials (Stannard et al, 1981), in which relatively small changes in assumed surface properties or ambient conditions can cause large changes in spacecraft floating potentials. Evidently, this phenomenon may frustrate attempts to make reliable predictions of spacecraft charging, and it is important to identify the parameter ranges in which such sensitivity effects occur.

This phenomenon is closely related to that of "threshold" effects, both predicted (Stannard et al, 1981), and observed (Gussenhoven and Mullen, 1982), in which no high-voltage charging occurs over a large range of environmental or surface conditions, but a small further change in conditions then results in a large change in surface potential from a small value (relative to space) to a value typically several kilovolts negative.

Another closely-related effect is that of sudden large changes in surface potential in response to relatively slow temporal changes in ambient plasma conditions (Sec. 2.3). This phenomenon was predicted by Prokopenko and Laframboise (1980) and Besse (1981), and subsequently observed both on the SCATHA (P78-2) satellite and in numerical simulations made using the NASA Charging Analyzer Program (NASCAP) (Schnuelle et al, 1981; Stannard et al, 1982).

In Secs. 3.2 and 3.3, we introduce the concept of threshold temperature as a property of a spacecraft surface material, and we show that all of the above-mentioned phenomena are unified and explained by this concept.

A separate phenomenon, which often controls the differential charging of other surfaces, including sunlit ones, relative to the most highly-charged surface, is the "barrier" effect; we discuss this in Sec. 4.5.

### 3.2 THE THRESHOLD-TEMPERATURE PROPERTY.

A typical secondary-electron yield curve is shown in Fig. 3.1(a). For most commonly-used spacecraft surface materials, there exists a region of this yield curve in which more than one secondary is produced on average per primary. This generally occurs for incident electron kinetic energies of a few hundred eV. In Fig. 3.1(b), energy-differential incident-electron flux (particle current density) curves are shown for Maxwellian electron velocity distributions at two representative values of electron temperature  $T_e$ . In the example shown, the peak of the lower-temperature curve is at almost the same energy as that of the secondary yield curve. In this situation, there is a large production of secondaries; in fact, the total secondary flux, which is given by an integral involving the product of these two functions [Eq. (2.10); Prokopenko and Laframboise (1977, 1980, Eq. 10)], will be greater than the incident primary flux if the maximum secondary yield  $\delta_{\max}$  per primary is greater than about 1.16 (Besse, 1981, Fig. 2). In contrast, the peak of the higher-temperature curve does not coincide closely with that of the secondary-emission curve, and in this case, the total secondary flux will be less than the incident flux. Evidently, a critical value of  $T_e$  must exist, intermediate between the two values indicated, at which emitted flux would exactly balance incident flux (H.I. Cohen, 1982, private communication). (There will also be another such critical temperature, below the peak of the secondary yield curve, but this is not of importance here.)

Maxwellian ambient distributions also have the special property that if they are retarded by a repelling (negative) surface potential, the distribution of particle kinetic energies reaching the surface is independent of the value of this potential. Therefore, for a Maxwellian ambient distribution, the preceding conclusions have a special property: they are independent of spacecraft surface potential (Besse, 1981; H.I. Cohen, private communication, 1982) as long as this potential is negative (with respect to space). Therefore, if the ambient electrons were Maxwellian at the critical temperature, incoming and outgoing fluxes would balance each other for all negative values of surface potential, and the surface then "would not know at what potential to float", i.e. the surface potential would become indeterminate, except for the (relatively small) current contribution from ambient ions. It is therefore evident that very large (negative) increases in floating potential will result for very small increases in ambient electron temperature in the neighbourhood of this critical value, which is a property of the surface material only. We will therefore refer to this critical value as the threshold material temperature T\* for high-voltage charging. In terms of this property, the first four effects mentioned in Sec. 3.1 can be immediately explained, as follows.

(1) Triple-root current-voltage characteristics have a simple explanation if the ambient electron velocity distribution can be approximated by a double Maxwellian. Such an approximation, although empirically-based, is often a very good one (Garrett and DeForest, 1979 ; Garrett et al, 1981). In this case, a characteristic will have three roots if (i) the temperature  $T_1$  of one Maxwellian is less than  $T^*$ , but the other one  $T_2$  is greater than  $T^*$ , and (ii) the total emitted electron (secondary and backscattered) flux at space potential is greater than the incident flux.

This can be proven as follows. The roots of the current-voltage characteristic are given by the zeros of the function:

$$J_{net} = J_i - J_e + J_{sec} + J_{scat} \quad (3.1)$$

where  $J_i$ ,  $J_e$ ,  $J_{sec}$  and  $J_{scat}$  are particle current densities (fluxes) for incident (ambient) ions and electrons, secondary electrons and backscattered electrons, respectively. Except at relatively large negative surface potentials  $\phi_s$  relative to space,  $J_i$  is relatively small, and will be neglected in what follows. For  $\phi_s < 0$ , we then have, in this approximation:

$$\begin{aligned}
 J_{net} &= (J_{sec,1} + J_{scat,1} - J_{e,1}) \exp(e\phi_s/kT_1) \\
 &+ (J_{sec,2} + J_{scat,2} - J_{e,2}) \exp(e\phi_s/kT_2) \\
 &\approx J_{net,1} \exp(e\phi_s/kT_1) + J_{net,2} \exp(e\phi_s/kT_2) \quad (3.2)
 \end{aligned}$$

where  $e > 0$  is the elementary charge,  $k$  is Boltzmann's constant, and all double-subscripted  $J$  are space-potential values. A triple-root characteristic must have an unstable root, i.e. a value of  $\phi_s$  such that (a)  $J_{net} = 0$ , and (b)  $dJ_{net}/d\phi_s > 0$ . This can happen only for  $\phi_s < 0$  because  $J_{sec}$  and  $J_{scat}$  both decrease rapidly at positive potentials (an exception to this, applicable at very small electron temperatures, has been found by Meyer-Vernet (1982)). Condition (a) requires that  $J_{net,1}$  and  $J_{net,2}$  have opposite signs, i.e.  $T^*$  is between  $T_1$  and  $T_2$ . Condition (b) implies that  $J_{net} > 0$  for all  $\phi_s$  values between this root and zero; this in turn implies that  $J_{net,1} + J_{net,2} > 0$ . This completes the proof of (i) and (ii). Even though this proof is only approximate for real velocity distributions, it will still be generally valid in terms of "temperatures" related in the usual way ( $\bar{E} = \frac{3}{2} kT$ ) to the mean energies obtained from a double-Maxwellian fit. Meyer-Vernet (1982) has shown that triple roots can also occur with Maxwellian electrons, when the electron temperature is less than the "temperature" of emission of secondary electrons. The unstable root then occurs at a positive rather than negative value of  $\phi_s$ .

(2) For  $T$  (or  $2\bar{E}/3k$ ) close to  $T^*$ , most current-voltage characteristics will have both a very small value and small slope over a large range of potentials, and the floating potential(s) will then be subject to large changes when only small changes in conditions occur. This explains "sensitivity" effects.

(3) For  $T$  slightly less than  $T^*$ ,  $J_{\text{sec}} + J_{\text{scat}} > J_e$  if  $\phi_p < 0$ , and the floating potential will generally be slightly positive. For  $T$  slightly greater than  $T^*$ ,  $J_{\text{sec}} + J_{\text{scat}} < J_e$  and the floating potential will generally be very negative. Clearly  $T^*$  is the temperature at which "threshold" effects may be expected.

(4) For a distribution which is (nearly) Maxwellian and has  $T \approx T^*$ , small (or gradual) changes in ambient conditions can cause the sign of  $J_{\text{sec}} + J_{\text{scat}} - J_e$  to change, resulting in large, sudden changes in floating potential. For a distribution which may not be near-Maxwellian but which leads to a triple-root characteristic, changes in ambient conditions may cause two of the three roots to coalesce and disappear, also producing large, sudden potential changes (Sec. 2.3; Prokopenko and Laframboise, 1980; Besse, 1981; Meyer-Vernet, 1982).



### 3.3 CALCULATION OF THRESHOLD TEMPERATURES; DISCUSSION

We have calculated threshold-temperature values (Table 2) for a variety of spacecraft surface materials; a listing of our computer program for doing this appears in Appendix B. In order to do this, we have calculate  $J_{\text{sec}} + J_{\text{scat}} - J_e$  as a function of  $T$  for Maxwellian incident distributions, and searched numerically for the value  $T^*$  at which this function changes from positive to negative as  $T$  increases.

For ambient electrons normally incident to a surface, we have used the secondary and backscattered flux expressions given by Prokopenko and Laframboise (1977, 1980), together with data given by Dekker (1958), Haenenberg and Brauer (1959, 1962), Gibbons (1966), Willis and Skinner (1973), Katz et al (1977, p. 38), Schnuelle et al (1979), Leung et al (1981), and Krainsky et al (1981).

The increased yields for electrons incident at other angles have an important influence on our results (last three columns of Table 2). For both secondary (Dekker, 1958; Salehi and Flinn, 1981; Krainsky et al, 1981) and backscattered (Darlington and Cosslett, 1972; Krainsky et al, 1981) electrons, it is found experimentally that the dependence of yield (average number of emitted electrons per incident electron)  $\delta(E, \theta)$  on angle of incidence  $\theta$  relative to the surface normal can be usefully approximated by a relation of the form

$$\ln \delta(E, \theta) = \ln \delta(E, 0) + \beta(1 - \cos \theta). \quad (3.3)$$

For secondary emission, the coefficient  $\beta$  appears to depend primarily on  $E/E_{\text{max}}$ , where  $E_{\text{max}}$  is the energy at which  $\delta$  is largest when  $\theta = 0^\circ$ . For backscattered emission,  $\beta$  appears to depend most strongly on the atomic number  $Z$  of the surface material, and only weakly on incident energy  $E$ . Also, available information on  $E$  dependence is fragmentary, and in any case, secondary emission predominates over backscattered emission at smaller values of  $E$ . For these reasons, we have ignored the  $E$  dependence.

The dependence given by Eq. (3.3) has the special advantage that for any isotropic ambient velocity distribution, the integration over angle in the emitted flux expression can be done analytically. In this case, we have:

$$\begin{aligned}
 J_{\text{sec}} \text{ or } J_{\text{scat}} &= \int f \delta v_n d^3\vec{v} \\
 &= \iiint f(E) \delta(E, \theta) (v \cos \theta) (v^2 \sin \theta dv d\theta d\phi) \\
 &= 2\pi \int_0^\infty f(E) \delta(E, 0) v^3 dv \int_0^{2\pi} e^{\beta(E)(1-\cos \theta)} \cos \theta \sin \theta d\theta
 \end{aligned} \tag{3.4}$$

where  $(v, \theta, \phi)$  are spherical coordinates in velocity space with polar axis normal to the surface,  $f \equiv d^6N/d^3\vec{r} d^3\vec{v}$  is the velocity distribution of ambient electrons,  $E = \frac{1}{2}mv^2$ , and  $v_n$  is the normal component of incident electron velocity.

The integral over  $\theta$  yields  $[\exp(\beta) - \beta - 1]/\beta^2$ , which has the value  $\frac{1}{2}$  when  $\beta = 0$ . After  $\beta$  is specified as a function of  $E$ , multiplication of  $\delta(E, 0)$  by the factor  $\Gamma = (2/\beta^2)[\exp(\beta) - \beta - 1]$  then corrects  $\delta(E, 0)$  to include angle-dependence of the secondary or backscattered yield [see also Whipple, 1981, Eq. (3.11)]. To obtain the resulting dependence of  $\delta \equiv \delta_{\text{sec}} + \delta_{\text{scat}}$  on  $E$ , we require that  $E_{\text{max}}$  and  $\delta_{\text{max}}$  for normal-incidence secondary yield be specified, together with  $Z$ . Our complete yield algorithm then is:

$$\xi = \ln(E/E_{\text{max}}); \quad \eta = 0.2755(\xi - 1.658) - \sqrt{[0.2755(\xi - 1.658)]^2 + 0.0228};$$

$$\beta_{\text{sec}} = e^\eta; \quad \Gamma_{\text{sec}} = (2/\beta_{\text{sec}}^2)[\exp(\beta_{\text{sec}}) - \beta_{\text{sec}} - 1]; \tag{3.5}$$

$$\beta_{\text{scat}} = 7.37Z^{-0.56875}; \quad \Gamma_{\text{scat}} = (2/\beta_{\text{scat}}^2)[\exp(\beta_{\text{scat}}) - \beta_{\text{scat}} - 1]$$

where the above expressions for  $\beta_{\text{sec}}$  and  $\beta_{\text{scat}}$  have been obtained by fits to the data of Dekker (1958), Darlington and Cosslett (1972), Salehi and Flinn (1981), and Krainsky et al (1981). Finally:

$$S(E) = \left[ 7.46 \frac{E}{E_{\max}} \exp\left(-2\sqrt{\frac{E}{E_{\max}}}\right) \right] \Gamma_{\text{sec}} + [A - B e^{-CE}] \Gamma_{\text{scat}} \quad (3.6)$$

where the factors multiplying  $\Gamma_{\text{sec}}$  and  $\Gamma_{\text{scat}}$  are, respectively, the secondary-yield curve of Sternglass (1954a), and an empirical factor given by Eq. 2.9 (See also Prokopenko and Laframboise, 1980, Eq. (9)), in which the coefficients A, B, and C are functions of Z obtained from the data of Sternglass (1954b) and Palluel (1947). These coefficients are also displayed in Table 2.  $J_{\text{sec}} + J_{\text{scat}}$  is then given by  $2\pi$  times the integral over  $v$  in (3.4) with  $f$  replaced by the Maxwellian distribution corresponding to temperature T, or more generally, by Eqs. (2.10) - (2.14).  $J_e = n_{\infty} (kT/2\pi m_e)^{1/2}$ , i.e. the usual random flux for a Maxwellian distribution (where  $n_{\infty}$  is ambient electron density and  $m_e$  is electron mass), or more generally, is given by Eqs. (2.1) - (2.3).

The resulting threshold temperatures  $T^*$  (labeled "TC3") appear in the last column of Table 1. Corresponding values of  $T^*$  for simplified forms of  $\delta(E)$  as indicated (labeled "TC1" and "TC2") appear in the two adjacent columns. It is clear from these results that angle-dependence of  $\delta_{\text{sec}}$  and  $\delta_{\text{scat}}$  has an important effect on values of  $T^*$ . The values labeled "TC1" can also be inferred from Fig. 2 of Besse (1981).

Clearly, those surface materials having the largest values of  $T^*$  will be the "most resistant" to high-voltage charging (leaving aside the effects of material conductivity) because the ambient environment will exceed their threshold temperature the least often. From this viewpoint, and using the data of Table 1,  $\text{MgF}_2$  is the "most resistant" material, followed by activated beryllium-copper, gold, and NASCAP 'BOOMAT', a spatially-averaged representation of a composite surface consisting of kapton partly covered with platinum strips, used on the SCATHA satellite (Schnuelle et al, 1979). The zero entries for  $T^*$  in Table 1 are those for which  $J_{\text{sec}} + J_{\text{scat}} < J_e$  at all values of T.

Our discussion so far has been almost completely concerned with "absolute" or "overall" surface charging, and has been based only on calculations of local currents to and from surfaces. Calculations of this type are usually sufficient to determine the floating potential of the most highly (usually negatively) charged portion of a spacecraft surface, which is usually in a shaded or partly-shaded region of the spacecraft. However, the most damaging effects of high-voltage charging are "differential" effects involving large potential differences between adjacent parts of a spacecraft. These effects are frequently dominated by non-local phenomena, an example of which we present in Sec. 4.6.

#### 4. CYLVIA: A TWO-DIMENSIONAL CHARGING SIMULATION FOR CYLINDRICAL SPACECRAFT CROSS-SECTIONS WITH ANGLE-DEPENDENCE.

##### 4.1 INTRODUCTION: THE QUASISTATIC ITERATION METHOD

We have constructed a numerical simulation program called CYLVIA (CYLinder Voltages in Ionosphere and Above) which combines the following features:

a) infinite circular cylindrical geometry with angle-dependence. We have chosen this geometry for the following reasons: A realistic model must be at least two-dimensional because the asymmetry between sunlit and shaded surfaces, or between surfaces with large and small secondary-electron emission currents, is a key feature of the differential charging problem. Cylindrical geometry is the simplest two-dimensional geometry, and it is also a useful approximation to many spacecraft shapes, including the DSCS and SCATHA mainframes, which are finite circular cylinders. Effects of finite cylinder length (three-dimensionality) on sheath potential profiles, which tend to cause a more rapid decrease of potential with radius, can be approximated by using a modified form of Poisson's equation (Sec. 4.3).

b) Quasistatic time-dependent iteration (Laframboise and Prokopenko, 1977). In this procedure, sheath potential changes during particle transit times are ignored. This leads to the following iteration scheme: a distribution of surface potentials is chosen. Poisson's equation is then solved to provide a radius- and angle-dependent static sheath potential [see (c) below]. Particle orbits are then followed numerically in this potential, yielding net surface charging rate as a function of surface position. Using this information, the surface potentials are updated. This process is repeated until a steady-state floating condition is obtained or in order to follow temporal changes in external conditions, such as spacecraft rotation or eclipse passage.

c) use of simplified space-charge density expressions (Sec. 4.2; Laframboise and Prokopenko, 1977), rather than numerical orbit-following,

in solving Poisson's equation for sheath potentials. Approximations of this type are good ones for geostationary-orbit situations, in which the Debye length of the ambient plasma is generally large enough that space-charge effects are almost negligible. They also yield an important saving of computer time.

Features (b) and (c) are now also used in the NASCAP (Katz et al, 1977, 1979) simulation program.

A listing of CYLVIA appears in Appendices C and D. The numerical solution of Poisson's equation in CYLVIA calculations uses the subroutines POIS, POISGN, POINIT, TRID, TRIDP, and NCHECK written by Swarztrauber and Sweet (1975).

#### 4.2 USE OF APPROXIMATE SPACE-CHARGE DENSITY EXPRESSIONS

At geostationary-orbit altitude, the Debye length  $\lambda_D$  for ambient particles is usually  $\sim 10$  m, so for satellites of ordinary size, effects of ambient space charge on sheath potentials will be relatively small. Any reasonably realistic approximation of this space charge can therefore be expected to produce only negligible errors in solving Poisson's equation for sheath potentials. Furthermore, large savings in computer time can be expected to result if one can avoid exact density calculations involving numerical orbit-following. In calculations using CYLVIA, only a relatively small amount of orbit-following is done, in order to calculate surface currents (Sec. 4.4).

A more significant space-charge effect near the spacecraft may be caused by emitted photoelectrons or secondary electrons (Soop, 1972; Schröder, 1973), because of their relatively low velocities compared to ambient values. However, effects of these are likely also to be small enough that any reasonably realistic approximations for their densities will yield good accuracy (Lafon, 1976). Such approximations must ultimately be verified by comparison with exact calculations. It is advantageous if such approximations depend on local potential only (rather than potentials at many locations), together with a relatively small number of other parameters, such as spacecraft potentials and potential barrier heights and locations. Laframboise and Prokopenko (1977) have developed such an approximation. Here we develop three

approximate expressions for ambient space-charge density [Eqs. (4.1)-(4.3)], based on the use of exact density expressions developed for collisionless, Maxwellian particles in the presence of obstacle-free potential wells of arbitrary shape by Laframboise and Parker (1973). The appropriate expression for our purposes is the result given by their Eq. (2) for three-dimensional wells. This is true even for an "infinite", that is, very long cylindrical spacecraft geometry, because of particle entry at the ends of such a geometry. For definiteness, we consider a negative well given by  $\phi(x,y,z) \leq 0$ , with  $\phi \rightarrow 0$  as  $x^2 + y^2 + z^2 \rightarrow \infty$ , where  $\phi$  is electric potential. If only ambient particles are considered, Poisson's equation is:

$$\nabla^2 \phi = \frac{e}{\epsilon_0} (N_e - N_i) \quad (4.1)$$

where  $e$  is magnitude of unit electron charge,  $\epsilon_0$  is permittivity of space, and  $N_e$ ,  $N_i$  are electron and ion number densities, respectively. Since positive ions are the attracted species in this well, we use Eq. (2) of Laframboise and Parker (1973) for ion density, and the usual Boltzmann factor for electron density. If  $\lambda_{De} = (\epsilon_0 k T_e / e^2 N_\infty)^{1/2}$ ,  $N_\infty$  is electron or ion density far from the spacecraft,  $L$  is a characteristic spacecraft length,  $\tilde{\nabla} = L \nabla$ ,  $\chi = e\phi / k T_e < 0$ ,  $k$  is Boltzmann's constant and  $T$  is temperature, Eq. (4.1) becomes:

$$\tilde{\nabla}^2 \chi = \left( \frac{L}{\lambda_{De}} \right)^2 \left\{ e^\chi - \frac{2}{\sqrt{\pi}} \left[ (-\chi T_e / T_i)^{1/2} + g(-\chi T_e / T_i)^{1/2} \right] \right\} \quad (4.2)$$

where  $g(s) = \frac{1}{2} \sqrt{\pi} \exp(s^2) \operatorname{erfc}(s) = \exp(s^2) \int_s^\infty \exp(-t^2) dt$ . An efficient method for calculating  $\operatorname{erfc}(s)$  has been given by Shepherd and Laframboise (1981).

The important feature of Eq. (4.2) for our purposes is that its right-hand side is a function of  $\chi$  only. For small  $\chi$ , Eq. (4.2) reduces to:

$$\tilde{\nabla}^2 \chi = (1 + T_e / T_i) (L / \lambda_{De})^2 \chi \quad (4.3)$$

where terms of order  $\chi^{3/2}$  and higher have been ignored. The linear form of (4.3) permits the use of direct Poisson-solvers for finding  $\chi$ . Another simplified form can be obtained by rederiving Eq. (4.2) with monoenergetic instead of Maxwellian ions assumed. The appropriate monoenergetic velocity

distribution (Chen, 1965; Laframboise, 1966, p. 14) is:

$$f \equiv \frac{d^3 N}{d^3 \vec{v}} = \frac{m_i^2 N_x}{4\pi} \frac{\delta(E - E_1)}{(2m_i E_1)^{1/2}} \quad (4.4)$$

where  $E_1 = 4kT_i/\pi$  and  $m_i$  is ion mass; this distribution duplicates the ambient number density and flux values of a Maxwellian at temperature  $T_i$ . Rederivation of (2) using this distribution yields the computationally simpler form:

$$\nabla^2 \chi = \left(\frac{L}{\lambda_{De}}\right)^2 \left[ e^\chi - \left(1 - \frac{\pi}{4} \frac{T_e}{T_i} \chi\right)^{1/2} \right]. \quad (4.5)$$

If any regions exist where  $\chi > 0$ , the roles of ions and electrons are interchanged, and Eqs. (4.2) - (4.5) must be modified accordingly.

The essential approximation contained in Eqs. (4.2) - (4.5) is the neglect of orbit depletion due to intersection with the spacecraft. The densities of ambient ions and electrons will therefore both be overestimated near the spacecraft in these results. As long as the spacecraft is at least moderately smaller than  $\lambda_{De}$ , the effects of this overestimate will be small. The attracted-species density will be overestimated by the greater amount for reasons involving the curvatures of attracted and repelled particle orbits. The sheath profiles predicted by (4.2) or (4.5) will therefore be steeper than real profiles, if electron emission effects are ignored. Laframboise and Prokopenko (1977, Secs. 2.4.2 and 2.4.3) have also discussed space-charge density approximations based on symmetric potentials and on equivalent potential wells, for ambient and emitted electrons.

#### 4.3 APPROXIMATE INCLUSION OF FINITE-CYLINDER - LENGTH (THREE-DIMENSIONAL) EFFECTS IN POISSON'S EQUATION.

Effects of finite spacecraft length on sheath potential profiles can be included in either of two approximate ways which lead to modifications of the two-dimensional Poisson equation to be solved. We include here a description of these methods. The first method is derived by pretending that the circular inner boundary of the computation grid, which



represents the spacecraft surface, is no longer a cross-section of an infinite cylinder, but rather is a cross-section through the equatorial plane of a prolate spheroid of polar-to-equatorial axis ratio  $L \geq 1$ .

We also assume that the sheath potential is (for some unspecified reason) independent of the latitude coordinate perpendicular to this plane.

This leads to a modified Poisson equation of the form

$$\tanh^2 \xi \frac{\partial^2 \chi}{\partial \xi^2} + \tanh \xi \frac{\partial \chi}{\partial \xi} + \frac{\partial^2 \chi}{\partial \theta^2} = \frac{\sinh^2 \xi}{\sinh^2 \xi_s} \left( \frac{R_s}{\lambda_D} \right)^2 (n_e - n_i) \quad (4.6)$$

where  $\chi = e\phi/kT_e$ ,  $\xi$  is a radial coordinate in the equatorial plane and is related to nondimensional radius  $r = R/R_s$ , defined in the same plane, by the relation

$r = (L^2 - 1)^{1/2} \sinh \xi$ ,  $\xi_s = \frac{1}{2} \ln [(L+1)/(L-1)]$ ,  $\theta$  is angular coordinate in the same plane,  $R_s$  is spacecraft radius,  $\lambda_D$  is Debye length, and  $n_e$  and  $n_i$  are the nondimensional electron and ion densities  $N_e/N_{e\infty}$  and  $N_i/N_{i\infty}$ , where  $N_0$  is ambient density of either species. Use of Eq. (4.6) in place of the usual polar-coordinate Poisson equation would result in sheath potential profiles which became increasingly steeper as  $L$  decreased, thus allowing for approximate estimates of sheath potentials around finite cylinders. The limiting case  $L=1$  would correspond to an assumed spherical geometry without latitude dependence; the limit  $L \rightarrow \infty$  leads to recovery of infinite cylindrical geometry.

The transformation  $s = \ln \coth \frac{1}{2} \xi$  leads to the alternative form

$$\frac{1}{\cosh^2 \xi} \frac{\partial^2 \chi}{\partial s^2} + \frac{\partial^2 \chi}{\partial \theta^2} = \frac{\sinh^2 \xi}{\sinh^2 \xi_s} \left( \frac{R_s}{\lambda_D} \right)^2 (n_e - n_i) \quad (4.7)$$

which contains no first-order terms. For small  $\xi$ ,  $s$  varies logarithmically with  $r$ ; for large  $\xi$ ,  $s$  varies as  $r^{-1}$ .

The second method is derived by first writing the nondimensional Poisson equation for cylindrical coordinates, which has the form

$$\frac{\partial^2 \chi}{\partial r^2} + \frac{1}{r} \frac{\partial \chi}{\partial r} + \frac{1}{r^2} \frac{\partial^2 \chi}{\partial \theta^2} + \frac{\partial^2 \chi}{\partial z^2} = \left( \frac{R_s}{\lambda_D} \right)^2 (n_e - n_i) \quad (4.8)$$

We then assume that  $\chi(r, \theta, z)$  is periodic in  $z$ , such that values of  $\chi$  repeat after nondimensional distance  $2l$  parallel to the  $z$  axis. In particular, we assume that  $\chi(r, \theta, z) = \text{some given dependence } \chi_2(r, \theta)$ ,

and that  $\chi(r, \theta, 0) = \chi_0(r, \theta)$  to be found. We further assume that  $\partial\chi/\partial z = 0$  at  $z = 0, z = \pm\ell, z = \pm 2\ell$ , etc, and that only the lowest Fourier component of the  $z$  dependence of  $\chi$  is present. Then

$$\chi(r, \theta, z) = \frac{1}{2}[\chi_0(r, \theta) + \chi_\ell(r, \theta)] + \frac{1}{2}[\chi_0(r, \theta) - \chi_\ell(r, \theta)] \cos\left(\frac{\pi z}{\ell}\right) \quad (4.9)$$

and, at  $z = 0$ , we have

$$\frac{\partial^2 \chi_0}{\partial z^2} = \frac{1}{2} \left(\frac{\pi}{\ell}\right)^2 [\chi_\ell(r, \theta) - \chi_0(r, \theta)] \quad (4.10)$$

The Poisson equation for  $\chi_0(r, \theta)$  now becomes

$$\frac{\partial^2 \chi_0}{\partial r^2} + \frac{1}{r} \frac{\partial \chi_0}{\partial r} + \frac{1}{r^2} \frac{\partial^2 \chi_0}{\partial \theta^2} - \frac{1}{2} \left(\frac{\pi}{\ell}\right)^2 \chi_0 = \left(\frac{R_s}{\lambda_D}\right)^2 (n_e - n_i) - \frac{1}{2} \left(\frac{\pi}{\ell}\right)^2 \chi_\ell(r, \theta) \quad (4.11)$$

We see that in this Poisson equation, effects of  $z$ -dependence are represented by a homogeneous "Helmholtz" term and a fictitious space charge contribution. The  $z$ -dependence incorporated into this equation could represent approximately the effects on sheath potentials of finite spacecraft length and/or features such as conductive circumferential bands. Equations (4.7) and (4.11) are both solvable by standard methods; both are linear. Both contain only two (radius and angle) independent variables.

#### 4.4 ORBIT INTEGRATION AND CURRENT CALCULATION

CYLVIA uses a form of the particle orbit equations in which particle total energy is explicitly conserved. This formulation was adopted because of a difficulty which arose when using more standard methods to integrate photoelectron orbits. Accumulation of numerical errors was occasionally found to change the total energy of an orbit by amounts large compared to the assumed thermal energy of emission (1.5V), especially near points where orbits were "reflected" by a potential barrier; this in turn produced large errors in calculations of photoelectron currents reimpacting spacecraft surfaces.

In order to derive the orbit equations, we consider the motion of a particle in a plane. We let  $(r, \theta)$  and  $(v_r, v_\theta)$  represent its position and

velocity components in polar coordinates (Fig. 4.1). We let  $s$  represent arc length along its orbit, and  $\hat{u}$  and  $\hat{n}$  represent unit tangent and unit normal vectors at a point on the orbit, the latter directed toward its local centre of curvature. We let  $\rho$  represent its local radius of curvature. We let  $q, m$ , and  $E$  represent particle charge, mass, and total energy, and  $\phi(r, \theta)$  represent electric potential. The equation of motion  $m \frac{d\vec{v}}{dt} = -q\nabla\phi$  reduces to:

$$v \frac{dv}{ds} \hat{u} + \frac{v^2}{\rho} \hat{n} = \frac{q}{m} \left( -\hat{n} \frac{\partial\phi}{\partial n} - \hat{u} \frac{\partial\phi}{\partial s} \right) \quad (4.12)$$

We equate respective components of Eq. (4.12) and use the relations  $ds = \rho d(\alpha + \theta)$ ,  $dr = \cos(\alpha) ds$ , and  $r d\theta = \sin(\alpha) ds$ . We then obtain the orbit equations in the following form:

$$\begin{aligned} \frac{d\alpha}{ds} &= - \frac{q}{mv^2} \left( \frac{\cos\alpha}{r} \frac{\partial\phi}{\partial\theta} - \sin\alpha \frac{\partial\phi}{\partial r} \right) - \frac{\sin\alpha}{r} \\ \frac{dr}{ds} &= \cos\alpha \\ \frac{d\theta}{ds} &= \frac{\sin\alpha}{r} \end{aligned} \quad (4.13)$$

$$v^2 = \frac{2}{m} \left[ E - q\phi(r, \theta) \right]$$

This system is reduced from fourth to third order because the last equation appears in integrated form. At points where particle reflection from potential barriers produces cusps or near-cusps in an orbit ( $d\alpha/ds$  becomes singular or large), a segment of the orbit is replaced by a parabolic arc.

We illustrate the current calculation method used by CYLVIA by first considering photoelectrons which arrive at a point on the surface whose normal makes an angle  $\theta$  with the sunward direction, each of them having originated at some other surface location  $\theta_0$  (Fig. 4.2a) and forced to return to the surface by a potential barrier which surrounds the spacecraft. Their current density at the surface location given by  $\theta$  is:

$$J(\theta) = \int_{v=0}^{v=\infty} \int_{\omega=0}^{\omega=\pi} \hat{f}(v, \omega) (v \sin \omega) (v \, dv \, d\omega) \quad (4.14)$$

where  $v = (v_r^2 + v_\theta^2)^{1/2}$  and  $\omega = \tan^{-1}(v_r/v_\theta)$  are polar coordinates in incident velocity space at the surface location  $\theta$ ,  $\hat{f} \equiv d^2N/dv_r dv_\theta$  is the two-dimensional velocity distribution of photoelectrons, and  $N$  is their number density. By Liouville's theorem,  $\hat{f}$  is constant along a particle orbit. Assuming that photoelectrons are emitted with a Maxwellian distribution corresponding to a temperature  $T$ , their emission flux  $J_{ph}(\theta_0)$  is related to  $\hat{f}$  as follows:

$$\hat{f} = \frac{1}{\sqrt{2\pi}} J_{ph}(\theta_0) \left( \frac{m}{kT} \right)^{3/2} e^{-mv_0^2/2kT} \quad (4.15)$$

If the sunlit side of the spacecraft has uniform material properties, then

$J_{ph}(\theta_0) = J_{ph}(0) \cos \theta_0$ . We introduce dimensionless variables as follows:

$$\chi = q\phi/kT; \quad u = v(m/2kT)^{1/2} \quad (4.16)$$

Since  $\frac{1}{2}mv^2 + q\phi = \frac{1}{2}mv_0^2 + q\phi_0$ , (4.15) and (4.14) become:

$$\hat{f} = \frac{1}{\sqrt{2\pi}} J_{ph}(\theta_0) \left( \frac{m}{kT} \right)^{3/2} e^{\chi_0 - \chi} e^{-u^2} \quad (4.17)$$

$$J(\theta) = \frac{2}{\sqrt{\pi}} \int_{u=0}^{u=\infty} du \, u^2 e^{-u^2} \int_{\omega=0}^{\omega=\pi} d\omega \sin \omega \left[ J_{ph}(\theta_0) e^{\chi_0 - \chi} \right] \quad (4.18)$$

The factor in square parentheses in (4.18) is evaluated for each  $u$  and  $\omega$  by integrating the corresponding photoelectron orbit backward to its origin to find  $\theta_0$  and  $\chi_0$ . To do the integrations in (4.18) we set up a polar-coordinate grid in velocity space at the surface location  $\theta$ , as shown in fig. 4.2b, where we have defined  $u_n = -u_r$ ,  $u_t = -u_\theta$ . We approximate  $F(u, \omega) \equiv (2/\sqrt{\pi}) J_{ph}(\theta_0) \exp(\chi_0 - \chi)$  in each cell  $u_i \leq u \leq u_{i+1}$ ,  $\omega_j \leq \omega \leq \omega_{j+1}$  by  $(A + Bu)(C + Dw)$  where  $A, \dots, D$  can be determined if the values of  $F$  at its four corners are found, again by integrating orbits backward. Equation (4.18) then becomes:

$$J(\theta) = \sum_{i,j} \int_{u_i}^{u_{i+1}} du u^2 e^{-u^2} (A_{ij} + B_{ij}u) \int_{\omega_j}^{\omega_{j+1}} d\omega \sin \omega (C_{ij} + D_{ij}\omega), \quad (4.19)$$

a form in which all integrals can be evaluated analytically. This method for evaluating  $J(\theta)$  is essentially equivalent to the "inside-out" method of Parker and Whipple (1967). The factor  $\exp(\chi_0 - \chi)$  in  $F(u, \omega)$  may vary strongly within individual cells. The potential barrier which surrounds a spacecraft is always of finite height, permitting some photoelectrons to escape and ambient electrons to reach it. This means that the integration in (4.19) must be performed over two regions of velocity space, labelled I and II in Fig. 4.2b, containing photoelectrons (and secondary and backscattered electrons), and ambient electrons, respectively. In general,  $\hat{f}$  will contain a discontinuity at the boundary between I and II (Whipple, 1976) which can produce large errors in the evaluation of  $J(\theta)$ . The integration method used in CYLVIA treats these discontinuities explicitly, using bisection searches to find points such as those circled in Fig. 4.2b. If the ambient electron velocity distribution is isotropic, then  $F$  in region II will be independent of  $\omega$ .

## 4.5 RESULTS AND DISCUSSION

Figure 4.3 shows a CYLVIA calculation of equipotential contours surrounding a cylindrical spacecraft cross-section whose surface consists of two independently floating conductive sectors, the smaller of which is shaded and subtends an angle of  $90^\circ$ . In this calculation the ambient ion and electron velocity distributions are double Maxwellians with the following properties:

$N_{i1} = 1 \text{ cm}^{-3}$	$N_{e1} = 1 \text{ cm}^{-3}$
$T_{i1} = 20 \text{ eV}$	$T_{e1} = 500 \text{ eV}$
$N_{i2} = 1 \text{ cm}^{-3}$	$N_{e2} = 1 \text{ cm}^{-3}$
$T_{i2} = 10^4 \text{ eV}$	$T_{e2} = 5000 \text{ eV}$

The photoelectron charge flux  $eJ_{ph}$  is  $45 \times 10^{-6} \text{ A/m}^2$  at normal sunlight incidence.  $T_{ph} = 1.5 \text{ eV}$ . Secondary and backscattered electron fluxes are assumed zero. Ambient ion and electron and photoelectron currents are calculated using numerical orbit-following as described in Sec. 4.4. The computation grid in  $(r, \theta)$  contains  $65 \times 48$  intervals. In this and subsequent calculations, the computation grid in  $(u, \omega)$  contains  $8 \times 16$  intervals for each Maxwellian component of each particle species, apart from bisection searches (Sec. 4.4) which give finer resolution. Linear space charge is assumed [Sec. 4.2; Laframboise and Prokopenko, 1977, Eq. (3)]. The above-mentioned plasma parameters imply an ambient Debye length of 32.5 meters; spacecraft radius  $r_s$  is 1 meter. The outer boundary of the computation grid is at  $e^5 r_s \approx 148 r_s$ . The most noteworthy feature of Fig. 4.3 is a negative saddle-point potential barrier which surrounds the larger sector, and whose height varies from about 2 volts at the sunward point to several hundred volts near the edges of this sector. The potential of the  $270^\circ$  sector ( $-2.265 \text{ kV}$ ) is controlled by blocking of electron escape caused by this barrier; this mechanism is discussed in more detail in Sec. 4.6. In Sec. 6.5, surface photocurrents obtained from this calculation are compared with values given by an analytic approximation. In this and subsequent calculations, calculated surface potentials are all within 10 volts of the values at which the residual currents change sign.

Figure 4.4 shows a CYLVIA calculation of equipotential contours around a spacecraft cross-section divided into four  $90^\circ$  sectors, two covered with aluminum and two with quartz. The aluminum sectors are electrically connected to each other. In this calculation the ambient velocity distributions are single Maxwellians with  $N_i = N_e = 3\text{cm}^{-3}$  and  $T_i = T_e = 1\text{ keV}$ . Photoelectron fluxes at normal sunlight incidence are 42 and  $32\ \mu\text{A/m}^2$  for aluminum and quartz, respectively.  $T_{ph} = 1.5\text{ eV}$  for both. Secondary and backscattered fluxes are assumed zero. The computation grid in  $(r,\theta)$  contains  $65 \times 16$  intervals. The outer boundary of this grid is at  $e^7 \times 1097$  spacecraft radii. The above-mentioned plasma parameters imply an ambient Debye length of 96 meters; spacecraft radius  $r_s$  is 1 meter. As in Fig. 4.3, a saddle-point barrier is present on the sunward side of the spacecraft (see Sec. 4.6), and controls the potential of the sunlit quartz sector and the two aluminum sectors.

In a separate calculation, which is not shown, we included secondary and backscattered electron emission; the calculated surface potentials then were all between 0 and +10V. This result can be readily interpreted in terms of the threshold material temperatures for high-voltage charging defined in Sec. 3 and listed in Table 2. Although the value of  $T_e$  for this case is greater than the threshold temperature of aluminum (Table 2), the aluminum sectors are partly sunlit, and photoemit enough to balance their ambient electron collection current. The threshold temperature of quartz is greater than  $T_e$ , so secondary and backscattered electron emission from these sectors is therefore enough to balance their ambient electron collection current. Thus in this case, no negative charging occurs on any sector. If  $T_e$  were made substantially larger than the threshold temperature of quartz (Table 2), then high-voltage negative charging of the shaded quartz sector would again occur.

In Fig. 4.5, the same spacecraft cross-section as in Fig. 4.4 has been rotated by  $90^\circ$  relative to the sunward direction. In this case the most negative potentials are those on the shaded regions of the quartz sectors, which float separately from the sunlit regions because the quartz is nonconductive. In this situation it is possible that

breakdown of orbit-limitation of the collection of ambient ions (Sec. 2.1) could occur, especially near the edges of these shaded regions, and this would restrict ion collection and cause their floating potentials to become even more negative than we have calculated, but the rather coarse  $\theta$ -interval of our computational grid has prevented us from resolving this question in this calculation.

Also in Fig. 4.5, we have this time a saddle-point barrier on the shaded side of the spacecraft; if the calculation had included secondary and backscattered electrons, this barrier would have controlled their escape. In this case a negative current flows from the shaded to the sunlit aluminum sector, so the sunlit sector floats at a much more negative potential than it would otherwise.

Figure 4.6 shows the distribution of surface potentials corresponding to the calculations of Figs. 4.4 and 4.5, together with the calculated surface potential distribution of a completely nonconductive ("quartz" but with secondary and backscattered electron emission not included) cylinder which is placed in the same environment.

Figure 4.7 shows again the same surface potential distribution for a nonconductive cylinder as in Fig. 4.6, together with another distribution for conditions which are unchanged except that the outer boundary  $r_B$  of the calculation is moved inward to 12 spacecraft radii  $r_S$ . A third calculation is shown, which has been done not using CYLVIA but using a program called TWOD, which combines the physical assumptions of the NASCAP program with circular cylindrical geometry (M. Mandell, Systems, Science and Software Inc., private communication). Except as noted, the physical situations treated in the CYLVIA and TWOD calculations are the same; in both cases  $r_B = 12 r_S$ , zero secondary and backscattered emission is assumed, and a 16-point angular discretization is used. In the TWOD calculation, zero space charge is assumed, but since  $\lambda_D = 96 r_S$  in the CYLVIA calculation, the comparison shown is probably unaffected by this



difference. In the TWOD calculation, photoelectron temperature and normal-incidence flux are 2 eV and  $20 \mu\text{A}/\text{m}^2$ , whereas for CYLVIA, the corresponding parameters are 1.5 eV and  $45 \mu\text{A}/\text{m}^2$ .

We see that rough agreement exists between the CYLVIA and the TWOD calculations. Either our higher photoemission flux, or the rather coarse angular discretization used in both calculations, may account for the differences; we have not yet investigated this question with further calculations. Even though the barrier which surrounds the sunlit side of the cylinder prevents almost all photoelectron escape in the (two) regions  $60^\circ \leq \theta < 90^\circ$  where the largest disagreement occurs, our larger assumed flux permits greater surface migration of photoelectrons (Sec. 6), and the resulting surface current will drain excess negative charge from these regions (to an extent which we have so far not determined). The large difference between the two CYLVIA calculations for  $r_B = 12r_S$  and  $r_B = e^7 r_S$  is symptomatic of the great sensitivity which two-dimensional Laplace-potential (or nearly Laplace-potential, as in our case) calculations have to outer-boundary position generally. On the other hand, tests with CYLVIA have indicated that  $r_B \gtrsim e^5 r_S$  is sufficient to overcome this sensitivity, especially when a small amount of linear (or other) space charge is included, as we have done.

#### 4.6 THE BARRIER EFFECT

As we have seen (Secs. 2 and 3), charging calculations based on local-current-balance considerations are usually sufficient to determine the floating potential of the most highly (usually negatively) charged portion of a spacecraft surface, which is usually in a shaded or partly-shaded region of the spacecraft. However, the most damaging effects of high-voltage charging are "differential" effects involving large potential differences between adjacent parts of a spacecraft. These effects are frequently dominated by non-local phenomena, several examples of which occurred in Sec. 4.5, and which we now examine in more detail.

The most important among these phenomena is the "barrier" effect, which often controls the differential charging of other surfaces, including sunlit ones, relative to the most highly-charged surface. In the "barrier" effect, a strong dipole or higher moment of the spacecraft's potential distribution produces "saddle-point" barriers over less-highly-charged portions of the spacecraft, limiting photoemitted or other electron escape from these portions and causing them to charge more negatively than otherwise. Space-charge effects are normally not important in the formation of such barriers. Their existence, and the resulting implications for differential charging, were first predicted by Fahleson (1973). Whipple (1976) presented evidence for the existence of such a barrier on the ATS-6 satellite. Other properties and consequences of these barriers were discussed by Prokopenko and Laframboise (1977,1980) and Laframboise and Prokopenko (1977). Katz et al (1979) performed a numerical simulation which showed the formation of such a barrier near a polyhedral "quasispherical" model satellite, together with the resulting effects for differential charging. Besse and Rubin (1980) developed an analytical treatment of the barrier effect for a spherical satellite. Purvis (1982) presented a variety of NASCAP numerical simulations to illustrate the prevalence of the barrier effect in high-voltage charging situations. Katz and Mandell (1982) examined mechanisms underlying the barrier effect, called by them the "field-reversal" effect, and in one particular application, the "snapover" effect. In this Section, we present results of a numerical simulation for circular cylindrical geometry, which emphasize the importance of the barrier effect for differential charging.

Using CYLVIA (Secs. 4.1 - 4.5), we have calculated the equilibrium charging state of a cylindrical spacecraft shape with a nonconductive surface in a model geostationary-orbit plasma with sunlight incident normally to the cylinder axis on one side. Figure 4.8 shows the results of a CYLVIA calculation in which we have deliberately made an important oversimplification: we have calculated the surface potential distribution on the basis of local current balance only. Because sunlight

strikes only one side of the spacecraft, photoelectrons are emitted only from this side. In this example, the escaping photoelectron flux from most of the sunlit side is sufficient to balance the ambient electron flux, so the sunlit side of the spacecraft floats at a potential of 5.1V, while the shaded side floats at -2.96 kV. As a result, the spacecraft potential has a strong dipole moment, resulting in the existence of a potential barrier which surrounds its sunlit side. The height of this barrier is -0.61 kV, while the assumed photoelectron emission temperature is only 1.5 eV, so almost all photoelectrons reflect from the barrier and return to the spacecraft, an effect which we have not taken into account in this calculation.

In Fig. 4.9 we have included this effect, and have allowed CYLVIA to converge to the resulting more-realistic steady state. As a result of photoelectron reflection from the barrier, the sunlit side of the spacecraft has charged to a more negative potential. As a result, the barrier height in the sunward direction has been reduced to -0.2V. A substantial fraction of the photo-electrons now escape over the barrier, permitting the local currents to come into balance. A further indication of this is that the saddle point has moved inward from 5.9 spacecraft radii almost to the spacecraft surface: such an inward movement was first predicted by Fahleson (1973), and is evident also in the results of Katz et al (1979, Figs. 17-21) and Besse and Rubin (1980).

The resulting changes in the potential profile along the spacecraft-sun line are shown in Fig. 4.10. The inward motion of the saddle point is again evident. Most importantly, the amount of differential charging between the sunlit and shaded sides has been reduced dramatically, from 2.96 kV to 1.19 kV. Potential-barrier formation evidently exerts a controlling effect on the differential charging. This is increasingly recognized as being the normal condition in differential-charging situations (Purvis, 1982; Katz and Mandell, 1982). Because the capacitances between various parts of a spacecraft are generally much larger than the free-space capacitance of the entire spacecraft, the

charging times for differential charging are usually much larger than those for absolute charging (Purvis, 1982).

It is clear from our example and also the examples presented in Sec. 4.5 (and also another example to be presented in Sec. 5.2), that the formation of potential barriers is very geometry-dependent. This is the case because in geostationary-orbit conditions, space-charge shielding around spacecraft of "ordinary" size (up to a few tens of meters) is a small effect (since the ambient Debye length is usually at least this large), and electric fields produced by charging on one part of a spacecraft surface readily surround other parts of it, even if these are on the other side of the spacecraft. Detailed simulations which include realistic representation of spacecraft geometry therefore appear likely to remain important for studies of spacecraft charging whenever the possibility of barrier effects exists.

In Fig. 4.11 we show another CYLVIA calculation which is discussed in detail in Sec. 5.

## 5. XYCIC: A SIMULATION FOR GENERAL PLANAR-SYMMETRIC (TWO-DIMENSIONAL) SPACECRAFT GEOMETRIES

### 5.1 INTRODUCTION

We have developed and partly tested a program called XYCIC [(X,Y) Charging Investigation Code], which is designed to permit simulation of a wider class of two-dimensional geometries than does CYLVIA. XYCIC is designed to treat any spacecraft cross-section which takes the form of one or more polygons, each of which joins a set of unit lattice points in a Cartesian plane with lines having slopes of 0,  $\pm\frac{1}{2}$ ,  $\pm 1$ ,  $\pm 2$ , or  $\infty$ . Thus a circular cylinder can be approximated by either an octagon or a hexadecagon (16-sided polygon). At present, the geometric features, or "object-generation" portion of XYCIC, and its Poisson-solver, have been completed and tested, and program segments incorporating the same plasma simulation features as in CYLVIA (Secs. 4.1-4.4) have been written and partly tested. A listing of the present version of XYCIC appears in Appendix E.

As noted in connection with Fig. 4.7, plasma simulations in two dimensions generally involve strong sensitivity to boundary effects, unless space-charge shielding intervenes, an effect which frequently does not occur at the large Debye lengths typical of geostationary-orbit conditions. In such cases, as we have seen, it may become necessary to place the outer boundaries of computational domains very far from a (simulated) spacecraft. In order to accomplish this in XYCIC without the penalty of excessive numbers of grid points, we have constructed its computational domain as a set of nested square grids, each of which is centered in the next larger one, and such that in crossing the boundary from each to the next larger one, the grid interval is doubled. A similar succession of nested sub-domains is used in three dimensions in NASCAP (Katz et al, 1977). On the boundary of the outermost domain, the potential is assumed to be zero.

## 5.2 PRELIMINARY RESULTS

Figure 5.1 shows a XYCIC calculation of equipotential contours around an octagonal approximation to the circular cylindrical geometry of Fig. 4.11. As in the case of Fig. 4.11, the surface potentials in Fig. 5.1 have the imposed values shown, rather than self-consistent values. A total of 7 nested grids have been used in this calculation, with the outermost grid boundary located at 27.4 half-widths of the simulated object.

This calculation, and the CYLVIA calculation shown in Fig. 4.11, have been done for comparison with a NASCAP calculation (Olsen, 1980, p. 190; Olsen and Whipple, 1980, Fig. 16) of potentials around an octagonal-cylinder "model object" which approximates the ATS-5 satellite. The feature of greatest interest in both sets of calculations is the potentials of the four saddle points which occur outside the 50 V sections of the spacecraft surface, which represent conductive areas from which electron emission occurred on the real spacecraft. Comparison of our results, Figs. 4.11 and 5.1, with each other indicates a satisfactory level of agreement between them with regard to the potentials and locations of the saddle points. This is the case even though the CYLVIA calculation contains a small amount of linear space charge, while the XYCIC calculation contains none.

Comparison of either result with that of Olsen and Whipple indicates that our saddle points are located about twice as far from the spacecraft surface as theirs, and have larger negative potentials (-56 to -59 V) than theirs (-53 V). These differences undoubtedly result from the fact that our simulation is two-dimensional and theirs is three-dimensional, even though our geometry in Fig. 5.1 is identical with that of their cross-section. Incorporation of three-dimensionality into our calculation, using the approximate method described in Sec. 4.3, would probably bring our results into much closer agreement with theirs, but we have not yet done this. In modifying our calculation in this fashion, it would probably be advantageous to perform our calculation as the superposition

of two modified calculations of the type described by Eqs. (4.8) to (4.11). One of these would have surface potentials given by the (uniform) average (taken over surface position) of those in our Figures, and the characteristic length  $\lambda$  used in it would be that of the ATS-5 model object. The other would have surface potentials given by the departures from this average, and its (much smaller) value of  $\lambda$  would be that of the conductive patches on the ATS-5 object. The disturbance potential of the patches would then decrease more quickly with radius, in better agreement with the Olsen and Whipple calculation.

Figure 5.2 shows a XYCIC prediction of equipotentials around a composite "object" which represents a cross-section through a hypothetical spacecraft-body-and-antenna combination. Again the surface potential values are given ones; in this case they are hypothetical. Other data pertinent to this calculation are given in the figure caption. If self-consistent calculations are made in the future with a geometry similar to the one shown, the "cutout" in the spacecraft body, and the region between the spacecraft body and the antenna, would both become examples of the "shaded cavities" discussed in connection with Fig. 2.8. It would then be possible to verify the prediction, made in Sec. 2.3, that electrically-isolated surfaces inside such cavities may charge to larger negative potentials than those elsewhere on the spacecraft. It would also be possible to investigate the relative importance of the two mechanisms, discussed in Sec. 2.3, which may produce such charging.

## 6. AN ANALYTIC CALCULATION OF SURFACE PHOTOCURRENTS

### 6.1 INTRODUCTION

Photoelectron migration can be an important cause of surface currents on spacecraft in charging situations. Numerical methods of calculating photoelectron migration involve following a large number of electron orbits which will generally be short (from origin to impact point) and have large curvature. Such a procedure can be a major source of expense in operating a simulation program. A good analytic approximation for surface photocurrent can therefore be of great value. If photoelectron migration takes place over a curved surface, the sunlight incidence angle will vary over this surface and therefore so will the photoemission flux. On the other hand, if the normal component of electric force on the electrons is attractive toward the surface and is large enough, the total distance of their travel along the surface will be short enough that effects of surface curvature on their orbits can be neglected, so a model situation involving a planar surface with a photoemission gradient along it becomes appropriate. In Section 6.2, we perform an analytic calculation of surface photocurrent for such a situation. In Section 6.3, we do a partial numerical verification of our result by comparing it with a numerical result obtained using CYLVIA.

### 6.2 THEORY

In this Section, we derive an analytic expression for the surface current density of photoelectron migration along a plane surface  $y=0$ , in the presence of: (a) a uniform normal electric field  $E_y > 0$ , which causes photoelectrons emitted from the surface to reimpact it (Fig. 6.1) (b) a uniform tangential electric field  $E_x$  (c) a uniform photoemission current density gradient  $J'_{ph} = dJ_{ph}/dx$ , so that the photoemission current per unit surface area is  $J_{ph}(x) = J_{ph,0} + J'_{ph} x$ . This photoemission gradient, or "production gradient", would ordinarily be caused by a spatial variation in the illumination of the surface. We also assume



that photoelectrons are emitted with a Maxwellian velocity distribution corresponding to a temperature  $T = T_{ph}$ . In the presence of (a) and (b), all photoelectron orbits are parabolas whose axes are parallel to the resultant electric field vector (Fig. 6.1). The impact location  $x$  for a photoelectron which originates at  $x_0$  with emission velocity components  $v_{x0}$  and  $v_{y0}$  is:

$$x = x_0 + \frac{2m}{eE_y} (v_{x0}v_{y0} - \frac{E_x}{E_y} v_{y0}^2) \quad (6.1)$$

where  $e$  is the magnitude of unit electronic charge. The surface current  $\Gamma$  in the  $x$  direction, per unit distance  $z$  perpendicular to the  $(x,y)$  plane, can now be found by integrating over position and velocity of emission to find the number of photoelectrons per unit  $z$  and unit time which cross the plane  $x = 0$  in the direction of increasing  $x$ , then subtracting the corresponding result for decreasing  $x$ . We note that  $v_{y0} \hat{f}(x_0, v_{x0}, v_{y0})$  is the number of photoelectrons produced per unit surface area per unit  $v_{x0}$  and  $v_{y0}$ , where  $\hat{f} \equiv d^2N/dv_x dv_y$  is the two-dimensional velocity distribution of photoelectrons and  $N$  is their number density. We obtain:

$$\Gamma = \int_{-\infty}^0 dx_0 \int_{-\infty}^{\infty} dv_{x0} \int_0^{\infty} dv_{y0} v_{y0} \hat{f}(x_0, v_{x0}, v_{y0}) H_+(x_0, v_{x0}, v_{y0}) \quad (6.2)$$

$$- \int_0^{\infty} dx_0 \int_{-\infty}^{\infty} dv_{x0} \int_0^{\infty} dv_{y0} v_{y0} \hat{f}(x_0, v_{x0}, v_{y0}) H_-(x_0, v_{x0}, v_{y0})$$

where  $\hat{f} = (1/2\pi) J_{ph}(x) (m/kT)^{3/2} \exp(-mv_0^2/2kT)$ , and  $H_+$  and  $H_-$  are equal to 1 if the impact location  $x$  given by (6.1) is positive or negative, respectively, and equal to 0 otherwise. We define:

$$v_0^2 = v_{x0}^2 + v_{y0}^2; \quad \psi = \tan^{-1}(v_{y0}/v_{x0}); \quad \xi = \tan^{-1}(E_y/E_x). \quad (6.3)$$

Since  $v_{y0} > 0$ , (6.1) implies that  $x \geq x_0$  if  $v_{x0} \geq (E_x/E_y)v_{y0}$ , or  $\psi \geq \xi$ .

Equation (6.2) now becomes:

$$\Gamma = \frac{1}{\sqrt{2\pi}} \left( \frac{m}{kT} \right)^{3/2} \int_0^{\infty} dv_0 v_0^2 \exp\left(-\frac{mv_0^2}{2kT}\right) \int_0^{\xi} d\psi \sin\psi \int_0^0 dx_0 (J_{ph,o} + J_{ph}' x_0)$$

$$- \frac{2mv_0^2}{eE_y} (\cos\psi \sin\psi - \cot\xi \sin^2\psi)$$

$$- \frac{2mv_0^2}{eE_y} (\cos\psi \sin\psi - \cot\xi \sin^2\psi)$$

$$- \frac{1}{\sqrt{2\pi}} \left( \frac{m}{kT} \right)^{3/2} \int_0^{\infty} dv_0 v_0^2 \exp\left(-\frac{mv_0^2}{2kT}\right) \int_{\xi}^{\pi} d\psi \sin\psi \int_0^{\pi} dx_0 (J_{ph,o} + J_{ph}' x_0) \quad (6.4)$$

We define:

$$\Gamma_o = J_{ph,o} kT/eE_y; \quad \gamma = \Gamma/\Gamma_o; \quad (6.5)$$

$$\tilde{x} = (eE_y/kT)x; \quad j' = J'_{ph} \Gamma_o/J_{ph,o}^2;$$

$$u = v_o \sqrt{m/2kT}.$$

Then (6.4) becomes:

$$\begin{aligned} \gamma &= \frac{2}{\sqrt{\pi}} \int_0^{\infty} du u^2 e^{-u^2} \int_0^{\pi} d\psi \left[ 4u^2 (\cos \psi \sin^2 \psi - \cot \xi \sin^3 \psi) \right. \\ &\quad \left. - 8u^4 j' (\cos^2 \psi \sin^3 \psi - 2\cos \psi \sin^4 \psi \cot \xi + \cot^2 \xi \sin^5 \psi) \right] \\ &= -4\cot \xi - j'(4 + 16\cot^2 \xi). \end{aligned} \quad (6.6)$$

Using (6.3) and (6.5), we finally obtain:

$$\Gamma = -\frac{4J_{ph,o} kT_{ph} E_x}{eE_y^2} - J'_{ph} \left( \frac{kT_{ph}}{eE_y} \right)^2 \left[ 4 + 16 \left( \frac{E_x}{E_y} \right)^2 \right]. \quad (6.7)$$

This result contains, respectively, a potential-gradient term, a production-gradient term, and a cross-term. The effect of the cross-term can be substantial: we see that it enhances the production-gradient term five-fold if  $(E_x/E_y)^2 = 1$ , in comparison with its value when  $E_x = 0$ . This is true regardless of the sign of  $E_x$ ; in other words, surprisingly, an "opposed" electric field causes the same enhancement as an "aligned" one.

The potential-gradient term is twice that given by Eq. (14) of Pelizzari and Criswell (1978); this can be seen as follows. If one assumes that photoelectrons are emitted isotropically, corresponding to a value of zero for the parameter  $b$  in their Eqs. (13) and (14), then in our notation, their Eq. (14) is:

$$-e\Gamma = \frac{4J_{ph,o} \left( \frac{3}{2} kT_{ph} \right) E_x}{3E_y^2} \quad (6.8)$$

where our quantities  $-e\Gamma$ ,  $J_{ph,o}$ , and  $\frac{3}{2}kT_{ph}$  are the same as their  $J_a$ ,  $F$ , and  $\langle E \rangle$ , respectively. It is readily seen that (6.7) with  $J'_{ph} = 0$  gives a result twice as large as (6.8), as just mentioned. To see why this difference occurs, we rederive Pelizzari and Criswell's result more rigorously, as follows. From our Eq. (6.1), the contribution of  $E_x$  to particle displacement in the  $x$  direction is

$$\frac{-2mE_x v_{y0}^2}{eE_y^2} \quad (6.9)$$

which is the same as their Eqs. (9) and (11) combined. The contribution due to  $v_{x0}$  in (6.1) averages to zero. Now the surface current density  $\Gamma$  per unit  $z$  equals the integral over  $v_{x0}$  and  $v_{y0}$  of: photoelectron production rate per unit  $v_{x0}$  and  $v_{y0}$  per unit surface area in the  $(x,z)$  plane, times distance travelled by particles of a given  $v_{y0}$  before impact [given by (6.9)]. This production rate in turn equals number per unit volume per unit  $v_{x0}$  and  $v_{y0}$ , times the value of  $v_{y0}$ .

Therefore:

$$\begin{aligned} \Gamma &= \int_0^\infty dv_{y0} \int_{-\infty}^\infty dv_{x0} \hat{f} v_{y0} \left( -\frac{2mE_x v_{y0}^2}{eE_y^2} \right) \\ &= \frac{J_{ph,o}}{\sqrt{2\pi}} \left( \frac{m}{kT} \right)^{\frac{3}{2}} \left( -\frac{2mE_x}{eE_y^2} \right) \int_{-\infty}^\infty dv_{x0} \exp\left(-\frac{mv_{x0}^2}{2kT}\right) \int_0^\infty dv_{y0} v_{y0}^3 \exp\left(-\frac{mv_{y0}^2}{2kT}\right) \\ &= -\frac{4J_{ph,o} kT_{ph}}{eE_y^2} \quad (6.10) \end{aligned}$$

in agreement with our result [Eq. (6.7)] rather than that of Pelizzari and Criswell. The reason for the difference evidently involves the fact that we have integrated Eq. (6.9) over  $v_{y0}$  but they did not. Thus we perform an integral containing  $v_{y0}^3$  [in the first line of (6.10)], but their procedure involves essentially an integral containing  $v_{y0}^2$  (to evaluate their quantity  $\langle E \rangle$ ), times a separate integral containing  $v_{y0}$  (to obtain  $J_{ph,o}$  from  $\hat{f}$ ). Their procedure therefore involves the use of incorrect moments of the velocity distribution function of photoemitted electrons.

## 6.3 COMPARISON WITH A NUMERICAL RESULT FROM CYLVIA

Figure 4.3 shows a CYLVIA calculation of equipotential contours surrounding a cylindrical spacecraft cross-section whose surface consists of two independently floating conductive sectors, the smaller of which is shaded and subtends an angle of  $90^\circ$ . Data pertinent to this calculation are given in Sec. 4.5. The most noteworthy feature of Fig. 4.3 is a negative saddle-point potential barrier which surrounds the larger sector, and whose height varies from about 2 volts at the sunward point to several hundred volts near the edges of this sector.

The resulting normalized current densities  $j_i, j_e,$  and  $j_{ph}$  of ambient ions, ambient electrons, and photoelectrons are shown as functions of surface position in Fig. 6.2. We have made a separate calculation of  $j_{ph}$  using Eq. (6.7) with the tangential electric field  $E_x$  set equal to zero since the spacecraft surfaces are conductive. To use (6.7), we note that the net photoelectron flux out of the surface is equal to the divergence of  $\Gamma$  with respect to surface coordinates. In our geometry, this means that

$$J_{ph,net\ in} \equiv J_{ph,in} - J_{ph,out} = \frac{-1}{r_s} \frac{d\Gamma}{d\theta} = \frac{4}{r_s^2} \frac{d}{d\theta} \left[ \left( \frac{kT_{ph}}{eE_r} \right)^2 \frac{dJ_{ph,out}}{d\theta} \right] \quad (6.11)$$

where

$$edJ_{ph,out}/d\theta = -45 \times 10^{-8} \sin \theta \text{ A/m}^2 \left( -\frac{1}{2}\pi < \theta < \frac{1}{2}\pi \right),$$

and the radial electric field  $E_r$  is obtained from the numerical solution for  $\phi(r, \theta)$  used to construct Fig. 4.3. Net photoelectron currents obtained in this way are shown as dashed curves in Fig. 6.2. We see that near  $\theta = 0^\circ$ , the net outward photocurrent is badly underestimated by Eq. (6.11) since the potential barrier for electrons at this location is not much higher than the photoelectron mean thermal energy, so a substantial fraction of photoelectrons escape, and this is not allowed for in Eqs. (6.7) and (6.11). However, in the interval  $30^\circ \lesssim \theta \lesssim 90^\circ$ , where photoelectron escape is negligible, agreement between Eq. (6.11) and the numerical result is much better. The numerical result is about 10% to 20% above that given by (6.11); the most important reason for this

difference is probably the fact that the tangential electric field, although zero at the spacecraft surface, is nonzero outside it, and the form of the cross-term in (6.7) indicates that the production-gradient current [which is the one calculated in Eq. (6.11)] is strongly sensitive to such fields. We have shown the photoelectron current as decreasing to zero almost discontinuously beyond  $\theta = 90^\circ$ , because the average angular distance of photoelectron migration in the electric fields at this point ( $E_\theta = 0$ ,  $E_r = 1824$  V/m) is about  $0.1^\circ$ .

Another noteworthy feature of Fig. 6.2 is the decrease in the flux of ambient electrons at larger  $\theta$ , caused by the increasing height of the potential barrier as one moves away from the sunward point  $\theta = 0^\circ$ .

## 7. FLUX AND DENSITY CALCULATION FOR COLLISIONLESS PARTICLE ORBITS

Calculation of current density deposited on a surface by particle orbits neighbouring a given orbit is of importance in several contexts related to spacecraft charging. Examples of these are: calculation of current density deposited on one part of a spacecraft by photoelectrons, secondary electrons, or beams of charged particles emitted from another point on it, or calculation of ion current density deposited on spacecraft surfaces in the presence of either a (model) infinite or a large but finite ion speed ratio. In this Section, a simple, general procedure is described for obtaining such information essentially as a byproduct of a numerical orbit calculation. The procedure is based on a perturbation of the orbit equations, and involves finding the evolution along an orbit of the axes of a differential tube of neighbouring orbits. The positions of these axes are given in terms of a set of integrals, contributions to which are collected as the orbit is followed numerically, and whose integrands involve the space derivatives  $\partial F_i / \partial x_j$  of the force components of points along it. At a surface impingement point, current density is then obtained by projecting the cross-section of this tube onto the surface tangent plane. The same formulation can also be used to obtain information about particle number density along an orbit.

In order to appreciate the usefulness of such a procedure it is instructive to compare it with the "standard" procedure which one would normally follow in calculating values of current density deposited on surfaces, and space charge density, of collisionless ions with negligible thermal motion flowing past a collecting object. The "standard" procedure is to numerically follow sets of neighbouring, initially-parallel particle orbits inward from an assumed unperturbed region far from the object, and to calculate flux and density everywhere between any two orbits by finding out how far apart they have become at their impingement points or elsewhere. This method has inherent difficulties: if the orbits chosen are too far apart initially, an orbit may eventually go off in a very different direction than the orbit next to it, making calculations of flux or density between them impossible or unrealistic. On the other hand, if they are initially too close together, inaccuracies in calculating either orbit may obscure the small difference which one is trying to calculate.

Our calculation proceeds as follows. The equations of particle motion are:

$$\frac{d^2 \vec{x}}{dt^2} = \frac{F(\vec{x}, t)}{m} \quad (7.1)$$

which is equivalent to:

$$\frac{d^2 x_i}{dt^2} = \frac{F_i(x_1, x_2, x_3, t)}{m} \quad (7.2)$$

Integration of this yields:

$$x_i(t) = x_i(0) + v_i(0)t + \int_0^t dt' \int_0^{t'} dt'' \frac{F_i[x_k(t''), t'']}{m} \quad (7.3)$$

For perturbed orbits, (7.2) is replaced by:

$$\frac{d^2}{dt^2} (x_i + \delta x_i) = \frac{F_i + \delta F_i}{m} \quad (7.4)$$

Subtraction of (7.2) from (7.4) yields:

$$\frac{d^2}{dt^2} \delta x_i = \frac{\delta F_i}{m} \quad (7.5)$$

We now assume that perturbations at any instant are small. Then:

$$\delta F_i = \sum_j \frac{\partial F_i}{\partial x_j} \delta x_j \quad (7.6)$$

i.e. we ignore  $(\delta x_j)^2$ ,  $(\delta x_j)^3$ , etc.

Equations (7.5) and (7.6) now imply, after integrating twice:

$$\delta x_i(t) = \frac{1}{m} \int_0^t dt' \int_0^{t'} dt'' \sum_j \frac{\partial F_i}{\partial x_j} [x_k(t''), t''] \delta x_j(t'') + \delta x_i(0) + t \delta v_i(0) \quad (7.7)$$

where the nine quantities  $\partial F_i / \partial x_j$  must be provided along the unperturbed orbit given by  $x_k(t'')$  and  $t''$ .

By noting that the region of integration in (7.7) is a triangle in  $(t', t'')$  coordinates, and then interchanging the order of integration, we can change (7.7) into the equivalent form (A.D. Stauffer, private communication):

$$\delta x_i(t) = \frac{1}{m} \int_0^t dt'' (t-t'') \sum_j \frac{\partial F_i}{\partial x_j} [x_k(t''), t''] \delta x_j(t'') + \delta x_i(0) + t \delta v_i(0) \quad (7.8)$$

which contains only a single integration.

We now consider a monokinetic particle beam having initial velocity  $(v_0, 0, 0)$ . This implies a zero initial perturbation velocity:  $\delta \vec{v}(0) = (0, 0, 0)$ . We choose two mutually orthogonal initial perturbations in position:

$$\delta_2 \vec{x}(0) = (0, 1, 0) \quad (7.9)$$

$$\delta_3 \vec{x}(0) = (0, 0, 1)$$

Since (7.8) is both linear and homogeneous in  $\delta \vec{x}$ , final values of  $\delta_2 \vec{x}$  and  $\delta_3 \vec{x}$  are proportional to initial values, as one expects for perturbation quantities.

Furthermore, if  $\delta \vec{x}(0) = a \delta_2 \vec{x}(0) + b \delta_3 \vec{x}(0)$ , then  $\delta \vec{x}(t) = a \delta_2 \vec{x}(t) + b \delta_3 \vec{x}(t)$ , where  $a$  and  $b$  are unchanged.

We now consider an initially circular differential tube of orbits defined by (7.9). As the unperturbed orbit is followed numerically, we simultaneously calculate  $\delta_2 \vec{x}$  and  $\delta_3 \vec{x}$  using (7.8). At the impingement point of the orbit, we project these onto the surface tangent plane (Fig. 7.1). The area of the ellipse thus generated is inversely proportional to the current density deposited on the surface.

For a monokinetic beam, this gives current density with no approximations.

The linearity of the perturbation equation (7.8) now implies that all orbits passing through  $A_0$  (Fig. 7.1) also pass through  $A$ . Therefore the total current carried by the tube is a constant, equal to  $A_0 j_0 = \frac{\pi}{4} j_0$ , where  $j_0$  is the current density through  $A_0$ .



The area A is given by:

$$A = \frac{\pi}{4} \left| \delta_2^{\vec{x}} \times \delta_3^{\vec{x}} \right| = \frac{\pi}{4} \left\| \begin{array}{ccc} \hat{i} & \hat{j} & \hat{k} \\ \delta_2^{x_1} & \delta_2^{x_2} & \delta_2^{x_3} \\ \delta_3^{x_1} & \delta_3^{x_2} & \delta_3^{x_3} \end{array} \right\| \quad (7.10)$$

where  $\hat{i}$ ,  $\hat{j}$ , and  $\hat{k}$  are unit vectors along the coordinate axes.

The current density at the surface therefore varies inversely as the projected tube area given by:

$$\frac{\pi}{4} \hat{n} \cdot (\delta_2^{\vec{x}} \times \delta_3^{\vec{x}}) = \frac{\pi}{4} \left\| \begin{array}{ccc} n_1 & n_2 & n_3 \\ \delta_2^{x_1} & \delta_2^{x_2} & \delta_2^{x_3} \\ \delta_3^{x_1} & \delta_3^{x_2} & \delta_3^{x_3} \end{array} \right\| \quad (7.11)$$

evaluated at the orbit impingement point on the surface, where  $\hat{n}$  is a unit vector perpendicular to the surface tangent plane (Fig. 7.1).

The current density at the surface therefore is:

$$j_{\text{surface}} = j_0 \left/ \left\| \begin{array}{ccc} n_1 & n_2 & n_3 \\ \delta_2^{x_1} & \delta_2^{x_2} & \delta_2^{x_3} \\ \delta_3^{x_1} & \delta_3^{x_2} & \delta_3^{x_3} \end{array} \right\| \right|_{\text{surface}} \quad (7.12)$$

It is possible for the plane of the ellipse to be perpendicular to the surface tangent plane. This occurs when the perturbed orbits happen to cross each other at the surface. The current density at the surface will then be infinite. This can occur only for a monokinetic distribution of initial velocities, which is only an approximation to real distributions.

We can also obtain an expression for number density  $n$  along the orbit, since  $n\vec{v}$  times the projection of A on a plane perpendicular to  $\vec{v}$  remains constant along the orbit.

i.e. the product  $\frac{\pi}{4} n \left| \vec{v} \cdot (\delta_2 \vec{x} \times \delta_3 \vec{x}) \right|$  is constant.

We therefore obtain:

$$n = n_0 v_0 / \left\| \begin{array}{ccc} v_1 & v_2 & v_3 \\ \delta_2 x_1 & \delta_2 x_2 & \delta_2 x_3 \\ \delta_3 x_1 & \delta_3 x_2 & \delta_3 x_3 \end{array} \right\| \quad (7.13)$$

For a monokinetic distribution,  $n$  can also become infinite if the perturbed orbits cross each other. For the same distribution,  $n$  (and  $j_{\text{surface}}$  if a surface is present) can also become infinite if one of the vectors  $\delta_2 \vec{x}$  or  $\delta_3 \vec{x}$ , or some linear combination of them, becomes zero. An example of this occurs on the (wake) axis of symmetry behind a sphere in a flowing collisionless plasma containing infinite-speed-ratio ions.

In two dimensions the perturbation produces a differential strip rather than tube. The corresponding results are:

$$j_{\text{surface}} = j_0 / \left\| \begin{array}{cc} n_1 & n_2 \\ \delta x_1 & \delta x_2 \end{array} \right\|_{\text{surface}} \quad (7.14)$$

$$n = n_0 v_0 / \left\| \begin{array}{cc} v_1 & v_2 \\ \delta x_1 & \delta x_2 \end{array} \right\| \quad (7.15)$$

We can also consider velocity-space rather than position-space initial perturbations. We assume that:

$$\delta_2 \vec{x} = \delta_3 \vec{x} = 0, \text{ but } \delta_2 \vec{v} = (0,1,0), \text{ and } \delta_3 \vec{v} = (0,0,1). \quad (7.16)$$

This permits us to treat situations where the ion speed ratio is large but not infinite. We can use (7.16) to do a calculation of ion defocusing on the wake axis behind a sphere, valid to order  $S_i^{-1}$ , where  $S_i$  is the ion speed ratio. We consider the situation shown in Fig. 7.2, in which an unperturbed orbit, initially parallel to the ion drift direction, has already been computed, in the presence of some known or given electric potential distribution e.g. a Coulomb potential. This orbit crosses the  $z$  axis at a downstream point  $z_0$ . Because

all orbits having the same impact parameter  $r_0$  cross at  $z_0$ , the ion density at this point is "infinite" unless the ions also have some random motion ( $S_i$  is finite). In reality the resulting space charge along this axis will influence ion orbits near it, but we ignore this effect here. We assume that values of  $\partial F_r / \partial r$ ,  $\partial F_r / \partial z$ ,  $\partial F_z / \partial r$ , and  $\partial F_z / \partial z$  are known along the unperturbed orbit. Our procedure is as follows. We choose two initial velocity perturbation vectors  $\delta_a \vec{v}(0)$  and  $\delta_b \vec{v}(0)$  in the plane of the unperturbed orbit (Fig. 7.2). We also choose  $\delta_2 \vec{x}(0) = \delta_3 \vec{x}(0) = 0$  at  $z_0$ . We now do our perturbation calculations backward, or "inside-out" along the ion orbit, even though we initially calculated the orbit forward, in the ion direction of motion. A single integration of (7.5) with (7.6) yields:

$$\delta v_i(t) = \frac{1}{m} \int_0^t dt' \sum_j \frac{\partial F_i}{\partial x_j} [x_k(t'), t'] \delta x_j(t') + \delta v_i(0). \quad (7.17)$$

For each of our two initial velocity perturbation vectors, we first integrate (7.8) from  $z_0$  to an upstream point at which the orbit is essentially no longer affected by the electric field of the sphere. We then use the resulting values of  $\delta x_j(t')$  [in this case  $\delta r(t')$  and  $\delta z(t')$ ] in (7.17) to calculate  $\delta v_i(t)$  [in this case  $\delta v_r(t)$  and  $\delta v_z(t)$ ] at the same upstream point. The linearity of the perturbation calculation

already discussed, implies now that multiplying  $\delta_a \vec{v}(0)$  and  $\delta_b \vec{v}(0)$  by any constants  $a$  and  $b$  means that  $\delta_a \vec{v}(t)$  and  $\delta_b \vec{v}(t)$  are also multiplied by  $a$  and  $b$ . Suppose now that the velocity distribution at the upstream point is a drifting Maxwellian. The linearity just mentioned now implies that velocity components in the  $(r, z)$  plane at the upstream point map linearly into those on the axis at  $z_0$ , so an integration over velocity space to find the density at  $z_0$  is easy to perform. This now will be found to yield a finite rather than infinite result, essentially because most ions will now have a small amount of angular momentum about the axis of symmetry and will no longer be found at  $z_0$ , and our perturbation calculation implicitly takes this into account.

As a final example, we consider the case of a nearly-monokinetic beam (the usual case for ion or electron guns on a spacecraft). We first need to calculate the five perturbation quantities  $\delta_2 \vec{x}, \dots, \delta_6 \vec{x}$  resulting from choosing initial perturbations given by (7.9) and by  $\delta_1 \vec{v}(0) = (1, 0, 0)$ ,  $\delta_2 \vec{v}(0) = (0, 1, 0)$ ,  $\delta_3 \vec{v}(0) = (0, 0, 1)$ . The values of  $\delta_2 \vec{x}$  and  $\delta_3 \vec{x}$  then give, as before, current density or space-charge density at any point of interest, but these are now differential

quantities with respect to the velocity distribution  $f \equiv d^3N/dv_1dv_2dv_3$  of the beam at its emission point; i.e. the values of these quantities found in this way are proportional to  $f(v_1, v_2, v_3)dv_1dv_2dv_3$ . The remaining perturbation quantities  $\delta_4\vec{x}$ ,  $\delta_5\vec{x}$ , and  $\delta_6\vec{x}$  then give the required information about the spread of the beam in position space. This may itself be due or partly due to beam space-charge; if this is the case, then the force derivatives  $\partial F_1/\partial x_j$  must themselves be found self-consistently, complicating the problem; in this case, calculations of the kind presented here would presumably become part of an iterative scheme.

If the beam is not nearly monokinetic (as will often be the case if it has not been deliberately accelerated) or it creates its own potential barrier around the spacecraft, so that part of it escapes and part does not, then evidently differential perturbations in velocity do not provide a realistic description of the result, and one would then need to replace calculations of  $\delta_4\vec{x}$ ,  $\delta_5\vec{x}$ , and  $\delta_6\vec{x}$  by separate, non-perturbation, orbit calculations for a representative discrete sample of the particle velocities most strongly represented in the beam.

## REFERENCES

- Allen, J.S., 1939, The emission of secondary electrons from metals bombarded with protons, Phys. Rev. 55, 336.
- Axford, W.I., 1968, Observations of the interplanetary plasma, Space Sci. Rev. 8, 331-365.
- Baragiola, R.A., Alonso, E.V., Florio, A.O., 1979, Electron emission from clean metal surfaces induced by low-energy light ions, Phys. Rev. B19, 121.
- Bernstein, I.B. and Rabinowitz, I.N., 1959, Theory of electrostatic probes in a low-density plasma, Phys. Fluids 2, 112.
- Besse, A.L. 1981, Unstable Potential of Geosynchronous Spacecraft, J. Geophys. Res. 86(A4), 2443-2446.
- Besse, A.L. and Rubin, A.G., 1980, A Simple Analysis of Spacecraft Charging Involving Blocked Photoelectron Currents, J. Geophys. Res. 85 (A5), 2324-2328.
- Chen, F.F., 1965, Numerical computations for ion probe characteristics in a collisionless plasma, Plasma Phys. (J. Nucle. Ener. Part C) 7, 47-68.
- Chung, M.S., and Everhart, T.E., 1974, Simple calculation of energy distribution of low-energy secondary electrons emitted from metals under electron bombardment, J. Appl. Phys. 45, 707.
- Cousinie, P., Colombié, N., Fert, C. and Simon, R., 1959, Variation du coefficient d'émission électronique secondaire de quelques métaux avec l'énergie des ions incidents, Compt. Rend. 249, 387.
- Darlington, E.H. and Cosslett, V.E. 1972, Backscattering of 0.5 - 10keV electrons from solid targets, J. Phys. D: Appl. Phys. 5, 1969- 1981.
- DeForest, S.E., 1972, Spacecraft charging at synchronous orbit, J. Geophys. Res. 77, 651.
- DeForest, S.E., 1977, The plasma environment at geosynchronous altitude, in: Proceedings of the Spacecraft Charging Technology Conference, edited by C.P. Pike and R.R. Lovell, pp. 37-52, Air Force Surveys in Geophysics, No. 364, Hanscom Air Force Base, Mass., Rep. AFGL-TR-77-0051/NASA TMX-73537.

- DeForest, S.E., and McIlwain, C.E., 1971, Plasma clouds in the magnetosphere, J. Geophys. Res. 76, 3587-3611.
- Dekker, A.J. 1958, Secondary Electron Emission, in: Solid State Physics, edited by F. Seitz and D. Turnbull, vol. 6, Academic, New York, p.251.
- Dessler, A.J., 1967, Solar wind and interplanetary magnetic field, Rev. Geophys. 5, 1-4.
- Fahleson, U. 1973, Plasma-Vehicle Interactions in Space - Some Aspects on Present Knowledge and Future Development, in: Photon and Particle Interaction with Surfaces in Space, edited by R.J.L. Garard, D. Reidel, Dordrecht, Holland, pp. 563-569.
- Garrett, H.B. and DeForest, S., 1979, An Analytical Simulation of the Geosynchronous Plasma Environment, Planet.Space Sci. 27, 1101-1109.
- Garrett, H.B., Schwank, D.C. and DeForest, S.E., 1981, A Statistical Analysis of the Low-Energy Geosynchronous Plasma Environment - I. Electrons, Planet.Space Sci. 29, (10), 1021-1044.
- Gibbons, D.J., 1966, Secondary Electron Emission, in: Handbook of Vacuum Physics, edited by A.H. Beck, Pergamon, Oxford, p. 301.
- Godard, R., 1975, A symmetrical model for cylindrical and spherical collectors in a flowing collisionless plasma, Ph.D. Thesis, York University, Toronto.
- Goldstein, H., 1950, Classical Mechanics, Addison-Wesley Pub. Co., Reading, Massachusetts.
- Goldstein, R. and Divine, N., 1977, Plasma distribution and spacecraft charging modeling near Jupiter. In: Proc. USAF-NASA Spacecraft Charging Technology Conference, C.P. Pike and R.R. Lovell, Editors, Report No. AFGL-TR-77-0051, Air Force Geophysics Laboratory, Hanscom AFB, Massachusetts/NASA TMX-73537, Lewis Research Center, Cleveland Ohio, pp. 131-141.
- Gussenhoven, M.S. and Mullen, E.G., A "Worst Case" Spacecraft Charging Environment as Observed by SCATHA on 24 April 1979, paper No. 82-0271, Amer. Inst. Aeron. Astron. 20th Aerospace Sciences Mtg., Jan. 82, Orlando, Florida.

- Hachenberg, O. and Brauer, W., 1959, Secondary Electron Emission from Solids, Advan. Electron. Electron Phys. 11, 413.
- Hachenberg, O. and Brauer, W., 1962, Advan. Electron. Electron Phys., 16, 145.
- Katz, I., Parks, D.E., Mandell, M.J., Harvey, J.M., Brownell, D.H. Jr., Wang, S.S. and Rotenberg, M., 1977, A Three Dimensional Dynamic Study of Electrostatic Charging in Materials, NASA Contractor Report No. CR-135256, Lewis Research Center, Cleveland, Ohio.
- Katz, I., Parks, D.E., Wang, S., and Wilson, A., 1977, Dynamic modeling of spacecraft in a collisionless plasma. In: Proc. USAF-NASA Spacecraft Charging Technology Conference, C.P. Pike and R.R. Lovell, Editors, Report No. AFGL-TR-77-0051, Air Force Geophysics Laboratory, Hanscom AFB, Massachusetts/NASA TMX-73537, Lewis Research Center, Cleveland, Ohio, pp. 319-330.
- Katz, I., Cassidy, J.J., Mandell, M.J., Schnuelle, G.W., Steen, P.G., and Roche, J.C., 1979, The Capabilities of the NASA Charging Analyzer Program, in: Spacecraft Charging Technology - 1978, NASA Conference Publication 2071/Report No. AFGL-TR-79-0082, Air Force Geophysics Laboratory, Massachusetts, pp. 101-122.
- Katz, I., and Mandell, M.J., 1982, Differential Charging of High-Voltage Spacecraft: The Equilibrium Potential of Insulated Surfaces, J. Geophys. Res. 87, 4533-4541.
- Kazan, B., and Knoll, M., 1968, Electronic Image Storage, Academic Press, New York.
- Knott, K., 1972, The equilibrium potential of a magnetospheric satellite in an eclipse situation, Planet. Space Sci. 20, 1137.
- Krainsky, I., Lundin, W., Gordon, W.L. and Hoffman, R.W., 1981, Secondary Electron Emission Yields, in: Spacecraft Charging Technology 1980, NASA Conference Publication 2182/Report No. AFGL-TR-81-0270, Air Force Geophysics Laboratory, Massachusetts, pp. 179-197.
- Lafon, J.-P.J., 1976, On the sheath surrounding a conductor emitting photoelectrons in an isotropic collisionless plasma, Radio Science 11, 483-493.

- Laframboise, J.G., 1966, Theory of spherical and cylindrical Langmuir probes in a collisionless, Maxwellian plasma at rest, Univ. of Toronto, Institute for Aerospace Studies, UTIAS Rep. 100.
- Laframboise, J.G., and Parker, L.W., 1973, Probe design for orbit-limited current collection, Phys. Fluids 16, 629-636.
- Laframboise, J.G., and Godard, R., 1974, Perturbation of an electrostatic probe by a spacecraft at small speed ratios, Planet. Space Sci. 22, 1145-1155.
- Laframboise, J.G. and Prokopenko, S.M.L., 1977, Numerical Simulation of Spacecraft Charging Phenomena, in: Proc. Spacecraft Charging Technology Conference, C.P. Pike and R.R. Lovell, Eds., Report No. AFGL-TR-77-0051, Air Force Geophysics Laboratory, Massachusetts/Report No. NASA TMX-73537, Lewis Research Center, Cleveland, Ohio, pp. 309-318.
- Laframboise, J.G., and Prokopenko, S.M.L., 1978, Predictions of high-voltage differential charging on geostationary spacecraft, in: Proc. 1978 Symposium on the Effect of the Ionosphere on Space and Terrestrial Systems, paper 4.4, Naval Research Lab./Office of Naval Research, Washington.
- Leung, M.S., Tueling, M.B. and Schnauss, E.R., 1981, Effects of Secondary Electron Emission on Charging, in: Spacecraft Charging Technology 1980, NASA Conference Publication 2182/Report No. AFGL-TR-81-0270, Air Force Geophysics Laboratory, Massachusetts, pp. 163-178.
- Manka, R.H., 1973, Plasma and potential at the lunar surface. In: Photon and Particle Interactions with Surfaces in Space, R.J.L. Gard, Editor, D. Reidel Pub. Co., Dordrecht, Holland, pp. 347-361.
- Mauk, B., 1975, Magnetospheric substorm pitch angle distribution, EOS 56, 423.
- McPherson, D.A., and Schober, W.R., 1976, Spacecraft charging at high altitudes: the Scatha satellite program, in: Spacecraft Charging by Magnetospheric Plasmas, edited by A. Rosen, American Institute of Aeronautics and Astronautics, New York, and MIT Press, Cambridge, Massachusetts.



- Meyer-Vernet, N., 1982, "Flip-Flop" of Electric Potential of Dust Grains in Space, Astron. Astrophys. 105, 98-106.
- Mott-Smith, H., Jr., and Langmuir, I., 1926, The theory of collectors in gaseous discharges, Phys. Rev. 28, 727.
- Olsen, R.C., 1980, Differential and Active Charging Results from the ATS Spacecraft. Univ. of California, San Diego, Ph.D. Thesis.
- Olsen, R.C. and Whipple, E.C., 1980, Analysis of Differential and Active Charging Phenomena on ATS-5 and ATS-6. University of California, San Diego, Center for Astrophysics and Space Sciences, Rep. CASS-80-1.
- Palluel, P., 1947, Composante rediffusée du rayonnement électronique secondaire des métaux, C.R. Acad. Sci. 224, 1492.
- Parker, L.W., 1978, Potential barriers and asymmetric sheaths due to differential charging of nonconducting spacecraft. Report No. AFGL-TR-78-0045, Air Force Geophysics Laboratory, Hanscom AFB, Massachusetts.
- Parker, L.W., and Whipple, E.C., Jr., 1967, Theory of a Satellite Electrostatic Probe. Ann. Phys. 44, 126-161.
- Pelizzari, M.A., and Criswell, D.R., 1978, Differential Photoelectric Charging of Nonconducting Surfaces in Space. J. Geophys. Res. 83, 5233-5244.
- Polychronopoulos, B., 1973, Effects of non-Maxwellian electron energy distributions on the orbital limited current-voltage characteristics of cylindrical and spherical Langmuir probes under collisionless conditions, Plasma Phys. 15, 37.
- Prokopenko, S.M.L. and Laframboise, J.G., 1977, Prediction of Large Negative Shaded-Side Spacecraft Potentials, in: Proc. Spacecraft Charging Technology Conference, C.P. Pike and R.R. Lovell, Eds., Report No. AFGL-TR-77-0051, Air Force Geophysics Laboratory, Massachusetts/Report No. NASA TMX-73537, Lewis Research Center, Cleveland, Ohio, pp. 369-387.
- Prokopenko, S.M.L. and Laframboise, J.G., 1980, High-Voltage Differential Charging of Geostationary Spacecraft, J. Geophys. Res. 85, (A8), 4125-4131.

- Purvis, C., 1982, Evolution of Spacecraft Charging Technology, Paper No. 82-0273, Amer. Inst. Aeron. Astron. 20th Aerospace Sciences Mtg., Jan. 82, Orlando, Florida.
- Ray, J.A., and Barnett, C.F., 1971, Secondary electron emission of metals bombarded with 120-eV to 5-keV protons, J. Appl. Phys. 42, 3260.
- Rosen, A., 1975, Large Arcs and Discharges on Spacecraft, Astronaut. Aeronaut., 13, 36.
- Salehi, M. and Flinn, E.A., 1981, Dependence of Secondary-Electron Emission from Amorphous Materials on Primary Angle of Incidence, J. Appl. Phys. 52 (2), 994-996.
- Sanders, N.L. and Inouye, G.T., 1979, Secondary Emission Effects on Spacecraft Charging: Energy Distribution Considerations, in: Spacecraft Charging Technology - 1978. NASA Conference Publication 2071/Report No. AFGL-TR-79-0082, Air Force Geophysics Laboratory, Massachusetts, pp. 747-755.
- Schnuelle, G.W., Parks, D.E., Katz, I., Mandell, M.J., Steen, P.G., Cassidy, J.J. and Rubin, A., 1979, Charging Analysis of the SCATHA satellite, in: Spacecraft Charging Technology - 1978, NASA Conference Publication 2071/Report No. AFGL-TR-79-0082, Air Force Geophysics Laboratory, Massachusetts, pp. 123-143.
- Schnuelle, G.W., Stannard, P.R., Katz, I. and Mandell, M.J., 1981, Simulation of Charging Response of SCATHA (P78-2) Satellite, in: Spacecraft Charging Technology 1980, NASA Conference Publication 2182/Report No. AFGL-TR-81-0270, Air Force Geophysics Laboratory, Massachusetts, pp. 580-591.
- Schröder, H., 1973, Spherically symmetric model of the photoelectron sheath for moderately large plasma Debye lengths. In: Photon and Particle Interactions with Surfaces in Space, R.J.L. Grard, Editor, D. Reidel Pub. Co., Dordrecht, Holland, pp. 51-58.
- Shepherd, M.M., and Laframboise, J.G., 1981, Chebyshev approximation of  $(1 + 2x)\exp(x^2)\operatorname{erfc}(x)$  in  $0 \leq x < \infty$ . Math. of Computation 36, 249.

- Shield, M.A., and Frank, L.A., 1970, Electron observations between the inner edge of the plasma sheet and the magnetosphere, J. Geophys. Res. 75, 5401-5414.
- Soop, M., 1972, Report on photo-sheath calculations for the satellite GEOS, Planet. Space Sci. 20, 859-870.
- Stannard, P.R., Schnuelle, G.W., Katz, I., and Mandell, M.J., 1981, Representation and Material Charging Response of GEO Plasma Environments, in: Spacecraft Charging Technology 1980, NASA Conference Publication 2182/Report No. AFGL-TR-81-0270, Air Force Geophysics Laboratory, Massachusetts, pp. 560-579.
- Stannard, P.R., Katz, I., Gedeon, L., Roche, J.C., Rubin, A.G. and Tautz, M.F., 1982, Validation of the NASCAP Model Using Spaceflight Data, Paper No. 82-0269, Amer. Inst. Aeron. Astron. 20th Aerospace Sciences Mtg., Jan. 82, Orlando, Florida.
- Sternglass, E.J., 1954, Theory of Secondary Electron Emission, Sci. Pap. 1772, Westinghouse Res. Lab., Pittsburgh, Pa.
- Sternglass, E.J., 1954, Backscattering of Kilovolt Electrons from Solids, Phys. Rev. 95, 345-358.
- Swarztrauber, P., and Sweet, R., 1975, Efficient FORTRAN Subprograms for the Solution of Elliptic Partial Differential Equations, Tech. Note NCAR-TN/IA-109, National Center for Atmospheric Research, Boulder, Colorado.
- Thomas, S., and Pattinson, E.B., 1970, Range of electrons and contribution of back-scattered electrons in secondary production in aluminum, J. Phys. D: Appl. Phys. 3, 349.
- Tsien, H.S., 1946, Superaerodynamics, mechanics of rarefied gases, J. Aero. Sci. 13, 653-664.
- Whipple, E.C., Jr., 1965, The Equilibrium Electric Potential of a Body in the Upper Atmosphere and in Interplanetary Space, Ph.D. Thesis, The George Washington Univ., Washington, D.C./Report No. X-615-65-296, NASA Goddard Space Flight Center, Greenbelt, Maryland.
- Whipple, E.C. Jr., 1976, Observation of Photoelectrons and Secondary Electrons Reflected from a Potential Barrier in the Vicinity of ATS 6, J. Geophys. Res. 81 (4), 715-719.
- Whipple, E.C., 1981, Potentials of Surfaces in Space, Rep. Prog. Phys. 44, 1197-1250.
- Willis, R.F., and Skinner, D.K., 1973, Secondary electron emission yield behaviour of polymers, Solid State Comm. 13, 685.

Table 1

Floating potentials of shaded surfaces of geostationary-altitude spacecraft, using the incident velocity spectra assumed by Knott [1972], with backscattered and secondary electron emission due to electron impacts included, with three-, two-, and one-dimensional velocity-space cutoffs corresponding to orbit-limited ion collection in spherical, infinite cylindrical and planar symmetries, respectively.

Material	Secondary Electron Emission Data		Back-scatter Data $\eta(5000\text{eV})$	Spectrum 1 "Quiet"			Spectrum 2b "Disturbed"		
	$\delta_{\text{max}}$	$E_{\text{max}}$ (eV)		Floating Potential (volts)			Floating Potential (volts)		
				3-dimen.	2-dimen.	1-dimen.	3-dimen.	2-dimen.	1-dimen.
Gold	1.45	800	.42	-39.9	-40.0	-40.8	-3470	-6430	-15,450
Aluminum	.97	300	.16	-1410	-2140	-5390	-6770	-11,500	-21,770
Aluminum with Oxide Coating	2.60	300	.12	+4.6 -630* -750	+3.0 -490* -1560	+1.9 -420* -4900	-6610	-11,360	-21,610
Quartz	2.50	420	.12	+3.9	+2.5	+1.5 -640* -4120	-6310	-10,960	-21,130
Aquadag	.75	350	.08	-1560	-2380	-5890	-7090	-12,010	-22,350
Beryllium Copper	2.20	300	.31	+4.7	+2.9	+1.9 -560* -3430	-5740	-9920	-19,890
Beryllium Copper Activated	5.00	400	.31	+8.0	+5.8	+4.2	+4.3 -900* -3950	+2.9 -830* -7580	+1.6 -770* -17,670
Teflon	3.00	300	.10	+5.2	+3.6 -660* -1370	+2.3 -490* -4870	-6640	-11,430	-21,700
Kapton	2.10	150	.07	+3.9 -170* -1580	+2.5 -170* -2440	+1.4 -170* -6040	-7180	-12,130	-22,520
No secondary or backscattered electrons	—	—	—	-1860	-2830	-6680	-7550	-12,690	-23,130

\* Unstable

TABLE 2

THRESHOLD TEMPERATURES T\* FOR SPACECRAFT SURFACE MATERIALS  
 TC1: INCLUDING SECONDARY ELECTRONS.  
 TC2: INCLUDING SECONDARY AND BACKSCATTERED ELECTRONS.  
 TC3: SAME AS TC2 EXCEPT THAT ANGULAR DEPENDENCE OF YIELD IS INCLUDED.

MATERIAL	SECONDARY		BACKSCATTERING							T* (keV)		
	E <sub>max</sub> (keV)	δ <sub>max</sub>	Z	A	B	C	TC1	TC2	TC3			
GOLD	.80	1.45	79.0	.4802	.3566	.6103	1.278	2.931	4.939			
ALUMINUM	.30	.97	13.0	.1569	.0303	.3431	0.000	0.000	.601			
ALUMINUM OXIDE	.30	2.60	10.0	.1238	.0172	.3435	1.116	1.777	1.931			
SiO <sub>2</sub> (QUARTZ)	.42	2.50	10.0	.1238	.0172	.3435	1.496	1.713	2.621			
FUSED SILICA	.33	3.46	10.0	.1238	.0172	.3435	1.645	1.847	2.707			
ARADAG(COLLOIDAL GRAPHITE)	.35	.75	6.0	.0800	0.0000	0.0000	0.000	0.000	0.000			
BERYLLIUM-COPPER	.30	2.20	29.0	.3136	.0692	.6207	.918	1.349	2.157			
BERYLLIUM-COPPER(ACTIVATED)	.40	5.00	29.0	.3136	.0692	.6207	2.754	3.692	5.423			
TEFLON	.30	3.00	8.0	.0900	0.0000	0.0000	1.299	1.977	2.102			
KAPTON (Willis and Skinner, 1973)	.15	2.10	5.3	.0700	0.0000	0.0000	.433	.474	.769			
KAPTON (Leung et al, 1981)	.25	1.80	5.3	.0700	0.0000	0.0000	.583	.647	1.096			
INDIUM OXIDE	.80	1.40	24.4	.2750	.0600	.5400	1.184	2.010	3.596			
MAGNESIUM	.25	.92	12.0	.1460	.0250	.3440	0.000	0.000	.441			
MAGNESIUM OXIDE	.40	4.00	10.0	.1738	.0172	.3435	2.280	2.548	3.686			
SILVER	.80	1.00	47.0	.3900	.2890	.6320	0.000	1.233	2.754			
ITO ON KAPTON	.35	2.55	15.3	.1830	.0370	.3820	1.275	1.550	2.370			
ITO ON 'FEP' TEFLON	.36	2.39	16.2	.1920	.0400	.3990	1.217	1.507	2.329			
ITO ON BOROSILICATE GLASS	.35	2.35	16.9	.2000	.0420	.4100	1.160	1.456	2.254			
ION-SPUTTERED ITO ON KAPTON	.39	1.52	15.3	.1830	.0370	.3820	.684	.921	1.587			
MGFL	.85	6.38	10.0	.1238	.0172	.3435	7.141	7.889	11.054			
NASCAP 'HPAI'	.15	2.10	5.0	.0600	0.0000	0.0000	.433	.468	.747			
NASCAP 'SOLA'	.41	2.05	10.0	.1238	.0172	.3435	1.147	1.338	2.123			
NASCAP 'CPAI'	.15	2.10	5.0	.0600	0.0000	0.0000	.433	.468	.747			
NASCAP 'WHITEN'	.15	2.10	5.0	.0600	0.0000	0.0000	.433	.468	.747			
NASCAP 'BLACKC YELLOWC'	.15	2.10	5.0	.0600	0.0000	0.0000	.433	.468	.747			
NASCAP 'GOLDF'	.72	1.03	70.1	.4560	.3380	.6120	0.000	1.392	2.857			
NASCAP 'YGOLDC'	.48	1.49	42.0	.3730	.2760	.6170	.810	1.392	2.444			
NASCAP 'REDHAT'	.59	1.86	63.4	.4380	.3250	.6130	1.443	2.596	4.203			
NASCAP 'MLI2'	.30	1.00	6.0	.0800	0.0000	0.0000	0.000	0.000	.602			

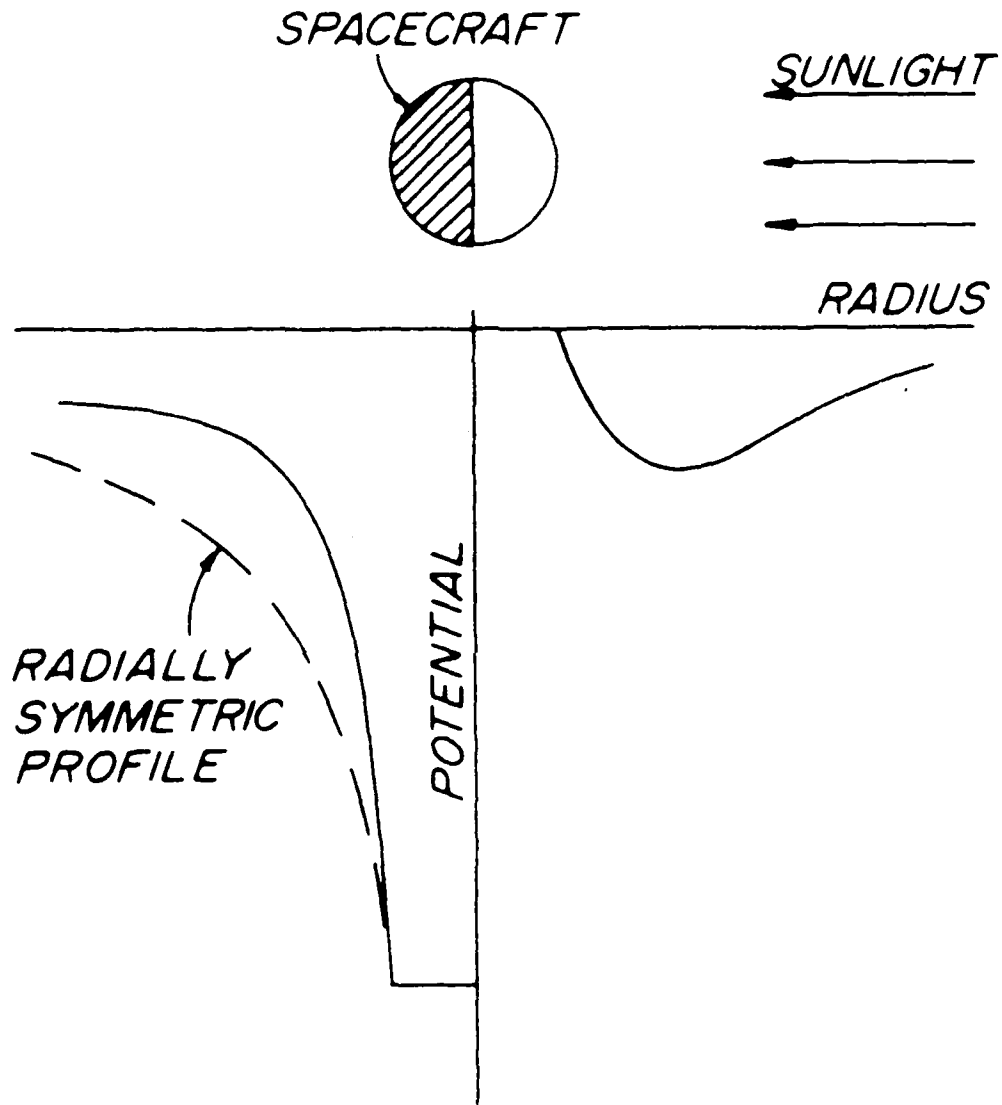


Fig. 2.1. Steepening of shaded-side potential profile, and sunlit-side potential barrier formation, caused by shaded-sunlit asymmetry on a spacecraft with an insulated surface, after Fahleson [1973].

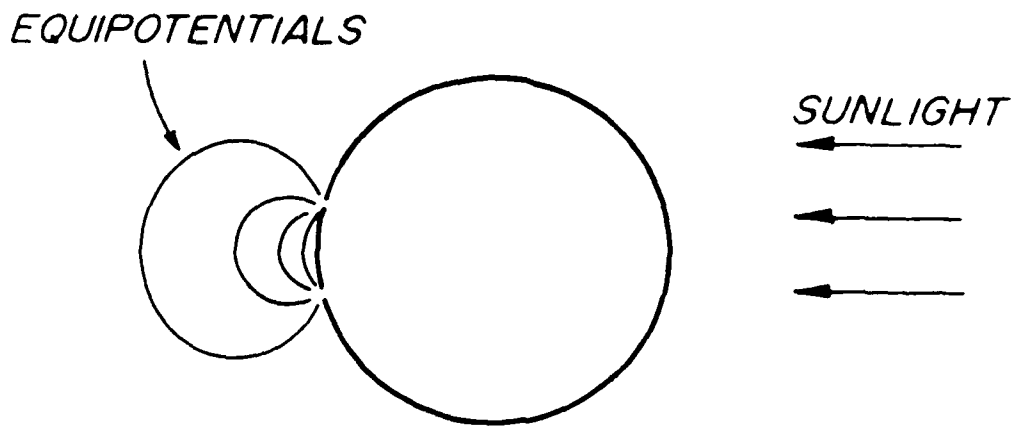


Fig.2.2. Conductive spacecraft with shaded isolated surface patch.

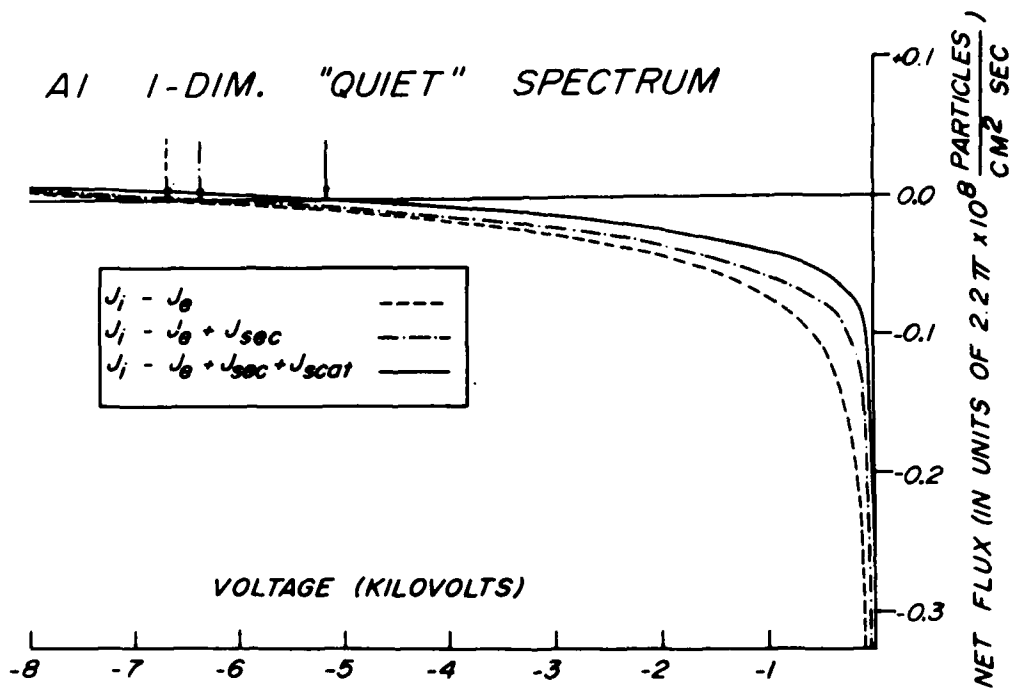


Fig. 2.3. Current-voltage characteristic for aluminum in "quiet" conditions, with a one-dimensional velocity-space cutoff. In Figures 2.3 - 2.7 the zeros of the characteristics are indicated by arrows.



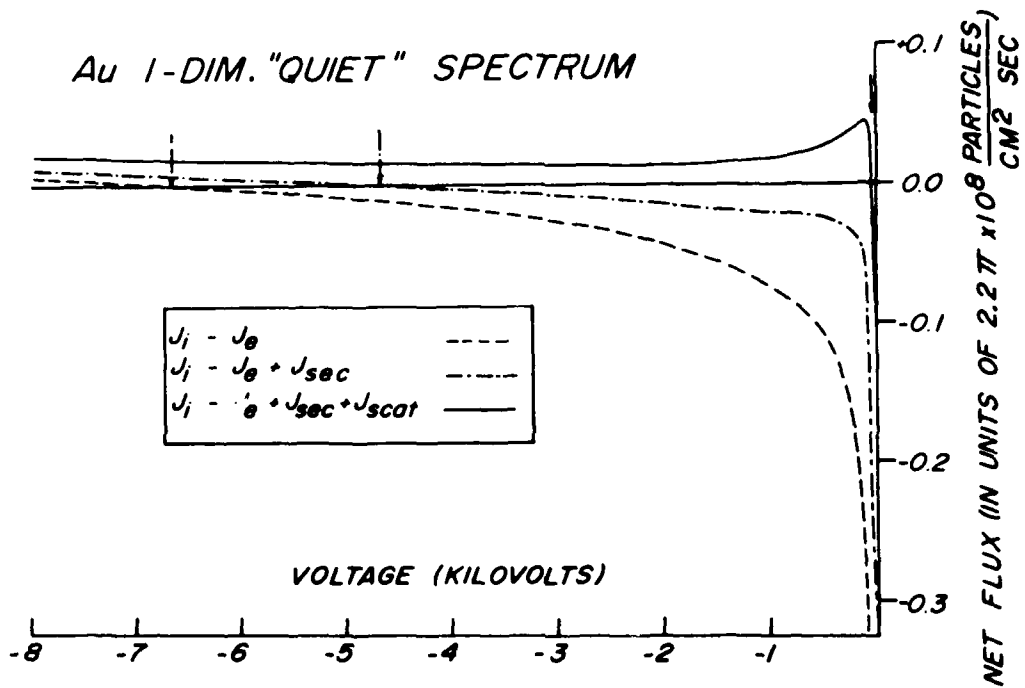


Fig. 2.4. Current-voltage characteristic for gold in "quiet" conditions, with a one-dimensional velocity-space cutoff.

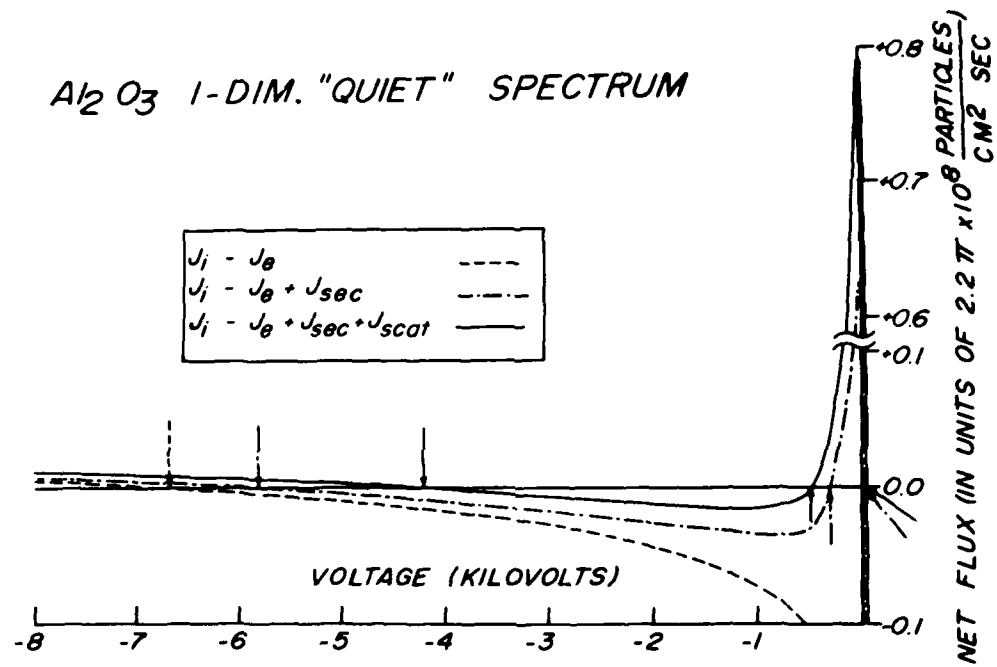


Fig. 2.5. Current-voltage characteristic for aluminum oxide in "quiet" conditions, with a one-dimensional velocity-space cutoff.

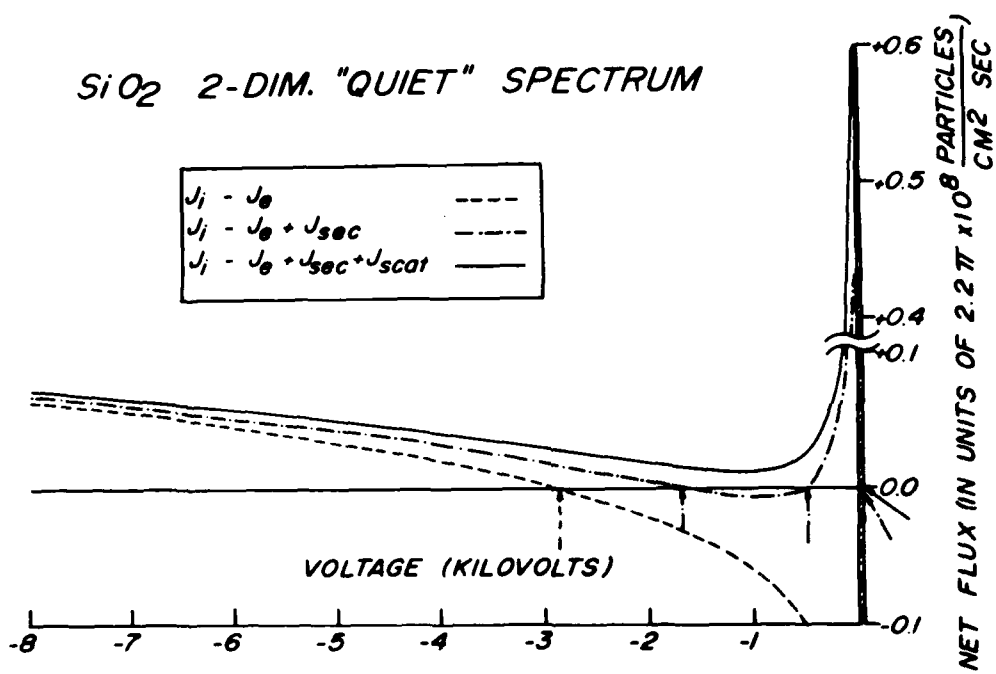


Fig. 2.6. Current-voltage characteristic for quartz in "quiet" conditions, with a two-dimensional velocity-space cutoff.

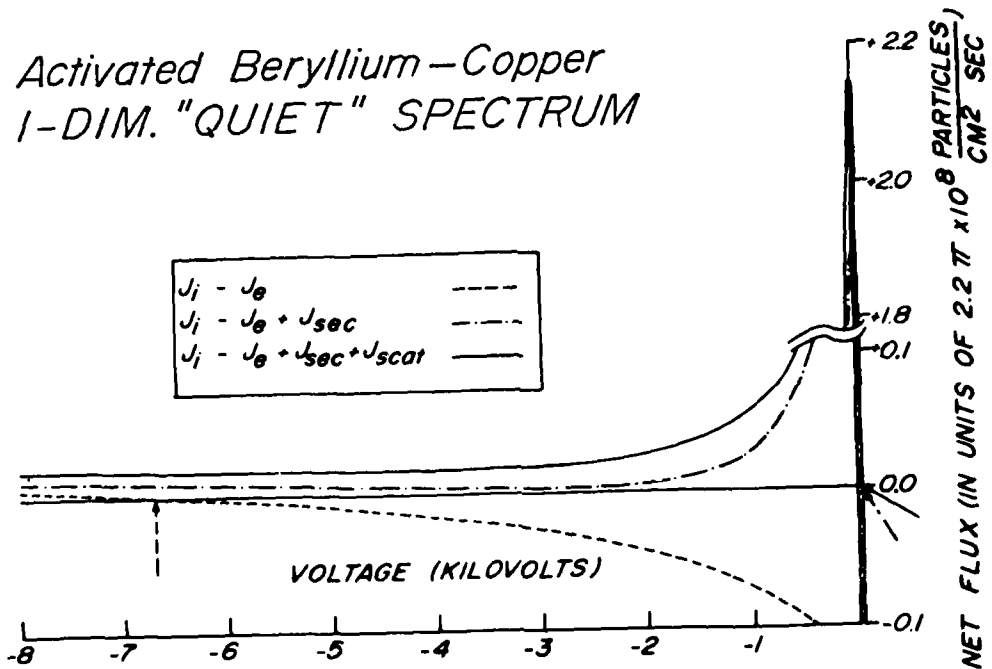


Fig. 2.7. Current-voltage characteristic for activated beryllium-copper in "quiet" conditions, with a one-dimensional velocity-space cutoff.

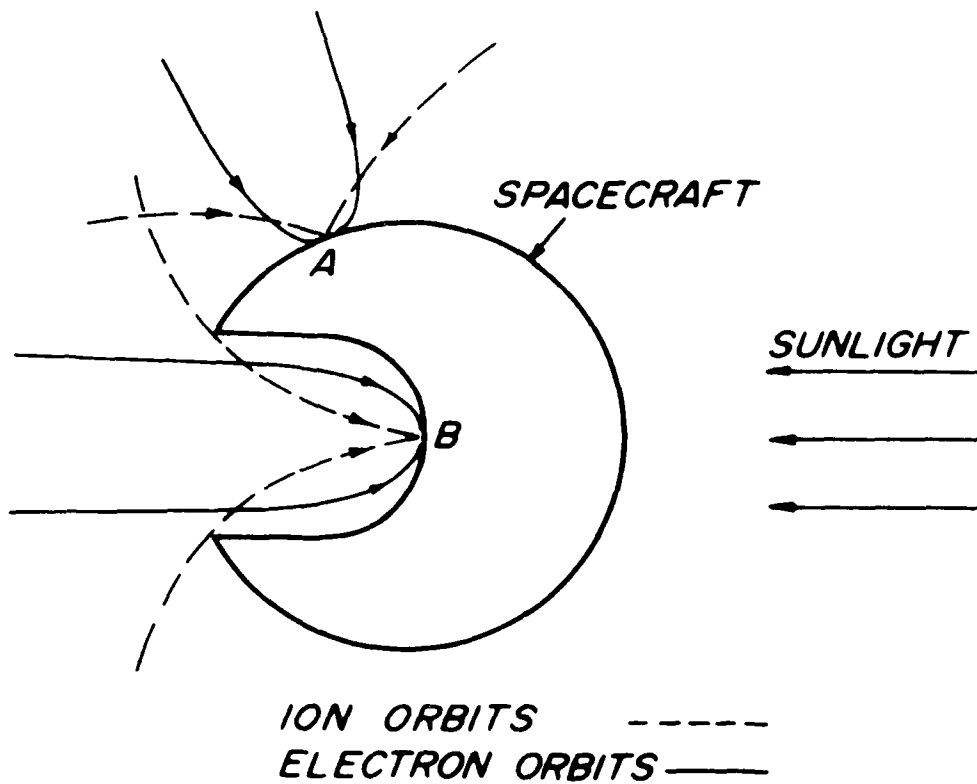


Fig. 2.8. Spacecraft with shaded isolated cavity, showing incident ion and electron orbits with energies close to the lowest for which collection of each species is possible. The orbits shown are cutoff orbits, defined as the most nearly tangential orbits for which incident particles of a given energy are able to reach a given point on the spacecraft surface, having tangential velocity component in a given direction.

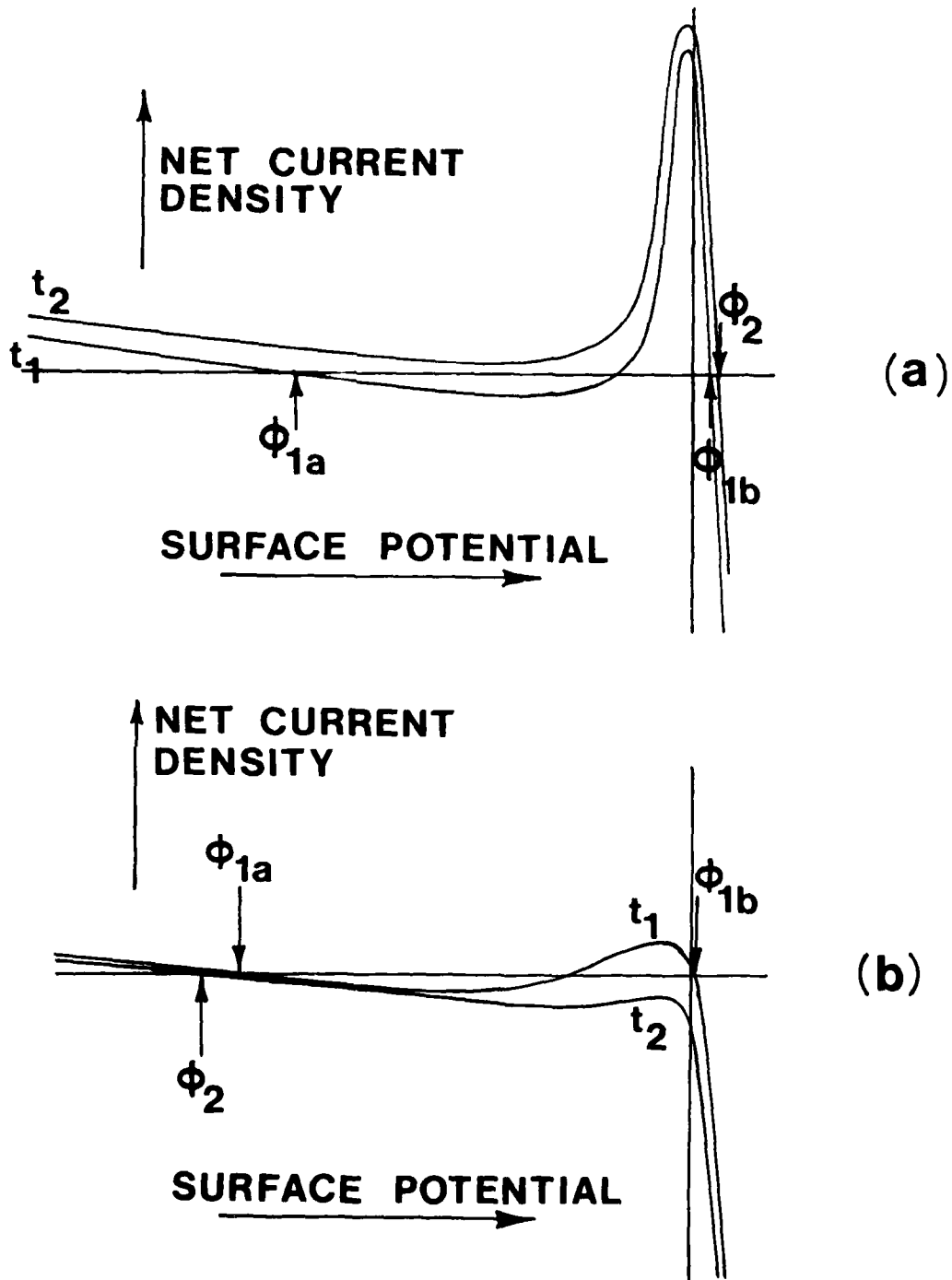


Fig. 2.9. Disappearance of multiple roots in the current-voltage characteristic of a spacecraft surface, as a result of temporal changes in ambient electron velocity distributions. These illustrations are schematic only but are representative of predicted behavior for various surface materials. Some combinations of materials and environments for which such behavior is predicted appear as clusters of three numbers in Table 1.

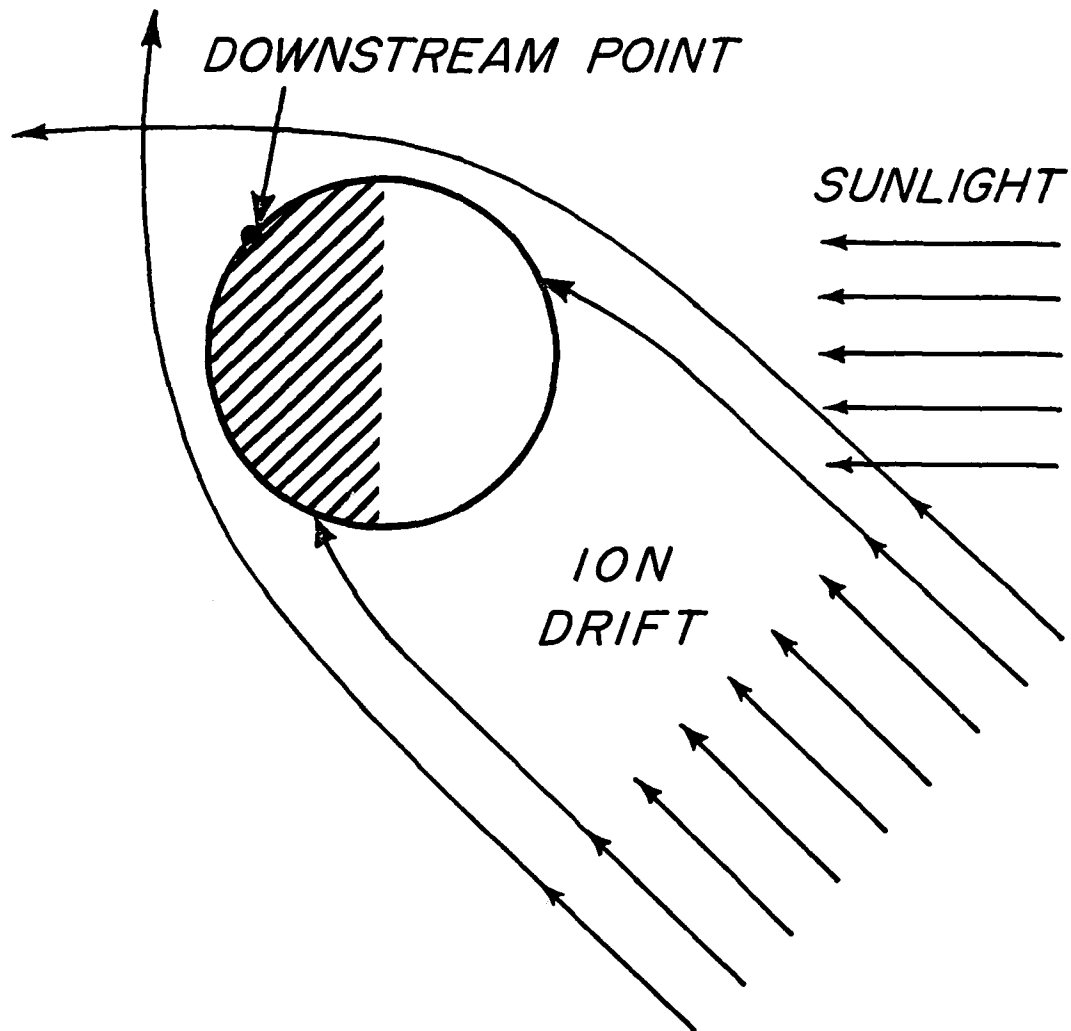


Fig. 2.10. Spherical spacecraft with downstream point (relative to ion drift direction) shaded.

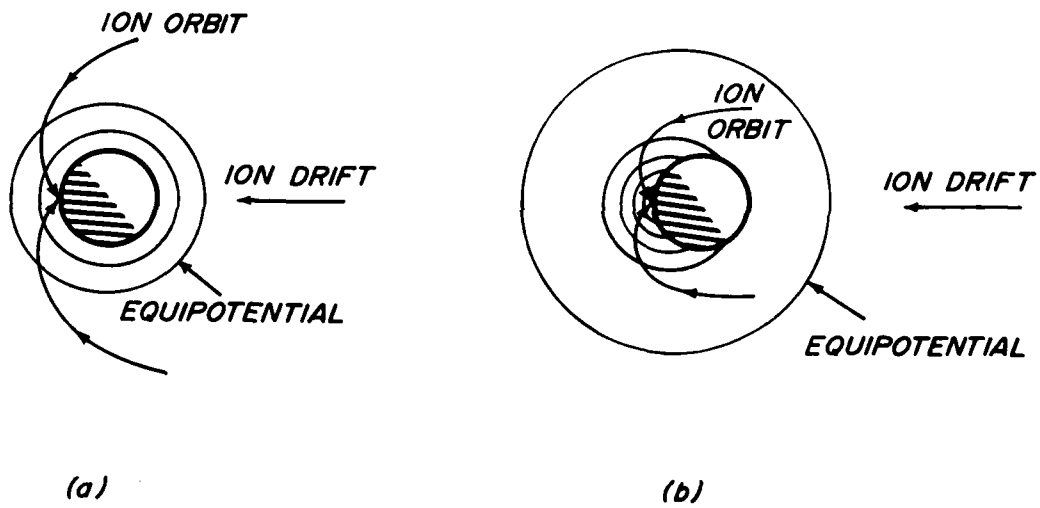


Fig. 2.11(a) Hypothetical symmetric equipotentials around a spherical spacecraft (b) nonsymmetric equipotentials around the same spacecraft.



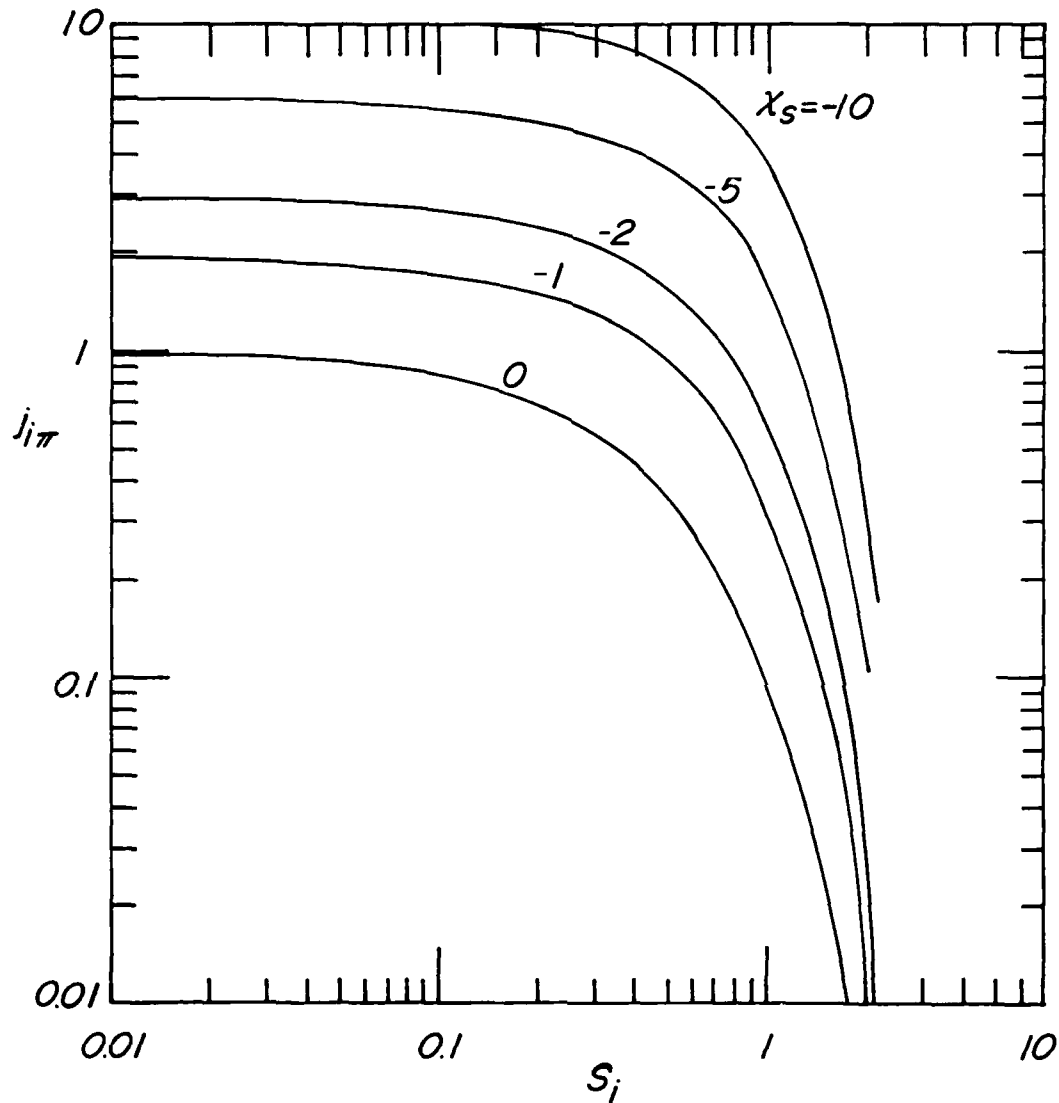


Fig. 2.12. Nondimensional downstream-point ion current density  $j_{i\pi} = J_{i\pi} / [N_{\infty} e (kT_i / 2\pi m_i)^{1/2}]$  as a function of ion speed ratio  $S_i = U / (2kT_i / m_i)^{1/2}$  for various nondimensional surface potentials  $\chi_s = e\phi_s / kT_i$ , assuming spherical geometry, zero magnetic field, uniform surface potential, collisionless large-Debye-length conditions, and drifting Maxwellian ions. For  $S_i \rightarrow 0$ ,  $j_{i\pi} \rightarrow 1 + |\chi_s|$  when  $\chi_s < 0$ .

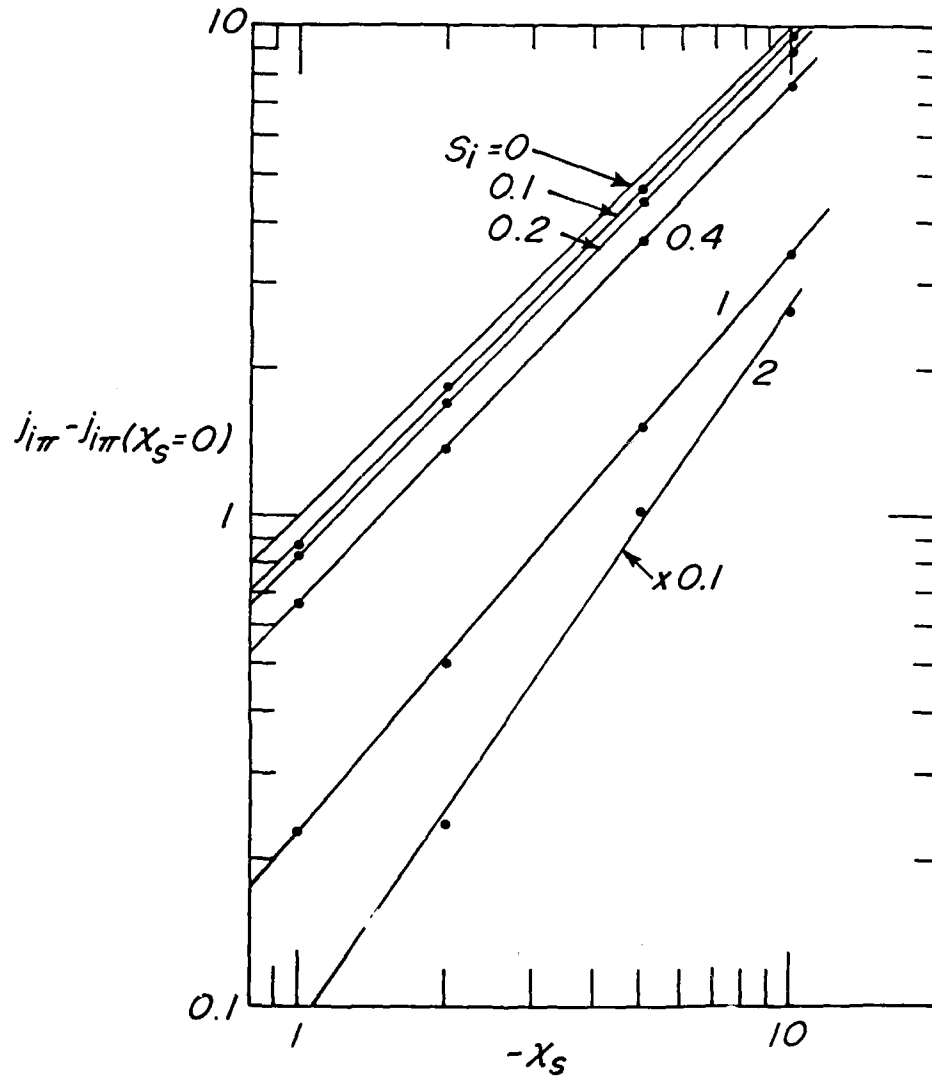


Fig. 2.13. Nondimensional downstream-point ion current density  $j_{i\pi}$  as a function of surface potential  $X_S$  for various ion speed ratios  $S_i$ , for the same conditions as in Fig. 2.12. The straight lines shown are power-law approximations.

AD-A130 043

NUMERICAL SIMULATION OF SPACECRAFT CHARGING PHENOMENA  
AT HIGH ALTITUDE (U) YORK UNIV DOWNSVIEW (ONTARIO)  
CENTRE FOR RESEARCH IN EXPERIME..

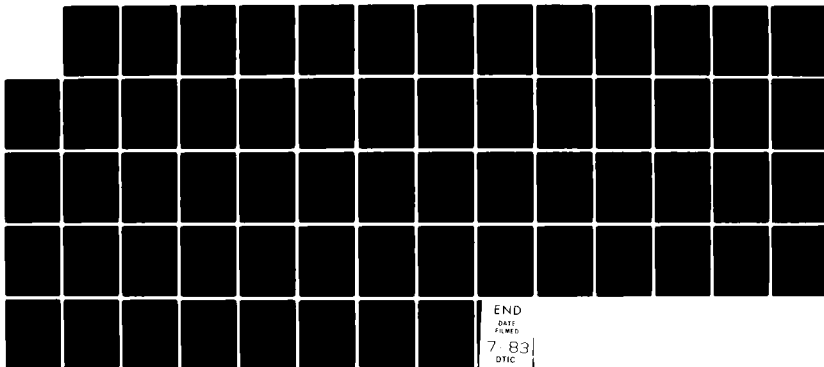
2/2

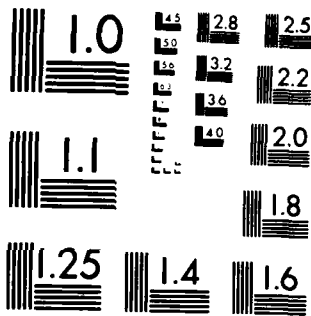
UNCLASSIFIED

J G LAFRAMBOISE ET AL. 10 AUG 82

F/G 22/2

NL





MICROCOPY RESOLUTION TEST CHART  
NATIONAL BUREAU OF STANDARDS-1963 A

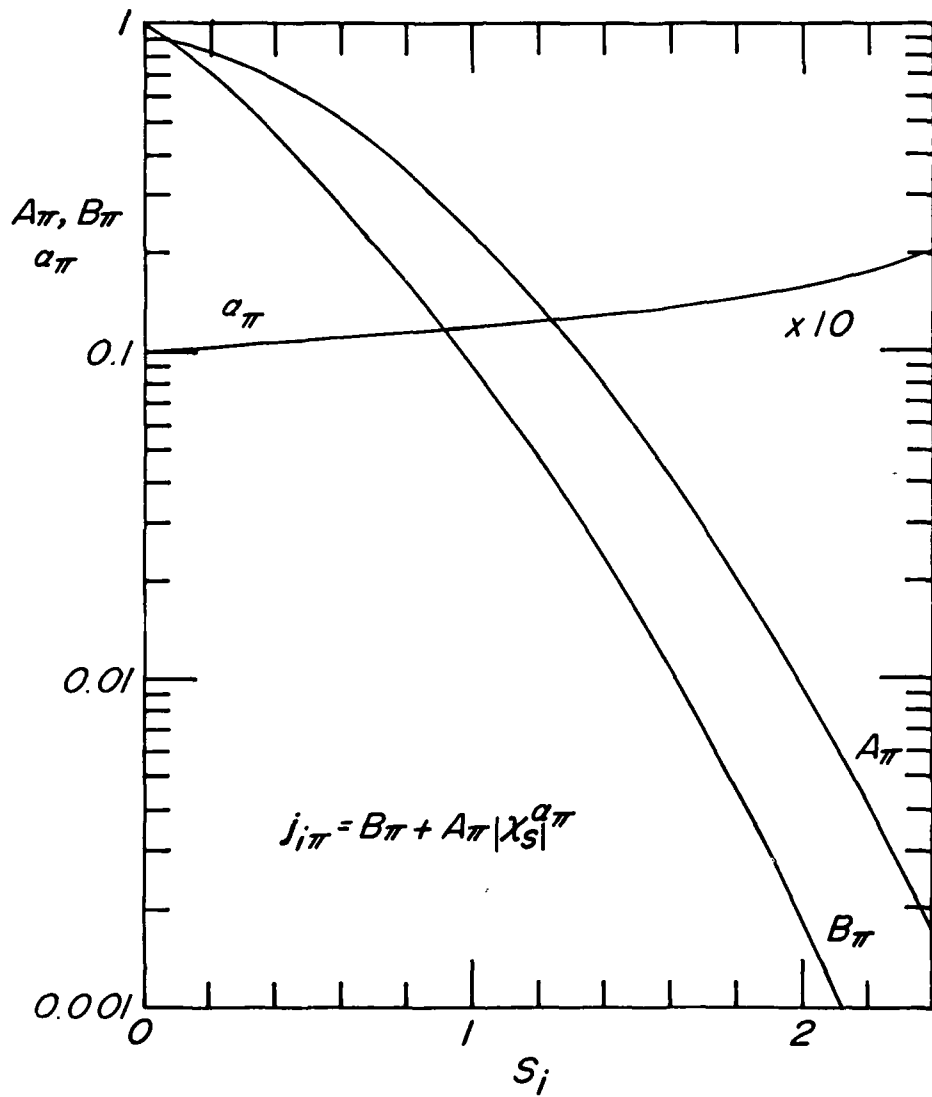


Fig. 2.14. Dependence of the power-law coefficients  $A_\pi$ ,  $B_\pi$  and  $\alpha_\pi$  on ion speed ratio  $S_i$ .

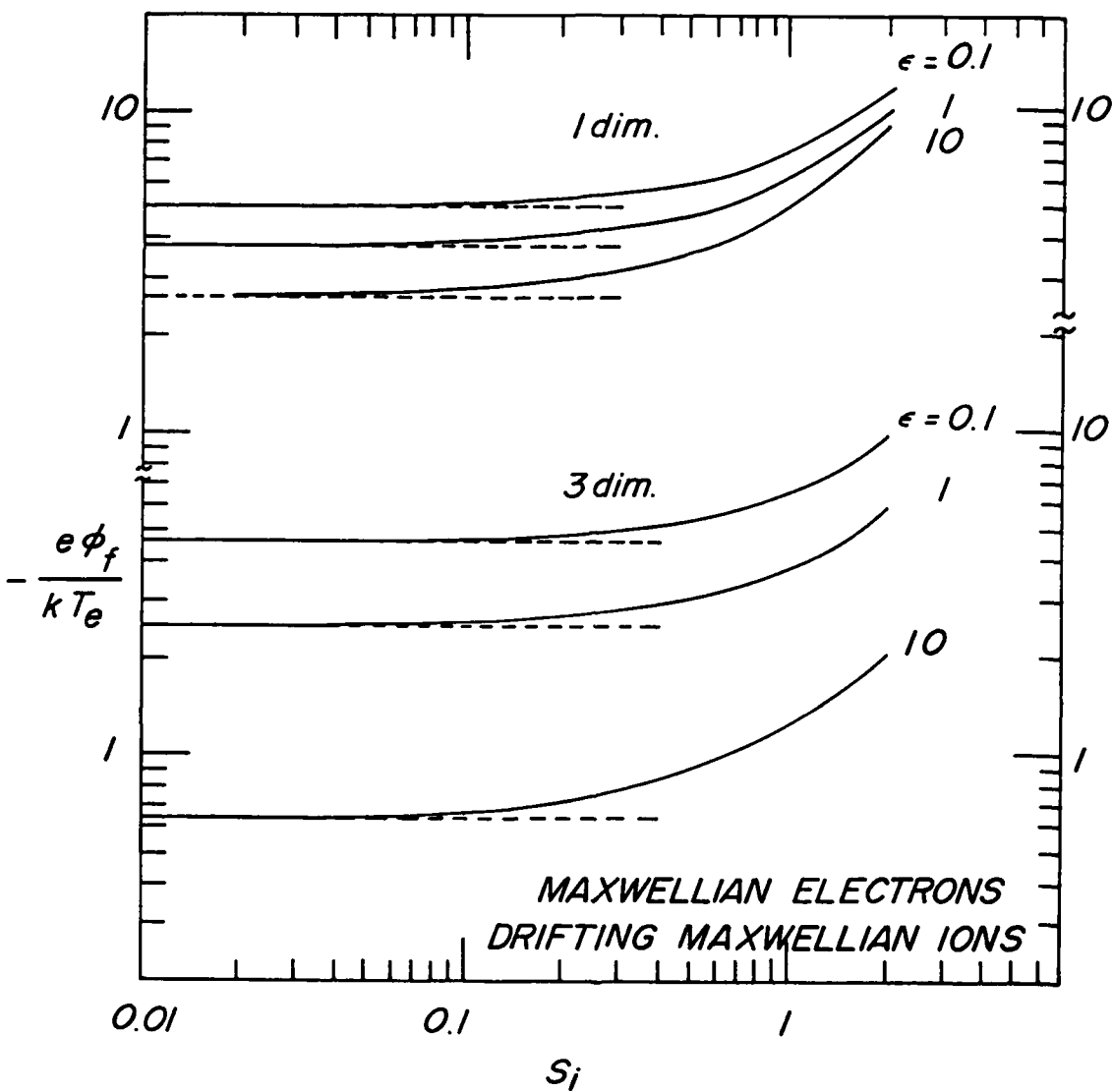


Fig. 2.15. Upper and lower bounds on floating potential  $\phi_f$  at shaded downstream point of spacecraft, as a function of ion speed ratio  $S_i$ , for various ion-to-electron temperature ratios  $\epsilon$ , for Maxwellian electrons and drifting Maxwellian ions, for one-dimensional and three-dimensional ion velocity space cutoffs.

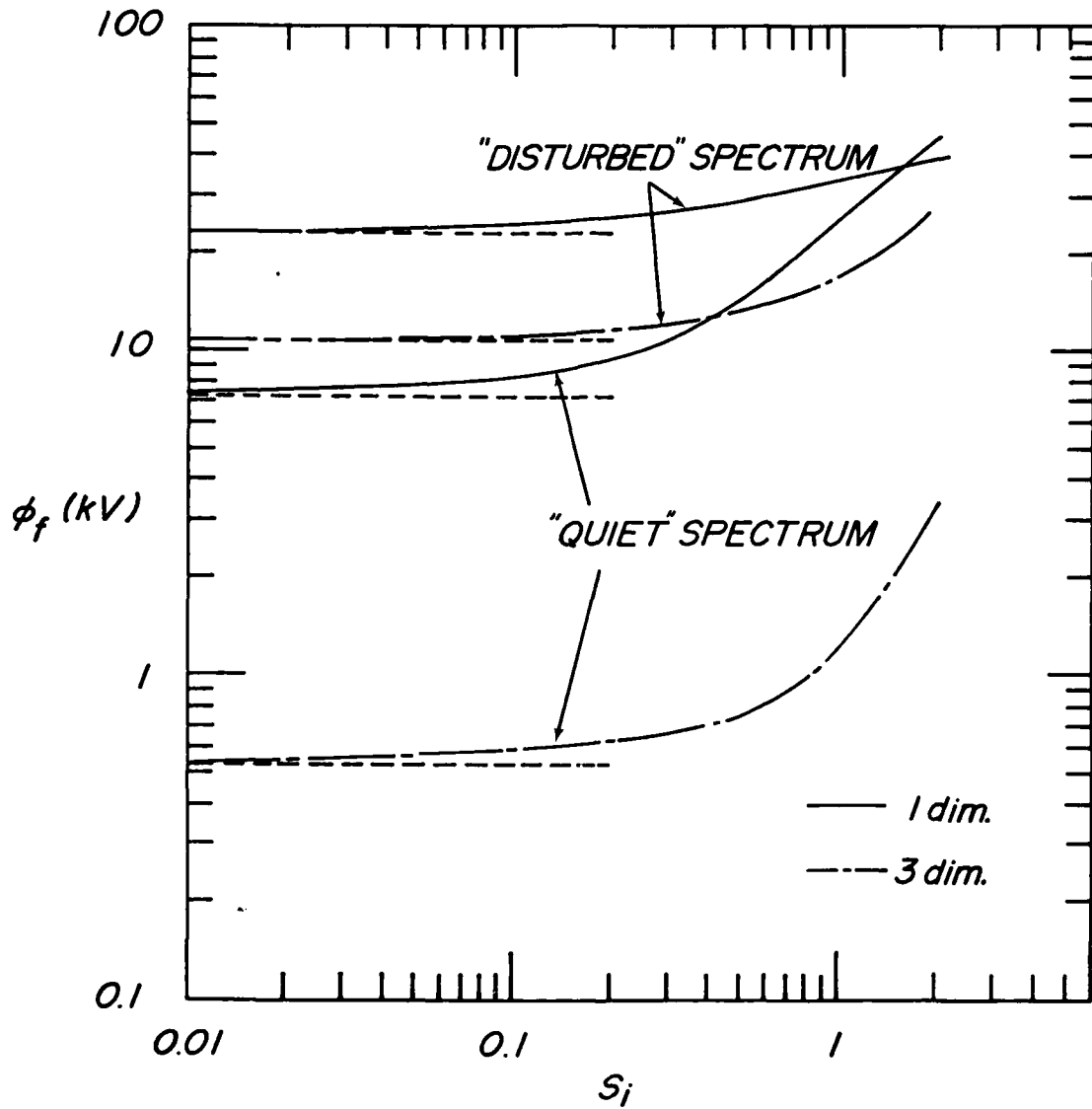


Fig. 2.16. Upper and lower bounds on floating potential  $\phi_f$  at shaded downstream point of spacecraft, as a function of ion speed ratio  $S_i$  for "disturbed" and "quiet" electron velocity spectra representing geostationary orbit conditions, for one-dimensional and three-dimensional ion velocity space cutoffs.

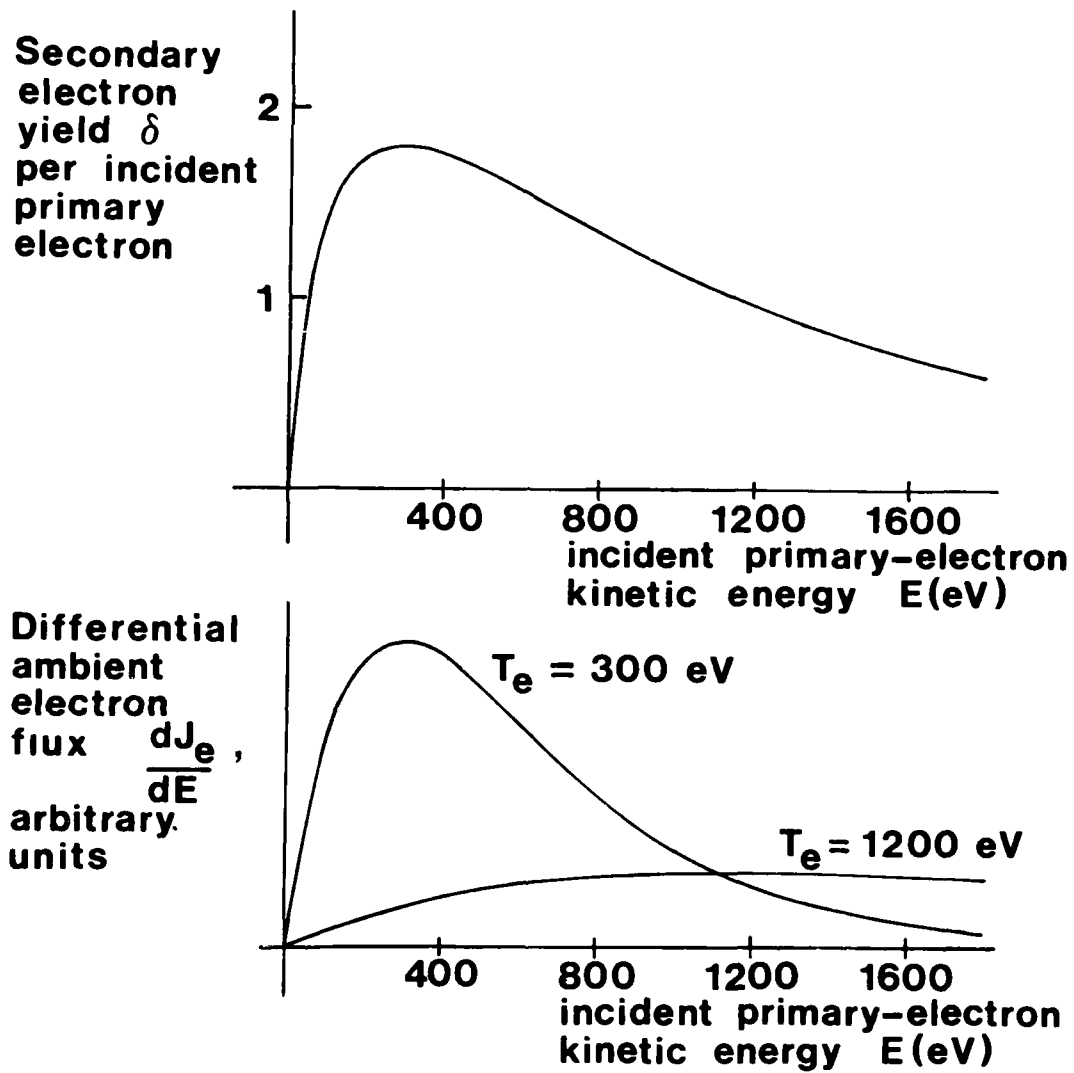


Fig. 3.1.(a) typical form of secondary-electron yield  $\delta$  (secondary electrons per incident primary electron), as a function of incident primary kinetic energy  $E$ , at normal incidence (b) energy-differential electron flux  $dJ_e/dE$  for Maxwellian ambient electron velocity distributions at two different temperatures. Total secondary-electron flux is obtained by integrating the product of these two functions [multiplied by another factor given in Eq. (2.10)] over energy  $E$ .



## PARTICLE ORBIT

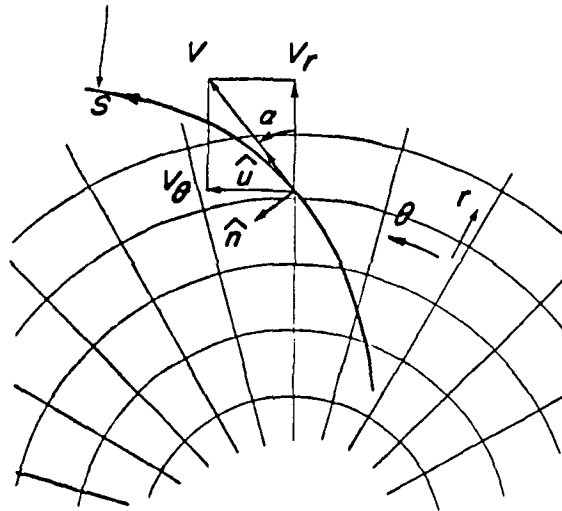


Fig. 4.1. Coordinate system and definitions for particle orbit integration.

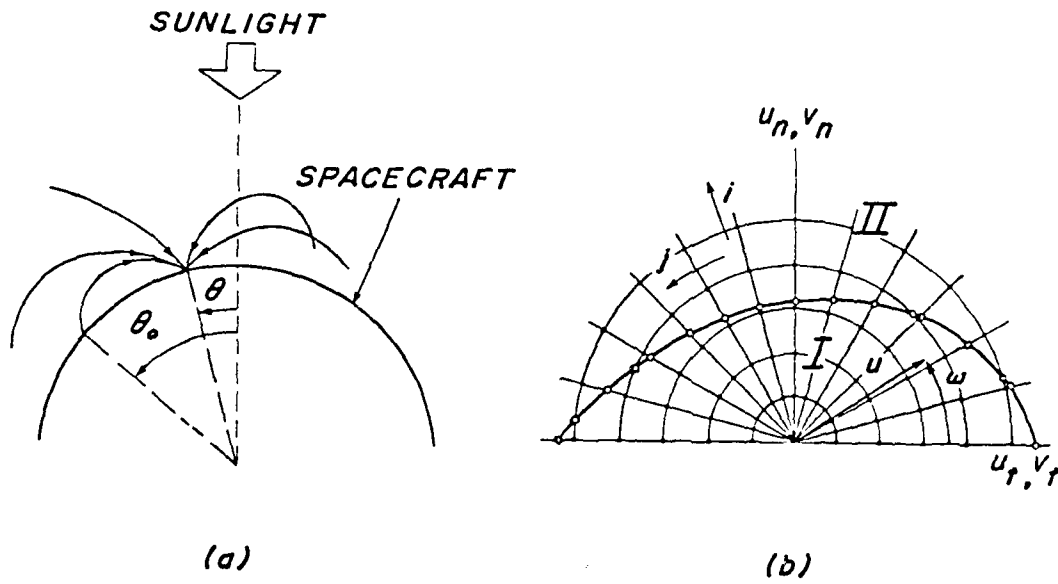


Fig. 4.2. Position-space (a) and velocity-space (b) coordinates for calculation of incident current density at a surface point. Figure 4.2a shows several particle orbits incident at a surface point  $\theta$ , one of them having originated at the surface point  $\theta_0$ .

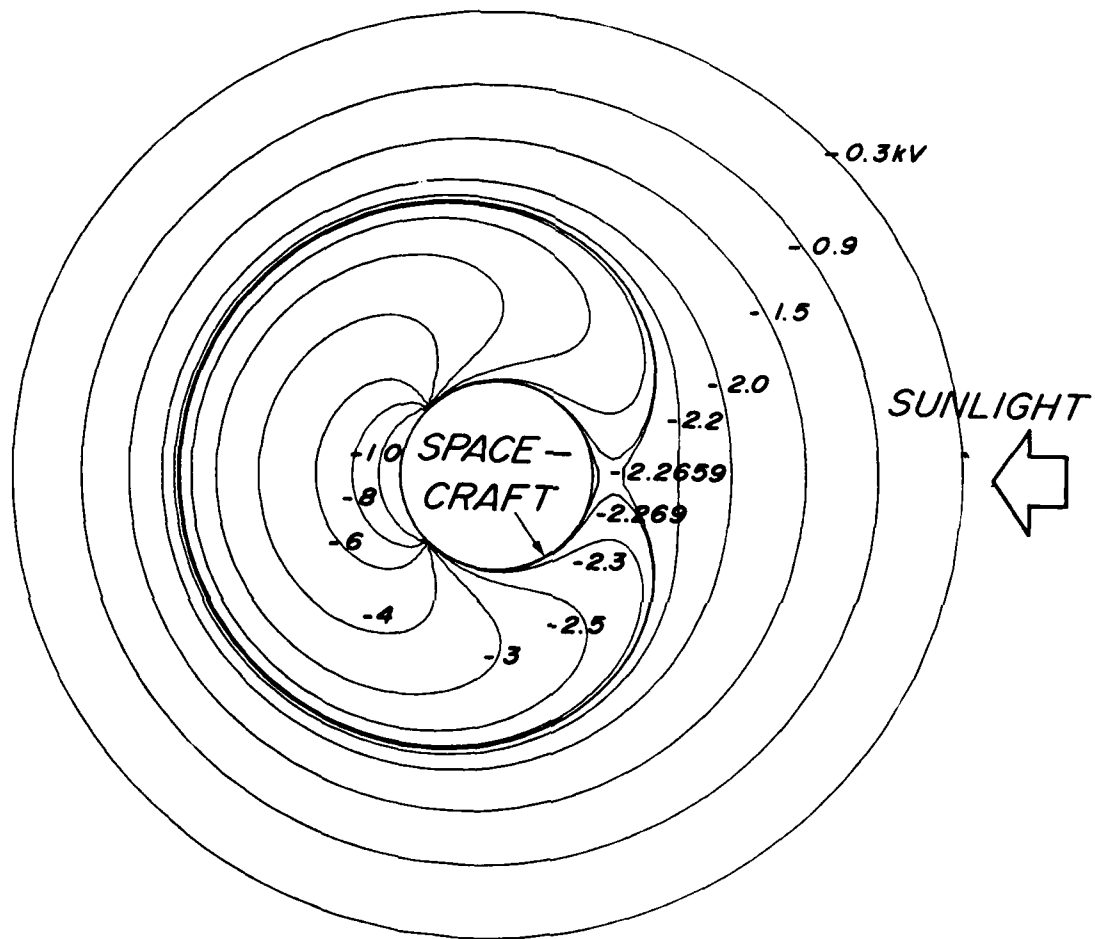


Fig. 4.3. Equipotential contours around a cylindrical spacecraft cross-section with two conductive sectors having angles of  $270^\circ$  and  $90^\circ$ . Sector potentials are  $-2.265$  kV and  $-11.88$  kV, respectively. Other data pertinent to this calculation are given in Sec. 4.5. The radial coordinate in Figs. 4.3 - 4.5, 4.8 and 4.9 is  $1 + \ln(r/r_s)$  where  $r_s$  is spacecraft radius.

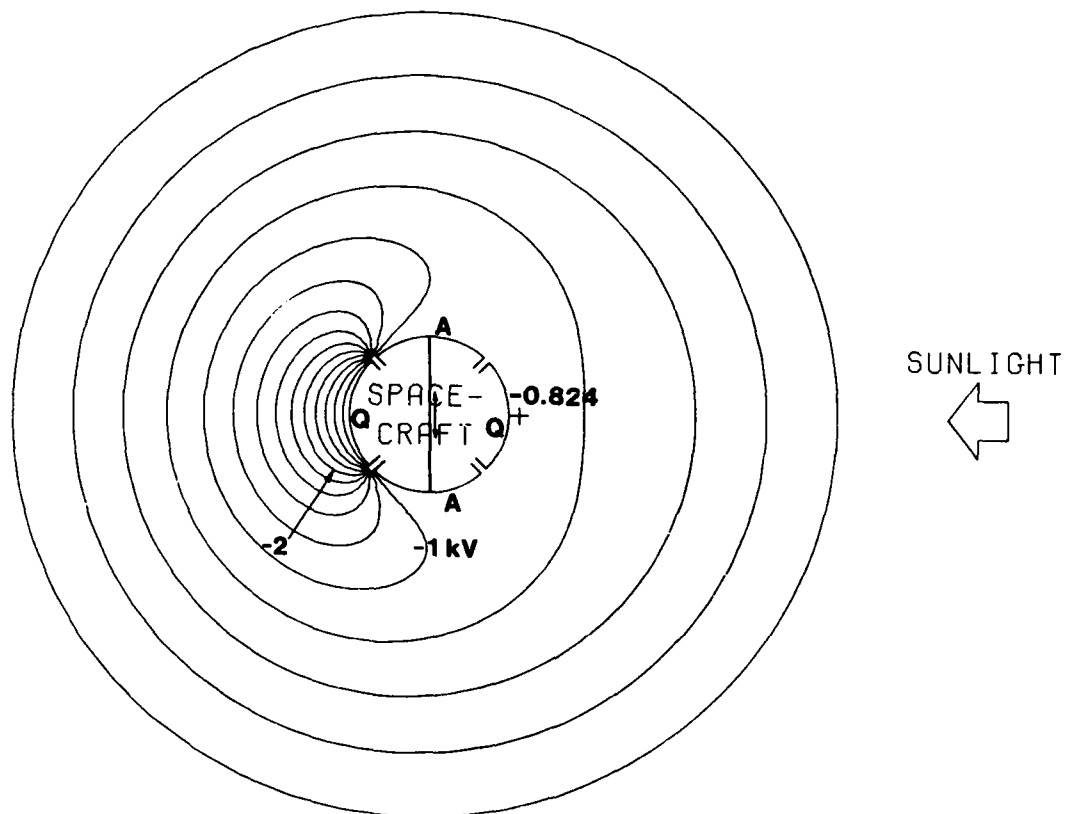


Fig. 4.4. CYLVIA calculation of equipotential contours around a cylindrical spacecraft cross-section with four sectors each having an angle of  $90^\circ$ . The two sectors labeled "A" are conductive, have the photoemission properties of aluminum, and are connected together electrically, as shown schematically in the figure. The two sectors labeled "Q" are nonconductive and have the photoemission properties of quartz. In this and subsequent figures, the symbol + indicates the location of a saddle point. Other data pertinent to this calculation are given in Sec. 4.5. The radial coordinate in this figure is as in Fig. 4.3. The floating surface potential distribution resulting from this calculation is shown in Fig. 4.6.

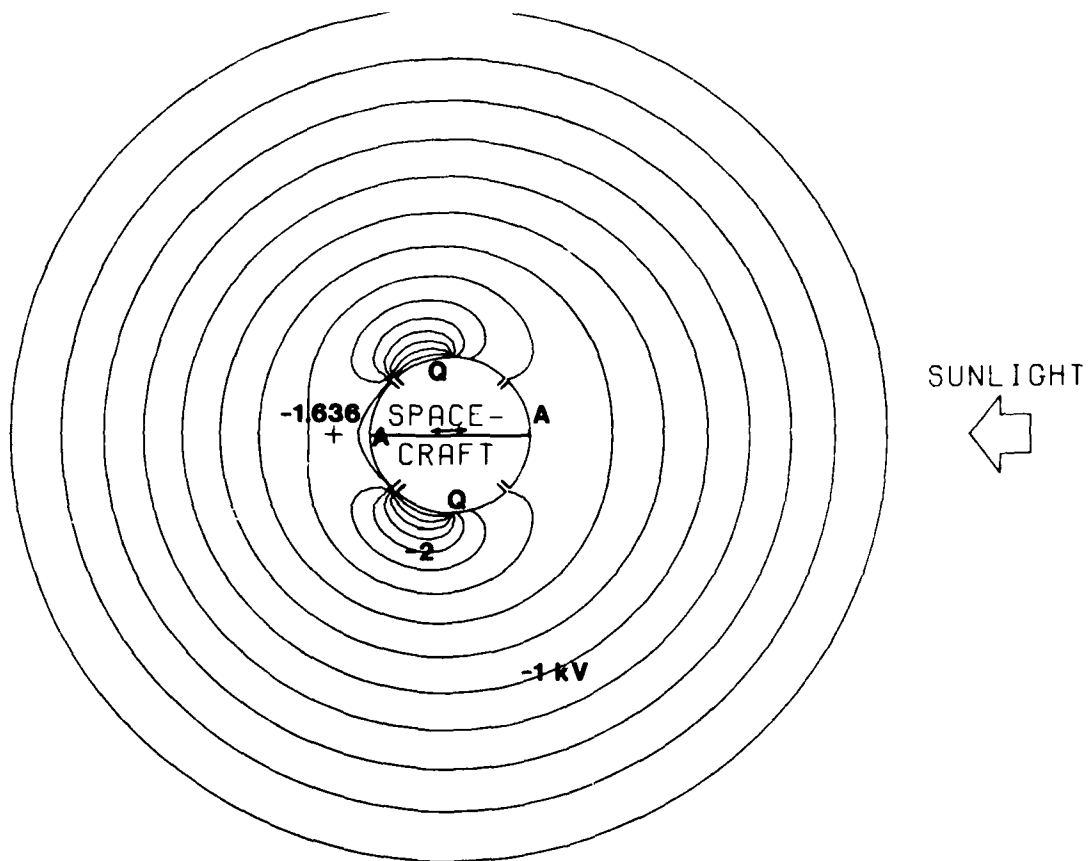


Fig. 4.5. Same as Fig. 4.4 except that the spacecraft has been rotated by  $90^\circ$ .

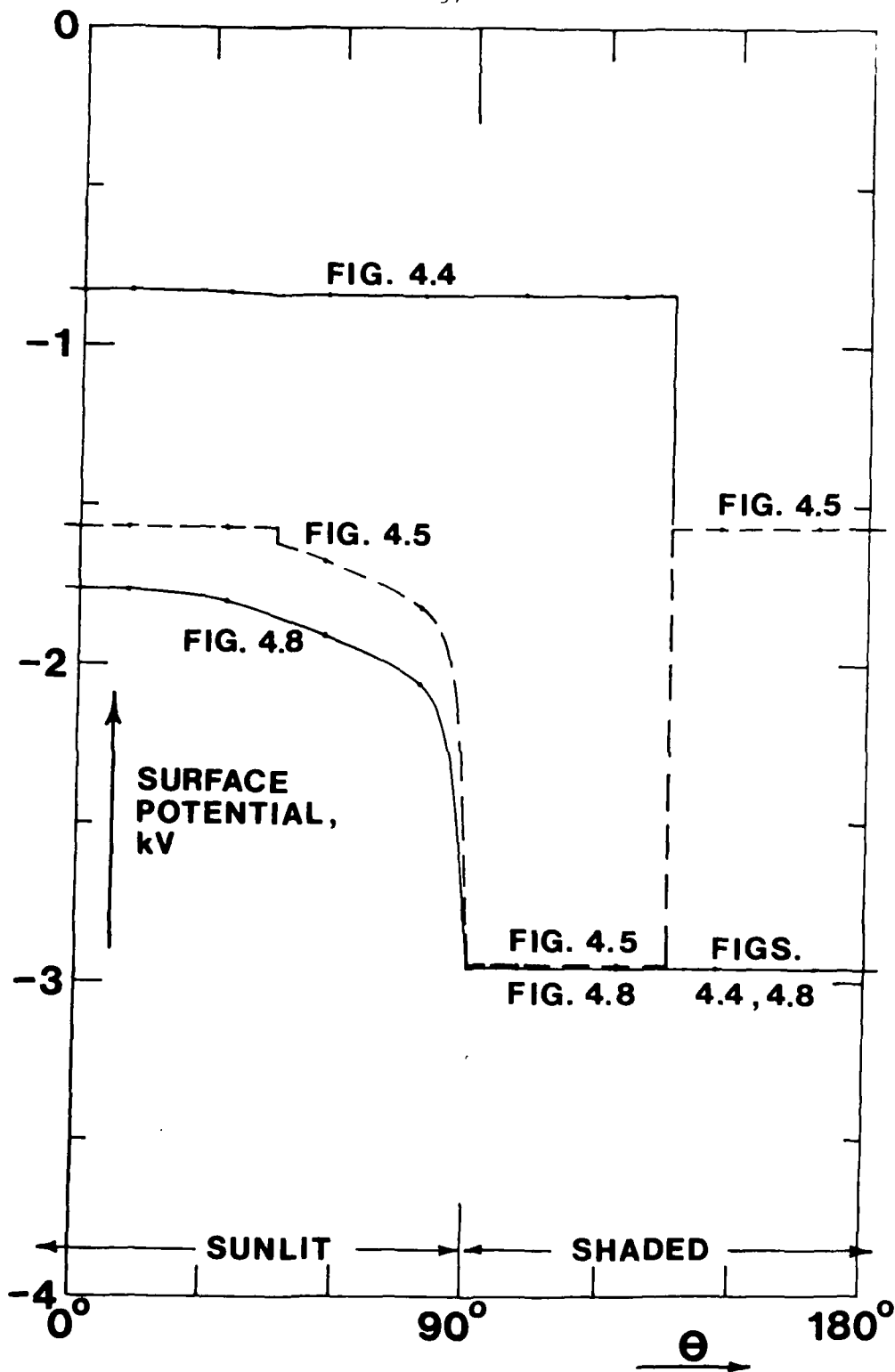


Fig. 4.6. Distributions of floating surface potential vs angle for the calculations shown in Figs. 4.4, 4.5, and 4.8.

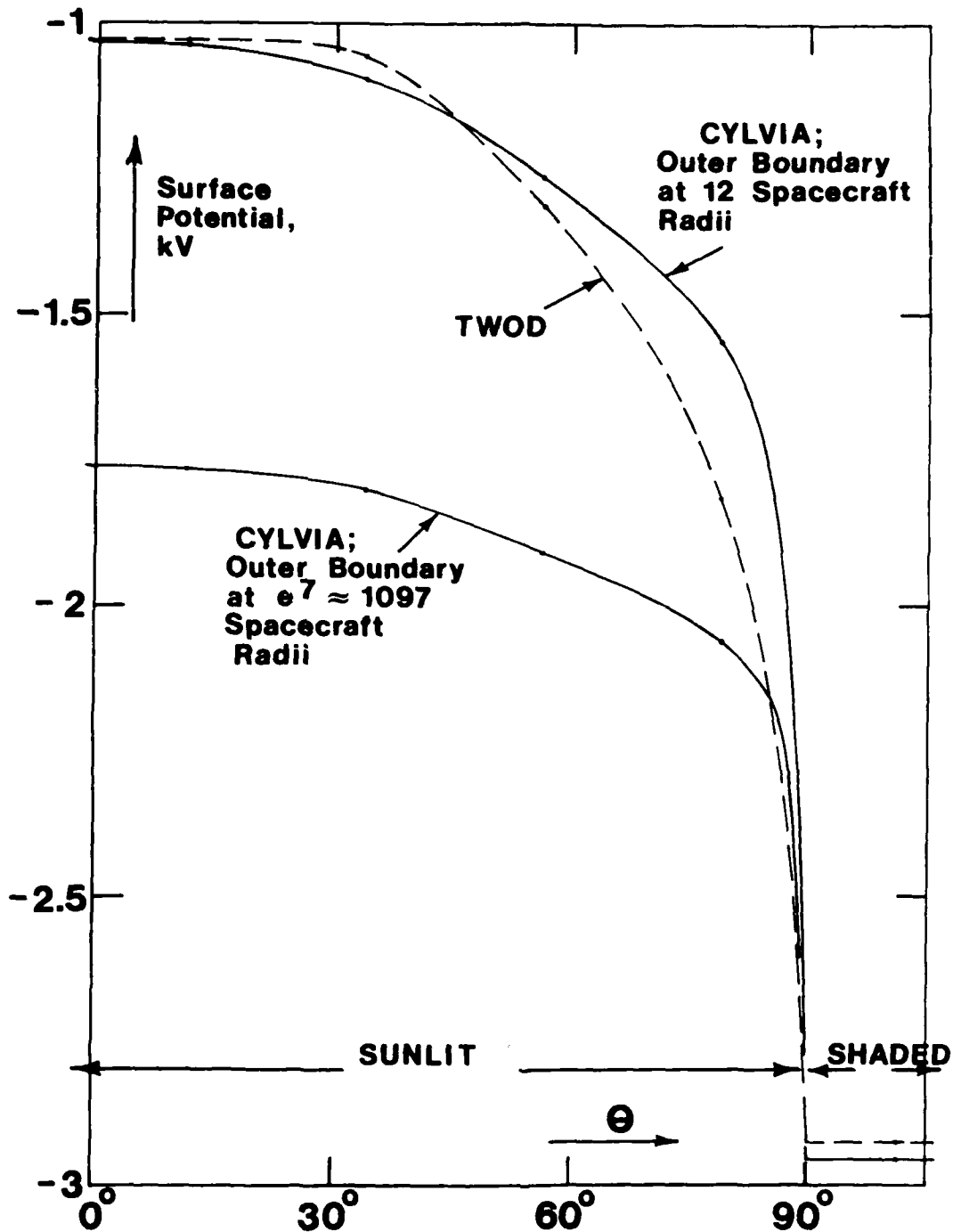


Fig. 4.7. Distributions of floating surface potentials vs angle for the calculation shown in Fig. 4.9, and also for another one which is the same except that the outer boundary of the calculation (which is held at space potential in all cases) is at  $12r_s$  rather than  $e^7 r_s$ . Also shown is another result for which the outer boundary is at  $12r_s$ , calculated using a program called TWOD, which combines NASCAP physical assumptions with circular cylindrical geometry (M. Mandell, Systems, Science and Software, Inc., private communication). Other data pertinent to these calculations are given in Sec. 4.5.

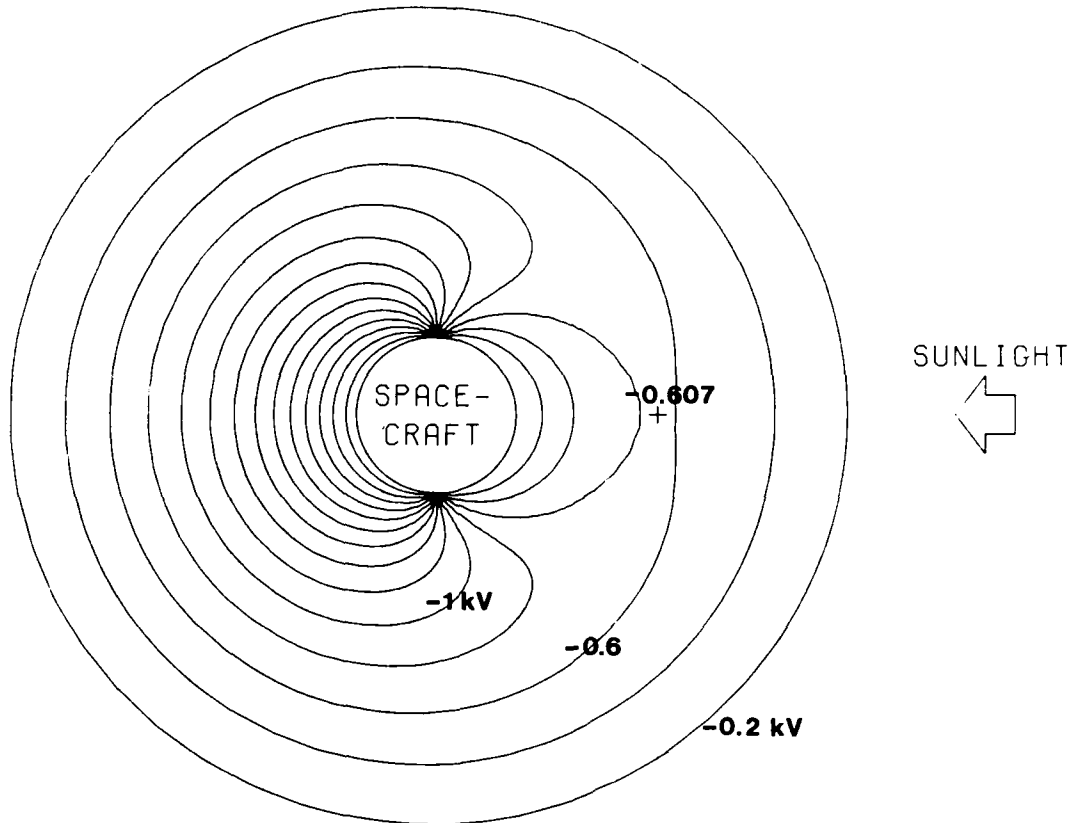


Fig. 4.8. CYLVIA calculation of equipotential contours around a cylindrical spacecraft cross-section having a nonconductive surface, corresponding to a surface potential distribution calculated assuming local current balance only (i.e., the presence of a potential barrier is ignored in calculating photoelectron escape). The symbol + indicates the location of a saddle point. The photoelectron charge flux  $eJ_{ph} = 4.2 \times 10^{-5} \text{A/m}^2$  at normal incidence.

$T_{ph} = 1.5 \text{ eV}$ . Ambient ion and electron distributions are single Maxwellians, each with  $n = 3 \text{ cm}^{-3}$  and  $T = 1 \text{ keV}$ . Secondary and backscattered electron fluxes are assumed zero. The polar-coordinate computation grids in position  $(r, \theta)$  and in velocity space contain  $65 \times 16$  and  $8 \times 16$  intervals, respectively. Outer grid boundary radius  $r_B$  is  $e^7$  times spacecraft radius  $r_S$ . Linearized ambient space charge (Eq. 4.3; Laframboise and Prokopenko, 1977), corresponding to a Debye length of  $96 r_S$ , is assumed. Radial coordinate in Figure is  $1 + \ln(r/r_S)$ .



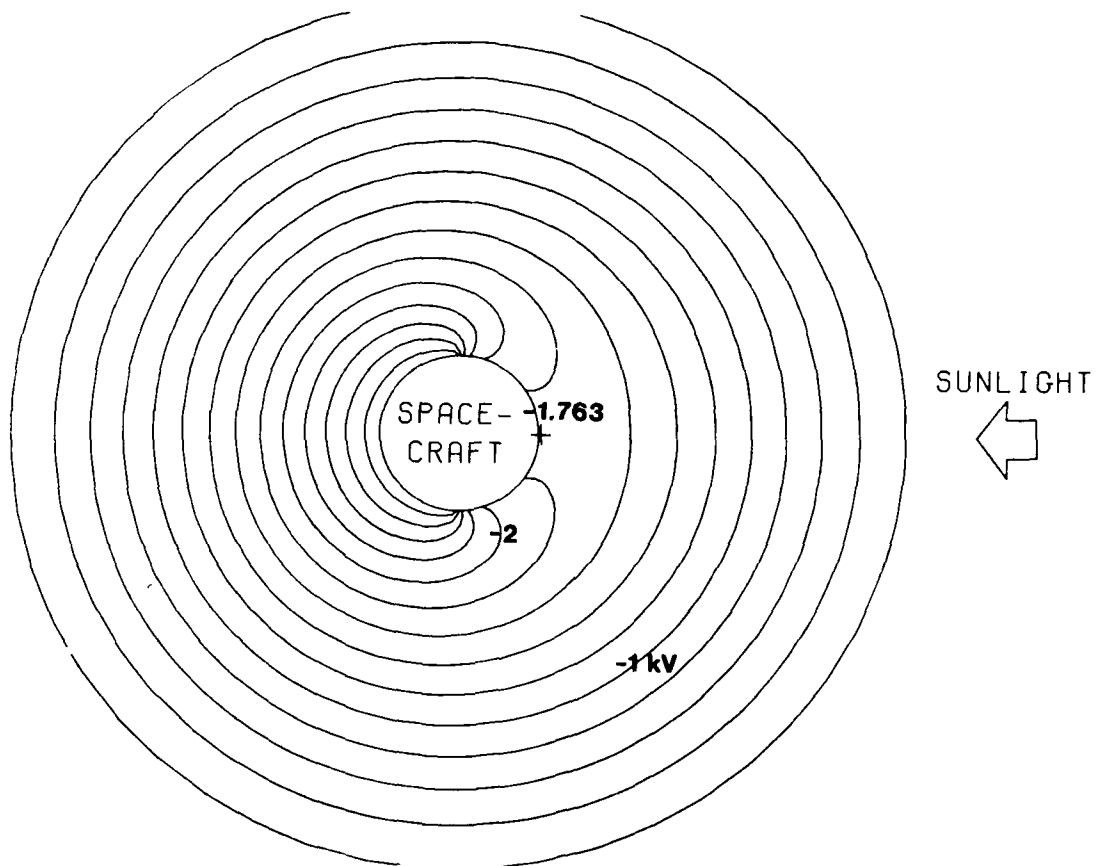


Fig. 4.9. Same as Figure 4.8 except that the calculation is now self-consistent including potential-barrier effects on photoelectron and other particle orbits.

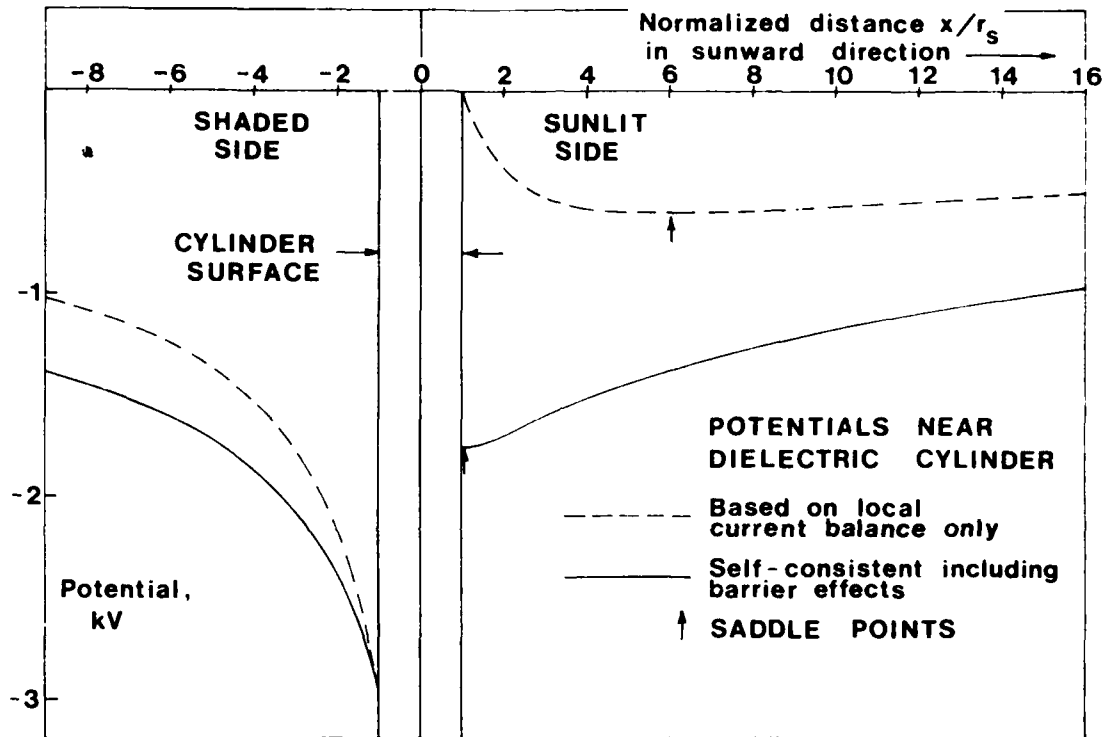


Fig. 4.10. Potentials vs distance along spacecraft-sun line for the situations shown in Figs. 4.8 and 4.9, showing the large decrease in differential charging which results when potential-barrier effects on particle (especially photoelectron) orbits are included. Without these effects, surface potentials at the sunward and anti-sunward points are 5.1V and -2.96 kV; with these effects, these potentials are -1.76 kV and -2.96 kV.

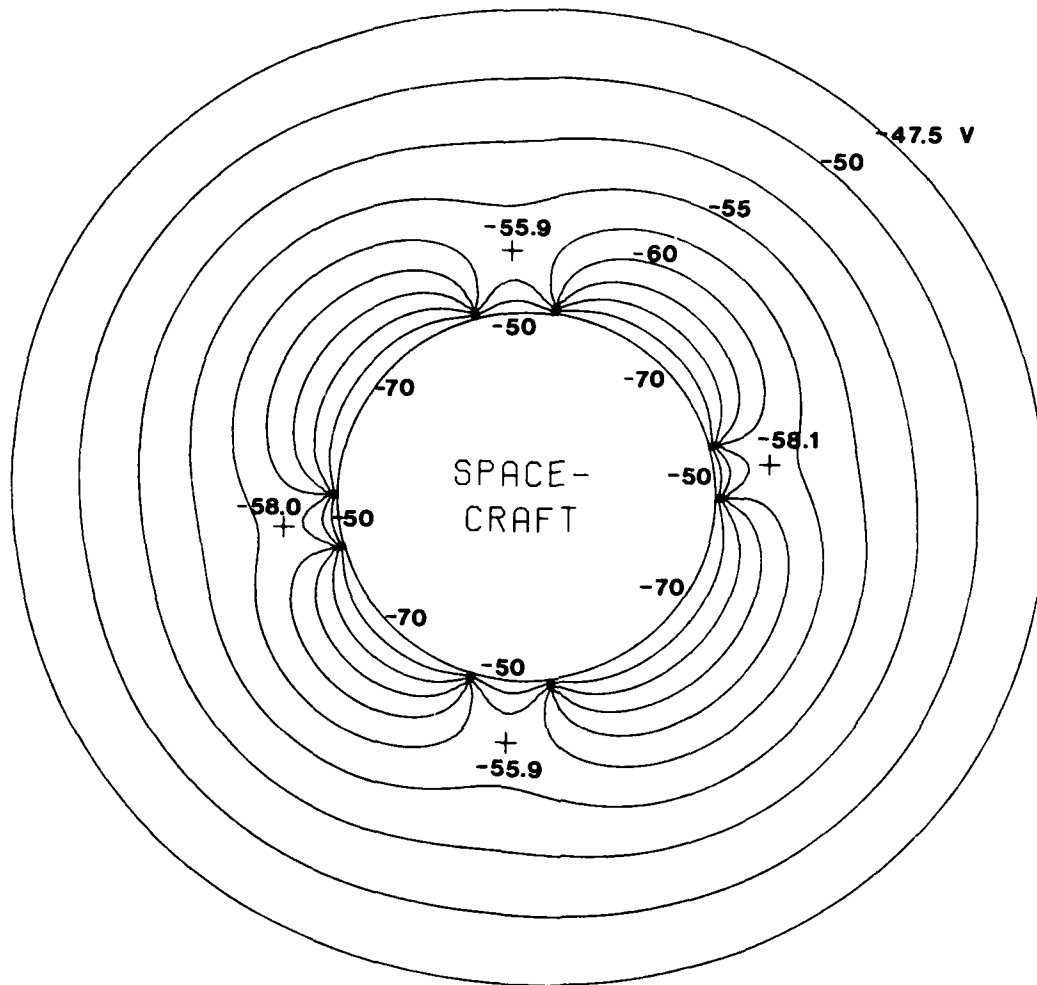


Fig. 4.11. CYLVIA calculation of equipotentials around a circular spacecraft cross-section with given rather than self-consistent surface potentials, as shown. In this Figure, the radial coordinate is proportional to radius. The computational grid in  $(r, \theta)$  contains  $65 \times 180$  intervals. The outer grid boundary is at  $e^5 \approx 148$  spacecraft radii. Linear space charge corresponding to  $\lambda_D = 32.5$  spacecraft radii is assumed. Other data pertinent to this calculation are given in Sec. 5.2. This calculation was done for the purpose of comparison with a XYCIC calculation shown in Fig. 5.1, and also with a similar but three-dimensional calculation done using NASCAP (Olsen, 1980, p. 190; Olsen and Whipple, 1980, Fig. 16). The results of this comparison are discussed in Sec. 5.2.

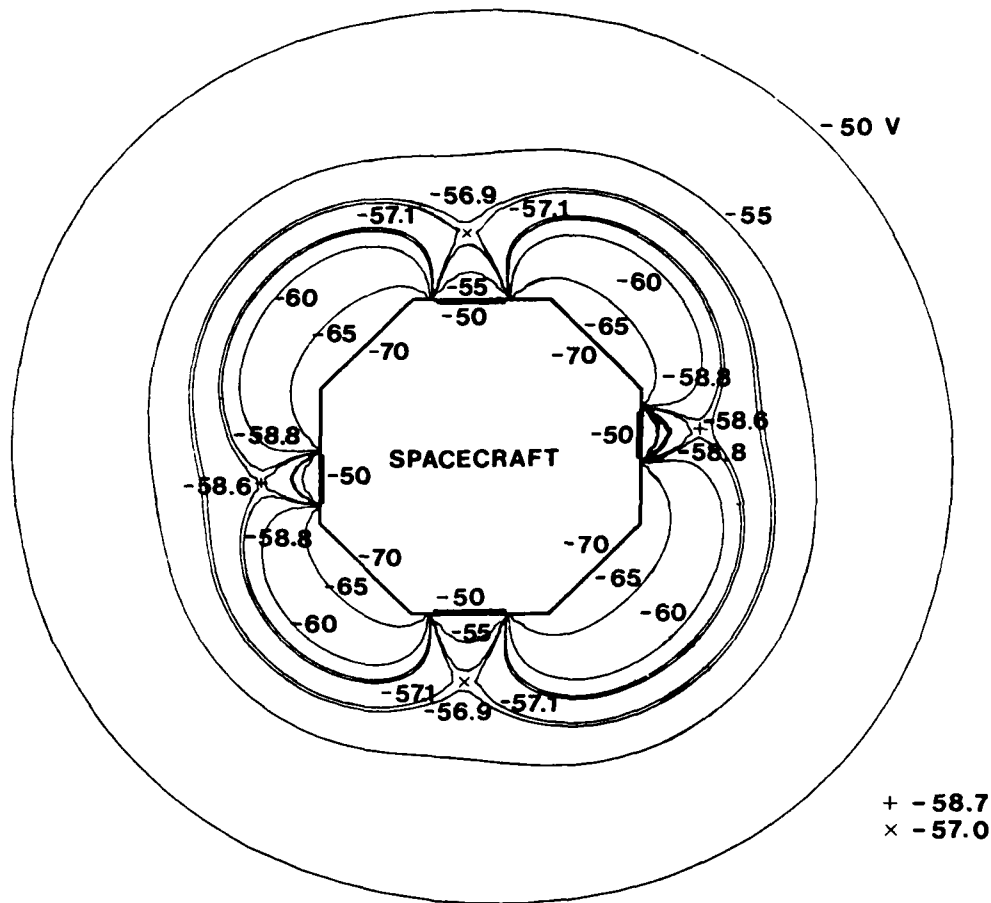


Fig. 5.1. Xycic calculation of equipotentials, corresponding to the CYLVIA calculation shown in Fig. 4.11. One difference between these two calculations is that in the Xycic calculation, zero space charge is assumed. The innermost grid used in the Xycic calculation contains  $40 \times 40$  intervals; the octagon has a dimension of  $28 \times 28$  intervals and is centred in this grid. Six other grids surround the innermost grid; the outermost grid boundary is a centred square of side 19.2 times as large as the innermost grid boundary, i.e. located at 27.4 object half-widths.

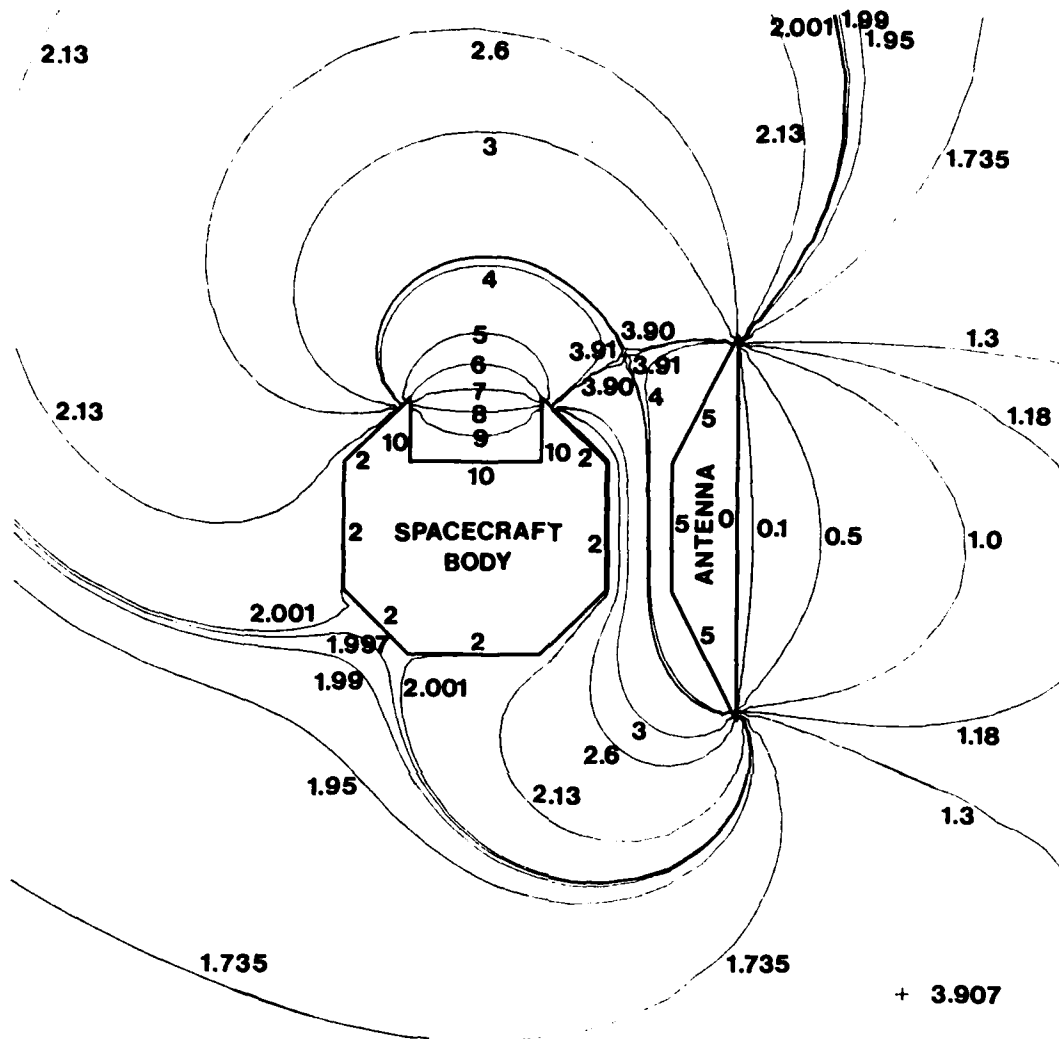


Fig. 5.2. XYCIC calculation of equipotentials around a cross-section through a hypothetical antenna + spacecraft body combination. As in Figs. 4.11 and 5.1, surface potentials are imposed (in this case, also hypothetical) values. Zero space charge is assumed. The innermost grid used contains  $32 \times 32$  intervals with the combined total width of the "object" being 24 intervals. Six other grids surround the innermost grid; the outermost grid boundary is a centred square of side 20 times the innermost grid boundary, i.e. located at 26.7 half-widths of the combined object.

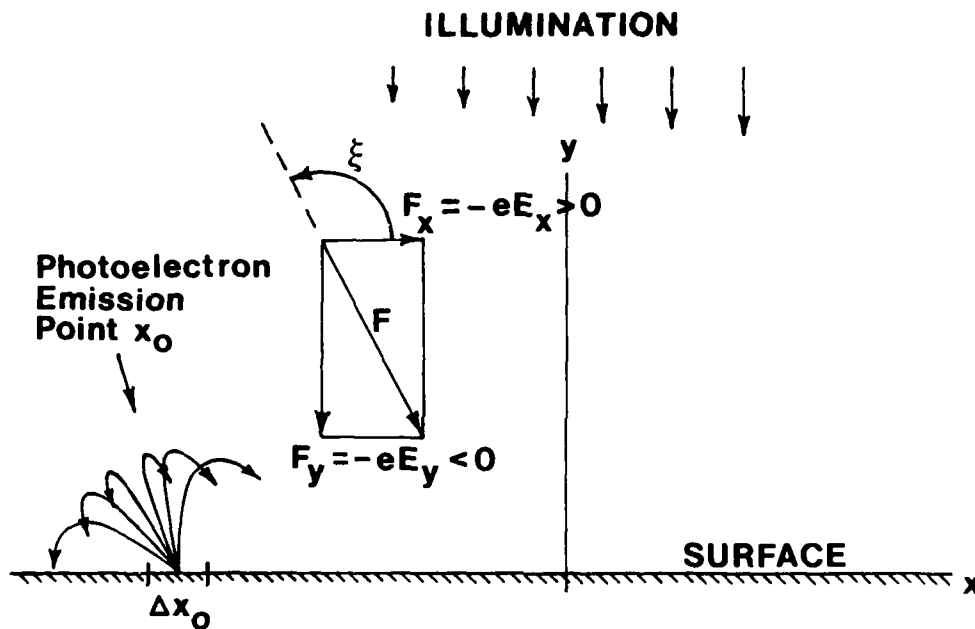


Fig. 6.1. Geometry for photocurrent sheet calculation. The illumination is assumed to vary linearly with  $x$ , producing a photoemission current density  $J_{ph}(x_0) = J_{ph,0} + J_{ph}'x_0$ . The electric field components  $E_x$  and  $E_y$  are assumed uniform, so that the surface potential varies linearly with  $x$ . The electron orbits are then tilted parabolas. Their impact points  $x$  can be found analytically (Eq. 6.1) for given values of emission position  $x_0$  and emission velocity components  $v_{x0}$  and  $v_{y0}$ .

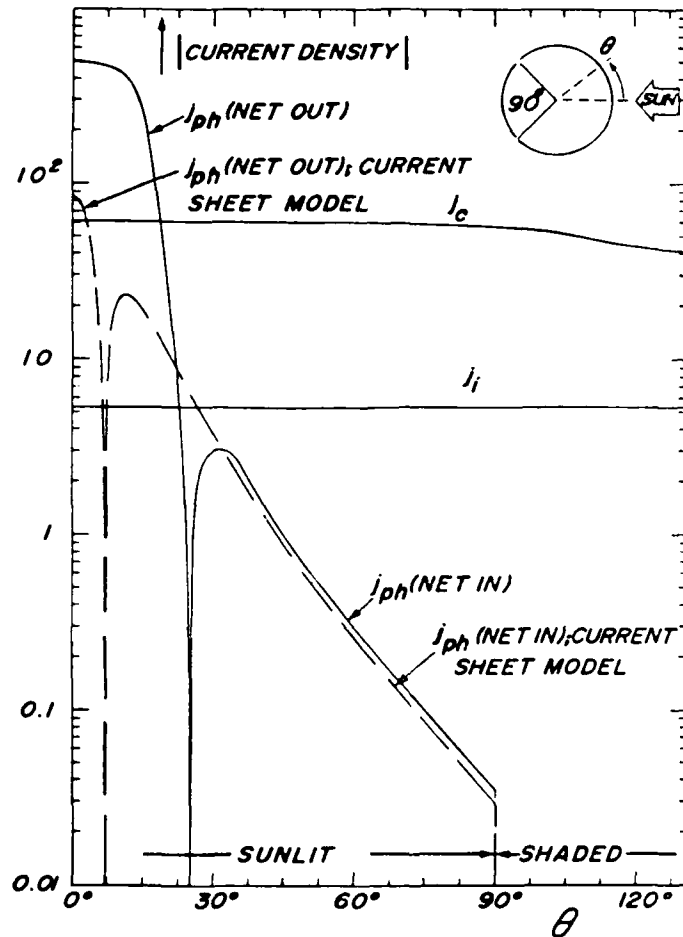


Fig. 6.2. Current densities vs surface position for the situation shown in Fig. 4.3 and described in Sec. 6.3. In this Figure, normalized current density  $j$  is defined as  $J/J_{\text{ref}}$ , where  $J_{\text{ref}}$  is the random flux of Maxwellian ions having a temperature and density of 1 keV and  $1 \text{ cm}^{-3}$ . Approximate photoelectron currents  $j_{\text{ph}}$  obtained using the approximate surface current ("current sheet") model given by Eqs. (6.7) and (6.8) are shown as dashed curves.

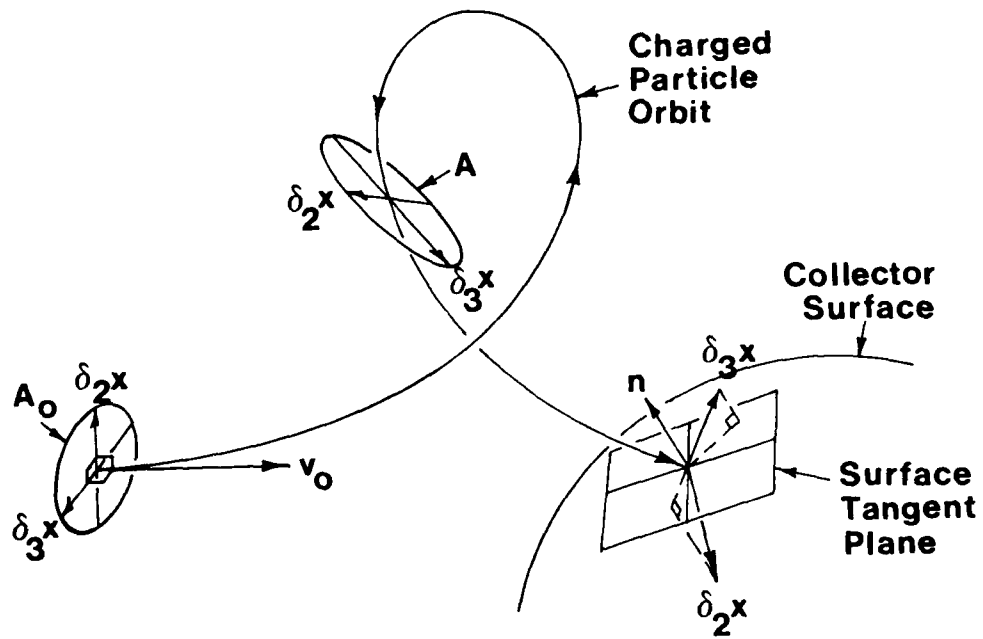


Fig. 7.1. Particle orbit geometry.



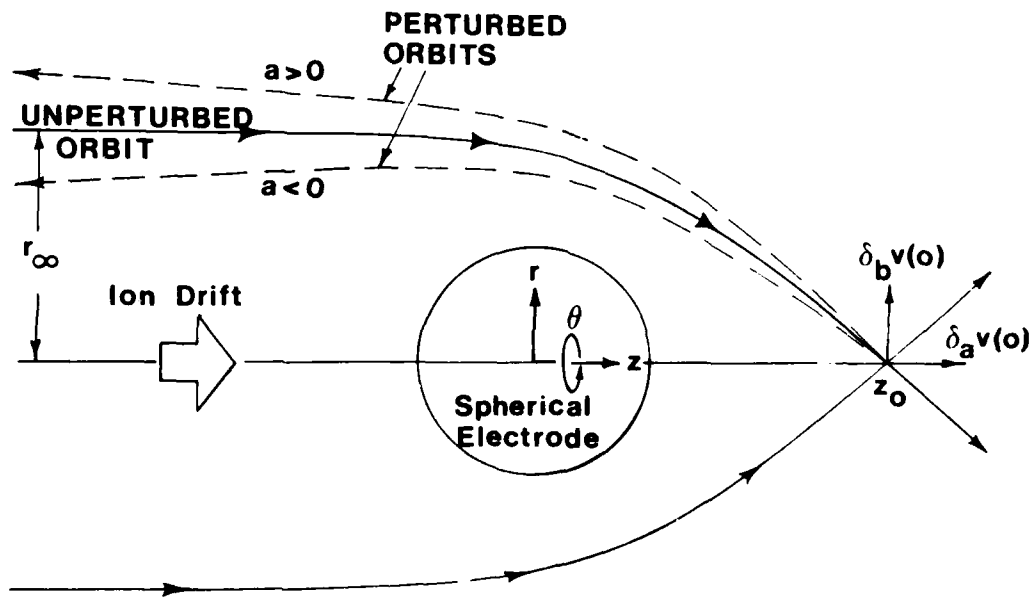


Fig. 7.2. Geometry for perturbation calculation of sphere axial defocusing.





```

40 CONTINUE
CSEC=FXSUM
GO TO 4
4 FXSUM=0
KON1=10.8KON
KON2=(CUTOFF+10.)/(CUTOFF-10.)
KON3=2.8(CUTOFF-10.)/EMAX
KON4=(CUTOFF+10.-2.8U)/(CUTOFF-10.)
KON10=4.58KON
KON30=18./EMAX
KON40=1.222222-U/4.5
KON11=KON
KON31=1.8/EMAX
KON41=1.222222-U/.45
KON12=25.8KON8(.1-CUTLOW)882
KON22=(.1+CUTLOW)/(1-CUTLOW)
KON32=2.8(.1-CUTLOW)/EMAX
KON42=KON22-2.8U/(1-CUTLOW)
KON8=2.8U/(CUTOFF-10.)
KON80=U/4.5
KON81=U/.45
KON82=2.8U/(1-CUTLOW)
KON13=12.58KON8(CUTLOW-U)883/CUTLOW
KON23=(CUTLOW+U)/(CUTLOW-U)
KON33=2.8(CUTLOW-U)/EMAX
DO 50 I=1,8
KON5=Y(I)+KON4
KON6=Y(I)+KON2
KON7=SQRT(KON38KON5)
KON50=Y(I)+KON40
KON60=Y(I)+1.222222
KON70=SQRT(KON308KON50)
KON51=Y(I)+KON41
KON61=Y(I)+1.222222
KON71=SQRT(KON318KON51)
KON52=Y(I)+KON42
KON62=Y(I)+KON22
KON72=SQRT(KON328KON52)
KON53=Y(I)+1
KON63=Y(I)+KON23
KON73=SQRT(KON338KON53)
FXH(I)=8(KON18KON58828EXP(-KON7)/KON6883
1/KON108KON508828EXP(-KON70)/KON60882+KON118KON518828EXP(-KON71)
1/KON61883+KON128KON528828EXP(-KON72)/KON62)
1/KON138KON538828EXP(-KON73)
FXSUM=FX+FXSUM

```

0.05	1.	.003	
0.1	50.	.001	
0.2	1.	1.	1.
0.3	1.	0.	0.
0.4	0.10	0.	.464

```

50 CONTINUE
CSEC=FXSUM
GO TO 5
5 KON1=10.8KON
KON2=(CUTOFF+10.)/(CUTOFF-10.)
KON3=2.8(CUTOFF-10.)/EMAX
KON4=(CUTOFF+10.-2.8U)/(CUTOFF-10.)
KON10=4.58KON
KON30=18./EMAX
KON40=1.222222-U/4.5
KON11=KON
KON31=1.8/EMAX
KON41=1.222222-U/.45
KON12=25.8KON8(.1-CUTLOW)882
KON22=(.1+CUTLOW)/(1-CUTLOW)
KON32=2.8(.1-CUTLOW)/EMAX
KON42=KON22-2.8U/(1-CUTLOW)
KON8=2.8U/(CUTOFF-10.)
KON80=U/4.5
KON81=U/.45
KON82=2.8U/(1-CUTLOW)
KON13=12.58KON8(CUTLOW-U)883
KON23=(CUTLOW+U)/CUTLOW
KON33=2.8CUTLOW/EMAX
KON43=1.-2.8U/CUTLOW
FXSUM=0
DO 60 I=1,8
KON5=Y(I)+KON4
KON6=Y(I)+KON2
KON7=SQRT(KON38KON5)
KON50=Y(I)+KON40
KON60=Y(I)+1.222222
KON70=SQRT(KON308KON50)
KON51=Y(I)+KON41
KON61=Y(I)+1.222222
KON71=SQRT(KON318KON51)
KON52=Y(I)+KON42
KON62=Y(I)+KON22
KON72=SQRT(KON328KON52)
KON53=Y(I)+1
KON63=Y(I)+KON23
KON73=SQRT(KON338KON53)
IF (KBRNCH.EG.1) FXH(I)=8(KON18KON58828EXP(-KON7)/KON6883
1/KON108KON508828EXP(-KON70)/KON60882+KON118KON518828EXP(-KON71)
1/KON61883+KON128KON528828EXP(-KON72)/KON62)
1/KON138KON538828EXP(-KON73)
IF (KBRNCH.EG.2) FXH(I)=8(KON18KON58(KON58883IN(SQRT(KON6/KON5))/KON
14+SQRT(KON8/KON6))8EXP(-KON7)/KON6882+KON108KON508(KON50883IN(SQR
2+(KON60/KON50))/KON60+SQRT(KON80/KON60))8EXP(-KON70)/KON60+KON11
288KON518(KON51883IN(SQRT(KON61/KON51))/KON61+SQRT(KON81/KON61))
38EXP(-KON71)/KON61882+KON128KON528(KON52883IN(SQRT(KON62/KON52)
4)/KON62+SQRT(KON82/KON62))8EXP(-KON72)
5+KON138KON538(KON53883IN(SQRT(KON63/KON53))/KON63)
68SQRT(KON83/KON63))8EXP(-KON73)
IF (KBRNCH.EG.3) FXH(I)=8(KON18KON588EXP(-KON7)/KON6882
1/KON108KON5088EXP(-KON70)/KON60882+KON118KON5188EXP(-KON71)/KON61882
1/KON128KON528EXP(-KON72)+KON138KON538KON638EXP(-KON73)
FXSUM=FX+FXSUM

```

```

60 CONTINUE
IF (KBRNCH.EG.2) FXSUM=.63661988FXSUM
CSEC=FXSUM
IF (U.LT.0.) CALL RETARD(U,CSEC,TSEC)
4 CSEC=CSEC/A1
8 RETURN
END
ENTRY
1414 4
-.9862938 .3511946E-01
-.9294349 .0015809E-01
-.8272913 .1215186
-.6872929 .1572032
-.5152488 .1895384
-.3191124 .2051985
-.1088548 .2152639
1.088549 .2152639
.3191124 .2051985
.5152488 .1895384
.6872929 .1572032
.8272913 .1215186
.9294349 .0015809E-01
.9862938 .3511946E-01

```

B1  
Appendix B: Listing of threshold temperatures program

PROGRAM THRESHOLD TEMPERATURES PROGRAM

```
104 PROGRAM THRESH
      DIMENSION N(100)
      COMMON /CTRL/ ENX(12), DRX(12), BSA(12), BSB(12), BSC(12), Z(12)
      COMMON /EM/ DM, KEM, A, B, C, F, Z, IFLG, ICHN, DINTG(10)
      DIMENSION ITC(12), DUMMY(12), IDUM(4), DOTS(2)
      EQUIVALENCE (DUMMY, IDUM)
      DATA EPS/1.0E-5, DOTS/0.05, ILO/
      DATA NUMS/17, NUME/29, IFLGE/3, NP1/17, NP2/29
      DATA LU/13, ITRAC/20, ISECT/0

      DO 500 N=NUMS, NUME
        WRITE(1,900) N
        I=KEM(N)
        NP=DRX(N)
        DO 500 NPART=NP1, NP2
          FAC=NPART/2.3
          DTS=DOTS*(NPART)
          WRITE(1,904) NPART
        904 FORMAT(10X, 'PART: ', I2)
        DO 500 IFLG=1, IFLGE
          IF (IFLG.GE.2) GO TO 90
          A=0.0
          B=0.0
          C=0.0
          IF (NPART.EQ.1) TS=EM
          IF (NPART.EQ.2) TS=EM/2.0
          GO TO 10
        90 A=BSA(N)
          B=BSB(N)
          C=BSC(N)
          IF (IFLG.EQ.2) GO TO 4
          D=DOUBLE(Z(N))
          BETAB=SNGL(7.37000DZ*(1.0-0.508750D))
          FZ=(EXP(BETAB)-BETAB-1.0)/BETAB**2.0
          WRITE(1,201) Z(N), BETAB
        201 FORMAT(10X, 'Z: ', F5.15X, ' BETAB: ', E15.7)
          GO TO 8
        8 FZ=1.0
          TS=TCN*(NPART)
          IF (NPART.EQ.1.AND.TS.LE.1.0E-4) TS=EM
          IF (NPART.EQ.2.AND.TS.LE.1.0E-4) TS=EM/2.0
        10 DT=DTS
          NPATH=1
        20 FL=RCUR(TS)
        30 TSS=TS+DT*FAC
          IF (TSS.LE.1.0E-4) GO TO 500
          FN=RCUR(TSS)
          WRITE(1,400) TS, FL, FN, DT
        400 FORMAT(4F15.7)
          IF (NPART.EQ.1.AND.TS.LE.1.0E-4) GO TO 500
          IF (NPART.EQ.2.AND.TS.LE.1.0E-4) GO TO 500
          IF (FL.FN) 50+50.40
        40 TS=TS+DT*FAC
          FL=FN
          GO TO (30,50), NPATH
        50 DT=DT/2.0
          NPATH=2
          IF (DT-EPS) 40,60,30
        60 NPAT=NPART+(IFLG-1)*2
          ITC(N, NPAT)=TS
          WRITE(1,200) IFLG, TS
        200 FORMAT(5X, ' IFLG: ', I1, '5X, ' TC: ', F8.4)
        500 CONTINUE
        CALL EXEC(2, LU, ENX+64, ITRAC, ISECT)
        CALL EXEC(2, LU, DRX+64, ITRAC, ISECT+1)
        CALL EXEC(2, LU, BSA+64, ITRAC, ISECT+2)
        CALL EXEC(2, LU, BSB+64, ITRAC, ISECT+3)
        CALL EXEC(2, LU, BSC+64, ITRAC, ISECT+4)
        CALL EXEC(2, LU, Z+64, ITRAC, ISECT+5)
        DO 300 J=1+6
          ISECT=ISECT+J+5
          DO 310 I=1+32
            DUMMY(I)=TC(I, J)
        310 CONTINUE
        CALL EXEC(2, LU, DUMMY+64, ITRAC, ISECT)
        300 CONTINUE
        IDUM(1)=NUMS
        IDUM(2)=NUME
        CALL EXEC(2, LU, IDUM+64, ITRAC, ISECT+12)
        STOP
      END
```

```
BLOCK DATA
COMMON /CTRL/ ENX(12), DRX(12), BSA(12), BSB(12), BSC(12), Z(12)
DATA ENX/0.8+0.3+0.3+0.42+0.33+0.35+0.34+0.34+0.39+0.85+0.15/
A0.25+0.8+0.25+0.4+0.8+0.35+0.36+0.33+0.39+0.85+0.15/
B0.41+0.15+0.15+0.15+0.72+0.48+0.59+0.3/
DATA DRX/1.45+0.97+2.6+2.5+3.46+0.75+2.2+5.0+3.0+2.1/
A1.8+1.4+0.92+4.0+1.0+2.55+2.39+2.35+1.52+6.38+2.1/
B2.05+2.1+2.1+1.03+1.49+1.86+1.0/
DATA Z/79.0+13.0+10.0+10.0+10.0+6.0+29.0+29.0+8.0+5.3/
A5.3+24.4+12.0+10.0+47.0+15.3+16.2+16.9+15.3+10.0+5.0/
B10.0+5.0+5.0+5.0+70.1+42.0+83.4+8.0/
DATA BSA/0.4802+0.1548+0.1238+0.1238+0.1238+0.08+0.3134/
A0.3134+0.09+0.07+0.07+0.275+0.146+0.1238+0.39+0.183+0.192/
B0.2+0.183+0.1238+0.06+0.1238+0.06+0.06+0.06+0.456+0.373/
C0.438+0.08/
DATA BSB/0.3566+0.0303+0.0172+0.0172+0.0172+0.0+0.0692/
A0.0692+0.0+0.0+0.0+0.04+0.025+0.0172+0.289+0.037+0.04/
B0.042+0.037+0.0172+0.0+0.0172+0.0+0.0+0.0+0.338+0.276/
C0.325+0.0/
DATA BSC/0.4103+0.3431+0.3435+0.3435+0.3435+0.0+0.6207/
A0.6207+0.0+0.0+0.0+0.56+0.346+0.3435+0.432+0.382+0.599/
B0.41+0.382+0.3435+0.0+0.3435+0.0+0.0+0.0+0.612+0.617/
C0.613+0.0/
END
```

```
SUBROUTINE INTG(EINTG)
COMMON /EM/ DM, KEM, A, B, C, F, Z, IFLG, ICHN, DINTG(10)
DATA ERROR/1.0E-4, ECUT/1.0E-7/
ITER=0
DO 100 I=1,200
  CUTOFF=1
  ECUT=EINTG(CUTOFF)
  IF (ECUT.LE.ECUT) GO TO 110
100 CONTINUE
WRITE(1,999)
999 FORMAT(' INSUFFICIENT # OF DOMAINS')
110 BE=CUTOFF/10.0
SUM1=ECUT
SUM=0.0
SUM2=0.0
F=BE
```

```
1000 SUM2=SUM2+INTG(E)
1100 E=BE
1101 CUTOFF=10.0*E
1001 SUM1=SUM1+INTG(E)
1102 E=BE
1103 CUTOFF=10.0*E
1002 INTG=BE/6.0*(SUM1+2.0*SUM2+4.0*SUM4)
ITER=ITER+1
IF (ITER.GT.6) GO TO 60
DINTG(1)=EINTG
GO TO 40
60 DINTG(2)=DINTG(1)
DINTG(3)=EINTG
40 IF (ABS(EINTG-SUM4)/EINTG-ERROR) 50,50+50
50 SUM2=SUM2+SUM4
SUM4=EINTG
IF (DE>.5)
  GO TO 4
50 DINTG(1)=CUTOFF
DINTG(2)=EINTG
DINTG(3)=DE
IF (ITER.EQ.1) RETURN
EINTG=(16.0*DINTG(5)-DINTG(4))/15.0
RETURN
END
FUNCTION RCUR(T)
COMMON /EM/ DM, KEM, A, B, C, F, Z, IFLG, ICHN, DINTG(10)
KEM=EM/7
CALL INTG(EINTG)
RCUR=KEM**2*EXP(2.0)*DM*EINTG*(A-B/(1.0+C*B)**2)*FZ-1.0
RETURN
END
FUNCTION FINTG(E)
COMMON /EM/ DM, KEM, A, B, C, F, Z, IFLG, ICHN, DINTG(10)
P1=2.0*SORT(E)-RENE
IF (IFLG.GE.3) GO TO 10
IF (P1.GT.-20.0) GO TO 5
FINTG=0.0
RETURN
5 FINTG=E**2*EXP(P1)
RETURN
10 F=0.2755*(ALOG(E)-1.658)
F=-0.0228/(1+50*F*(1+0.226*F))
BETAS=EXP(F)
F2=P1*BETAS
IF (P1.GT.-20.0) GO TO 15
FINTG=(E/BETAS)**2*EXP(P2)*B2.0
RETURN
15 FINTG=(E/BETAS)**2*(EXP(P2)-EXP(P1))*(BETAS+1.0)**2.0
RETURN
END
END8
```









```

READ(LUM9,20) (IPANEL(I),I=1,NSECT)
DO 100 I=1,NSECT
C
IP=IPANEL(I)
READ(LUM9,20) (PERFAN(I),I=1,IP)
WRITE(LUM9,90) I,IPANEL(I),PERFAN(I),I=1,IP)
100 CONTINUE
901 FORMAT (1X,SECTOR NUMBER 8+12,8 NUMBER OF PANELS 8+12,
1 8 NR OF GRID POINTS PER PANEL 8+14)
READ(LUM9,20) (PANIND(J),J=1,NPOINT)
IF (IFAILT(13),EQ,0) RETURN
READ(LUM9,20) (IDTL(I),I=1,NSECT)
WRITE(LUM9,900) (IDTL(I),I=1,NSECT)
900 FORMAT (//,10X,SECTORS WHERE WE WANT A FINE STRUCTURE(//,1614))
C
READ(LUM9,20) (JDTL(J),J=1,NPOINT)
WRITE(LUM9,902) (JDTL(J),J=1,NPOINT)
902 FORMAT (//,10X,GRID POINTS WHERE WE WANT A FINE STRUCTURE(//,1616))
RETURN
99 WRITE(LUM9,30)
10 FORMAT (8,ERROR IN SECTOR DATA(//,))
WRITE(LUM9,35) NPOINT
15 FORMAT (8,NUMBER OF INDICES 8+13,8 IS NOT EQUAL
170 NUMBER OF POINTS 8+13)
C
C STOP
98 WRITE(LUM9,30)
WRITE(LUM9,31) I,J,SECIND(J)
31 FORMAT (8,INDEX(8,13,8) 8+13,8) 8+13)
C
C STOP
97 WRITE(LUM9,30)
WRITE(LUM9,32) I,SECIND(I)
32 FORMAT (8,INDEX(8,13,8) 8+13,8 IS LESS THAN UNITY)
C
C STOP
96 WRITE(LUM9,30)
WRITE(LUM9,33) I,SECIND(I),NPOINT
33 FORMAT (8,INDEX(8,13,8) 8+13,8 IS GREATER THAN
170 NUMBER OF POINTS 8+13)
C
C STOP
END
SUBROUTINE FINGRD
C
C PURPOSE:
C
C TO RESET ALL ARRAYS FOR A FINE DETAIL STRUCTURE OF SURFACE
C IN ORDER TO RESPECT GEOMETRY,INTERVALLES ARE DIVIDED BY THREE.
C
INTEGER PERSEC,SECIND,PERPAN,PANIND
COMMON PSAVE(144,10),CSAVE(144,10),PSECTR(144),CSECTR(144),
1DELEE(20),DELMAX(144),ENAX(144),ETA(20),BSCAT1(144),
2BSCAT2(144),BSCAT3(144),PHO(20,40),
3IANG(40),CPHMAX(144),SUMANG,ANGD,BOUNDL(20,40),BOUNDI(20,40),
4ANGL(20,40),VII(20,40),ICHECK(20,40),RATIO(13),IRODT(144),
5IFAULT(14),JLOCAL(144),ICOM(144),
6IVI(20),EVI(8),NLEU,NFINES,ILEV,TIMIN(20),TINAX(20),VINUM(20),
7A(144),B(144),C(144),BB(144),BM(144),TM(144),DM(144),
8SEM(144),TMOCOS(700),
9IFLG,NPOINT,ISYR,ISYR,IPDS,NSECT,PPEROD,PPEROD,IDIHY,
10GAMMA,DVUX(70,48),DVY(70,48),Y(144),DELTAK,DELTAY,
11YS(48,48),XS(48),XS(70),
12IVARBLE(4),T,DELT,SBOUND,NDIR,POT,M,J1,RPI,RP12,RPINAF,SOTPI,
132SAY,TEMP1,TEMP2,DEME1,DEME2,DEMI1,DEMI2,TEMP11,TEMP12,
14TEMP,LUM5,LUM6,LUM7,LUM8,LUM9,LUM10,
15IDTL(144),JDTL(144),PERSEC(144),SECIND(144),IPANEL(144),
16PERPAN(144,4),PANIND(144),
17ICION(144),CELEC(144),CSEC(144),CSECI(144),CPHOTO(144),
182CPHOT1(144),CBSCAT(144),CBSCA1(144),SECPRI(144),SECPRI(144),
193PMI(144),CGUM(144),
20IKASE,JOM,DPMI,NANG,RAD,PBOUND,OMEGA,ALPHA,SO,JP,IS,ECS,
212XPV12(20),EFTVI(20),IERROR,TETMIN,TETMAX,BETA1,BETA2,JLESS,
223LCARRIV,CPH,XI,CSECEL,CSECE1,CS,CB,CSI,CBI
EQUIVALENCE (IRODT(1),IDUMMY(1))
C
C *****
C
C IOLD=NSECT
C JOLD=NPOINT
C NPOINT=3*JOLD
C ANGD=ANGD/3.0
C SUMANG=SUMANG/3.0
C
C FIND NEW FLAGS OF CORRESPONDING GRID POINTS
C FIRST SAVE OLD VALUES
C
DO 100 J=1,JOLD
IF (JDTL(J),EQ,0) GO TO 102
IDUMMY(J83-2)=1
IDUMMY(J83-1)=1
IDUMMY(J83)=1
GO TO 100
102 IDUMMY(J83-2)=0
IDUMMY(J83-1)=1
IDUMMY(J83)=0
100 CONTINUE
C
C
C
C NOW RESET ARRAY
DO 110 J=1,NPOINT
110 JDTL(J)=IDUMMY(J)
C
C
C FIND NEW INDICES OF CORRESPONDING GRID POINTS
L=0
II=0
DO 112 I=1,IOLD
N=PERSEC(I)
N2=L*N
N1=L+1
DO 113 J=N1,N2
J=SECIND(NJ)
IF (ICOM(I),EQ,0,AND,ISYR,EQ,2) GO TO 1100
IDUMMY(NJ83-2)=J83-2
IDUMMY(NJ83-1)=J83-1
IDUMMY(NJ83)=J83
II=II+3
GO TO 113
1100 II=II+6
IDUMMY(II-5)=J83-2
IDUMMY(II-4)=SECIND(NJ+1)+83

```

```

IDUMMY(II-3)=J83-1
IDUMMY(II-2)=SECIND(NJ+1)+83
IDUMMY(II-1)=J83
GO TO 1111
1111 CONTINUE
C
1111 CONTINUE
L=L*N
112 CONTINUE
C
C NOW RESET ARRAY
DO 114 J=1,NPOINT
SECIND(J)=IDUMMY(J)
114 CONTINUE
C
C SET UP NEW INDICES OF GRID POINTS PER PANEL (FAMIND)
L=0
II=0
DO 251 I=1,IOLD
N=PERSEC(I)
N2=L*N
N1=L+1
DO 250 NJ=N1,N2
J=PANIND(NJ)
IF (ICOM(I),EQ,0,AND,ISYR,EQ,2) GO TO 2500
IDUMMY(NJ83-2)=J83-2
IDUMMY(NJ83-1)=J83-1
IDUMMY(NJ83)=J83
II=II+3
GO TO 250
2500 II=II+6
IDUMMY(II-5)=J83-2
IDUMMY(II-4)=PANIND(NJ+1)+83
IDUMMY(II-3)=J83-1
IDUMMY(II-2)=PANIND(NJ+1)+83-1
IDUMMY(II-1)=J83
IDUMMY(II)=PANIND(NJ+1)+83-2
GO TO 2501
250 CONTINUE
2501 CONTINUE
L=L*N
251 CONTINUE
C
CRESET ARRAY
DO 260 J=1,NPOINT
260 PANIND(J)=IDUMMY(J)
C
C
C FIND NEW NUMBER OF POINTS (PERSEC) PER NEW SECTOR
C IF AN OLD SECTOR IS INSULATOR,IT IS BROKEN INTO 3 NEW SECTORS
L=0
II=0
DO 120 I=1,IOLD
N=PERSEC(I)
IF (ICOM(I),EQ,1) II=II+1
IF (ICOM(I),EQ,1) IDUMMY(II)*38K
IF (ICOM(I),EQ,1) GO TO 120
II=II+3
IDUMMY(II-2)=1
IF (ISYR,NE,0) IDUMMY(II-2)=2
IDUMMY(II-1)=K
IDUMMY(II)=1
IF (ISYR,NE,0) IDUMMY(II)=2
120 CONTINUE
C
NSECT=II
C
C
C NOW REORGANIZE ARRAYS
DO 130 I=1,NSECT
130 PERSEC(I)=IDUMMY(I)
C
C
C SET NEW FLAGS IDTL FOR SECTORS
II=0
DO 140 I=1,IOLD
IF (ICOM(I),EQ,1) II=II+1
IF (ICOM(I),EQ,1) IDUMMY(II)=1
IF (ICOM(I),EQ,0,AND,IDTL(I),EQ,0) GO TO 150
IF (ICOM(I),EQ,0,AND,IDTL(I),EQ,1) GO TO 140
GO TO 140
150 II=II+3
IDUMMY(II-2)=0
IDUMMY(II-1)=1
IDUMMY(II)=0
GO TO 140
160 II=II+3
IDUMMY(II-2)=1
IDUMMY(II-1)=1
IDUMMY(II)=1
140 CONTINUE
C
C
C NOW REORGANIZE ARRAY
DO 170 I=1,NSECT
170 IDTL(I)=IDUMMY(I)
C
C
C SET UP NEW NUMBER OF GRID POINTS PER PANEL
II=0
DO 270 I=1,IOLD
IP=IPANEL(I)
IF (ICOM(I),EQ,1) II=II+1
IF (ICOM(I),EQ,1) IDUMMY(II)=IP
IF (ICOM(I),EQ,1) GO TO 280
II=II+3
IDUMMY(II-2)=1
IF (ISYR,NE,0) IDUMMY(II-2)=2
IDUMMY(II-1)=IP
IDUMMY(II)=1
IF (ISYR,NE,0) IDUMMY(II)=2
ID=IDUMMY(II-2)
DO 275 L=1,IB
IDUM(II-2,L)=1
275 IDUM(II)=L+1
C
280 DO 290 L=1,IP
IF (ICOM(I),EQ,1) IDUM(II,L)=PERPAN(I,L)
IF (ICOM(I),EQ,0) IDUM(II,L)=1
290 CONTINUE
270 CONTINUE
C
C
C NOW RESET ARRAYS
DO 284 I=1,NSECT

```

```

IPANEL(I)=IDUMMY(I)
IF(IPANEL(I) .EQ. 1)
  DO 295 I=1,IP
  PERPAN(I,L)=IDUM(I,L)
295 CONTINUE
C
C
C CONNECTIVITY OF NEW SECTORS
I1=0
DO 300 I=1,IOLD
  IF (ICOM(I).EQ.1) I1=I+1
  IF (ICOM(I).EQ.1) IDUMMY(I)=1
  IF (ICOM(I).EQ.1) GO TO 300
  I1=I+3
  IDUMMY(I1-2)=0
  IDUMMY(I1-1)=0
  IDUMMY(I1)=0
300 CONTINUE
C
C NOW REORGANIZE ARRAYS
DO 310 I=1,NSECT
  ICOM(I)=IDUMMY(I)
310 CONTINUE
C
C
C
C NOW RESET SURFACE PROPERTIES
C FIRST SAVE OLD J VALUES
DO 450 J=1,JOLD
  IDUMMY(J)=JLOCAL(J)
450 CONTINUE
C
  DO 460 J=1,JOLD
  JLOCAL(J83-2)=IDUMMY(J)
  JLOCAL(J83-1)=IDUMMY(J)
  JLOCAL(J83)=IDUMMY(J)
460 CONTINUE
C
C
C FIND NEW SURFACE PROPERTIES
C
  DO 470 J=1,NPOINT
  REWIND LUN3
480 READ(LUN3,500) JFIRST
500 FORMAT (I2)
  IF(JLOCAL(J).NE.JFIRST) GO TO 480
  READ(LUN3,301) DELMAX(J),EMAX(J),CPHONX(J)
  READ(LUN3,301) DELTAY(J),DELTAY(J),BSCAT2(J),BSCAT3(J)
  READ(LUN3,301) DELP(J),EXP(J)
470 CONTINUE
C
  WRITE(LUN9,900)
  900 FORMAT (//10X,'THE FINAL DETAIL STRUCTURE IS NOW SET UP',10X,40
  1('B'))
C
C WRITE NEW VALUES
C
  WRITE(LUN9,901) (JDTL(J),J=1,NPOINT)
  WRITE(LUN9,901) (SECIND(J),J=1,NPOINT)
  WRITE(LUN9,901) (PERSEC(I),I=1,NSECT)
  WRITE(LUN9,902) (IDTL(I),I=1,NSECT)
  WRITE(LUN9,901) (PANIND(J),J=1,NPOINT)
  WRITE(LUN9,902) (ICOM(I),I=1,NSECT)
  WRITE(LUN9,902)
  902 FORMAT (/)
  901 FORMAT (I2I2)
  DO 903 I=1,NSECT
  IP=IPANEL(I)
  WRITE(LUN9,902)
  WRITE(LUN9,901) (PERPAN(I,L),L=1,IP)
  903 CONTINUE
C
C
C
C RETURN
END
SUBROUTINE INTPOL(DUMMY)
C *****
C PURPOSE: TO INTERPOLATE VARIABLES FOR FINEGRID STRUCTURE
C *****
C
C
C DIMENSION DUMMY(1)
C DIMENSION X(144),Y(144),D(144)
C INTEGER PERSEC,SECIND,PERPAN,PANIND
C COMMON PSAVE(144,10),CSAVE(144,10),PSECTR(144),CSECTR(144),
C JDELE(20),DELMAX(144),EMAX(144),ETA(20),BSCATS(144),
C 2BSCAT2(144),BSCAT3(144),PHO(20,40),
C 1AND(40),CPHONX(144),BUNMD,AMND,BOUNDL(20,40),BOUNDS(20,40),
C 2ANGL(20,40),V(120,40),ICHECK(20,40),RATIO(13),IRDOT(144),
C 3IFAULT(14),JLOCAL(144),ICOM(144),
C IVI(20),EV(B),NLEV,NNTIME,ILEV,TIMN(20),TIMAX(20),VINUM(20),
C 26(144),B(144),C(144),BP(144),BM(144),TU(144),DU(144),
C SEM(144),IMOC(700)
C 1IFLG,NPOINT,N1,IGCRN,ISYN,IPDIS,NSECT,NPEROD,PPEROD,IDIHY,
C 20ANNA,DVUX(70,48),DVY(70,48),Y(144),DELTAY,DELTAY,
C 3VS(44,48),XS(44),XSB(70)
C 1VARBLE(4),T,DELT,BOUNDB,NDR,POT,N,J1,RP1,RP12,RPINAF,SBTP1,
C 2SAV,TEMP1,TEMP2,DEME,DENE2,DENI1,DENI2,TEMP11,TEMP12,
C 3TEMPR,LUN3,LUN4,LUN5,LUN6,LUN7,LUN8,LUN9,LUN10,
C 1DTL(144),JDL(144),PERSEC(144),SECIND(144),IPANEL(144),
C 2PERPAN(144,8),PANIND(144),
C 1ICOM(144),CELEC(144),CSEC(144),CSECI(144),CPHOTD(144),
C 2CPHOT1(144),CBSCAT(144),CBSCA1(144),SECPRN(144),SECPR1(144),
C 3PHI(144),COUM(144)
C 1RASE,JOML,BPHI,MMND,RAD,PBOND,OMEGA,ALPHA,SO,JP,IS,ECS,
C 2EXPUS(20),EFUS(20),IERROR,TEHIN,TEHAX,BETA1,BETA2,JLESS,
C 3L2,CARRIV,CPH,VI,CSECEL,CCECEI,CS,CP,CS1,CD1
C EQUIVALENCE (X(1),A(1)),(Y(1),B(1)),(D(1),DM(1))
C
C
C IF SECTORS ARE CONDUCTORS, INTERPOLATION IS DONE PER PANEL
C IF SECTORS ARE INSULATORS, INTERPOLATION IS DONE BETWEEN ADJACENT SECT
C
C DESCRIPTION OF VARIABLES
C JSTART: INDEX WHERE TO FIND FIRST GRID POINT OF SECTOR
C XX AND YY: TEMPORARY STORAGE FOR INTERPOLATION
C B,C,D COEFFICIENT FOR SPLINE
C
  JSTART=1
  I=0

```

```

C LOOP OVER SECTORS
1000 I=1
  IF (I.DT.NSECT) RETURN
C DO DIFFERENT SHERES IF INSULATORS OR CONDUCTORS
  IF (ICOM(I).EQ.0) GO TO 10
C
C NOW DO INTERPOLATION FOR CONDUCTORS, FIND NO OF PANELS
  IP=IPANEL(I)
C FIND NR OF GRID POINTS PER PANEL AND ACCUMULATE FUNCTION VALUES
C WHEN JDTL(I)=1
  DO 2 J1=1,IP
  JF=PERPAN(J1,I)
  JEND=JF+JSTART-1
C NOW ACCUMULATE DATA
  DO 3 J1=JSTART,JEND
  JF=JF+1
  JF=PANIND(J1)
  IF (JDTL(J1).EQ.1) XX(J1)=DELTAY(J1-1)
  IF (JDTL(J1).EQ.1) YY(J1)=DUMMY(J1)
  3 CONTINUE
C
C NOW CALL INTERPOLATION ROUTINE
C IF JF=JP NO INTERPOLATION NEEDED FOR THAT PANEL
  IF (JF.EQ.JP) GO TO 8
C
  CALL SPLINE (JF,XX,YY,B,C,D)
C
  DO 7 J1=JSTART,JEND
  JF=PANIND(J1)
  IF (JDTL(J1).EQ.0) DUMMY(J1)=SPIDER(J1,DELTAY(J1-1),XX,Y,B,C,D)
  7 CONTINUE
C
  8 JSTART=JEND+1
  2 CONTINUE
  GO TO 1000
C
C INTERPOLATION FOR INSULATORS
C
  10 CONTINUE
C DO INTERPOLATION OF EXTRAPOLATION BETWEEN KNOWN SECTORS,
C TAKING INTO ACCOUNT THE SURFACE PROPERTIES OF SECTORS
C
  IF (IDTL(I).EQ.1) JSTART=JSTART+PERSEC(I)
  IF (IDTL(I).EQ.1) GO TO 1000
C
C SEE IF WE CAN DO AN INTERPOLATION
  J1=JSTART
  I1=1
  11 I1=I1-1
  IF (I1.LE.0) GO TO 20
  J1=J1-PERSEC(I1)
  IF (IDTL(I1).EQ.0) GO TO 11
  I2=I1
  J2=JSTART
  12 I2=I2+1
  IF (I2.GT.NSECT) GO TO 30
  J2=J2+PERSEC(I2-1)
  IF (IDTL(I2).EQ.0) GO TO 12
C
C FUNCTION IS NOW KNOWN AT SECTORS I1 AND I2
C NOW CHECK IF SURFACE PROPERTIES ARE IDENTICAL AT I1 AND I2
  IF (ICOM(I1).NE.0) GO TO 20
  IF (ICOM(I2).NE.0) GO TO 30
  JJ=SECIND(I)
  J1=SECIND(I1)
  J2=SECIND(I2)
  IF (JLOCAL(J1).NE.JLOCAL(J2)) GO TO 20
  IF (JLOCAL(J2).NE.JLOCAL(J1)) GO TO 30
  40 DUMMY(J1)=(DUMMY(J2)-DUMMY(J1))/(Y(J2)-Y(J1))*Y(J1)+(DUMMY(J1)
  1+DUMMY(J2))
  IF (ISYN.EQ.2) DUMMY(NPOINT-JJ+1)=DUMMY(J1)
  JSTART=JSTART+PERSEC(I)
  GO TO 1000
C
C DO EXTRAPOLATION FROM RIGHT OF I
  20 I1=1
  J1=JSTART
  21 I1=I1+1
  J1=J1+PERSEC(I1-1)
  IF (ICOM(I1).EQ.0) GO TO 21
  I2=I1
  J2=J1
  22 I2=I2+1
  J2=J2+PERSEC(I2-1)
  IF (ICOM(I2).EQ.0) GO TO 22
  GO TO 40
C
C DO EXTRAPOLATION FROM LEFT OF I
  30 I1=1
  J1=JSTART
  31 I1=I1-1
  J1=J1-PERSEC(I1)
  IF (ICOM(I1).EQ.0) GO TO 31
  I2=I1
  J2=J1
  32 I2=I2-1
  J2=J2-PERSEC(I2)
  IF (ICOM(I2).EQ.0) GO TO 32
  GO TO 40
C
C
C SUBROUTINE SPLINE(N,X,Y,B,C,D)
C REF: HALLON AND ROLLER
C DIMENSION X(N),Y(N),B(N),C(N),D(N)
C
C THE COEFFICIENTS B(I),C(I),AND D(I), I=1,2,...,N ARE COMPUTED
C FOR A CUBIC INTERPOLATING SPLINE
C
C SX=X(I)+B(I)X(X-I)+C(I)X(X-I)**2+D(I)X(X-I)**3
C
C FOR X(I)-LE.X(I+1)
C
C INPUT
C N=NUMBER OF DATA POINTS
C X=ABSCISSA
C Y=ORDINATES
C
C OUTPUT
C B,C,D=ARRAYS OF SPLINE COEFFICIENTS
C
  N=N-1
  IF (N.LT.2) STOP
  IF (N.LT.3) GO TO 50
C
C SET UP TRIANGULAR SYSTEM

```



```

      U=UANKIV/CPN*XI*CSCEC/CSCE1*CS*CB*CS1*CB1
      DATA NLUN9/10.0/
      N=NPOINT
      IF (IFIG.EQ.1) GO TO 100
      COMPUTE LINEAR SPACE CHARGE
      RLNDA=0.0
      DEBY=AVSQR(TEMPR*1.6E-19/(DENI181.JNL-21))
      IF (IFALT(14).EQ.1)
      1 RLNDA=RAD/DEBY**2*(DENI1/TEMPE1+DENE2/TEMPE2+DENI2/TEMPI1+
      1 DENI2/TEMPI2+TEMPI/DEMI1
      DELTAX=SRND/FLD*H*1
      DELTAY=RP12/FLD*H*1
      SYX=(DELTAY/DELTAX)**2
      GENERATE GRID POINTS, COEFFICIENTS AND RHS OF EQUATION (1,N,1)
      100 NMI=1
      DO 200 J=1,N
      Y(J)=FLOAT(J-1)*DELTAY+ANGD
      IF (Y(J).LT.0.0.OR.Y(J).GT.RP12) STOP
      YS(N,J)=SYX*SRND
      DO 210 I=2,NMI
      YS(I,J)=0.
      210 CONTINUE
      200 CONTINUE
      PREPARE DATA FOR POISSON SOLVER
      TLNDA=RLNDA*DELTAX**2
      DO 220 I=1,N
      XS(I)=FLOAT(I)*DELTAX
      AC(I)=SYX
      B(I)=-2.*SYX-TLNDA*EXP(2.*XS(I))
      C(I)=SYX
      220 CONTINUE
      AC(1)=0.
      C(N)=0.
      250 IF (IPOIS-1) 300,301,310
      CALL GUESS FIELD
      300 CALL GUESS
      IPOIS=IPOIS+1
      301 DO 230 J=1,N
      YS(I,J)=SYX*PHI(J)
      230 CONTINUE
      CALL POISSON SOLVER
      CALL POT
      IF (ERROR.NE.0) WRITE(LUN9,121) IERROR
      121 FORMAT(8 ERROR IN POISSON FIELD,IERROR=8,13////)
      COMPUTE APPROXIMATE STEPSIZE FOR ORBIT INTEGRATION
      H=DELTAX/HCONS
      IF (H)
      RETURN
      READ IN POTENTIAL AT THE SURFACE
      310 WRITE(LUN9,2345)
      2345 FORMAT (//////20X,8THE INITIAL POTENTIAL AT THE SURFACE IS,
      1 /20X8-----9//)
      READ(LUN10,122) (PHI(J),J=1,N)
      122 FORMAT(AE12.5)
      WRITE(LUN9,1220) (PHI(J),J=1,N)
      1220 FORMAT(41X,1PE12.5)
      IPOIS=1
      GO TO 301
      END
      SUBROUTINE DIVPOT
      C *****
      C PURPOSE
      C TO COMPUTE DERIVATIVES OF POTENTIAL IN X AND Y DIRECTIONS AND
      C TO RESET POTENTIAL ARRAY.
      C DESCRIPTION OF THE VARIABLES
      C DVDX IS N.D. FINITE DIFFERENCE DERIVATIVE OF POTENTIAL IN X DIR
      C DVDY IS N.D. FINITE DIFFERENCE DERIVATIVE OF POTENTIAL IN Y DIR
      C N IS NUMBER OF INTERVALS IN Y DIRECTION
      C NP2 IS NUMBER OF GRID POINTS IN X DIRECTION
      C PHI IS POTENTIAL AT THE SURFACE OF SPACECRAFT
      C PBOUNL IS OUTER BOUNDARY FOR POTENTIAL
      C SBOUNL IS OUTER LIMIT FOR RADIAL DISTANCE
      C XS IS RADIAL DISTANCE IN I DIRECTION INCLUDING BOUNDARY POINTS
      C XSB IS ARRAY USED IN FUNCTION RANGE
      C YS IS POTENTIAL MATRIX CHANGED TO INCLUDE BOUNDARY POINTS
      C *****
      C EXTERNALS NONE
      C *****
      INTEGER PERSEC,SECIND,PERPAN,PANIND
      IMPLICIT REAL8 (A-H,O-Z)
      COMMON PSAVE(144,10),CSAVE(144,10),PSECTR(144),CSECTR(144),
      1DELEE(20),DELMAX(144),ENAX(144),ETA(20),BSCAT1(144),
      2BSCAT2(144),BSCAT3(144),PHI(20,40),
      1ANG(40),CPNDX(144),SUMANG,ANGD,BOUNDL(20,40),BOUNL(20,40),
      2ANGL(20,40),V1(20,40),ICHECK(20,40),RATIO(13),TRODT(144),
      3IFALT(14),ALCAL(144),ICOM(144),
      1V1(20),EV(8),NLEV,NTIME,ILEV,TIRIN(20),TIPAK(20),VIMUN(20),
      2A1(144),B1(144),C1(144),B1(144),BM(144),TM(144),DM(144),
      3EM(144),TMDCS(700),
      1IFLO,MPDINT,N,IOEDN,ISYN,IPOIS,NSECT,NPEROD,NPEROD,IBINY,
      2GAMMA,DVXB(70,40),DVY(70,40),Y(144),DELTAX,DELTAY,
      3YS(66,40),XS(66),XS(70),
      1VARIABLE(4),T,DELT,SBOUNL,NDIN,POT,N,J1,RP1,RP12,RP1NF,SBTPI,
      2BAY,TEMPE1,TEMPE2,DENE1,DENE2,DENI1,DENI2,TEMPI2,
      3TEMPI,LUM1,LUM4,LUM5,LUM6,LUM7,LUM8,LUM9,LUM10,
      1IDTL(144),JDTL(144),PERSEC(144),SECIND(144),IPANEL(144),
      2PERPANI(144,4),PANIND(144),
      1ICOM(144),CELEC(144),CSEC(144),CSEC1(144),CPHOTO(144),
      2CPHOT1(144),CBSCAT(144),CBSCA1(144),BECPRN(144),BECPR1(144),
      3PHI(144),COLN(144),
      1KASE,JOHL,DPHI,MMAG,RAD,PBOUND,ONEGA,ALPHA,SO,JP,IS,ECS,
      2EPTV1(20),EPTV2(20),IERROR,TETMIN,TETMAX,BETA1,BETA2,ALSS,
      3L2,CARRIV,CPN,XI,CSCEC,CSECE1,CS,CB,CS1,CB1
      NP3=NP3
      NP2=NP2
      NP1=NP1
      N=NPOINT
      XSB(NP2)=SBOUNL
      DO 10 I=2,NP1
      IPA=NP2-I
      IF (IPA)
      XS(I)=XS(IPA)
      10 CONTINUE
      XS(1)=SO
      XS(N)=SO
      XS(2)=NO*DELTAX
      NP2=1+NP2
      XS(N)=XS-1+DELTAX
      20 CONTINUE
      XS(NP2)=SBOUNL
      DO 40 J=1,N
      YS(NP2,J)=PBOUND
      DO 30 I=2,NP1
      DVDX(I,J)=-(YS(I,J)+YS(I-1,J)-1.0*YS(1,J))/2./DELTAX
      DVDX(NP2,J)=(3.0*YS(NP2,J)-4.0*YS(NP1,J)+YS(N,J))/2./DELTAX
      30 CONTINUE
      DVX(NP2,J)=-(3.0*YS(NP2,J)-4.0*YS(NP1,J)+YS(N,J))/2./DELTAX
      40 CONTINUE
      COMPUTATION OF THE DERIVATIVES IN RADIAL DISTANCES
      C BY FINITE DIFFERENCES
      DO 50 J=1,N
      DVDX(I,J)=-(YS(I,J)+YS(I-1,J)-1.0*YS(1,J))/2./DELTAX
      DVX(NP2,J)=(3.0*YS(NP2,J)-4.0*YS(NP1,J)+YS(N,J))/2./DELTAX
      50 CONTINUE
      DO 60 J=1,N
      DO 60 I=2,NP2
      DVDX(I,J)=(YS(I,J)-YS(I-1,J))/DELTAX
      60 CONTINUE
      CALCULATION OF DVDY IN J DIRECTION OR ANGLES
      DO 70 I=1,NP2
      DO 70 J=1,N
      JP1=J+1
      IF (J.EQ.N) JP1=1
      DVDX(I,J)=(YS(I,JP1)-YS(I,J))/DELTAY
      70 CONTINUE
      RETURN
      END
      SUBROUTINE ION
      C *****
      C PURPOSE
      C TO COMPUTE ION CURRENT AT A GIVEN GRID POINT. THE DISTRIBUTION FUNCTIO
      C IS APPROXIMATED BY A DISCRETE NUMBER OF LEVELS. FOR EACH OF THESE
      C LEVELS, THE PHASE SPACE BOUNDARIES ARE DETERMINED BY FOLLOWING
      C ION TRAJECTORIES BACKWARDS.
      C I=SUM FROM J=1 TO J=JMAX OF INTEGRAL FROM U(I) TO U(I+1) OF
      C DUBF(U)*SUBS(COS(ANG1(U))-COS(ANG2(U)))
      C *****
      C DESCRIPTION OF THE VARIABLES
      C BETAI=V182 IS NONDIMENSIONAL ENERGY OF IONS AT INFINITY
      C BETAJ=BETA1*PHI(J) IS ION KINETIC ENERGY AT SURFACE.
      C IOM IS ION CURRENT
      C DELP COEFFICIENT FOR SECONDARY EMISSION DUE TO PROTONS
      C EXMP COEFFICIENT FOR SECONDARY EMISSION DUE TO PROTONS
      C N IS NUMBER OF GRID POINT AT SURFACE
      C NLEV IS TOTAL NUMBER OF NONDEGENERATE LEVELS
      C ILEV SELECTS THE NUMBER OF NONDEGENERATE LEVELS USED (ILEV=2
      C ITER NUMBER OF ITERATIONS
      C JOHL IS FLAG
      C IF JOHL=0,ORBITS ARE FOLLOWED NUMERICALLY.
      C SECPRN CURRENT DUE TO SECONDARY ELECTRONS INDUCED BY PROTONS
      C SECPR1 CURRENT DUE TO SECONDARY ELECTRONS INDUCED BY PROTONS
      C LEAVING THE SURFACE.
      C TETMIN MAXIMUM ACCEPTANCE ANGLE
      C TETMIN MINIMUM ACCEPTANCE ANGLE
      C UACC IS ACCURACY DESIRED ON VELOCITY SPACE MINIMUM
      C VZERO IS MINIMUM KINETIC VELOCITY AT SPACECRAFT SURFACE.
      C *****
      C EXTERNALS
      C ANAX1
      C COEFF
      C EXP
      C DEMORB
      C ORBIT
      C *****
      INTEGER PERSEC,SECIND,PERPAN,PANIND
      IMPLICIT REAL8 (A-H,O-Z)
      COMMON PSAVE(144,10),CSAVE(144,10),PSECTR(144),CSECTR(144),
      1DELEE(20),DELMAX(144),ENAX(144),ETA(20),BSCAT1(144),
      2BSCAT2(144),BSCAT3(144),PHI(20,40),
      1ANG(40),CPNDX(144),SUMANG,ANGD,BOUNDL(20,40),BOUNL(20,40),
      2ANGL(20,40),V1(20,40),ICHECK(20,40),RATIO(13),TRODT(144),
      3IFALT(14),ALCAL(144),ICOM(144),
      1V1(20),EV(8),NLEV,NTIME,ILEV,TIRIN(20),TIPAK(20),VIMUN(20),
      2A1(144),B1(144),C1(144),B1(144),BM(144),TM(144),DM(144),
      3EM(144),TMDCS(700),
      1IFLO,MPDINT,N,IOEDN,ISYN,IPOIS,NSECT,NPEROD,NPEROD,IBINY,
      2GAMMA,DVXB(70,40),DVY(70,40),Y(144),DELTAX,DELTAY,
      3YS(66,40),XS(66),XS(70),
      1VARIABLE(4),T,DELT,SBOUNL,NDIN,POT,N,J1,RP1,RP12,RP1NF,SBTPI,
      2BAY,TEMPE1,TEMPE2,DENE1,DENE2,DENI1,DENI2,TEMPI2,
      3TEMPI,LUM1,LUM4,LUM5,LUM6,LUM7,LUM8,LUM9,LUM10,
      1IDTL(144),JDTL(144),PERSEC(144),SECIND(144),IPANEL(144),
      2PERPANI(144,4),PANIND(144),
      1ICOM(144),CELEC(144),CSEC(144),CSEC1(144),CPHOTO(144),
      2CPHOT1(144),CBSCAT(144),CBSCA1(144),BECPRN(144),BECPR1(144),
      3PHI(144),COLN(144),
      1KASE,JOHL,DPHI,MMAG,RAD,PBOUND,ONEGA,ALPHA,SO,JP,IS,ECS,
      2EPTV1(20),EPTV2(20),IERROR,TETMIN,TETMAX,BETA1,BETA2,ALSS,
      3L2,CARRIV,CPN,XI,CSCEC,CSECE1,CS,CB,CS1,CB1
      DATA UACC/1.E-3/
      C *****

```

```

      IF (TEMP11.NE.0.0) C11=1.0/SAY(SORT(XI/RATIO8))
      1 COEFF(SORT(XI/RATIO8))=RATIO10
      IF (TEMP12.NE.0.0) C12=1.0/SAY(SORT(XI/RATIO11))
      1 COEFF(SORT(XI/RATIO11))=RATIO12/DEN12/DEN11
      C10M(J)=C11+C12
      GO TO 714
*13 IF (TEMP11.NE.0.0) C11=EXP(-XI/RATIO8)*RATIO10
      IF (TEMP12.NE.0.0) C12=EXP(-XI/RATIO11)*RATIO12/DEN12/DEN11
      C10M(J)=C11+C12
      GO TO 715
*14 CONTINUE
*****
C LOOP IF MAXWELLIAN DISTRIBUTION
      NDIM=4
      DO 710 J=1,2
      IF (J.NE.1) GO TO 711
      GAMMA=RATIO8
      TEMP1=TEMP11
      DEN1=1.0
      RATE=RATIO7
      GO TO 712
*11 CONTINUE
      GAMMA=RATIO11
      TEMP1=TEMP12
      DEN1=DEN12/DEN11
      RATE=RATIO12
*12 CONTINUE
C
      NUM=1
      IF (DEN.EQ.0.0) GO TO 710
      NTOUR=1
      IF (PHI(J).GT.0.0) NUM=1
C COMPUTE MINIMUM KINETIC VELOCITY AT COLLECTOR SURFACE.
      VZERO=0.0
      IF (PHI(J).NE.0.0)
      1 VZERO=AMX1(10.0)/PHI(J)/GAMMA/SORT(ABS(PHI(J)/GAMMA))/
      2 ABS(PHI(J)/GAMMA)
C
C COMPUTE FOR WHICH ENERGY LEVELS PARTICLES ARE ESCAPING.
      DO 700 I=1,MLEV
      BETA1=V1+I*BE2
      BETA2=BETA1-PHI(J)/GAMMA
      IF (BETA2.LE.0.) GO TO 700
C IF ENERGY AT SURFACE (BETA2) IS LESS THAN ZERO, GO ON TO NEXT ENERGY
      TETMIN=0.0
      TETMAX=PI
C COMPUTE ACCEPTANCE ANGLES FOR A GIVEN ENERGY LEVEL
C IF ORBITS CORRESPONDING TO LOW ENERGY LEVELS ARE OML, DO NOT
C COMPUTE ORBITS FOR HIGHER ENERGY LEVELS.
      IF (NTOUR.EQ.1)
      1 CALL GENORB
      IF (TETMIN.LE.0.0.AND.TETMAX.GE.PI) NTOUR=0
      NUM=NUM+1
      TIRIN(NUM)=TETMIN
      TIRAX(NUM)=TETMAX
      VINUM(NUM)=SORT(BETA2)
C COMPUTE COEFFICIENT FOR SECONDARY ELECTRONS INDUCED BY PROTONS
      IF (IFAU1(9).EQ.1)
      1 DELEC(NUM)=DELP(J)*SORT(1.0010BETA20TEMP1)/(1.0+BETA20TEMP1/
      1 EXPR(J))
      700 CONTINUE
C
      IF (NUM.LE.1) GO TO 705
C
C COMPUTE ACCEPTANCE ANGLES FOR THE LOWEST ENERGY LEVEL
      TZERO=(TIRIN(2)+TIRAX(2))/2.
      UNIN=VINUM(2)
      810 VMBD=(VMBD+TZERO)/2.
      VARBLE(1)=SO
      VARBLE(2)=VMBD*(1+TZERO)
      VARBLE(3)=Y(J)
      VARBLE(4)=VMBD*COS(TZERO)
      7=0.
      DELT=H
      BETA1=VMBD+VPHI(J)/GAMMA
      CALL ORBIT
      IF (VARBLE(1).GE.(SBOUND-DELTAX)) UNIN=VMBD
      IF (VARBLE(1).LT.SVZERO) VMBD
      IF (ABS(UNIN-TZERO).GT.VACC) GO TO 810
      VINUM(1)=UNIN
      BETA2=VMBD+BE2
      BETA1=BETA2+PHI(J)/GAMMA
      TETMIN=TIRIN(2)
      TETMAX=TIRAX(2)
      TIRIN(1)=TZERO
      TIRAX(1)=TZERO
      CALL GENORB
      IF (J.LESS.EQ.2) GO TO 800
      TIRIN(1)=TETMIN
      TIRAX(1)=TETMAX
      800 NUM1=NUM-1
      IF (IFAU1(9).EQ.1)
      1 DELEC(1)=DELP(J)*SORT(1.0010BETA20TEMP1)/(1.0+BETA20TEMP1/
      1 EXPR(J))
      WRITE (LUM6,610) J, J, TIRIN(1), I=1, NUM1
      610 FORMAT (1X, I=0, 15, 7J, 8, 15, 8ACCEPTANCE ANGLES FOR IONS#
      1 (101X, 1P10, 3))
      WRITE (LUM6,611) TIRAX(1), I=1, NUM1
      611 FORMAT (101X, 1P10, 3)
      WRITE (LUM6,612)
      612 FORMAT (1X, 8, 15, 8VELOCITY LEVELS FOR IONS#)
      WRITE (LUM6,613) (VINUM(I), I=1, NUM1)

```

```

      CUFF=1.0/PHI(J)/GAMMA/SORT(
      AMX1(10.0)
      MLEV=0
      ADEL=0.0
      MDEL=0.0
      DO 810 I=1, NUM1
      DENM(VINUM(I)+VINUM(I))
      AMIN=(COS(TIRIN(I))+COS(TIRIN(I))) DENM
      MMIN=(COS(TIRIN(I))-AMIN)/VINUM(I)
      AMAX=(COS(TIRAX(I))+COS(TIRAX(I))) DENM
      MMAX=(COS(TIRAX(I))-AMAX)/VINUM(I)
      AMI1=AMIN-AMAX
      MLI1=MMIN-MMAX
      LUM1=CUFF*EXP(-VINUM(I)*BE2)/(AMAX1-AMIX0)*C1(VINUM(I)*BE2)
      LUMI11=MMI10*(VINUM(I)+CDEFT(VINUM(I)))
      IF (IFAU1(9).EQ.0.0) GO TO 815
      ADEL1=COS(TIRIN(I))*DELEC(I)+1-COS(TIRIN(I))/MNUM
      MDEL1=DELEC(I)*SLOS(TIRIN(I))-ADEL(VINUM(I))
      AMI1M=(COS(TIRAX(I))*DELEC(I)+1-COS(TIRAX(I))/DENM
      MDEL1M=DELEC(I)*SLOS(TIRAX(I))-ADEL(VINUM(I))
      ADEL1=ADEL1-AMIN1
      MDEL1=MDEL1-MMIN1
      LUM1=CUFF*EXP(-VINUM(I)*BE2)/(ADEL1-ADEL0)*C1(VINUM(I)*BE2)
      1 (MDEL1-MDEL0)/(VINUM(I)+CDEFT(VINUM(I)))
      AMI10=ADEL1
      MLI10=MDEL1
      810 AMIX0=AMI11
      MLI0=MLI11
      810 CONTINUE
C
C COMPUTATION OF ION CURRENT
C
      C10M(J)=C10M(J)+CUFF*ICUR1*BRATE*DEN
      CUR2=CUR2
      IF (PHI(J).GT.0.0) CUR2=
      1 (2.0/SAY(SORT(1-PHI(J)/RATIO(13))+CDEFT(SORT(1-PHI(J)/
      2 RATIO(13))))*EXP(PHI(J)/RATIO(13))*CLWC
      SECPRM(J)=SECPRM(J)+CUFF*ICUR2*BRATE*DEN
      SECPRI(J)=SECPRI(J)+CUFF*ICUR2*BRATE*DEN
      GO TO 710
*705 CONTINUE
*710 CONTINUE
*715 CONTINUE
      RETURN
      END
SUBROUTINE ELEC
*****
C PURPOSE
C TO COMPUTE ELECTRON CURRENT AT EACH GRID POINT AND
C CURRENT DUE TO EMITTED SECONDARIES AND BACKSCATTERS
C 1=SUM FROM I TO J=MAX OF INTEGRAL FROM U(1) TO U(I+1)
C OF DUB(U)*SUB(CDS(ALPHA2(U))-COS(ALPHA(U)))
C
C DESCRIPTION OF THE VARIABLES
C BETA1=MI*BE2 IS NONDIMENSIONAL ELECTRON ENERGY.
C BETA2=BETA1-ALPHA(J)/GAMMA IS ELECTRON KINETIC ENERGY AT SURFACE
C CSEC IS SECONDARY CURRENT
C CSECI IS SECONDARY CURRENT LEAVING THE SURFACE
C CBSCAT IS BSCATTER CURRENT
C CBSCAT1 IS BSCATTER CURRENT LEAVING THE SURFACE
C IFA IS COEFFICIENT USED IN THE COMPUTATION OF BSCATTERS.
C DELEC IS COEFFICIENT USED IN THE COMPUTATION OF SECONDARIES
C *THE COEFFICIENTS IN THE FORMULAE CORRESPOND TO STERNGLASS
C EQUATION, THEY ARE TAKEN FROM AMOTT'S PAPER.
C ILEV SELECTS THE NUMBER OF MONOENERGETIC LEVELS BEFORE
C ITER IS NUMBER OF ITERATIONS
C IFAU1 IS A FLAG FOR SECONDARIES AND BSCATTERS.
C JOML IS A FLAG
C JOML=0, ACCEPTANCE ANGLES ARE COMPUTED NUMERICALLY.
C JOML=1, ACCEPTANCE ANGLES ARE ASSUMED TO BE OML
C TETMAX IS MAXIMUM ACCEPTANCE ANGLE.
C VACC IS ACCURACY DESIRED ON VELOCITY SPACE MINI
C VZERO IS MINIMUM KINETIC VELOCITY AT COLLECTOR SURFACE
C
C EXTERNALS
C AMAX1
C CDEFT
C EXP
C GENORB
C ORBIT
*****
      IMPLICIT REAL8 (A-H,O-Z)
      INTEGER PERSEC, BECIB, PERPAN, PANIND
      COMMON PSAVE(144,10), CSAVE(144,10), PBECTR(144), CBECTR(144),
      1 BELEC(20), DELMAX(144), EMAX(144), ETA(20), BSCAT1(144),
      2 BSCAT2(144), BSCAT3(144), PMD(20,40),
      3 IAND(40), CPMD(144), BUNARD, ARND, BOUNDL(20,40), BOUND1(20,40),
      4 2NML(20,40), V1(20,40), ICHECK(20,40), RATIO(13), IROOT(144),
      5 IFAULT(14), JLOCAL(144), ICON(144),
      6 V1(20), EV(8), MLEV, NTINEB, ILEV, TIRIN(20), TIRAX(20), VINUM(20),
      7 2A(144), B(144), C(144), BB(144), BU(144), DU(144),
      8 SEM(144), TWCOR(700),
      9 IFLG, NPODIR, ICOND, ISTN, IPOIS, HSECT, NPEROD, NPEROD, IDIRY,
      10 26GAMMA, DUBX(70,40), DUBY(70,40), Y(144), DELTAX, DELTAY,
      11 3YB(44,40), X5(44), X5B(70),
      12 VARBLE(4), T, DELT, SBOUND, MDIN, PDT, H, J1, RPI, RP12, RPINAF, SOTPI,
      13 28AY, TPE1, TPE2, DEBE1, DEBE2, DEN1, DEN12, DEN13, TEMP11, TEMP12,
      14 STPRP, LUM3, LUM4, LUM5, LUM6, LUM7, LUM8, LUM9, LUM10,
      15 IDTL(144), JDTL(144), PERSEC(144), SECIND(144), IPANEL(144),
      16 2PERPAN(144,4), PANIND(144),
      17 IC10M(144), CELEC(144), CSEC(144), CBECI(144), CPNOTD(144),
      18 2CPNOTD(144), CBSCAT(144), CBSCA(144), SECPRI(144), SECPRI1(144),
      19 3PHI(144), COUN(144),
      20 IASE, JOML, DPPI, MAND, RAD, PBOUND, DPEGA, ALPHA, BO, JP, IS, ECB,
      21 2EXP12(20), EFTV(20), IERROR, TETMIN, TETMAX, BETA1, BETA2, JLESS,
      22 3L2, CARRIV, CPH, XI, CSECEL, CSECEL, CB, CB, CB1, CB1
      DATA VACC/1.E-3/
*****
      J=JP
C INITIALIZE CURRENTS TO ZERO
      NDIM=4
      CELEC(J)=0.0
      CSECI(J)=0.0
      CBSCAT(J)=0.0
      CBSCA(J)=0.0
      CBECI(J)=0.0
      IF (JOML.EQ.0) GO TO 714
C COMPUTE ELECTRON CURRENT USING OML CONDITIONS
      XI=PHI(J)
      CS=0.0
      CB=0.0
      CB1=0.0
      CB1=0.0
      CEI=0.0
      CEI=0.0
      IF (IFAU1(3).NE.0.0) IF (IFAU1(4).NE.0.0) CALL CBS
      CSECI(J)=CS
      PARF(1)=CF1

```





```

      INTEGRA PERSEC=SECIND*PERPAN*PANIND
      COMMON PSAVE(144,10),CSAVE(144,10),PSECTR(144),CSECTR(144),
      1DELEE(20),DELMAX(144),EMAX(144),ETA(20),BSCAT(144),
      2BSCAT(144),BSCAT3(144),PHO(20,40),
      3LANG(40),CPHOMX(144),SUNANG,ANGD,BOUNDL(20,40),BOUND(20,40),
      4WANGL(20,40),VII(20,40),ICHECK(20,40),RATIO(13),IROOT(144),
      5IFAULT(14),JLOCAL(144),ICOM(144),
      6IVI(20),EVB(8),NLEV,NTIMES,ILEV,TIMIN(20),TIMAX(20),VINUM(20),
      7TA(144),B(144),C(144),BB(144),BM(144),TM(144),DM(144),
      8SEM(144),TWCOS(700),
      9IFLG,NPOINT,N,IGEDN,ISYN,IPDIS,NSECT,NPEROD,NPEROD,IDIAY,
      10GAMMA,DVUX(70,48),DVUY(70,48),Y(144),DELTA,DELTA,
      113YS(66,48),XS(66),XSS(70),
      12VARIABLE(4),T,DELTA,SBOUND,NDIM,POT,M,J1,RP1,RP12,RP1NAF,SGTPI,
      13SAY,TEMP1,TEMP2,DEME1,DEME2,DEMI1,DEMI2,TEMP11,TEMP12,
      143TEMPR,LUN3,LUN4,LUN5,LUN6,LUN7,LUN8,LUN9,LUN10,
      15IDTL(144),JDTL(144),PERSEC(144),SECIND(144),IPANEL(144),
      16PERPAN(144,4),PANIND(144),
      17ICDM(144),CSECEL(144),CSECI(144),CSECI(144),CPHOT(144),
      182CPHOT1(144),CBSCAT(144),CBSCA1(144),SECPRN(144),SECPRI(144),
      193PHI(144),CGUN(144),
      20IKASE,JOHL,DPHI,NANG,RAD,PBOUND,OMEGA,ALPHA,SO,JP,IS,ECS,
      21CEXP(20),EFTVI(20),IERROR,TETMIN,TETMAX,BETA1,BETA2,JLESS,
      223L,CARRIV,CPH,XI,CSECEL,CSECI,CS,CS,CS1,CS1
C THIS SUBROUTINE CALCULATES THE SECONDARY CURRENT CSEC
C CSEC CONSISTS OF TWO PARTS:CSEL,MAIN SECONDARY CURRENT
C LEAVING A LOCATION,AND CARRIV,SECONDARY
C CURRENT ARRIVING AT A LOCATION FROM OTHER PORTIONS OF THE CRAFT
C PHI IS POTENTIAL ON SPACECRAFT SURFACE
C N IS NUMBER OF GRID POINTS ON SPACECRAFT SURFACE
C NANG IS NUMBER OF INTERVALS THAT HALF-ANGLE (RPI/2) GRID FOR
C SECONDARIES IS DIVIDED INTO. NANG SHOULD BE ODD SO THAT THERE IS
C A GRID POINT FOR RPI/2
C NLEV IS NUMBER OF VELOCITY LEVELS USED
C PHO IS ACTUAL CONTRIBUTION AT EACH POINT
C ANG IS LOCATION OF EACH GRID POINT. NOTE THAT ANG AND PHO ARE
C NLEV X NANG MATRICES.
      DATA DAMG/0.017
      DATA FAC/1.0/DVI/0.01/
      DATA AL/O/
      DATA ANL/O/
      GAMMA=RATIO(3)
      NDIM=3
      DELANG=.5RPI/FLOAT(NANG-1)
      L1=2*NANG-1
      L2=L1-1
C GENERATE COEFFICIENTS PHO(I,L) AND ANG(L) FOR USE IN CALCULATING
C SECONDARY CURRENT DUE TO SECONDARIES ARRIVING FROM OTHER
C PORTIONS OF THE SPACECRAFT
      IOHL=1
      DO 300 I=1,NLEV
      DO 191 L=L1,L1
      IF(L,EG.0) ICHECK(I,L)=1
      IF(L,EG.1) ICHECK(I,L)=0
      PHO(I,L)=0.0
      IF(IOHL,EG.0) GO TO 191
      ANG(L)=DELANG*FLOAT(L-1)
      BETA1=VI(I)*RPI(2)/GAMMA
      IF(BETA1,LT.0.0) GO TO 180
      VARIABLE(1)=SO
      VARIABLE(2)=ANG(L)
      VARIABLE(3)=Y(J)
      COSA=COS(ANG(L))
      DBETA=COSAR*DVUX(1,J)/(2.0*VUI(I)*RPI(2)*GAMMA)+COSA
      IF(L,EG.1,AND,DBETA,LT.0.0) GO TO 180
      IF(L,EG.L1,AND,DBETA,GT.0.0) GO TO 180
      T=0.
      CALL ORBIT(SO,BETA1,J)
      IF(VARIABLE(1),GE,(SBOUND-DELTA)) GO TO 190
      IF (ABS((PHI(J)-POT)/RATIO(3)),LT.100.)
      1 PHO(I,L)=2.0CSEC(J)*EXP((POT-PHI(J))/RATIO(3))/
      2 SGTPI
      IF (PHO(I,L),EQ.0.0) ICHECK(I,L)=1
      GO TO 191
180 PHO(I,L)=2.0CSEC(I,J)/SGTPI
190 CONTINUE
191 CONTINUE
      IOHL=0
      DO 300 L=L1,L1
      IF(PHO(I,L),NE.0.0) IOHL=IOHL+1
300 CONTINUE
C
C
      DO 197 L=L1,L1
      DO 197 I=1,NLEV
      BOUNDL(I,L)=PHO(I,L)
      BOUND(I,L)=PHO(I,L)
      VII(I,L)=VUI(I)
      ANG(L)=ANG(L)
197 CONTINUE
C
C
      IF(L,EG.0) GO TO 2100
      DO 200 I=1,NLEV
      DO 200 L=L1,L2
      IF (ICHECK(I,L),EQ.1,OR,ICHECK(I,L+1),EQ.1) GO TO 200
      IF (PHO(I,L),EQ.0.0,AND,PHO(I,L+1),NE.0.0) GO TO 201
      IF (PHO(I,L),NE.0.0,AND,PHO(I,L+1),EQ.0.0) GO TO 202
      GO TO 200
201 LCUT=L
      ANGA=ANG(L)
      ANGB=ANG(L+1)
      GO TO 203
202 LCUT=L+1
      ANGA=ANG(L+1)
      ANGB=ANG(L)
203 ANGLE=0.5*(ANGA+ANGB)
204 ANGL=ANGLE
      VARIABLE(1)=SO
      VARIABLE(2)=ANGLE
      VARIABLE(3)=Y(J)
      T=0.0
      BETA1=VI(I)*VUI(I)+PHI(J)/GAMMA
      IF(BETA1,LT.0.0) BOUNDL(I,LCUT)=2.0CSEC(I,J)/SGTPI
      IF(BETA1,LT.0.0) GO TO 207
      CALL ORBIT(SO,BETA1,J)
      IF (VARIABLE(1),GE,(SBOUND-DELTA)) GO TO 204
      IF (ABS((PHI(J)-POT)/GAMMA),LT.100.)
      1 BOUNDL(I,LCUT)=2.0CSEC(I,J)*EXP((POT-PHI(J))/GAMMA)/SGTPI
207 ANGB=ANGLE
      GO TO 205
204 ANGA=ANGLE
205 ANGLE=0.5*(ANGA+ANGB)
      IF (ABS(ANGLE-ANGL),GT.DAMG) GO TO 204
      ANGL(I,LCUT)=ANGLE
200 CONTINUE
C
C
      NLEVI=NLEV-1
      DO 210 L=L1,L1
      DO 210 I=1,NLEVI
      IF (CARRIV(I,L),EQ.1,OR,CARRIV(I,L+1),EQ.1) GO TO 210
      IF (PHO(I,L),EQ.0.0,AND,PHO(I,L+1),EQ.0.0) GO TO 210
      IF (PHO(I,L),NE.0.0,AND,PHO(I,L+1),EQ.0.0) GO TO 210
      IF (PHO(I,L),EQ.0.0,AND,PHO(I,L+1),EQ.0.0) GO TO 210
      GO TO 210
211 ICUT=L
      IF(ABS((PHI(J)-POT)/GAMMA),LT.100.)
      1 VIV=VI(I)
      VIV=VUI(I)
      GO TO 213
212 ICUT=L+1
      VIV=VUI(I)
      VIV=VUI(I)
      GO TO 213
213 VIV=0.5*(VIV+VIV)
214 VIOLD=VIV
      BETA1=VIV*PHI(J)/GAMMA
      IF(BETA1,LT.0.0) BOUNDL(I,LCUT)=2.0CSEC(I,J)/SGTPI
      IF (BETA1,LE.0.0) GO TO 214
      VARIABLE(1)=SO
      VARIABLE(2)=ANG(L)
      VARIABLE(3)=Y(J)
      T=0.0
      CALL ORBIT(SO,BETA1,J)
      IF (VARIABLE(1),GE,(SBOUND-DELTA)) GO TO 214
      IF (ABS((PHI(J)-POT)/GAMMA),LT.100.)
      1 BOUNDL(I,LCUT)=2.0CSEC(I,J)*EXP((POT-PHI(J))/GAMMA)/SGTPI
217 VIV=VIV
      GO TO 215
214 VIV=VIV
      GO TO 215
215 VIV=0.5*(VIV+VIV)
      IF (ABS((PHI(J)-POT)/GAMMA),LT.100.)
      1 BOUNDL(I,LCUT)=2.0CSEC(I,J)*EXP((POT-PHI(J))/GAMMA)/SGTPI
      VII(I,LCUT)=VIV
210 CONTINUE
C
C
2100 CONTINUE
C
C
C CALCULATE CSEC
      CURRIN=0.
      CURRAT(144)=BSCAT3(144),PHO(20,40)
      CARRIV=0.
      IF(IFAULT(7),EQ.0)GO TO 4000
      CPH=0.0
      DO 350 L=L1,L1
      IF(PHO(I,L),NE.0.0,OR,PHI(J),GT.0.0)
      1 CPH=2.0CSEC(I,J)/SGTPI
350 CONTINUE
      WRITE (LUN6,6000) J
6000 FORMAT (/IX,PSAMPLING IN VELOCITY SPACE FOR SECONDARIES FOR J=,
      1 IX/)
      WRITE (LUN6,600) ((PHO(I,L),I=1,NLEV),L=L1,L1)
600 FORMAT (8(IX,IPEP,2))
359 CONTINUE
      CALL FT(L2,CARRIV,CURRIN,CURRAT,J,CPH,PHI,N,GAMMA)
4000 CONTINUE
360 CSEC(J)=CSEC(J)+CARRIV
400 CONTINUE
      RETURN
C
      SUBROUTINE BSCATR(N,NANG,PHI,CBSCAT,ITER,IGEDN,OMEGA,SO,J,CPH,CSCA1)
      INTEGER PERSEC,SECIND,PERPAN,PANIND
      COMMON PSAVE(144,10),CSAVE(144,10),PSECTR(144),CSECTR(144),
      1DELEE(20),DELMAX(144),EMAX(144),ETA(20),BSCAT(144),
      2BSCAT(144),BSCAT3(144),PHO(20,40),
      3LANG(40),CPHOMX(144),SUNANG,ANGD,BOUNDL(20,40),BOUND(20,40),
      4WANGL(20,40),VII(20,40),ICHECK(20,40),RATIO(13),IROOT(144),
      5IFAULT(14),JLOCAL(144),ICOM(144),
      6IVI(20),EVB(8),NLEV,NTIMES,ILEV,TIMIN(20),TIMAX(20),VINUM(20),
      7TA(144),B(144),C(144),BB(144),BM(144),TM(144),DM(144),
      8SEM(144),TWCOS(700),
      9IFLG,NPOINT,N,IGEDN,ISYN,IPDIS,NSECT,NPEROD,NPEROD,IDIAY,
      10GAMMA,DVUX(70,48),DVUY(70,48),Y(144),DELTA,DELTA,
      113YS(66,48),XS(66),XSS(70),
      12VARIABLE(4),T,DELTA,SBOUND,NDIM,POT,M,J1,RP1,RP12,RP1NAF,SGTPI,
      13SAY,TEMP1,TEMP2,DEME1,DEME2,DEMI1,DEMI2,TEMP11,TEMP12,
      143TEMPR,LUN3,LUN4,LUN5,LUN6,LUN7,LUN8,LUN9,LUN10,
      15IDTL(144),JDTL(144),PERSEC(144),SECIND(144),IPANEL(144),
      16PERPAN(144,4),PANIND(144),
      17ICDM(144),CSECEL(144),CSECI(144),CSECI(144),CPHOT(144),
      182CPHOT1(144),CBSCAT(144),CBSCA1(144),SECPRN(144),SECPRI(144),
      193PHI(144),CGUN(144),
      20IKASE,JOHL,DPHI,NANG,RAD,PBOUND,OMEGA,ALPHA,SO,JP,IS,ECS,
      21CEXP(20),EFTVI(20),IERROR,TETMIN,TETMAX,BETA1,BETA2,JLESS,
      223L,CARRIV,CPH,XI,CSECEL,CSECI,CS,CS,CS1,CS1
C THIS SUBROUTINE CALCULATES THE BSCATTER CURRENT CBSCAT
C CBSCAT CONSISTS OF TWO PARTS:CBSCAT,MAIN BSCATTER CURRENT
C LEAVING A LOCATION,AND CARRIV,BSCATTER
C CURRENT ARRIVING AT A LOCATION FROM OTHER PORTIONS OF THE CRAFT
C PHI IS POTENTIAL ON SPACECRAFT SURFACE
C N IS NUMBER OF GRID POINTS ON SPACECRAFT SURFACE
C NANG IS NUMBER OF INTERVALS THAT HALF-ANGLE (RPI/2) GRID FOR
C BSCATTERS IS DIVIDED INTO. NANG SHOULD BE ODD SO THAT THERE IS
C A GRID POINT FOR RPI/2
C NLEV IS NUMBER OF VELOCITY LEVELS USED
C PHO IS ACTUAL CONTRIBUTION AT EACH POINT
C ANG IS LOCATION OF EACH GRID POINT. NOTE THAT ANG AND PHO ARE
C NLEV X NANG MATRICES.
      DATA DAMG/0.017
      DATA FAC/1.0/DVI/0.01/
      DATA AL/O/
      DATA ANL/O/
      GAMMA=RATIO(4)
      DELANG=.5RPI/FLOAT(NANG-1)
      L1=2*NANG-1
      L2=L1-1
      NDIM=3
C GENERATE COEFFICIENTS PHO(I,L) AND ANG(L) FOR USE IN CALCULATING
C BSCATTER CURRENT DUE TO BSCATTERS ARRIVING FROM OTHER
C PORTIONS OF THE SPACECRAFT
      IOHL=1
      DO 300 I=1,NLEV
      DO 190 L=L1,L1
      IF(L,EG.0) ICHECK(I,L)=1
      IF(L,EG.1) ICHECK(I,L)=0
      PHO(I,L)=0.0
      IF(IOHL,EG.0) GO TO 190
      ANG(L)=DELANG*FLOAT(L-1)
      BETA1=VI(I)*RPI(2)/GAMMA
      IF(BETA1,LT.0.0) GO TO 180
      VARIABLE(1)=SO
      VARIABLE(2)=ANG(L)
      VARIABLE(3)=Y(J)
      COSA=COS(ANG(L))
      DBETA=COSAR*DVUX(1,J)/(2.0*VUI(I)*RPI(2)*GAMMA)+COSA
      IF(L,EG.1,AND,DBETA,LT.0.0) GO TO 180
      IF(L,EG.L1,AND,DBETA,GT.0.0) GO TO 180
      T=0.
      CALL ORBIT(SO,BETA1,J)
      IF(VARIABLE(1),GE,(SBOUND-DELTA)) GO TO 190
      IF (ABS((PHI(J)-POT)/RATIO(4)),LT.200.)
      1 PHO(I,L)=2.0CBSCA1(J)*EXP((POT-PHI(J))/RATIO(4))/
      2 SGTPI
      IF (PHO(I,L),EQ.0.0) ICHECK(I,L)=1
      GO TO 191
180 PHO(I,L)=2.0CBSCAT(I,J)
190 CONTINUE
191 CONTINUE
      IOHL=0
      DO 300 L=L1,L1
      IF(PHO(I,L),NE.0.0) IOHL=IOHL+1
300 CONTINUE
C
C
      DO 197 L=L1,L1
      DO 197 I=1,NLEV
      BOUNDL(I,L)=PHO(I,L)
      BOUND(I,L)=PHO(I,L)
      VII(I,L)=VUI(I)
      ANG(L)=ANG(L)
197 CONTINUE
C
C
      IF(L,EG.0) GO TO 2100
      DO 200 I=1,NLEV
      DO 200 L=L1,L2
      IF (ICHECK(I,L),EQ.1,OR,ICHECK(I,L+1),EQ.1) GO TO 200
      IF (PHO(I,L),EQ.0.0,AND,PHO(I,L+1),NE.0.0) GO TO 201
      IF (PHO(I,L),NE.0.0,AND,PHO(I,L+1),EQ.0.0) GO TO 202
      GO TO 200
201 LCUT=L
      ANGA=ANG(L)
      ANGB=ANG(L+1)
      GO TO 203
202 LCUT=L+1
      ANGA=ANG(L+1)
      ANGB=ANG(L)
203 ANGLE=0.5*(ANGA+ANGB)
204 ANGL=ANGLE
      VARIABLE(1)=SO
      VARIABLE(2)=ANGLE
      VARIABLE(3)=Y(J)
      T=0.0
      BETA1=VI(I)*VUI(I)+PHI(J)/GAMMA
      IF(BETA1,LT.0.0) BOUNDL(I,LCUT)=2.0CBSCAT(I,J)/SGTPI
      IF(BETA1,LT.0.0) GO TO 207
      CALL ORBIT(SO,BETA1,J)
      IF (VARIABLE(1),GE,(SBOUND-DELTA)) GO TO 204
      IF (ABS((PHI(J)-POT)/GAMMA),LT.100.)
      1 BOUNDL(I,LCUT)=2.0CBSCAT(I,J)*EXP((POT-PHI(J))/GAMMA)/SGTPI
207 ANGB=ANGLE
      GO TO 205
204 ANGA=ANGLE
205 ANGLE=0.5*(ANGA+ANGB)
      IF (ABS(ANGLE-ANGL),GT.DAMG) GO TO 204
      ANGL(I,LCUT)=ANGLE
200 CONTINUE
C
C
      NLEVI=NLEV-1
      DO 210 L=L1,L1
      DO 210 I=1,NLEVI
      IF (CARRIV(I,L),EQ.1,OR,CARRIV(I,L+1),EQ.1) GO TO 210
      IF (PHO(I,L),EQ.0.0,AND,PHO(I,L+1),EQ.0.0) GO TO 210
      IF (PHO(I,L),NE.0.0,AND,PHO(I,L+1),EQ.0.0) GO TO 210
      IF (PHO(I,L),EQ.0.0,AND,PHO(I,L+1),EQ.0.0) GO TO 210
      GO TO 210
211 ICUT=L
      IF(ABS((PHI(J)-POT)/GAMMA),LT.100.)
      1 VIV=VI(I)
      VIV=VUI(I)
      GO TO 213
212 ICUT=L+1
      VIV=VUI(I)
      VIV=VUI(I)
      GO TO 213
213 VIV=0.5*(VIV+VIV)
214 VIOLD=VIV
      BETA1=VIV*PHI(J)/GAMMA
      IF(BETA1,LT.0.0) BOUNDL(I,LCUT)=2.0CBSCAT(I,J)/SGTPI
      IF (BETA1,LE.0.0) GO TO 214
      VARIABLE(1)=SO
      VARIABLE(2)=ANG(L)
      VARIABLE(3)=Y(J)
      T=0.0
      CALL ORBIT(SO,BETA1,J)
      IF (VARIABLE(1),GE,(SBOUND-DELTA)) GO TO 214
      IF (ABS((PHI(J)-POT)/RATIO(4)),LT.200.)
      1 BOUNDL(I,LCUT)=2.0CBSCAT(I,J)*EXP((POT-PHI(J))/RATIO(4))/
      2 SGTPI
      VII(I,LCUT)=VIV
210 CONTINUE
C
C

```



```

140 PHO(I,L)=2.08CSCA(J)/SOTPI
140 UNCONTINUE
      IOML=0
      DO 100 L=1,L1
      IF (PHO(I,L).NE.0.0) IOML=IOML+1
300 CONTINUE
C
      DO 197 L=1,L1
      DO 197 I=1,MLEV
      ROUNDL(I,L)=PHO(I,L)
      ROUNDI(I,L)=PHO(I,L)
      VII(I,L)=VI(I)
      ANGL(I,L)=ANG(L)
197 CONTINUE
C
      IF (KL.EQ.0) GO TO 2100
      DO 200 I=1,MLEV
      DO 200 L=1,L2
      IF (ICHECK(I,L).EQ.1.OR.ICHECK(I+1,L).EQ.1) GO TO 200
      IF (PHO(I,L).EQ.0.0.AND.PHO(I+1,L).NE.0.0) GO TO 201
      IF (PHO(I,L).NE.0.0.AND.PHO(I+1,L).EQ.0.0) GO TO 202
      GO TO 200
201 LCUT=L
      ANGA=ANG(L)
      ANGB=ANG(L+1)
      GO TO 203
202 LCUT=L+1
      ANGA=ANG(L+1)
      ANGB=ANG(L)
203 ANGLE=58(ANGA+ANGB)
204 AOL=ANGLE
      VARBLE(1)=50
      VARBLE(2)=ANGLE
      VARBLE(3)=Y(J)
      T=0.0
      BETA=VI(I)*VI(I)+PHI(J)/GAMMA
      IF (BETA.LT.0.0) BOUNDL(I,LCUT)=2.08CSCA(J)/SOTPI
      IF (BETA.LT.0.0) GO TO 207
      CALL ORBIT(50,BETA,I)
      IF (VARBLE(1).GE.(SBOUND-DELTA)) GO TO 204
      IF (ABS(PHI(J)-POT)/GAMMA.LT.100.0)
      IBOUND(I,LCUT)=2.08CSCA(J)*EXP((POT-PHI(J))/GAMMA)/SOTPI
207 ANGB=ANGLE
      GO TO 205
204 ANGA=ANGLE
205 ANGLE=0.58(ANGA+ANGB)
      IF (ABS(ANGLE-AOL).GT.DANG) GO TO 204
      ANGL(I,LCUT)=ANGLE
200 CONTINUE
C
      MLEV1=MLEV-1
      DO 210 L=1,L1
      DO 210 I=1,MLEV1
      IF (ICHECK(I,L).EQ.1.OR.ICHECK(I+1,L).EQ.1) GO TO 210
      IF (PHO(I,L).EQ.0.0.AND.PHO(I+1,L).NE.0.0) GO TO 211
      IF (PHO(I,L).NE.0.0.AND.PHO(I+1,L).EQ.0.0) GO TO 212
      GO TO 210
211 ICUT=I
      VIA=VI(I)
      VIB=VI(I+1)
      GO TO 213
212 ICUT=I+1
      VIA=VI(I+1)
      VIB=VI(I)
213 VIN=0.58(VIA+VIB)
214 VIOL=VIN
      BETA=VIN*VIN+PHI(J)/GAMMA
      IF (BETA.LT.0.0) BOUNDI(ICUT,L)=2.08CSCA(J)/SOTPI
      IF (BETA.LT.0.0) GO TO 217
      VARBLE(1)=50
      VARBLE(2)=ANG(L)
      VARBLE(3)=Y(J)
      T=0.0
      CALL ORBIT(50,BETA,I)
      IF (VARBLE(1).GE.(SBOUND-DELTA)) GO TO 214
      IF (ABS(PHI(J)-POT)/GAMMA.LT.100.0)
      IBOUND(ICUT,L)=2.08CSCA(J)*EXP((POT-PHI(J))/GAMMA)/SOTPI
217 VIB=VIN
      GO TO 215
214 VIA=VIN
      GO TO 215
215 VIN=0.58(VIA+VIB)
      IF (ABS(VIN-VIOL).GT.DV18(VI(I+1)-VI(I))) GO TO 214
      VI(ICUT,L)=VIN
210 CONTINUE
C
2100 CONTINUE
C CALCULATE CBSCAT
      CURRIN=0.
      CARRIV=0.
      IF (IFAIL(I).EQ.0) GO TO 4000
      CPH=0.0
      DO 350 L=1,L1
      IF (PHO(I,L).NE.0.0.OR.PHI(J).GT.0.0)
      I CPH=2.08CSCA(J)/SOTPI
350 CONTINUE
      WRITE (LUNG,6000) J
4000 FORMAT (/IX,6000) J
      WRITE (LUNG,600) (PHO(I,L),I=1,MLEV),L=1,L1)
400 FORMAT (8(IX,1PE9.2))
      CALL FIT(I2,CARRIV,CURRIN,CURRIN,J,CPH,PHI,N,GAMMA)
4000 CONTINUE
401 FORMAT (/)
360 CBSCAT(J)=CBSCAT(J)+CARRIV
400 CONTINUE
      RETURN
      END
      SUBROUTINE ELPRH(N,MANG,PHI,SECPH,ITER,IBEON,OMEGA,SO,J,SECPRI)
      INTEGER PERSEC,SECTINB,PERPAN,PANIND
      COMMON PSAVE(144,10),CSAVE(144,10),PSECTR(144),CSECTR(144),
      IDELEC(20),DELMAX(144),EMAX(144),ETA(20),BSCAT(144),
      BSCAT2(144),BSCAT3(144),PHO(20,40),
      IAND(40),CPHMAX(144),BUNNGB(144),BUNNGB(20,40),BUNNGB(20,40),
      ZANG(20,40),VII(20,40),ICHECK(20,40),RATIO(13),IROOT(144),
      IFAULT(144),J,OCAL(144),ICOM(144),
      VI(20),FV(8),MLEV,MTIME,ILEV,ITRN(20),ITMAX(20),VINUN(20),
      ZAT(44),B(144),C(144),BB(144),BW(144),TW(144),DW(144),
      SFU(144),TUCDB(700)
      IFLB=MOD(ITER,IBEON)-IBYN,IPDIS,IBSECT,IPEROD,IPEROD,IBIRY,
      ZOHANNA,BVBD(70,48),BVBD(70,48),Y(144),DELTA,DELTA,
      JYS(44,48),X(44),Y(70)
      IVARBL(4),T,DELT,SBOUND,NDIR,POT,N,J,RP1,RP12,RP1MF,SOTPI,
      ZSAY,TEMP1,TEMP2,DEMI,DEME,DEMI,DEMI2,TEMP11,TEMP12,
      TEMP13,TEMP14,TEMP15,TEMP16,TEMP17,TEMP18,TEMP19,TEMP20

```

```

      IEDTL(144),IDTL(144),PERSEC(144),SECTINB(144),IPANEL(144),
      ZPERPAN(144,4),PANIND(144),
      ICION(144),ELEEC(144),CSEC(144),CSEI(144),CPHID(144),
      ZCPHDI(144),LSCAT(144),CBSCA(144),SECPRN(144),SELPRI(144),
      IPI(144),CDUM(144),
      IKA5E,IOML,DPHI,MANG,RAD,FBOUND,OMEGA,ALPHA,SO,J,IS,ECS,
      ZEKPI2(20),EFVIL(20),IERROR,ITRN,ITMAX,BETA,DELAZ,ALISS,
      ILZ,CARRIV,CPH,XI,CSECEL,CSECE1,CS,CP,CS1,CBI
      C*****
      C THIS SUBROUTINE CALCULATES THE SECONDARY CURRENT SECPRN
      C SECPRN CONSISTS OF TWO PARTS:SECPRN,MAIN SECONDARY CURRENT
      C LEAVING A LOCATION,AND CARRIV,SECONDARY
      C CURRENT ARRIVING AT A LOCATION FROM OTHER PORTIONS OF THE CRAFT
      C PHI IS PDENTIAL ON SPACECRAFT SURFACE
      C N IS NUMBER OF GRID POINTS ON SPACECRAFT SURFACE
      C MANG IS NUMBER OF INTERVALS THAT HALF-ANGLE (RPI/2) GRID FOR
      C SECONDARIES IS DIVIDED INTO. MANG SHOULD BE ODD SO THAT THERE IS
      C A GRID POINT FOR RPI/2
      C MLEV IS NUMBER OF VELOCITY LEVELS USED
      C PHO IS LOCAL CONTRIBUTION AT EACH POINT
      C ANGL IS LOCATION OF EACH GRID POINT. NOTE THAT ANGL AND PHO ARE
      C MLEV X MANG MATRICES.
      DATA DANG/0.1/
      DATA FAC/1.0/DUI/0.017/
      DATA KL/0./
      GAMMA=RATIO(13)
      DELANG=58RPI/FLOAT(MANG-1)
      L1=2*MANG-1
      L2=L1-1
      NDIM=3
      C GENERATE COEFFICIENTS PHO(I,L) AND ANGL(L) FOR USE IN CALCULATING
      C SECONDARY CURRENT DUE TO SECONDARIES ARRIVING FROM OTHER
      C PORTIONS OF THE SPACECRAFT
      IOML=1
      DO 300 I=1,MLEV
      DO 190 L=1,L1
      IF (KL.EQ.0) ICHECK(I,L)=1
      IF (KL.EQ.1) ICHECK(I,L)=0
      PHO(I,L)=0.0
      IF (IOML.EQ.0) GO TO 190
      ANGL(L)=DELANG*FLOOR(L-1)
      BETA=VI(I)*VI(I)+PHI(J)/GAMMA
      IF (BETA.LT.0.0) GO TO 180
      VARBLE(1)=50
      VARBLE(2)=ANG(L)
      VARBLE(3)=Y(J)
      COSA=COS(ANG(L))
      DISTAN=COS(DUI*(J-1))/(2.0*VI(I)*BUNNGB(MANG)+COSA)
      IF (L.EQ.1.AND.DBETA.LT.0.0) GO TO 180
      IF (L.EQ.L1.AND.DBETA.GT.0.0) GO TO 180
      T=0.
      CALL ORBIT(50,BETA,I)
      IF (VARBLE(1).GE.(SBOUND-DELTA)) GO TO 190
      IF (ABS(POT-PHI(J))/RATIO(13).LT.100.)
      I PHO(I,L)=2.08SECPRI(J)*EXP((POT-PHI(J))/RATIO(13))/
      5 SOTPI
      IF (PHO(I,L).EQ.0.0) ICHECK(I,L)=1
      GO TO 190
180 PHO(I,L)=2.08SECPRI(J)/SOTPI
190 CONTINUE
      IOML=0
      DO 300 L=1,L1
      IF (PHO(I,L).NE.0.0) IOML=IOML+1
300 CONTINUE
C
      DO 197 L=1,L1
      DO 197 I=1,MLEV
      ROUNDL(I,L)=PHO(I,L)
      ROUNDI(I,L)=PHO(I,L)
      VII(I,L)=VI(I)
      ANGL(I,L)=ANG(L)
197 CONTINUE
C
      IF (KL.EQ.0) GO TO 2100
      DO 200 I=1,MLEV
      DO 200 L=1,L2
      IF (ICHECK(I,L).EQ.1.OR.ICHECK(I+1,L).EQ.1) GO TO 200
      IF (PHO(I,L).EQ.0.0.AND.PHO(I+1,L).NE.0.0) GO TO 201
      IF (PHO(I,L).NE.0.0.AND.PHO(I+1,L).EQ.0.0) GO TO 202
      GO TO 200
201 LCUT=L
      ANGA=ANG(L)
      ANGB=ANG(L+1)
      GO TO 203
202 LCUT=L+1
      ANGA=ANG(L+1)
      ANGB=ANG(L)
203 ANGLE=0.58(ANGA+ANGB)
204 AOL=ANGLE
      VARBLE(1)=50
      VARBLE(2)=ANGLE
      VARBLE(3)=Y(J)
      T=0.0
      BETA=VI(I)*VI(I)+PHI(J)/GAMMA
      IF (BETA.LT.0.0) BOUNDL(I,LCUT)=2.08SECPRI(J)/SOTPI
      IF (BETA.LT.0.0) GO TO 207
      CALL ORBIT(50,BETA,I)
      IF (VARBLE(1).GE.(SBOUND-DELTA)) GO TO 204
      IF (ABS(PHI(J)-POT)/GAMMA.LT.100.0)
      IBOUND(ICUT,L)=2.08SECPRI(J)*EXP((POT-PHI(J))/GAMMA)/SOTPI
207 ANGB=ANGLE
      GO TO 205
204 ANGA=ANGLE
205 ANGLE=0.58(ANGA+ANGB)
      IF (ABS(ANGLE-AOL).GT.DANG) GO TO 204
      ANGL(I,LCUT)=ANGLE
200 CONTINUE
C
      MLEV1=MLEV-1
      DO 210 L=1,L1
      DO 210 I=1,MLEV1
      IF (ICHECK(I,L).EQ.1.OR.ICHECK(I+1,L).EQ.1) GO TO 210
      IF (PHO(I,L).EQ.0.0.AND.PHO(I+1,L).NE.0.0) GO TO 211
      IF (PHO(I,L).NE.0.0.AND.PHO(I+1,L).EQ.0.0) GO TO 212
      GO TO 210
211 ICUT=I
      VIA=VI(I)
      VIB=VI(I+1)
      GO TO 213
212 ICUT=I+1
      VIA=VI(I+1)
      VIB=VI(I)
213 VIN=0.58(VIA+VIB)
214 VIOL=VIN
      BETA=VIN*VIN+PHI(J)/GAMMA
      IF (BETA.LT.0.0) BOUNDI(ICUT,L)=2.08SECPRI(J)/SOTPI
      IF (BETA.LT.0.0) GO TO 217
      VARBLE(1)=50
      VARBLE(2)=ANG(L)
      VARBLE(3)=Y(J)
      T=0.0
      CALL ORBIT(50,BETA,I)
      IF (VARBLE(1).GE.(SBOUND-DELTA)) GO TO 214
      IF (ABS(PHI(J)-POT)/GAMMA.LT.100.0)
      IBOUND(ICUT,L)=2.08SECPRI(J)*EXP((POT-PHI(J))/GAMMA)/SOTPI
217 VIB=VIN
      GO TO 215
214 VIA=VIN
      GO TO 215
215 VIN=0.58(VIA+VIB)
      IF (ABS(VIN-VIOL).GT.DV18(VI(I+1)-VI(I))) GO TO 214
      VI(ICUT,L)=VIN
210 CONTINUE
C
2100 CONTINUE
C
      MLEV1=MLEV-1
      DO 210 L=1,L1
      DO 210 I=1,MLEV1
      IF (ICHECK(I,L).EQ.1.OR.ICHECK(I+1,L).EQ.1) GO TO 210
      IF (PHO(I,L).EQ.0.0.AND.PHO(I+1,L).NE.0.0) GO TO 211
      IF (PHO(I,L).NE.0.0.AND.PHO(I+1,L).EQ.0.0) GO TO 212
      GO TO 210
211 ICUT=I
      VIA=VI(I)
      VIB=VI(I+1)
      GO TO 213
212 ICUT=I+1
      VIA=VI(I+1)
      VIB=VI(I)
213 VIN=0.58(VIA+VIB)
214 VIOL=VIN
      BETA=VIN*VIN+PHI(J)/GAMMA
      IF (BETA.LT.0.0) BOUNDI(ICUT,L)=2.08SECPRI(J)/SOTPI
      IF (BETA.LT.0.0) GO TO 217
      VARBLE(1)=50
      VARBLE(2)=ANG(L)
      VARBLE(3)=Y(J)
      T=0.0
      CALL ORBIT(50,BETA,I)
      IF (VARBLE(1).GE.(SBOUND-DELTA)) GO TO 214
      IF (ABS(PHI(J)-POT)/GAMMA.LT.100.0)
      IBOUND(ICUT,L)=2.08SECPRI(J)*EXP((POT-PHI(J))/GAMMA)/SOTPI
217 VIB=VIN
      GO TO 215
214 VIA=VIN
      GO TO 215
215 VIN=0.58(VIA+VIB)
      IF (ABS(VIN-VIOL).GT.DV18(VI(I+1)-VI(I))) GO TO 214
      VI(ICUT,L)=VIN
210 CONTINUE
C
      MLEV1=MLEV-1
      DO 210 L=1,L1
      DO 210 I=1,MLEV1
      IF (ICHECK(I,L).EQ.1.OR.ICHECK(I+1,L).EQ.1) GO TO 210
      IF (PHO(I,L).EQ.0.0.AND.PHO(I+1,L).NE.0.0) GO TO 211
      IF (PHO(I,L).NE.0.0.AND.PHO(I+1,L).EQ.0.0) GO TO 212
      GO TO 210
211 ICUT=I
      VIA=VI(I)
      VIB=VI(I+1)
      GO TO 213
212 ICUT=I+1
      VIA=VI(I+1)
      VIB=VI(I)
213 VIN=0.58(VIA+VIB)
214 VIOL=VIN
      BETA=VIN*VIN+PHI(J)/GAMMA
      IF (BETA.LT.0.0) BOUNDI(ICUT,L)=2.08SECPRI(J)/SOTPI
      IF (BETA.LT.0.0) GO TO 217
      VARBLE(1)=50
      VARBLE(2)=ANG(L)
      VARBLE(3)=Y(J)
      T=0.0
      CALL ORBIT(50,BETA,I)
      IF (VARBLE(1).GE.(SBOUND-DELTA)) GO TO 214
      IF (ABS(PHI(J)-POT)/GAMMA.LT.100.0)
      IBOUND(ICUT,L)=2.08SECPRI(J)*EXP((POT-PHI(J))/GAMMA)/SOTPI
217 VIB=VIN
      GO TO 215
214 VIA=VIN
      GO TO 215
215 VIN=0.58(VIA+VIB)
      IF (ABS(VIN-VIOL).GT.DV18(VI(I+1)-VI(I))) GO TO 214
      VI(ICUT,L)=VIN
210 CONTINUE
C
      MLEV1=MLEV-1
      DO 210 L=1,L1
      DO 210 I=1,MLEV1
      IF (ICHECK(I,L).EQ.1.OR.ICHECK(I+1,L).EQ.1) GO TO 210
      IF (PHO(I,L).EQ.0.0.AND.PHO(I+1,L).NE.0.0) GO TO 211
      IF (PHO(I,L).NE.0.0.AND.PHO(I+1,L).EQ.0.0) GO TO 212
      GO TO 210
211 ICUT=I
      VIA=VI(I)
      VIB=VI(I+1)
      GO TO 213
212 ICUT=I+1
      VIA=VI(I+1)
      VIB=VI(I)
213 VIN=0.58(VIA+VIB)
214 VIOL=VIN
      BETA=VIN*VIN+PHI(J)/GAMMA
      IF (BETA.LT.0.0) BOUNDI(ICUT,L)=2.08SECPRI(J)/SOTPI
      IF (BETA.LT.0.0) GO TO 217
      VARBLE(1)=50
      VARBLE(2)=ANG(L)
      VARBLE(3)=Y(J)
      T=0.0
      CALL ORBIT(50,BETA,I)
      IF (VARBLE(1).GE.(SBOUND-DELTA)) GO TO 214
      IF (ABS(PHI(J)-POT)/GAMMA.LT.100.0)
      IBOUND(ICUT,L)=2.08SECPRI(J)*EXP((POT-PHI(J))/GAMMA)/SOTPI
217 VIB=VIN
      GO TO 215
214 VIA=VIN
      GO TO 215
215 VIN=0.58(VIA+VIB)
      IF (ABS(VIN-VIOL).GT.DV18(VI(I+1)-VI(I))) GO TO 214
      VI(ICUT,L)=VIN
210 CONTINUE
C
      MLEV1=MLEV-1
      DO 210 L=1,L1
      DO 210 I=1,MLEV1
      IF (ICHECK(I,L).EQ.1.OR.ICHECK(I+1,L).EQ.1) GO TO 210
      IF (PHO(I,L).EQ.0.0.AND.PHO(I+1,L).NE.0.0) GO TO 211
      IF (PHO(I,L).NE.0.0.AND.PHO(I+1,L).EQ.0.0) GO TO 212
      GO TO 210
211 ICUT=I
      VIA=VI(I)
      VIB=VI(I+1)
      GO TO 213
212 ICUT=I+1
      VIA=VI(I+1)
      VIB=VI(I)
213 VIN=0.58(VIA+VIB)
214 VIOL=VIN
      BETA=VIN*VIN+PHI(J)/GAMMA
      IF (BETA.LT.0.0) BOUNDI(ICUT,L)=2.08SECPRI(J)/SOTPI
      IF (BETA.LT.0.0) GO TO 217
      VARBLE(1)=50
      VARBLE(2)=ANG(L)
      VARBLE(3)=Y(J)
      T=0.0
      CALL ORBIT(50,BETA,I)
      IF (VARBLE(1).GE.(SBOUND-DELTA)) GO TO 214
      IF (ABS(PHI(J)-POT)/GAMMA.LT.100.0)
      IBOUND(ICUT,L)=2.08SECPRI(J)*EXP((POT-PHI(J))/GAMMA)/SOTPI
217 VIB=VIN
      GO TO 215
214 VIA=VIN
      GO TO 215
215 VIN=0.58(VIA+VIB)
      IF (ABS(VIN-VIOL).GT.DV18(VI(I+1)-VI(I))) GO TO 214
      VI(ICUT,L)=VIN
210 CONTINUE
C
      MLEV1=MLEV-1
      DO 210 L=1,L1
      DO 210 I=1,MLEV1
      IF (ICHECK(I,L).EQ.1.OR.ICHECK(I+1,L).EQ.1) GO TO 210
      IF (PHO(I,L).EQ.0.0.AND.PHO(I+1,L).NE.0.0) GO TO 211
      IF (PHO(I,L).NE.0.0.AND.PHO(I+1,L).EQ.0.0) GO TO 212
      GO TO 210
211 ICUT=I
      VIA=VI(I)
      VIB=VI(I+1)
      GO TO 213
212 ICUT=I+1
      VIA=VI(I+1)
      VIB=VI(I)
213 VIN=0.58(VIA+VIB)
214 VIOL=VIN
      BETA=VIN*VIN+PHI(J)/GAMMA
      IF (BETA.LT.0.0) BOUNDI(ICUT,L)=2.08SECPRI(J)/SOTPI
      IF (BETA.LT.0.0) GO TO 217
      VARBLE(1)=50
      VARBLE(2)=ANG(L)
      VARBLE(3)=Y(J)
      T=0.0
      CALL ORBIT(50,BETA,I)
      IF (VARBLE(1).GE.(SBOUND-DELTA)) GO TO 214
      IF (ABS(PHI(J)-POT)/GAMMA.LT.100.0)
      IBOUND(ICUT,L)=2.08SECPRI(J)*EXP((POT-PHI(J))/GAMMA)/SOTPI
217 VIB=VIN
      GO TO 215
214 VIA=VIN
      GO TO 215
215 VIN=0.58(VIA+VIB)
      IF (ABS(VIN-VIOL).GT.DV18(VI(I+1)-VI(I))) GO TO 214
      VI(ICUT,L)=VIN
210 CONTINUE
C
      MLEV1=MLEV-1
      DO 210 L=1,L1
      DO 210 I=1,MLEV1
      IF (ICHECK(I,L).EQ.1.OR.ICHECK(I+1,L).EQ.1) GO TO 210
      IF (PHO(I,L).EQ.0.0.AND.PHO(I+1,L).NE.0.0) GO TO 211
      IF (PHO(I,L).NE.0.0.AND.PHO(I+1,L).EQ.0.0) GO TO 212
      GO TO 210
211 ICUT=I
      VIA=VI(I)
      VIB=VI(I+1)
      GO TO 213
212 ICUT=I+1
      VIA=VI(I+1)
      VIB=VI(I)
213 VIN=0.58(VIA+VIB)
214 VIOL=VIN
      BETA=VIN*VIN+PHI(J)/GAMMA
      IF (BETA.LT.0.0) BOUNDI(ICUT,L)=2.08SECPRI(J)/SOTPI
      IF (BETA.LT.0.0) GO TO 217
      VARBLE(1)=50
      VARBLE(2)=ANG(L)
      VARBLE(3)=Y(J)
      T=0.0
      CALL ORBIT(50,BETA,I)
      IF (VARBLE(1).GE.(SBOUND-DELTA)) GO TO 214
      IF (ABS(PHI(J)-POT)/GAMMA.LT.100.0)
      IBOUND(ICUT,L)=2.08SECPRI(J)*EXP((POT-PHI(J))/GAMMA)/SOTPI
217 VIB=VIN
      GO TO 215
214 VIA=VIN
      GO TO 215
215 VIN=0.58(VIA+VIB)
      IF (ABS(VIN-VIOL).GT.DV18(VI(I+1)-VI(I))) GO TO 214
      VI(ICUT,L)=VIN
210 CONTINUE
C
      MLEV1=MLEV-1
      DO 210 L=1,L1
      DO 210 I=1,MLEV1
      IF (ICHECK(I,L).EQ.1.OR.ICHECK(I+1,L).EQ.1) GO TO 210
      IF (PHO(I,L).EQ.0.0.AND.PHO(I+1,L).NE.0.0) GO TO 211
      IF (PHO(I,L).NE.0.0.AND.PHO(I+1,L).EQ.0.0) GO TO 212
      GO TO 210
211 ICUT=I
      VIA=VI(I)
      VIB=VI(I+1)
      GO TO 213
212 ICUT=I+1
      VIA=VI(I+1)
      VIB=VI(I)
213 VIN=0.58(VIA+VIB)
214 VIOL=VIN
      BETA=VIN*VIN+PHI(J)/GAMMA
      IF (BETA.LT.0.0) BOUNDI(ICUT,L)=2.08SECPRI(J)/SOTPI
      IF (BETA.LT.0.0) GO TO 217
      VARBLE(1)=50
      VARBLE(2)=ANG(L)
      VARBLE(3)=Y(J)
      T=0.0
      CALL ORBIT(50,BETA,I)
      IF (VARBLE(1).GE.(SBOUND-DELTA)) GO TO 214
      IF (ABS(PHI(J)-POT)/GAMMA.LT.100.0)
      IBOUND(ICUT,L)=2.08SECPRI(J)*EXP((POT-PHI(J))/GAMMA)/SOTPI
217 VIB=VIN
      GO TO 215
214 VIA=VIN
      GO TO 215
215 VIN=0.58(VIA+VIB)
      IF (ABS(VIN-VIOL).GT.DV18(VI(I+1)-VI(I))) GO TO 214
      VI(ICUT,L)=VIN
210 CONTINUE
C
      MLEV1=MLEV-1
      DO 210 L=1,L1
      DO 210 I=1,MLEV1
      IF (ICHECK(I,L).EQ.1.OR.ICHECK(I+1,L).EQ.1) GO TO 210
      IF (PHO(I,L).EQ.0.0.AND.PHO(I+1,L).NE.0.0) GO TO 211
      IF (PHO(I,L).NE.0.0.AND.PHO(I+1,L).EQ.0.0) GO TO 212
      GO TO 210
211 ICUT=I
      VIA=VI(I)
      VIB=VI(I+1)
      GO TO 213
212 ICUT=I+1
      VIA=VI(I+1)
      VIB=VI(I)
213 VIN=0.58(VIA+VIB)
214 VIOL=VIN
      BETA=VIN*VIN+PHI(J)/GAMMA
      IF (BETA.LT.0.0) BOUNDI(ICUT,L)=2.08SECPRI(J)/SOTPI
      IF (BETA.LT.0.0) GO TO 217
      VARBLE(1)=50
      VARBLE(2)=ANG(L)
      VARBLE(3)=Y(J)
      T=0.0
      CALL ORBIT(50,BETA,I)
      IF (VARBLE(1).GE.(SBOUND-DELTA)) GO TO 214
      IF (ABS(PHI(J)-POT)/GAMMA.LT.100.0)
      IBOUND(ICUT,L)=2.08SECPRI(J)*EXP((POT-PHI(J))/GAMMA)/SOTPI
217 VIB=VIN
      GO TO 215
214 VIA=VIN
      GO TO 215
215 VIN=0.58(VIA+VIB)
      IF (ABS(VIN-VIOL).GT.DV18(VI(I+1)-VI(I))) GO TO 214
      VI(ICUT,L)=VIN
210 CONTINUE
C
      MLEV1=MLEV-1
      DO 210 L=1,L1
      DO 210 I=1,MLEV1
      IF (ICHECK(I,L).EQ.1.OR.ICHECK(I+1,L).EQ.1) GO TO 210
      IF (PHO(I,L).EQ.0.0.AND.PHO(I+1,L).NE.0.0) GO TO 211
      IF (PHO(I,L).NE.0.0.AND.PHO(I+1,L).EQ.0.0) GO TO 212
      GO TO 210
211 ICUT=I
      VIA=VI(I)
      VIB=VI(I+1)
      GO TO 213
212 ICUT=I+1
      VIA=VI(I+1)
      VIB=VI(I)
213 VIN=0.58(VIA+VIB)
214 VIOL=VIN
      BETA=VIN*VIN+PHI(J)/GAMMA
      IF (BETA.LT.0.0) BOUNDI(ICUT,L)=2.08SECPRI(J)/SOTPI
      IF (BETA.LT.0.0) GO TO 217
      VARBLE(1)=50
      VARBLE(2)=ANG(L)
      VARBLE(3)=Y(J)
      T=0.0
      CALL ORBIT(50,BETA,I)
      IF (VARBLE(1).GE.(SBOUND-DELTA)) GO TO 214
      IF (ABS(PHI(J)-POT)/GAMMA.LT.100.0)
      IBOUND(ICUT,L)=2.08SECPRI(J)*EXP((POT-PHI(J))/GAMMA)/SOTPI
217 VIB=VIN
      GO TO 215
214 VIA=VIN
      GO TO 215
215 VIN=0.58(VIA+VIB)
      IF (ABS(VIN-VIOL).GT.DV18(VI(I+1)-VI(I))) GO TO 214
      VI(ICUT,L)=VIN
210 CONTINUE
C
      MLEV1=MLEV-1
      DO 210 L=1,L1
      DO 210 I=1,MLEV1
      IF (ICHECK(I,L).EQ.1.OR.ICHECK(I+1,L).EQ.1) GO TO 210
      IF (PHO(I,L).EQ.0.0.AND.PHO(I+1,L).NE.0.0) GO TO 211
      IF (PHO(I,L).NE.0.0.AND.PHO(I+1,L).EQ.0.0) GO TO 212
      GO TO 210
211 ICUT=I
      VIA=VI(I)
      VIB=VI(I+1)
      GO TO 213
212 ICUT=I+1
      VIA=VI(I+1)
      VIB=VI(I)
213 VIN=0.58(VIA+VIB)
214 VIOL=VIN
      BETA=VIN*VIN+PHI(J)/GAMMA
      IF (BETA.LT.0.0) BOUNDI(ICUT,L)=2.08SECPRI(J)/SOTPI
      IF (BETA.LT.0.0) GO TO 217
      VARBLE(1)=50
      VARBLE(2)=ANG(L)
      VARBLE(3)=Y(J)
      T=0.0
      CALL ORBIT(50,BETA,I)
      IF (VARBLE(1).GE.(SBOUND-DELTA)) GO TO 214
      IF (ABS(PHI(J)-POT)/GAMMA.LT.100.0)
      IBOUND(ICUT,L)=2.08SECPRI(J)*EXP((POT-PHI(J))/GAMMA)/SOTPI
217 VIB=VIN
      GO TO 215
214 VIA=VIN
      GO TO 215
215 VIN=0.58(VIA+VIB)
      IF (ABS(VIN-VIOL).GT.DV18(VI(I+1)-VI(I))) GO TO 214
      VI(ICUT,L)=VIN
210 CONTINUE
C
      MLEV1=MLEV-1
      DO 210 L=1,L1
      DO 210 I=1,MLEV1
      IF (ICHECK(I,L).EQ.1.OR.ICHECK(I+1,L).EQ.1) GO TO 210
      IF (PHO(I,L).EQ.0.0.AND.PHO(I+1,L).NE.0.0) GO TO 211
      IF (PHO(I,L).NE.0.0.AND.PHO(I+1,L).EQ.0.0) GO TO 212
      GO TO 210
211 ICUT=I
      VIA=VI(I)
      VIB=VI(I+1)
      GO TO 213
212 ICUT=I+1
      VIA=VI(I+1)
      VIB=VI(I)
213 VIN=0.58(VIA+VIB)
214 VIOL=VIN
      BETA=VIN*VIN+PHI(J)/GAMMA
      IF (BETA.LT.0.0) BOUNDI(ICUT,L)=2.08SECPRI(J)/SOTPI
      IF (BETA.LT.0.0) GO TO 217
      VARBLE(1)=50
      VARBLE(2)=ANG(L)
      VARBLE(3)=Y(J)
      T=0.0
      CALL ORBIT(50,BETA,I)
      IF (VARBLE(1).GE.(SBOUND-DELTA)) GO TO 214
      IF (ABS(PHI(J)-POT)/GAMMA.LT.100.0)
      IBOUND(ICUT,L)=2.08SECPRI(J)*EXP((POT-PHI(J))/GAMMA)/SOTPI
217 VIB=VIN
      GO TO 215
214 VIA=VIN
      GO TO 215
215 VIN=0.58(VIA+VIB)
      IF (ABS(VIN-VIOL).GT.DV18(VI(I+1)-VI(I))) GO TO 214
      VI(ICUT,L)=VIN
210 CONTINUE
C
      MLEV1=MLEV-1
      DO 210 L=1,L1
      DO 210 I=1,MLEV1
      IF (ICHECK(I,L).EQ.1.OR.ICHECK(I+1,L).EQ.1) GO TO 210
      IF (PHO(I,L).EQ.0.0.AND.PHO(I+1,L).NE.0.0) GO TO 211
      IF (PHO(I,L).NE.0.0.AND.PHO(I+1,L).EQ.0.0) GO TO 212
      GO TO 210
211 ICUT=I
      VIA=VI(I)
      VIB=VI(I+1)
      GO TO 213
212 ICUT=I+1
      VIA=VI(I+1)
      VIB=VI(I)
213 VIN=0.58(VIA+VIB)
214 VIOL=VIN
      BETA=VIN*VIN+PHI(J)/GAMMA
      IF (BETA.LT.0.0) BOUNDI(ICUT,L)=2.08SECPRI(J)/SOTPI
      IF (BETA.LT.0.0) GO TO 217
      VARBLE(1)=50
      VARBLE(2)=ANG(L)
      VARBLE(3)=Y(J)
      T=0.0
      CALL ORBIT(50,BETA,I)
      IF (VARBLE(1).GE.(SBOUND-DELTA)) GO TO 214
      IF (ABS(PHI(J)-POT)/GAMMA.LT.100.0)
      IBOUND(ICUT,L)=2.08SECPRI(J)*EXP((POT-PHI(J))/GAMMA)/SOTPI
217 VIB=VIN
      GO TO 215
214 VIA=VIN
      GO TO 215
215 VIN=0.58(VIA+VIB)
      IF (ABS(VIN-VIOL).GT.DV18(VI(I+1)-VI(I))) GO TO 214
      VI(ICUT,L)=VIN
210 CONTINUE
C
      MLEV1=MLEV-1
      DO 210 L=1,L1
      DO 210 I=1,MLEV1
      IF (ICHECK(I,L).EQ.1.OR.ICHECK(I+1,L).EQ.1) GO TO 210
      IF (PHO(I,L).EQ.0.0.AND.PHO(I+1,L).NE.0.0) GO TO 211
      IF (PHO(I,L).NE.0.0.AND.PHO(I+1,L).EQ.0.0) GO TO 212
      GO TO 210
211 ICUT=I
      VIA=VI(I)
      VIB=VI(I+1)
      GO TO 213
212 ICUT=I+1
      VIA=VI(I+1)
      VIB=VI(I)
213 VIN=0.58(VIA+VIB)
214 VIOL=VIN
      BETA=VIN*VIN+PHI(J)/GAMMA
      IF (BETA.LT.0.0) BOUNDI(ICUT,L)=2.08SECPRI(J)/SOTPI
      IF (BETA.LT.0.0) GO TO 217
      VARBLE(1)=50
      VARBLE(2)=ANG(L)
      VARBLE(3)=Y(J)
      T=0.0
      CALL ORBIT(50,BETA,I)
      IF (VARBLE(1).GE.(SBOUND-DELTA)) GO TO 214
      IF (ABS(PHI(J)-POT)/GAMMA.LT.100.0)
      IBOUND(ICUT,L)=2.08SECPRI(J)*EXP((POT-PHI(J))/GAMMA)/SOTPI
217 VIB=VIN
      GO TO 215
214 VIA=VIN
      GO TO 215
215 VIN=0.58(VIA+VIB)
      IF (ABS(VIN-VIOL).GT.DV18(VI(I+1)-VI(I))) GO TO 214
      VI(ICUT,L)=VIN
210 CONTINUE
C
      MLEV1=MLEV-1
      DO 210 L=1,L1
      DO 210 I=1,MLEV1
      IF (ICHECK(I,L).EQ.1.OR.ICHECK(I+1,L).EQ.1) GO TO 210
      IF (PHO(I,L).EQ.0.0.AND.PHO(I+1,L).NE.0.0) GO TO 211
      IF (PHO(I,L).NE.0.0.AND.PHO(I+1,L).EQ.0.0) GO TO 212
      GO TO 210
211 ICUT=I
      VIA=VI(I)
      VIB=VI(I+1)
      GO TO 213
212 ICUT=I+1
      VIA=VI(I+1)
      VIB=VI(I)
213 VIN=0.58(VIA+VIB)
214 VIOL=VIN
      BETA=VIN*VIN+PHI(J)/GAMMA
      IF (BETA.LT.0.0) BOUNDI(ICUT,L)=2.08SECPRI(J)/SOTPI
      IF (BETA.LT.0.0) GO TO 217
      VARBLE(1)=50
      VARBLE(2)=ANG(L)
      VARBLE(3)=Y(J)
      T=0.0
      CALL ORBIT(50,BETA,I)
      IF (VARBLE(1).GE.(SBOUND-DELTA)) GO TO 214
      IF (ABS(PHI(J)-POT)/GAMMA.LT.100.0)
      IBOUND(ICUT,L)=2.08SECPRI(J)*EXP((POT-PHI(J))/GAMMA)/SOTPI
217 VIB=VIN
      GO TO 215
214 VIA=VIN
      GO TO 215
215 VIN=0.58(VIA+VIB)
      IF (ABS(VIN-VIOL).GT.DV18(VI(I+1)-VI(I))) GO TO 214
      VI(ICUT,L)=VIN
210 CONTINUE
C
      MLEV1=MLEV-1
      DO 210 L=1,L1
      DO 210 I=1,MLEV1
      IF (ICHECK(I,L).EQ.1.OR.ICHECK(I+1,L).EQ.1) GO TO 210
      IF (PHO(I,L).EQ.0.0.AND.PHO(I+1,L).NE.0.0) GO TO 211
      IF (PHO(I,L).NE.0.0.AND.PHO(I+1,L).EQ.0.0) GO TO 212
      GO TO 210
211 ICUT=I
      VIA=VI(I)
      VIB=VI(I+1)
      GO TO 213
212 ICUT=I+1
      VIA=VI(I+1)
      VIB=VI(I)
213 VIN=0.58(VIA+VIB)
214 VIOL=VIN
      BETA=VIN*VIN+PHI(J)/GAMMA
      IF (BETA.LT.0.0) BOUNDI(ICUT,L)=2.08SECPRI(J)/SOTPI
      IF (BETA.LT.0.0) GO TO 217
      VARBLE(1)=50
      VARBLE(2)=ANG(L)
      VARBLE(3)=Y(J)
      T=0.0
      CALL ORBIT(50,BETA,I)
      IF (VARBLE(1).GE.(SBOUND-DELTA)) GO TO 214
      IF (ABS(PHI(J)-POT)/GAMMA.LT.100.0)
      IBOUND(ICUT,L)=2.08SECPRI(J)*EXP((POT-PHI(J))/GAMMA)/SOTPI
217 VIB=VIN
      GO TO 215
214 VIA=VIN
      GO TO 215
215 VIN=0.58(VIA+VIB)
      IF (ABS(VIN-VIOL).GT.DV18(VI(I+1)-VI(I))) GO TO 214
      VI(ICUT,L)=VIN
210 CONTINUE
C
      MLEV1=MLEV-1
      DO 210 L=1,L1
      DO 210 I=1,MLEV1
      IF (ICHECK(I,L).EQ.1.OR.ICHECK(I+1,L).EQ.1) GO TO 210
      IF (PHO(I,L).EQ.0.0.AND.PHO(I+1,L).NE.0.0) GO TO 211
      IF (PHO(I,L).NE.0.0.AND.PHO(I+1,L).EQ.0.0) GO TO 212
      GO TO 210
211 ICUT=I
      VIA=VI(I)
      VIB=VI(I+1)
      GO TO 213
212 ICUT=I+1
      VIA=VI(I+1)
      VIB=VI(I)
213 VIN=0.58(VIA+VIB)
214 VIOL=VIN
      BETA=VIN*VIN+PHI(J)/GAMMA
      IF (BETA.LT.0.0) BOUNDI(ICUT,L)=2.08SECPRI(J)/SOTPI
      IF (BETA.LT.0.0) GO TO 217
      VARBLE(1)=50
      VARBLE(2)=ANG(L)
      VARBLE(3)=Y(J)
      T=0.0
      CALL ORBIT(50,BETA,I)
      IF (VARBLE(1).GE.(SBOUND-DELTA)) GO TO
```

```

VARIABLES=ANG(L)
VARIABLES=Y(J)
I=0
CALL ORBIT(SO,BETA,L)
IF (VARIABLES,GE,(SBOUND-DELTA)) GO TO214
VIB=VIB
SECPRI(1,0)=WEIGHT*SECPRI(J)+WEIGHT*SECPRI(J)
ROUND((ICUT-L)*2,0)SECPRIEXP((POT-PHI(J))/GAMMA)/SDTPI
GO TO 215
214 VIA=VIB
GO TO 215
215 VIM=0.58*(VIA+VIB)
IF (ABS(VIM-VIOLD),GT,DUI*(VI(I+1)-VI(I))) GO TO 216
217 VII(ICUT,L)=VIM
210 CONTINUE
C
C
C
2100 CONTINUE
C
C
C
CALCULATE SECPRI
CURRINO=0
CURMAX=0
CARRIV=0
IF (IFAULT(8),EQ,0) GO TO 4000
CPH=0
DO 350 L=1,L1
IF (PHO(I,L),NE,0,OR,PHI(J),GT,0,0)
1 CPH=2,08SECPRI(J)/SDTPI
350 CONTINUE
WRITE (LUM6,600) J
4000 FORMAT (1X,'SAMPLING IN VELOCITY SPACE FOR ELEC INDUCED AT J=',
1 I3)
WRITE (LUM6,600) (PHO(I,L),I=1,NLEV,L=1,L1)
600 FORMAT (81X,'PEV,2)
CALL FIT(L2,CARRIV,CURRIN,CURMAX,J,CPH,PHI,N,GAMMA)
4000 CONTINUE
360 SECPRI(J)=SECPRI(J)+CARRIV
400 CONTINUE
RETURN
END
SUBROUTINE GUM
C-----
C PURPOSE TO COMPUTE THE CURRENT DUE TO THE EMISSION OF A GUM
C-----
COMMON/COMR/CUM(144),CELEC(144),CSECI(144),CSECI(144),CNOT(144)
1 CPHOT(144),CBSCAT(144),CBSCAI(144),SECPRI(144),SECPRI(144)
2 PHI(144),CUM(144)
RETURN
END
SUBROUTINE FIT(L2,CARRIV,CURRIN,CURMAX,J,PHO,PHI,N,GAMMA)
C-----
C THIS SUBROUTINE CALCULATES SECONDARY CURRENT FROM OTHER POINTS.
C IT IS USED IN THE COMPUTATION OF PHOTOELECTRONS,SECONDARIES,AND
C BACKSCATTERED ELECTRONS.
C
C PURPOSE
C
C TO COMPUTE THE CURRENT DENSITY=SUM OVER (VELOCITY) AND SUM OVER L
C (ANGLE) OF (A+B*ANG(L)+C*VELOCITY+D*ANGLE*VELOCITY)*EXP(-VELOCITY**2)
C (VELOCITY**2)*SIN(ANGLE)*SIN(ANGLE)*SIN(VELOCITY)
C TACKING INTO ACCOUNT THE FACT THAT FOR CERTAIN INCIDENT ENERGIES
C AND CERTAIN DIRECTIONS, ELECTRON ORBITS DO CONNECT BACK TO THE AMBIENT
C PLASMA.
C DESCRIPTION OF THE VARIABLES
C CARRIV/TOTAL ARRIVING SECONDARY CURRENT AT A GIVEN GRID POINT
C CURENT/ARRIVING CURRENT FOR ONE ELEMENTARY CELL IN VELOCITY SPACE
C PHO(I,L) MEANTIME FACTORS IN CURRENT INTEGRATION
C A,B,C,D COEFFICIENTS IN BILINEAR INTERPOLATION
C ANGLE SAMPLING ANGLE IN VELOCITY SPACE,ANGLES ARE SAMPLED FROM 0 T
C ZERO TO PI
C VII SAMPLING IN KINETIC VELOCITY
C NLEV/ NUMBER OF ENERGY LEVELS USED IN THE COMPUTATION
C L2/ NUMBER OF ANGLES IN VELOCITY SPACE USED IN THE COMPUTATION
C
INTEGER PERSEC,SECIND,CPH,PAN,PANIND
COMMON PSAVE(144,10),PSAVE(144,10),PSECTR(144),CSECTR(144),
1 DELEC(20),DELEX(144),ENAX(144),ETA(20),BSCAT(144),
2 BSCAI(144),BSCAT(144),BSCAI(144),PHO(20,40),
1 ANGB(40),CPHON(144),SUMANG,AMBO,BOUND(20,40),BOUND(20,40),
2 ANGL(20,40),VII(20,40),ICHECK(20,40),RATIO(13),IROOT(144),
3 IFAULT(14),JLOCAL(144),ICOM(144),
1 VI(20),EVI(8),NLEV,NTHES,ILEV,FININ(20),FINUM(20),
2 TA(144),BI(144),CI(144),BI(144),BI(144),TU(144),DU(144),
3 SEI(144),THODS(700),
1 IFL/MPINT,N,ISEM,ISYN,IPDIS,INJECT,NPEROD,NPEROD,IDIHY,
2 GAMMA,BVBT(70,48),DVBV(70,48),Y(144),DELTA,DELTA,
3 YR(48,48),X(48),XSB(70),
1 IANGL(14),T,DELTA,BOUND,MIN,POT,N,J1,RP1,RP12,RPINAF,SDTPI,
2 BAY,TEMP1,TEMP2,BENI,DENE,DENI,DENI2,TEMP1,TEMP2,
3 ITEMP,LUM3,LUM4,LUM5,LUM6,LUM7,LUM8,LUM9,LUM10,
1 IDTL(144),JDTL(144),PERSEC(144),SECIND(144),IPANEL(144),
2 PERPANI(144),PHIIND(144),
1 CIDM(144),CELEC(144),CSECI(144),CSECI(144),CPHOT(144),
2 CPHOT(144),CBSCAT(144),CBSCAI(144),SECPRI(144),SECPRI(144),
3 PHI(144),CUM(144),
1 INAME,JOH,IPHI,PHO,RAD,PSOUND,OMEGA,ALPHA,BO,JP,IS,ECS,
2 EXPV2(20),EFTVI(20),TEROR,TEMP,TEMPAN,BETA1,BETA2,A,EBB,
3 L2,CARRIV,CPH,XI,CSECEL,CSECFI,CB,CB,CS,CBI
C
C
C
DATA KSTEP/5/
C
DO 390 I=1,NLEV
DO 300 L=1,L2
IF (.GT.1)GO TO 320
IF (PHI(J)/GAMMA,LT,0,0) GO TO 340
IF (PHO(I,L),EQ,0,OR,PHO(I,L+1),EQ,0,0) GO TO 340
DEMON=VI(I)*(ANG(L)-ANG(L+1))
A=PHO
B=0,0
C=(PHO(I,L+1)*BAND(L)-PHO(I,L)*BAND(L+1))+PHO(I,ANG(L+1)-
1 ANGL(L)))/DENOM
D=(PHO(I,L+1)*BAND(L+1)-PHO(I,L)*BAND(L+1))/DENOM
UPRINE=(A+B*ANG(L))/SCOS(ANG(L))-((A+B*ANG(L+1))/
1 COS(ANG(L+1))+B*SIN(ANG(L+1))-SIN(ANG(L)))
CURRENT=UPRINE*(0.58*VI(I)*EXPV2(I-1)+0.25SDTPI*EFTVI(I))
UPRINE=0.58*(EXPV2(I-1)*0.4*VI(I-1)*0.02)-EXPV2(I)*0.1*
1 VI(I)*0.02)
CURRENT=CURRENT+UPRINE*(C1*(COS(ANG(L))-COS(ANG(L+1))+SIN(ANG(L)*
1 COS(ANG(L+1))-SIN(ANG(L+1))))
CARRIV=CARRIV+CURRENT
GO TO 340
C
C
C
CASE NO 1-----
400 CONTINUE
PA=BOUND(I,L+1)
PB=BOUND(I,L+1)
PD=(PHO(I,L+1)-PHO(I,L))/(ANG(L+1)-ANG(L))
1 (ANG(L+1)-ANG(L))+PHO(I,L)
C
C
C
REGION 1
D1=(PB-PD)*PHO(I,L)+PHO(I,L+1)/(ANG(L+1)-ANG(L))*VII(I)-
1 VII(I-1)
C1=(ANG(L+1)-ANG(L))/(PHO(I,L)-PHO(I,L+1))-ANG(L)*(PB-PD)/
1 (ANG(L+1)-ANG(L))*VII(I)-VII(I-1)
B1=(PB-PD)/(ANG(L+1)-ANG(L))-D1*VII(I)
A1=PB-B1*ANG(L+1)-C1*VII(I)-D1*ANG(L+1)*VII(I)
C
C
C
REGION 2
VA=VII(I,L+1)
AMB=ANG(I,L+1)
D2=(PB-PD)*(VA-VI(I-1))-((PA-PHO(I,L+1))*VII(I)-VII(I-1))/
1 ((VA-VI(I-1))*VII(I)-VII(I-1))*(AMB-ANG(L+1))
C2=(PB-PD)*BAND(L+1)*(VA-VI(I-1))-((PA-PHO(I,L+1))*BANDS(VI(I)-
1 VII(I-1)))/(VA-VI(I-1))*VII(I)-VII(I-1))*(AMB(L+1)-AMB)
B2=(PB-PHO(I,L+1))/(AMB-ANG(L+1))-D2*VII(I-1)
A2=PHO(I,L+1)-B2*AMB(L+1)-C2*VII(I-1)-D2*VII(I-1)*BAND(L+1)
C
C
C
STEP=(AMB(L+1)-AMB)/FLOAT(KSTEP)
STEP=AMB
STEP=VII(I,L+1)-VII(I)/FLOAT(KSTEP)
STEP=VII(I)
C
DO 401 K=1,KSTEP
STEP=STEP+STEP
UPRINE=(A2+B2*STEP)*SCOS(STEP)-(A2+B2*STEP)*SCOS(STEP)+
1 B2*(SIN(STEP)-SIN(STEP))
CURRENT=CURRENT+UPRINE*(0.58*(VI(I-1)*EXPV2(I-1)-VII(I)*EXPV2(I)
1 0.25SDTPI*EFTVI(I))-VI(I)-VII(I))
UPRINE=0.58*(EXPV2(I-1)*0.4*VI(I-1)*0.02)-EXPV2(I)*0.1*
1 (0.4*STEP*0.02)
CURRENT=CURRENT+UPRINE*(C2*(COS(STEP)-COS(STEP))+
1 B2*(STEP*SCOS(STEP)-STEP*SCOS(STEP)+SIN(STEP)-SIN(STEP)))
STEP=STEP+STEP
STEP=STEP
401 CONTINUE
CARRIV=CARRIV+CURRENT
CUR=CURRENT
901 FORMAT(1X,CUR,3I3,IP10,3)
WRITE(9,901) J,I,L,CUR
C
GO TO 340
C
C
CASE NO 2-----
410 B1=(BOUND(I,L+1)-PHO(I,L+1))*VII(I,L+1)-VII(I-1)-VII(I,L+1)-
1 VII(I-1)*(BOUND(I,L)-PHO(I,L))/(ANG(L+1)-ANG(L))*VII(I,L+1)
2 (VII(I,L+1)-VII(I-1))*ANG(L+1)*VII(I,L+1)-VII(I-1)*VII(I,L+1)-
3 VII(I-1)
C1=(BOUND(I,L)-PHO(I,L)+BAND(L+1)*VII(I-1)-VII(I,L+1))/(VII(I,L+1)
1 -VII(I-1))
B=(PHO(I,L)-PHO(I,L+1)-B*VII(I-1))/(ANG(L+1)-ANG(L))
1 ANG(L+1)
A=PHO(I,L+1)-B*ANG(L+1)-C*VII(I-1)-B*ANG(L+1)*VII(I-1)
CURRENT=CARRIV+CURRENT
STEP=AMB(I)-AMB(I)/FLOAT(KSTEP)

```



```

1     PSAVE(144,10),CSAVE(144,10),PSECTR(144),CSECTR(144),
1DELE(1,20),DELTA(1,144),EMAX(144),ETA(20),BSCAT1(144),
2     BNA(1,144),BSCAT2(144),PHO(20,40),
3     LANG(40),CPHONX(144),SUMANG,ANGD,BOUNDL(20,40),BOUNDI(20,40),
4     ANGL(20,40),V1(1,20,40),ICHECK(20,40),RATIO(13),IROOT(144),
5     JIFAU(1,144),JLOCAL(144),ICOM(144),
6     IVI(20),EVB(1),MLEV,NTINES,ILEV,TIMIN(20),TIMAX(20),VIMUH(20),
7     2A(144),B(144),C(144),BB(144),BM(144),TM(144),DM(144),
8     TEM(144),TMOCCS(700),
9     IFFLG,NPRINT,M,IGEOM,ISYN,IPOIS,NSECT,NPEROD,NPEROD,INDIM,
10    GAMMA,DVUX(70,48),DVUY(70,48),Y(144),DELTA,DELTA,
11    SYS(66,48),XS(66),XSS(70),
12    IVARLE(4),T,DELTA,SBOUND,NDIN,PQT,H,J1,RP1,RP12,RPIMAF,SOTPI,
13    2SAY,TEMPE1,TEMPE2,DEME1,DEME2,DEM11,DEM12,TEMPI1,TEMPI2,
14    3TEMPR,LUM3,LUM4,LUM5,LUM6,LUM7,LUM8,LUM9,LUM10,
15    IIDI(144),JDTL(144),PERSEC(144),SECIND(144),IPANEL(144),
16    2PERPAN(144,4),PANIND(144),
17    ICION(144),CELEC(144),CSEC(144),CSECI(144),CPHOTO(144),
18    2CPHOT1(144),CBSCAT(144),CBSCA1(144),SECPRN(144),SECPRI(144),
19    3PHI(144),CGUM(144),
20    IKASE,JOHL,DPHI,NANG,RAD,PBOUND,OMEGA,ALPHA,SO,JP,IS,ECS,
21    2EXPIV(20),EFTVI(20),IERROR,TETHIN,TETMAX,BETA1,BETA2,JLESS,
22    3L2,CARRIV,CPH,XI,CSECEL,CSECE1,CS,CS,CS1,CB1
23    DATA DELMIN,ACCIN/18.,1.E-2/
24
25
26
27
28
29
30
31
32
33
34
35
36
37
38
39
40
41
42
43
44
45
46
47
48
49
50
51
52
53
54
55
56
57
58
59
60
61
62
63
64
65
66
67
68
69
70
71
72
73
74
75
76
77
78
79
80
81
82
83
84
85
86
87
88
89
90
91
92
93
94
95
96
97
98
99
100
101
102
103
104
105
106
107
108
109
110
111
112
113
114
115
116
117
118
119
120
121
122
123
124
125
126
127
128
129
130
131
132
133
134
135
136
137
138
139
140
141
142
143
144
145
146
147
148
149
150
151
152
153
154
155
156
157
158
159
160
161
162
163
164
165
166
167
168
169
170
171
172
173
174
175
176
177
178
179
180
181
182
183
184
185
186
187
188
189
190
191
192
193
194
195
196
197
198
199
200
201
202
203
204
205
206
207
208
209
210
211
212
213
214
215
216
217
218
219
220
221
222
223
224
225
226
227
228
229
230
231
232
233
234
235
236
237
238
239
240
241
242
243
244
245
246
247
248
249
250
251
252
253
254
255
256
257
258
259
260
261
262
263
264
265
266
267
268
269
270
271
272
273
274
275
276
277
278
279
280
281
282
283
284
285
286
287
288
289
290
291
292
293
294
295
296
297
298
299
300
301
302
303
304
305
306
307
308
309
310
311
312
313
314
315
316
317
318
319
320
321
322
323
324
325
326
327
328
329
330
331
332
333
334
335
336
337
338
339
340
341
342
343
344
345
346
347
348
349
350
351
352
353
354
355
356
357
358
359
360
361
362
363
364
365
366
367
368
369
370
371
372
373
374
375
376
377
378
379
380
381
382
383
384
385
386
387
388
389
390
391
392
393
394
395
396
397
398
399
400
401
402
403
404
405
406
407
408
409
410
411
412
413
414
415
416
417
418
419
420
421
422
423
424
425
426
427
428
429
430
431
432
433
434
435
436
437
438
439
440
441
442
443
444
445
446
447
448
449
450
451
452
453
454
455
456
457
458
459
460
461
462
463
464
465
466
467
468
469
470
471
472
473
474
475
476
477
478
479
480
481
482
483
484
485
486
487
488
489
490
491
492
493
494
495
496
497
498
499
500
501
502
503
504
505
506
507
508
509
510
511
512
513
514
515
516
517
518
519
520
521
522
523
524
525
526
527
528
529
530
531
532
533
534
535
536
537
538
539
540
541
542
543
544
545
546
547
548
549
550
551
552
553
554
555
556
557
558
559
560
561
562
563
564
565
566
567
568
569
570
571
572
573
574
575
576
577
578
579
580
581
582
583
584
585
586
587
588
589
590
591
592
593
594
595
596
597
598
599
600
601
602
603
604
605
606
607
608
609
610
611
612
613
614
615
616
617
618
619
620
621
622
623
624
625
626
627
628
629
630
631
632
633
634
635
636
637
638
639
640
641
642
643
644
645
646
647
648
649
650
651
652
653
654
655
656
657
658
659
660
661
662
663
664
665
666
667
668
669
670
671
672
673
674
675
676
677
678
679
680
681
682
683
684
685
686
687
688
689
690
691
692
693
694
695
696
697
698
699
700
701
702
703
704
705
706
707
708
709
710
711
712
713
714
715
716
717
718
719
720
721
722
723
724
725
726
727
728
729
730
731
732
733
734
735
736
737
738
739
740
741
742
743
744
745
746
747
748
749
750
751
752
753
754
755
756
757
758
759
760
761
762
763
764
765
766
767
768
769
770
771
772
773
774
775
776
777
778
779
780
781
782
783
784
785
786
787
788
789
790
791
792
793
794
795
796
797
798
799
800
801
802
803
804
805
806
807
808
809
810
811
812
813
814
815
816
817
818
819
820
821
822
823
824
825
826
827
828
829
830
831
832
833
834
835
836
837
838
839
840
841
842
843
844
845
846
847
848
849
850
851
852
853
854
855
856
857
858
859
860
861
862
863
864
865
866
867
868
869
870
871
872
873
874
875
876
877
878
879
880
881
882
883
884
885
886
887
888
889
890
891
892
893
894
895
896
897
898
899
900
901
902
903
904
905
906
907
908
909
910
911
912
913
914
915
916
917
918
919
920
921
922
923
924
925
926
927
928
929
930
931
932
933
934
935
936
937
938
939
940
941
942
943
944
945
946
947
948
949
950
951
952
953
954
955
956
957
958
959
960
961
962
963
964
965
966
967
968
969
970
971
972
973
974
975
976
977
978
979
980
981
982
983
984
985
986
987
988
989
990
991
992
993
994
995
996
997
998
999
1000

```



```

EXPV1(20),EFTV1(20),ERROR,TETMIN,TETMAX,METAI,BETA2,JEBS,
SL2,CARRIV,CPH,XI,CSECEL,CSECE1,US,CS,CB,CSI,CBI
INTEGER I,J,N,N1,N,N1
DATA IXL,5,DE,3
DATA ISMITH,0
DO I=1,NHSECT
CURP(I)=0.0
CURP(I)=0.0
PHIN(I)=0.0
PHIP(I)=0.0
CONTINUE
C
NTOUR=1
10 NTOUR=NTOUR+1
IF (NTOUR.GE.900) WRITE (9,400)
400 FORMAT (1X,400 CONVERGENCE IN GUESS FIELD AFTER 900 ITER)
IF (NTOUR.GE.900) STOP
L=0
DO 100 I=1,NHSECT
ECS=0.0
CE1(I)=0.0
CN=0.0
N=PERSEC(I)
N=L*N
T=L*I
C
DO 90 J=T,N
N=SECIND(J)
ECB=ECB+CURRENT*(PHI(N)-Y(N),CE,CPH,CS,CB,CSECEL)
CET(I)=CET(I)+CE
PSECTR(I)=PHI(I)
90 CONTINUE
L=L*N
CSECTR(I)=ECS
100 CONTINUE
C
PREPARE DATA FOR REGULAR FALSI METHOD
IF (NTOUR-1) 201,401,401
201 DO 210 I=1,NHSECT
IF (CSECTR(I).GT.0.0) GO TO 111
CURN(I)=CSECTR(I)
PHIN(I)=PSECTR(I)
PSECTR(I)=PSECTR(I)-3.0
GO TO 210
111 CURP(I)=CSECTR(I)
PHIP(I)=PSECTR(I)
PSECTR(I)=PSECTR(I)+1.0
210 CONTINUE
C
GO TO 500
C
BEGIN REGULA FALSI ITERATION
401 K=0
DO 410 I=1,NHSECT
IF (ABS(CSECTR(I)).LE.TOLCET(I)) GO TO 410
IF (CURN(I).EQ.0.0) PHIN(I)=PSECTR(I)
IF (CURN(I).EQ.0.0) CURN(I)=CSECTR(I)
IF (CURP(I).EQ.0.0) PHIP(I)=PSECTR(I)
IF (CURP(I).EQ.0.0) CURP(I)=CSECTR(I)
K=K+1
IF (CURN(I)*CSECTR(I).GE.0.0) GO TO 420
CURP(I)=CSECTR(I)
PHIP(I)=PSECTR(I)
GO TO 430
420 CURN(I)=CSECTR(I)
PHIN(I)=PSECTR(I)
430 IF (CURN(I)*CURP(I).LE.0.0) GO TO 440
IF (CURN(I).GE.0.0) PSECTR(I)=PSECTR(I)+1.0
IF (CURP(I).LE.0.0) PSECTR(I)=PSECTR(I)-1.0
GO TO 410
440 PSECTR(I)=(PHIN(I)*CURP(I)-PHIP(I)*CURN(I))/(CURP(I)-CURN(I))
410 CONTINUE
IF (K.NE.0) GO TO 500
WRITE (9,401)
401 FORMAT (1X,8 DK PAST GUESS FIELD)
WRITE (9,400) (PHI(J),J=1,NPOINT)
4001 FORMAT (4(1X,1PE12.5))
ISMITH=1
C
500 L=0
DO 501 I=1,NHSECT
PHINEM=PSECTR(I)
K=PERSEC(I)
N=L*K
T=L*I
DO 510 J=T,N
N=SECIND(J)
PHI(N)=PHINEM
510 CONTINUE
L=L*K
501 CONTINUE
IF (ISMITH.EQ.1) RETURN
GO TO 10
END
FUNCTION CURRENT (J,XI,YY,CE,CPH,CS,CB,CSECEL)
C *****
C PURPOSE: TO COMPUTE CURRENT COLLECTION AT GRID POINTS FOR GUESS FIELD.
C *****
INTEGER PERSEC,SECIND,PERPAN,PANIND
COMMON PSAME(144,10),CBAME(144,10),PSECTR(144),CSECTR(144),
1DELE(20),DELMAX(144),ENAX(144),ETA(20),BSCAT(144),
2BSCAT2(144),BSCAT3(144),PHO(20,40),
1AND(40),CPHMX(144),BUNANG,ANDB,BOUNDL(20,40),BOUNDI(20,40),
2ANBL(20,40),VII(20,40),ICHECK(20,40),RATIO(13),IROOT(144),
3IFALT(14),J.OCAL(144),ICOM(144),
1VI(20),EVC(8),NLEV,NTINEB,ILEV,TININ(20),TINAX(20),VINUN(20),
2A(144),B(144),C(144),BB(144),BM(144),TU(144),BU(144),
3EM(144),TMOCS(700),
1IFLO,NPOINT,N,IGEON,IBYN,IPDIS,NHSECT,NPEROD,NPEROD,IDIHY,
2GANGA,DVX(70,40),DVY(70,40),Y(144),DELTA,DELTA,
3YS(66,40),XB(66),XSB(70),
1VARIABLE(4),T,DELT,SBUND,MBIN,POT,M,J1,RP1,RP12,RP1MF,BOTPI,
2SAY,TEMP1,TEMP2,DEME1,DEME2,DEMI1,DEMI2,TEMP11,TEMP12,
3TEMPR,LUN3,LUN4,LUN5,LUN6,LUN7,LUN8,LUN9,LUN10,
1IDL(144),JDL(144),PERSEC(144),SECIND(144),IPANEL(144),
2PERPAN(144,4),PANIND(144),
1CION(144),CELEC(144),CSEC(144),CSEC1(144),CPHOTO(144),
2CPHOT(144),CBSCAT(144),CBSCA1(144),BECPRN(144),BECPRI(144),
3PHI(144),COLM(144),
1BASE,JOH,DPHI,NAND,RAB,PROUD,ONEGA,ALPHA,BO,JP,IS,ECB,
2EXPV1(20),EFTV1(20),ERROR,TETMIN,TETMAX,METAI,BETA2,JEBS,
3L2,CARRIV,CPH,XI,CSECEL,CSECE1,CS,CB,CSI,CBI
L=0
DO 100 I=1,NHSECT
ECS=0.0
K=PERSEC(I)
N=L*K
T=L*I
DO 90 J=T,N
N=SECIND(J)
ECB=ECB+CET*(PHI(N))
PSECTR(I)=PHI(N)
90 CONTINUE
L=L*K
CSECTR(I)=ECS
100 CONTINUE
WRITE (9,401) (CSECTR(I),I=1,NHSECT)
401 FORMAT (8(1X,1PE10.3))
RETURN
END
FUNCTION CETT(J)
C *****
C ALL CURRENTS ARE DIMENSIONALIZED WITH RESPECT TO REF TEMP
C CION N-B ION CURRENT
C CIPP N-B FICTION CURRENT

```

```

C CSEC N-D SLC CURRENT
C BSCAT BACA-SCATTER ELECTRON CURRENT
C CPHOTO N-D PHOTO ELECTRON CURRENT
C CETT NET CURRENT
C SECPRN N-D SEC ELECTRON CURRENT INDUCED BY PROTONS
C XI N-D POTENTIAL
C*****
C INTEGER PERSEC,SECIND,PERPAN,PANIND
COMMON PSAVE(144,10),CSAVE(144,10),PSECTR(144),CSECTR(144),
1 DELEE(20),DELMAX(144),EMAX(144),ETA(20),BSCAT(144),
2 BSCAT2(144),BSCAT3(144),PHO(20,40),
1ANG(40),CPHOX(144),SUMANG,ANGD,BOUNDL(20,40),BOUNDI(20,40),
2AMGL(20,40),V1I(20,40),ICHECK(20,40),RATIO(13),IRODT(144),
3IFAU(144),JOCAL(144),ICOM(144),
1V(20),EV(8),MLEV,NTINES,ILEV,TIMIN(20),TIMAX(20),VINUM(20),
2A(144),B(144),C(144),BB(144),BM(144),TM(144),DM(144),
3EM(144),TMOCS(700),
1IFLG,NPOINT,N,IGDGM,ISYM,IPDIS,HSECT,NPEROD,NPEROD,IDIHY,
2GAMMA,DUD(70,48),DUDY(70,48),Y(144),DELTA,DELTA,T,
3YS(46,48),XS(66),XSS(70),
1VARIABLE(4),T,DELTA,SBOUND,NDIM,POT,H,J1,RPI,RP12,RPIMAF,SOTPI,
2SAY,TEMPE1,TEMPE2,DEME1,DEME2,DENI1,DENI2,TEMP11,TEMP12,
3TEMPR,LUM3,LUM4,LUM5,LUM6,LUM7,LUM8,LUM9,LUM10,
1IDL(144),JDTL(144),PERSEC(144),SECIND(144),IPANEL(144),
2PERPAN(144,4),PANIND(144),
1CIOM(144),CELEC(144),CSEC(144),CSECI(144),CPHOTO(144),
2CPHOT(144),CBSCAT(144),CBSCAL(144),SECPRN(144),SECPRI(144),
3PHI(144),CDUM(144),
1KASE,DOML,DPMI,HAND,RAD,PBOUND,OMEGA,ALPHA,SO,JP,IS,ECS,
2EXPVIZ(20),EFTVI(20),IERROR,TETHIN,TETMAX,BETA1,BETA2,JLESS,
3L2,CARRIV,CPH,XI,CSECEL,CSECEI,CS,CB,CSI,CBI
C
C IF (IFAU(1),EQ.0) CIOM(J)=0.0
C IF (IFAU(2),EQ.0) CELEC(J)=0.0
C IF (IFAU(3),EQ.0) CSEC(J)=0.0
C IF (IFAU(4),EQ.0) CBSCAT(J)=0.0
C IF (IFAU(5),EQ.0) CPHOTO(J)=0.0
C CPHOTO(J)=CPHOT(J)*RATIO(9)
C CPHOT(J)=CPHOT(J)*RATIO(9)
C IF (IFAU(9),EQ.0) SECPRN(J)=0.0
C CETT=CIOM(J)+CELEC(J)+CBSCAT(J)+CPHOTO(J)+SECPRN(J)
C WRITE (LUM4,400) J,PHI(J),CETT,CIOM(J),CELEC(J),CPHOTO(J),CPHOT(J)
C I,CSEC(J),CSECI(J),CBSCAT(J),CBSCAL(J),SECPRN(J),SECPRI(J)
400 FORMAT(13,12,1PE10,3)
C RETURN
C END
C SUBROUTINE CBS(XI,J,CS,CB,CSI,CBI)
C*****
C PURPOSE IS TO FIND THE CONTRIBUTION OF SEC AND BACKS ELECTRONS TO THE
C GUESS FIELD.
C
C*****
C INTEGER PERSEC,SECIND,PERPAN,PANIND
COMMON PSAVE(144,10),CSAVE(144,10),PSECTR(144),CSECTR(144),
1 DELEE(20),DELMAX(144),EMAX(144),ETA(20),BSCAT(144),
2 BSCAT2(144),BSCAT3(144),PHO(20,40),
1ANG(40),CPHOX(144),SUMANG,ANGD,BOUNDL(20,40),BOUNDI(20,40),
2AMGL(20,40),V1I(20,40),ICHECK(20,40),RATIO(13),IRODT(144),
3IFAU(144),JOCAL(144),ICOM(144),
1V(20),EV(8),MLEV,NTINES,ILEV,TIMIN(20),TIMAX(20),VINUM(20),
2A(144),B(144),C(144),BB(144),BM(144),TM(144),DM(144),
3EM(144),TMOCS(700),
1IFLG,NPOINT,N,IGDGM,ISYM,IPDIS,HSECT,NPEROD,NPEROD,IDIHY,
2GAMMA,DUD(70,48),DUDY(70,48),Y(144),DELTA,DELTA,T,
3YS(46,48),XS(66),XSS(70),
1VARIABLE(4),T,DELTA,SBOUND,NDIM,POT,H,J1,RPI,RP12,RPIMAF,SOTPI,
2SAY,TEMPE1,TEMPE2,DEME1,DEME2,DENI1,DENI2,TEMP11,TEMP12,
3TEMPR,LUM3,LUM4,LUM5,LUM6,LUM7,LUM8,LUM9,LUM10,
1IDL(144),JDTL(144),PERSEC(144),SECIND(144),IPANEL(144),
2PERPAN(144,4),PANIND(144),
1CIOM(144),CELEC(144),CSEC(144),CSECI(144),CPHOTO(144),
2CPHOT(144),CBSCAT(144),CBSCAL(144),SECPRN(144),SECPRI(144),
3PHI(144),CDUM(144),
1KASE,DOML,DPMI,HAND,RAD,PBOUND,OMEGA,ALPHA,SO,JP,IS,ECS,
2EXPVIZ(20),EFTVI(20),IERROR,TETHIN,TETMAX,BETA1,BETA2,JLESS,
3L2,CARRIV,CPH,XI,CSECEL,CSECEI,CS,CB,CSI,CBI
C
C DO 710 J=1,2
C IF (J,NE.1) GO TO 711
C GAMMA=RATIO(2)
C TEMPE=TEMPE1
C RATE=RATIO(4)
C DEN=DEN1/DENI1
C GO TO 712
711 GAMMA=RATIO(10)
C TEMPE=TEMPE2
C RATE=RATIO(11)
C DEN=DEN2/DENI1
712 CONTINUE
C IF (DEN,EG.0.0) GO TO 710
C NUM=1
C VZERO=0.0
C IF (XI,NE.0.0)
C VZERO=MAX(1.0,-XI/GAMMA)*ABS(XI/GAMMA)/ABS(XI/GAMMA)
C DO 705 I=1,MLEV,ILEV
C BETA1=VI(I)*82
C BETA2=BETA1-XI/GAMMA
C IF (BETA2,LE.0.0) GO TO 705
C NUM=NUM+1
C VINUM(NUM)=SORT(BETA2)
C DELEE(NUM)=7.48*DELMAX(J)*BETA2*TEMPE*EXP(-2.08*SORT(BETA2*TEMPE/
C EMAX(J)))/EMAX(J)
C BSC=BSCAT3(J)*BETA2*GAMMA
C ETA(NUM)=BSCAT1(J)
C IF (BSC,LE.100.0)
C ETA(NUM)=BSCAT1(J)-BSCAT2(J)*EXP(-BSC)
705 CONTINUE
C IF (NUM,EG.1) GO TO 710
C VINUM(1)=VZERO
C BETA2=VZERO*82
C DELEE(1)=7.48*DELMAX(J)*BETA2*TEMPE*EXP(-2.08*SORT(BETA2*TEMPE/
C EMAX(J)))/EMAX(J)
C BSC=BSCAT3(J)*BETA2*GAMMA
C ETA(1)=BSCAT1(J)
C IF (BSC,LE.100.0)
C ETA(1)=BSCAT1(J)-BSCAT2(J)*EXP(-BSC)
C NUM1=NUM-1
C CUR2=0.0
C CUR3=0.0
C COFF1=EXP(-XI/GAMMA)/SOTPI
C ABEL0=0.0
C BDEL0=0.0
C ASCA0=0.0
C BSCA0=0.0
C
C DO B1A I=1,NUM1
C DENOM=VINUM(I+1)-VINUM(I)
C ABEL1=(DELEE(I+1)-DELEE(I))/DENOM
C BDEL1=DELEE(I)-ABEL1*VINUM(I)
C ABEL1=2.0*ABEL1
C BDEL1=2.0*BDEL1
C CUR2=CUR2+EXP(-VINUM(I)*82)*((ABEL1-ABEL0)/(1.0+VINUM(I)*82)
C 1 (BDEL1-BDEL0)/(VINUM(I)+COEFF(VINUM(I))))
C ABEL0=ABEL1
C BDEL0=BDEL1
B1A CONTINUE
C CUR2=CUR2
C CUR3=CUR3
C IF (XI,LE.0.0) GO TO B17
C CUR2=(2.08*YS(SORT(-XI/RATIO(3)))*COEFF(SORT(-XI/RATIO(3))))*8
C 1 CUR2*EXP(XI/RATIO(3))
C CUR3=(2.08*YS(SORT(-XI/RATIO(4)))*COEFF(SORT(-XI/RATIO(4))))*8
C 1 CUR3*EXP(XI/RATIO(4))
C
C B17 CONTINUE
C IF (IFAU(3),EQ.0.0) CUR2=0.0
C IF (IFAU(4),EQ.0.0) CUR3=0.0
C CS=RATE*COFF1*CUR2*DEN+CS
C CB=RATE*COFF1*CUR3*DEN+CB
C CSI=CSI+RATE*COFF1*CUR2*DEN
C CBI=CBI+RATE*COFF1*CUR3*DEN
710 CONTINUE
C RETURN
C END
C SUBROUTINE SECEL(XI,CSECEL,CSECEI)
C*****
C*****
C PURPOSE TO COMPUTE SECONDARY ELECTRONS INDUCED BY PROTONS FOR THE
C GUESS FIELD.
C
C*****
C EXTERNALS NONE
C*****
C INTEGER PERSEC,SECIND,PERPAN,PANIND
COMMON PSAVE(144,10),CSAVE(144,10),PSECTR(144),CSECTR(144),
1 DELEE(20),DELMAX(144),EMAX(144),ETA(20),BSCAT(144),
2 BSCAT2(144),BSCAT3(144),PHO(20,40),
1ANG(40),CPHOX(144),SUMANG,ANGD,BOUNDL(20,40),BOUNDI(20,40),
2AMGL(20,40),V1I(20,40),ICHECK(20,40),RATIO(13),IRODT(144),
3IFAU(144),JOCAL(144),ICOM(144),
1V(20),EV(8),MLEV,NTINES,ILEV,TIMIN(20),TIMAX(20),VINUM(20),
2A(144),B(144),C(144),BB(144),BM(144),TM(144),DM(144),
3EM(144),TMOCS(700),
1IFLG,NPOINT,N,IGDGM,ISYM,IPDIS,HSECT,NPEROD,NPEROD,IDIHY,
2GAMMA,DUD(70,48),DUDY(70,48),Y(144),DELTA,DELTA,T,
3YS(46,48),XS(66),XSS(70),
1VARIABLE(4),T,DELTA,SBOUND,NDIM,POT,H,J1,RPI,RP12,RPIMAF,SOTPI,
2SAY,TEMPE1,TEMPE2,DEME1,DEME2,DENI1,DENI2,TEMP11,TEMP12,
3TEMPR,LUM3,LUM4,LUM5,LUM6,LUM7,LUM8,LUM9,LUM10,
1IDL(144),JDTL(144),PERSEC(144),SECIND(144),IPANEL(144),
2PERPAN(144,4),PANIND(144),
1CIOM(144),CELEC(144),CSEC(144),CSECI(144),CPHOTO(144),
2CPHOT(144),CBSCAT(144),CBSCAL(144),SECPRN(144),SECPRI(144),
3PHI(144),CDUM(144),
1KASE,DOML,DPMI,HAND,RAD,PBOUND,OMEGA,ALPHA,SO,JP,IS,ECS,
2EXPVIZ(20),EFTVI(20),IERROR,TETHIN,TETMAX,BETA1,BETA2,JLESS,
3L2,CARRIV,CPH,XI,CSECEL,CSECEI,CS,CB,CSI,CBI
C
C CSECI=0.0
C CSECEI=0.0
C DO 710 J=1,2
C IF (J,NE.1) GO TO 711
C GAMMA=RATIO(8)
C TEMP1=TEMP11
C DEN=DEN1/DENI1
C RATE=RATIO(7)
C GO TO 712
711 CONTINUE
C GAMMA=RATIO(1)
C TEMP1=TEMP12
C DEN=DEN2/DENI1
C RATE=RATIO(12)
712 CONTINUE
C IF (TEMP1,EG.0.0) GO TO 710
C NUM=1
C VZERO=0.0
C IF (XI,NE.0.0)
C VZERO=MAX(1.0,-XI/GAMMA)*ABS(XI/GAMMA)/ABS(XI/GAMMA)
C DO 700 I=1,MLEV,ILEV
C BETA1=VI(I)*82
C BETA2=BETA1-XI/GAMMA
C IF (BETA2,LE.0.0) GO TO 700
C NUM=NUM+1
C VINUM(NUM)=SORT(BETA2)
C DELEE(NUM)=BETP(J)*SORT(0.001*BETA2*TEMP1)/(1.0+BETA2*TEMP1/
C 1 EXP(J))
700 CONTINUE
C IF (NUM,EG.1) GO TO 710
C VINUM(1)=VZERO
C BETA2=VINUM(1)*82
C DELEE(1)=BETP(J)*SORT(0.001*BETA2*TEMP1)/(1.0+BETA2*TEMP1/
C 1 EXP(J))
C
C CUR2=0.0
C COFF1=EXP(-XI/GAMMA)/SOTPI
C ABEL0=0.0
C BDEL0=0.0
C NUM1=NUM-1
C DO B1A I=1,NUM1
C DENOM=VINUM(I+1)-VINUM(I)
C ABEL1=(DELEE(I+1)-DELEE(I))/DENOM
C BDEL1=DELEE(I)-ABEL1*VINUM(I)
C ABEL1=2.0*ABEL1
C BDEL1=2.0*BDEL1
C CUR2=CUR2+EXP(-VINUM(I)*82)*((ABEL1-ABEL0)/(1.0+VINUM(I)*82)
C 1 (BDEL1-BDEL0)/(VINUM(I)+COEFF(VINUM(I))))
C ABEL0=ABEL1
C BDEL0=BDEL1
B1A CONTINUE
C CUR2=CUR2
C CUR3=CUR3
C IF (XI,GT.0.0) CUR2=(2.08*YS(SORT(-XI/RATIO(13)))*
C 1 COEFF(SORT(-XI/RATIO(13))))*EXP(XI/RATIO(13))*CUR2
C CSECEL=CSECEL+COFF1*CUR2*RATE*DEN
C CSECEI=CSECEI+COFF1*CUR3*RATE*DEN
710 CONTINUE
C RETURN
C END
C SUBROUTINE POI(IFLG,NPEROD,N,PEROD,H,A,B,C,IDIHY,T,IERROR,M)
C
C
C
C

```





```

WRITE (1,*) '***** DELTAX=BXAX,SO=OMEGA
600 FORMAT ('X',IPE10,3)
H=(DELTAX/DELTAY)/(DELTA/INITIAT)*HCONS)
KELUN
END
SUBROUTINE PLOTIT(SBOUND,PBOUND,N,MP0INT,SUMANG,CMT)
C
C POTENTIAL CONTOURS AROUND A SPACECRAFT UNDER MAGNETOSPHERIC
C CONDITIONS.
C
DIMENSION X(70)
DIMENSION Y(181)
COMMON/CDIV/YS(66,180),XS(70),SY(66,181)
COMMON/PIE/RP1,RP12,RP1HF,SDPI,SAY
COMMON/POT/GAMMA,DELTAX,DELTAY,Y(180),RAD,RPLDT
COMMON/BLK2/PHI(180),DELPHI(180),CN(20),NCH,ISCALE
DATA FAC/1000./
KP=RPLDT
N1=MP0INT+1
MP2=MP2
MP1=MP1
DELTAX=SBOUND/FLQAT(MP2-1)
C
C RELOCATE ELEMENTS OF THE ARRAYS XS AND YS.
C
DO 300 J=1,MP0INT
YS(MP2,J)=PBOUND*FAC
DO 310 I=2,MP1
IPA=MP2-I
IPB=IPA+1
YS(IPB,J)=YS(IPA,J)*FAC
310 CONTINUE
YS(1,J)=PHI(J)*FAC
300 CONTINUE
DO 320 I=1,MP2
320 XS(I)=DELTAX*FLQAT(I-1)
IF(DELTAX/DELTAY.LT.1.6) GO TO 99
C
C GRID CELLS ARE TOO ELONGATED RADIALY. FIX THIS USING INTERPOLATION.
C
MP1=MINO(MP182,64)
MP2=MP1+1
M=MP1-1
M1=M-1
M2=M-2
DELTAX=DELTAX/2.0
DO 91 I=1,MP2+2
IU=MP2+1-I
KV=(IU+1)/2
DO 91 J=1,MP0INT
91 YS(IU,J)=YS(KV,J)
DO 92 J=1,MP0INT
YS(2,J)=(3.0*YS(1,J)+4.0*YS(3,J)-YS(5,J))/8.0
YS(MP1,J)=(3.0*YS(MP2,J)+4.0*YS(M,J)-YS(M+2,J))/8.0
DO 92 I=4,MP2
92 YS(I,J)=(9.0*(YS(I-1,J)+YS(I+1,J))-YS(I-3,J)-YS(I+3,J))/16.0
DO 93 I=1,MP2
93 XS(I)=DELTAX*FLQAT(I-1)
WRITE(6,90) N
90 FORMAT('//IX',RADIAL GRID INTERVAL HALVED, NEW N =',I3)
C
C SET UP EXPANDED ARRAY OF POTENTIAL VALUES FOR USE BY PLOTTER.
C
99 DO 1 I=1,MP2
SY(I,M1)=YS(I,1)
DO 1 J=1,MP0INT
SY(I,J)=YS(I,J)
1 CONTINUE
C
C GENERATE GRID
C
DO 2 J=1,MP0INT
YY(J)=Y(J)
2 CONTINUE
YY(M1)=RP12+Y(1)
C
DO 3 I=1,MP2
IF(ISCAL.EQ.0) X(I)=MPS(1.0*FLQAT(I-1)*DELTAX)
IF(ISCAL.EQ.1) X(I)=MPS*EXP(FLQAT(I-1)*DELTAX)
3 CONTINUE
C
C INITIALIZE PLOTTER
C
CALL START
CALL SYMBOL(0.0,0.10,5.0,15,'PLEASE MOUNT BLACK FINE POINT PEN IN 1'
1,270,0.38)
CALL PLOT(1.0,0.0,-3)
CALL PLOT(8.0,5.5,-3)
C
C *** IF THE FIRST DIMENSION OF THE ARRAY BY IS CHANGED, IDX MUST BE
C CHANGED. ***
C
IDX=66
DO 100 I=1,NCH
CH(I)=CH(I)*FAC
CALL CNTOUR (X,MP2,YY,M1,SY,IDX,CN(I),CNT,CN(I))
100 CONTINUE
C
C
C ARCHED=M1/N1*(X(MP2)+DELTAX*.5)
SIZE=1.0
CALL PLOT(ARCHEB+0.0,3)
CALL PLOT(ARCHEB+0.375*SIZE+0.5*SIZE,2)
CALL PLOT(ARCHEB+0.375*SIZE+0.25*SIZE,2)
CALL PLOT(ARCHEB+0.75*SIZE+0.25*SIZE,2)
CALL PLOT(ARCHEB+0.75*SIZE+0.25*SIZE,2)
CALL PLOT(ARCHEB+0.375*SIZE+0.25*SIZE,2)
CALL PLOT(ARCHEB+0.375*SIZE+0.5*SIZE,2)
CALL PLOT(ARCHEB+0.0,2)
C
C
C CALL SYMBOL(ARCHEB-0.5*SIZE+0.625*SIZE+0.25*SIZE,'SUNLIGHT',0.0,0)
CALL SYMBOL(-0.75*SIZE+0.125*SIZE+0.25*SIZE,'SPACE',0.0,6)
CALL SYMBOL(-0.625*SIZE+0.375*SIZE+0.25*SIZE,'CRAFT',0.0,5)
C
C CALL CTRCL(RP-0.0,0.0,0.360,0,RP,RP,0.0)
C
DO 102 I=1,MP2
DO 102 J=1,MP0INT
YS(I,J)=YS(I,J)/FAC
102 CONTINUE
RE TURN
END
SUBROUTINE TOUR(IX,YR,YR,XS,YS)
RADR=YR
RADS=YS
YR=IRBSIN(RADR)
XR=IRBCOS(RADR)
YS=IRBSIN(RADS)
XS=IRBCOS(RADS)
RE TURN
END

```

```

SUBROUTINE BARRIER(MP2,N)
C
C *****
C PURPOSE
C TO COMPUTE HEIGHT AND RADIAL DISTANCE OF POTENTIAL BARRIERS
BY FITTING A PARABOLA.
C DESCRIPTION OF THE VARIABLES
C XBAR AND YBAR ARE BARRIER LOCATION AND HEIGHT
C EXTERNALS= NONE
C *****
COMMON/CDIV/YS(66,180),XS(70),SY(66,181)
COMMON/PIE/RP1,RP12,RP1HF,SDPI,SAY
COMMON/POT/GAMMA,DELTAX,DELTAY,Y(180),RAD,RPLDT
DIMENSION BRADP(180),BRADN(180),BDEGP(180),BDEGN(180),BPOTP(180),
BPOTN(180),IP(180),IN(180),JP(180),JN(180)
MP1=MP2-1
MNB=0
MNB=0
DO 400 J=1,N
IF (YS(1,J).GT.YS(MP2,J))GO TO 405
YMIN=YS(1,J)
IRMIN=1
YMAX=YS(MP2,J)
IRMAX=MP2
GO TO 403
405 YMAX=YS(1,J)
IRMAX=1
YMIN=YS(MP2,J)
IRMIN=MP2
403 DO 410 I=2,MP1
IF(Y(I,J).GT.YMAX) IRMAX=I
IF(Y(I,J).GT.YMIN) YMAX=YS(I,J)
IF(YS(I,J).LT.YMIN) IRMIN=I
IF(YS(I,J).LT.YMIN) YMIN=YS(I,J)
410 CONTINUE
IF(IRMAX.EQ.1.AND.IRMIN.EQ.MP2)GO TO 400
IF(IRMAX.EQ.MP2.AND.IRMIN.EQ.1)GO TO 400
C
C A BARRIER HAS BEEN FOUND AT ANGLE J.
C
DO 400 K=1,2
GO TO(401,402),K
401 IF (IRMAX.EQ.1.OR.IRMAX.EQ.MP2)GO TO 400
I=IRMAX
MNB=MNB+1
GO TO 440
402 IF(IRMIN.EQ.1.OR.IRMIN.EQ.MP2) GO TO 400
I=IRMIN
MNB=MNB+1
C
C CALCULATION OF HEIGHT AND RADIAL LOCATION OF POTENTIAL BARRIER BY
C FITTING A PARABOLA TO THREE POINTS
C
460 DIM1=(YS(I,J)-YS(I-1,J))/DELTAX
DIPI=(YS(I,J)-YS(I-1,J))/DELTAX
APAR=(DIPI-DIM1)/(2.0*DELTAX)
BPAR=DIPI-APAR*(XS(I)+XS(I+1))
CPAR=YS(I,J)-APAR*(XS(I)+XS(I+1))
XB=BPAR/(2.0*APAR)
YB=APAR*(XB+2.0*XB)+CPAR
GO TO (411,412),K
411 IP(MNB)=I
JP(MNB)=J
BRADP(MNB)=EXP(XB)
BDEGN(MNB)=Y(J)*180.0/RP1
BPOTP(MNB)=YB
GO TO 400
412 IN(MNB)=I
JN(MNB)=J
BRADN(MNB)=EXP(XB)
BDEGN(MNB)=Y(J)*180.0/RP1
BPOTN(MNB)=YB
400 CONTINUE
C
IF(MNB.EQ.0) GO TO 421
WRITE(6,422)
422 FORMAT('//IX','POSITIVE BARRIERS')
WRITE(6,429) (IP(L),JP(L),BRADP(L),BDEGN(L),BPOTP(L),L=1,MNB)
429 FORMAT('//IX,3(4I,'I',3H',J',2X,'RAD/RS',1X,'DEGREES',1X,
1,'HEIGHT(KV)')/(1X,2(14,OP2B,3,IPE12,3)))
421 IF(MNB.EQ.0) GO TO 423
WRITE(6,424)
424 FORMAT('//IX','NEGATIVE BARRIERS')
WRITE(6,429) (IN(L),JN(L),BRADN(L),BDEGN(L),BPOTN(L),L=1,MNB)
423 RETURN
END
SUBROUTINE SADDLE
C PURPOSE IS TO IDENTIFY SADDLE POINTS
C
COMMON/CPOISA/N,M,KBPOTS,NDCNCS
COMMON/CDIV/YS(66,180),XS(70),SY(66,181)
COMMON/PIE/RP1,RP12,RP1HF,SDPI,SAY
COMMON/POT/GAMMA,DELTAX,DELTAY,Y(180),RAD,RPLDT
COMMON/BLK2/PHI(180),DELPHI(180),CN(20),NCH,ISCALE
DIMENSION BX(66,180),BYR(180),BYV(180)
C
DO 100 J=1,N
BYR(J)=-(YS(3,J)+4.0*YS(2,J)-3.0*PHI(J))/(2.0*DELTAX*BRAD)
JP=J+1
IF(JP.GT.N) JP=1
IF(LN.EQ.0) JN=N
BYV(J)=(PHI(JP)-PHI(J))/(2.0*DELTAY*BRAD)
100 CONTINUE
C
WRITE(6,600)
600 FORMAT('//IX','RADIAL ELECTRIC FIELD AT THE SURFACE (KV/METER)')
WRITE(6,700) (BYR(J),J=1,N)
700 FORMAT(10(1X,IPE12,5))
WRITE(6,800)
800 FORMAT('//IX','TANGENTIAL ELECTRIC FIELD AT THE SURFACE',
1,' (KV/METER)')
WRITE(6,700) (BYV(J),J=1,N)
WRITE(6,850)
850 FORMAT('///)
C
C
MP1=M+1
MP2=M+2
DO 1 J=1,N
DO 1 I=2,MP2
SX(I,J)=999.
1 CONTINUE
C
C
DO 2 J=1,N
DO 2 I=2,MP1
P=(YS(I+1,J)-YS(I-1,J))/(2.0*DELTAX)
JP=J+1
IF(I.PE.N) M=1

```

```

      INI=J-1
      IF (J.EQ.1) JMI=N
      O=((YS(I,J)-YS(I,JMI))/(2.0*DELTA))
      PX=(YS(I,J)-2.0*YS(I,JMI)+YS(I,J))/DELTA*DELTA
      OY=(YS(I,J)-2.0*YS(I,JMI)+YS(I,JMI))/DELTA*DELTA
      PY=(YS(I,J)-YS(I,JMI)-YS(I,JMI)+YS(I,JMI))/
      1 DELTA*DELTA*0.0
      7 OX=PY
C
      DEN=PX*OY-OX*PY
      IF (DEN.NE.0.0) SK(I,J)=(O*PY-P*OX)/DEN
      IF (DEN.NE.0.0) SY(I,J)=(P*OX-O*PY)/DEN
      IF (ABS(SK(I,J)).LT.DELTA.AND.ABS(SY(I,J)).LT.DELTA)
      1 GO TO 3
      SK(I,J)=999.
C
      2 CONTINUE
C
C IF THERE IS NO SADDLE POINT-RETURN
C
      ICH=0
      DO 10 J=1,N
      DO 10 I=2,NP1
      IF (SX(I,J).EQ.999.0) ICH=ICH+1
      10 CONTINUE
      IF (ICH.NE.0) GO TO 11
      WRITE(A,900)
      900 FORMAT(IX,'NO SADDLE POINT FOUND')
      RETURN
C
C FIND ACCURATE LOCATION OF SADDLE POINTS
C
      11 DO 20 J=1,N
      JP1=J+1
      IF (J.EQ.N) JP1=1
      DO 20 I=1,NP1
C
C CHECK IF A SADDLE POINT HAS BEEN OBSERVED IN THE GRID CELL ABOVE
C AND TO THE RIGHT OF THE POINT(I,J).
C
      ANDYX=0.0
      ANDY=0.0
      AN=0.0
      JMI=J-1
      IF (I.EQ.1) GO TO 22
      IF (SX(I,J).EQ.999.0.OR.SX(I,J).LT.0.0.OR.SY(I,J).LT.0.0)
      1 GO TO 21
      AN=AN+1.0
      ANDYX=ANDYX+SX(I,J)
      ANDY=ANDY+SY(I,J)
      21 IF (SX(I,JP1).EQ.999.0.OR.SX(I,JP1).LT.0.0.OR.SY(I,JP1).GT.0.0)
      1 GO TO 22
      AN=AN+1.0
      ANDYX=ANDYX+SX(I,JP1)
      ANDY=ANDY+SY(I,JP1)*DELTA
C
      22 IF (I.EQ.NP1) GO TO 24
      IF (SX(I+1,J).EQ.999.0.OR.SX(I+1,J).GT.0.0.OR.SY(I+1,J).LT.0.0)
      1 GO TO 23
      AN=AN+1.0
      ANDYX=ANDYX+SX(I+1,J)*DELTA
      ANDY=ANDY+SY(I+1,J)
      23 IF (SX(I+1,JP1).EQ.999.0.OR.SX(I+1,JP1).GT.0.0.OR.SY(I+1,JP1).GT.
      0.0) GO TO 24
      AN=AN+1.0
      ANDYX=ANDYX+SX(I+1,JP1)*DELTA
      ANDY=ANDY+SY(I+1,JP1)*DELTA
      24 CONTINUE
      IF (AN.EQ.0.0) GO TO 20
      AX=ANDYX/AN
      AY=ANDY/AN
      MAXX=ABS(AX)
      MAXY=ABS(AY)
      XSB=ABS(DELTA*AX)
      YSB=ABS(DELTA*AY)
      SADDPT=(YS(I+1,J)*XSB+YS(I,J)*S(1.0-XSB))/S(1.0-YSB)
      1*(YS(I+1,JP1)*XSB+YS(I,JP1)*S(1.0-XSB))/YSB
C
      SARRAD=EXP(MAXX)
      SARRB=MAXY/S(1.0/NP1)
      WRITE(A,401) I,J,SARRAD,SARRB,SADDPT,AN
      401 FORMAT(IX,'SADDLE POINT DETECTED IN CELL',2I3,' RAD/RB= ',
      A7.3,' DEGREE= ',F7.3,' POTENTIAL(KV)= ',E12.3,
      8' NUMBER OF DETECTIONS ',D994.1)
      IF (AN.LT.4.0) GO TO 20
      IF (ISCALE.EQ.0) SRRAD=NPLOTS*(1.0+MAXX)
      IF (ISCALE.EQ.1) SRRAD=NPLOTS*EXP(MAXX)
      SARR=SPRAB*SCS(MAXY)
      SARRB=SPRAB*SCS(MAXY)
      IF (ABS(SARR).GT.3.25) GO TO 20
      IF (ABS(SARRB).GT.3.0) GO TO 20
      CALL SYMBOL(SARR,SARRB,0.20,4.45,0.0)
      20 CONTINUE
      CALL FINISH
      RETURN
      END
      SUBROUTINE SPOTS
C
C THIS SUBROUTINE GETS THE SURFACE POTENTIAL VALUES PHI(1,2,.....N)
C IN A MANNER DEPENDING ON THE VALUE OF KSPOTS.
C
      COMMON/CP01SA/N,N,KSPOTS,NBCSIS
      COMMON/BLK2/PHI(100),DELPHI(100),CH(20),NCH,ISCALE
C
      IF (KSPOTS.GT.2) GO TO 900
C
      IF (N.NE.100) GO TO 900
      DO 11 J=1,N
      PHI(J)=-0.07
      IF (J.GE.1.AND.J.LE.8) PHI(J)=-0.06
      IF (J.GE.42.AND.J.LE.53) PHI(J)=-0.06
      IF (J.GE.91.AND.J.LE.98) PHI(J)=-0.06
      IF (J.GE.128.AND.J.LE.139) PHI(J)=-0.06
      11 CONTINUE
      RETURN
C
      900 WRITE(A,901) N,KSPOTS
      901 FORMAT(IX,'SPOTS CALLED INCORRECTLY. N = ',I3,
      A' KSPOTS = ',I3)
      RETURN
      END
      ENDS

```

E1  
Appendix E: Listing of XYCIC

```

FTN4
SEMA(AEPA1,0)
PROGRAM OBJCT(3,150)
C
C THIS IS THE MAIN ROUTINE FOR THE OBJECT DEFINITION SECTION
C OF XYCIC.
C
C (COMMON/AEPA1/XD(2560),YD(2560),IG(2560,4),IL(53,53),
C ICH(53,53),ICA(52,52)
C COMMON/CNE SH/INSHIN,INSHIN,INSHX,INSHX,IMO,JMO-DX,BY
C COMMON/CNST1/NEST(10),NNI(10),NNJ(10),NOUTER(10),RS(10),
C IRE(10),KAR(10),KARA(10),RNU(10),RMA(10)
C COMMON/CNST2/NESSMAX,NAHDD,NAKLE,NOBOUT,MODIN,KELOUT,
C IRELIN,MODINS
C COMMON/CONV/MCONV(10,4,4)
C COMMON/CREP/LNRN,LNRB(32),LNRX(32),LNRV(32)
C COMMON/CSUM/SANGL,NSUMB(32),XSUMB(32),YSUMB(32),ASUNS(64),
C INSUM(120),NSUM
C COMMON/IDBT/LUN,LU,ITRACS
C COMMON/OBJ1/MOJCT,NSGO(5),ISPACE(64),JSPACE(64),XSSEG(64),
C YSSEG(64),XSEGO(4),YSEGO(4),ISLP(64),IVEC(64),PLPSEG(64),
C XCOX(5),COY(5)
C COMMON/OBJ2/ISP(120),YSP(120),XEP(120),YEP(120),MSP(120),
C ISEP(120),MSP(32),MPAT(5),MXPAT
C COMMON/PSOLV/ISY,IPQISS,IPGT,REBY,CPOIS
C COMMON/RPI/MP1,P1,MP13,P12,SP1,SP12
C COMMON/BLK1/XS(15,6),YS(15,6),XE(15,6),YE(15,6),TY(15,7),
C TYR1(15,3),TYR2(15,3)
C COMMON/BLK2/BUF1(15),BUF2(15),BUF3(15),BUF4(15)
C COMMON/BLK3/BUF5(15),BUF6(15),BUF7(15),BUF8(20),BUF9(30)
C COMMON/BLK4/BUF1(25),BUF2(25),BUF3(25),BUF4(25)
C COMMON/BLK5/LR(4,4),LT(5,4),RX(9),RY(9),RX(4),RCB(4,6),
C ILLC(15,9)
C COMMON/BLK6/XO,YO,MO,MS,DH1,DH2,DH3,DH4,DH5
C COMMON/BLK7/NO,IO,JO,MO,KO,LO,MO,MC1,MC2,MC3,IRN,JRN
C COMMON/BLK8/MS,ME,IBUM1,IBUM2,IBUM3,IBUM4,IBUM5,IBUM6
C COMMON/BLK9/I1,I2,I3,I4,I5,I6,I7,I8,I9,I10
C DIMENS ION NAME(3)
C DATA NAME/2ND,2MPT,2M1 /
C
C WRITE(LUN,999)
C *** FORMAT(///10X,'888'XYCIC' SATTELLITE SIMULATION888')
C CALL EXEC(B,NAME)
C
C STOP
C END
C BLOCK DATA
C COMMON/CNE SH/INSHIN,INSHIN,INSHX,INSHX,IMO,JMO-DX,BY
C COMMON/CNST1/NEST(10),NNI(10),NNJ(10),NOUTER(10),RS(10),
C IRE(10),KAR(10),KARA(10),RNU(10),RMA(10)
C COMMON/CNST2/NESSMAX,NAHDD,NAKLE,NOBOUT,MODIN,KELOUT,
C IRELIN,MODINS
C COMMON/CONV/MCONV(10,4,4)
C COMMON/CREP/LNRN,LNRB(32),LNRX(32),LNRV(32)
C COMMON/CSUM/SANGL,NSUMB(32),XSUMB(32),YSUMB(32),ASUNS(64),
C INSUM(120),NSUM
C COMMON/IDBT/LUN,LU,ITRACS
C COMMON/OBJ1/MOJCT,NSGO(5),ISPACE(64),JSPACE(64),XSSEG(64),
C YSSEG(64),XSEGO(4),YSEGO(4),ISLP(64),IVEC(64),PLPSEG(64),
C XCOX(5),COY(5)
C COMMON/OBJ2/ISP(120),YSP(120),XEP(120),YEP(120),MSP(120),
C ISEP(120),MSP(32),MPAT(5),MXPAT
C COMMON/PSOLV/ISY,IPQISS,IPGT,REBY,CPOIS
C COMMON/RPI/MP1,P1,MP13,P12,SP1,SP12
C COMMON/BLK1/XS(15,6),YS(15,6),XE(15,6),YE(15,6),TY(15,7),
C TYR1(15,3),TYR2(15,3)
C COMMON/BLK2/BUF1(15),BUF2(15),BUF3(15),BUF4(15)
C COMMON/BLK3/BUF5(15),BUF6(15),BUF7(15),BUF8(20),BUF9(30)
C COMMON/BLK4/BUF1(25),BUF2(25),BUF3(25),BUF4(25)
C COMMON/BLK5/LR(4,4),LT(5,4),RX(9),RY(9),RX(4),RCB(4,6),
C ILLC(15,9)
C COMMON/BLK6/XO,YO,MO,MS,DH1,DH2,DH3,DH4,DH5
C COMMON/BLK7/NO,IO,JO,MO,KO,LO,MO,MC1,MC2,MC3,IRN,JRN
C COMMON/BLK8/MS,ME,IBUM1,IBUM2,IBUM3,IBUM4,IBUM5,IBUM6
C COMMON/BLK9/I1,I2,I3,I4,I5,I6,I7,I8,I9,I10
C DIMENS ION NAME(3)
C DATA NAME/2ND,2MPT,2M1 /
C
C ***** AND TRACKS WHERE I/O DATA STORAGE STARTS.
C DATA LUN6/LU/SI/ITRACS/0/
C ***** CONSTANTS WITH RESPECT TO 'PI'.
C DATA MP1,PI,MP13,P12,SP1,SP12/1.570796326794897,
C A3.141592653589793,4.712388980384690,6.283185307179586,
C B1.772453850905516,1.1037716999031/
C
C END
C SUBROUTINE SORT(N)
C COMMON/BLK4/IA(25),IB(25),IC(25),ID(25)
C
C N1=N-1
C M=1
C 1 N1=N+1
C 2 IF(IA(N).LE.IA(N1)) GO TO 3
C I1=IA(N)
C I2=IB(N)
C IA(N)=IA(N1)
C IB(N)=IB(N1)
C IA(N1)=I1
C IB(N1)=I2
C 3 N1=N-1
C IF(N1.LE.N) GO TO 2
C N=N+1
C IF(IA(N1).GT.IA(N)) GO TO 1
C RETURN
C END
C ENDS

```



```

DO 90 I=INMS,INNE
DO 90 J=JNMS,JNNE
IF (ICM(I,J).LE.-1) GO TO 90
IF (ICM(I,J).LE.-1) OR (ICM(I,J).LE.-1) OR
1 ICM(I,J).LE.-1) OR (ICM(I,J).LE.-1) OR
2 ICM(I,J).LE.-1) OR (ICM(I,J).LE.-1) OR
3 ICM(I,J).LE.-1) OR (ICM(I,J).LE.-1) ICM(I,J)+1
90 CONTINUE

92 DO 95 I=INMS,INNE
DO 95 J=JNMS,JNNE
JJ=ICM(I,J)
IF (JJ.LE.-1) OR (JJ.EQ.1) GO TO 95
MS1=MS1+1
IL(I,J)=MS1
YG(MS1)=FLOAT(I-INO)SDX
YG(MS1)=FLOAT(J-JNO)SDY
95 CONTINUE
MODINS=MS1+1

DO 100 I=INMS,INNE
DO 110 J=JNMS,JNNE
JI=ICM(I,J)
IF (JI.EQ.-1) GO TO 120
IF (JI.EQ.0) GO TO 110
MS1=MS1+1
IL(I,J)=MS1
XG(MS1)=FLOAT(I-INO)SDX
YG(MS1)=FLOAT(J-JNO)SDY
GO TO 130
120 IL(I,J)=-1
130 IF (I.EQ.INMS) OR (I.EQ.INNE) GO TO 110
IF (J.EQ.JNMS) OR (J.EQ.JNNE) GO TO 110
I1=ICK(I-1,J)
I2=ICK(I,J)
IF (I1.EQ.5) AND (I1.LE.8) GO TO 140
GO TO 110
140 IF (I2.EQ.5) AND (I2.LE.8) GO TO 150
GO TO 110
150 MS1=MS1+1
XG(MS1)=FLOAT(I-INO)SDX
YG(MS1)=FLOAT(J-JNO)SDY
HI=HI+1
H=(H+1)SD3
IBI(M+1)=I
IBI(M+2)=J
IBI(M+3)=MS1
110 CONTINUE

C
IF (I.EQ.INNE) GO TO 100

C
DO 160 J=JNMS,JNNE
JI=ICK(I,J-1)
J2=ICK(I,J)
IF (J1.EQ.9) AND (J1.LE.12) GO TO 170
GO TO 160
170 IF (J2.EQ.9) AND (J2.LE.12) GO TO 180
GO TO 160
180 MS1=MS1+1
XG(MS1)=FLOAT(I-INO)SDX
YG(MS1)=FLOAT(J-JNO)SDY
HJ=HJ+1
H=(H+1)SD3
IBJ(M+1)=I
IBJ(M+2)=J
IBJ(M+3)=MS1
160 CONTINUE
100 CONTINUE
MAXNO=MS1
KE(1)=MS1
KAM(1)=KE(1)-KE(1)+1

C
WRITE(LUN,123) MAXNO
123 FORMAT('00 MAXNO='//I4)

C
K=KELOUT
DO 200 I=1,INMHIN
DO 210 J=1,JNMHIN
MM=ICK(I,J)
IF (MM.EQ.-1) GO TO 210
K=K+1
IF (MM.EQ.0) GO TO 220

C
IG(K,1)=IL(I,J)
IG(K,2)=IL(I01,J)
IG(K,3)=IL(I01,J01)
GO TO 270
220 IF (MM.EQ.5) AND (MM.LE.8) GO TO 280
IF (MM.EQ.9) AND (MM.LE.12) GO TO 360
GO TO (230,240,250,260),MM

C
230 IG(K,1)=IL(I,J)
IG(K,2)=IL(I01,J)
IG(K,3)=IL(I01,J01)
GO TO 270
240 IG(K,1)=IL(I,J)
IG(K,2)=IL(I01,J)
IG(K,3)=IL(I01,J01)
GO TO 270
250 IG(K,1)=IL(I,J)
IG(K,2)=IL(I01,J01)
IG(K,3)=IL(I01,J01)
GO TO 270
260 IG(K,1)=IL(I01,J)
IG(K,2)=IL(I01,J01)
IG(K,3)=IL(I01,J01)
GO TO 270
270 ICK(I,J)=-1
GO TO 210

C
280 DO 290 M=1,M1
MM=(M+1)SD3
IF (IBI(MM+1).NE.101) GO TO 290
IF (IBI(MM+2).NE.J) GO TO 290
IS=IBI(MM+3)
GO TO 300
290 CONTINUE
300 M1=MM+4
GO TO (310,320,330,340),M1

C
110 IG(K,1)=IL(I,J)
IG(K,2)=IL(I01,J)
IG(K,3)=IS
K=K+1
IG(K,1)=IL(I01,J)
IG(K,2)=IL(I02,J)
IG(K,3)=IS
K=K+1
IG(K,1)=IS
IG(K,2)=IL(I01,J)
IG(K,3)=IL(I01,J01)
K=K+1
IG(K,1)=IL(I01,J01)
IG(K,2)=IS
IG(K,3)=IL(I02,J01)
GO TO 350
IG(K,1)=IL(I01,J01)
IG(K,2)=IS
IG(K,3)=IL(I01,J01)
K=K+1
IG(K,1)=IL(I01,J01)
IG(K,2)=IS
IG(K,3)=IL(I02,J01)
K=K+1
IG(K,1)=IL(I02,J)
IG(K,2)=IS
IG(K,3)=IL(I02,J)
ICK(I,J)=-1
ICK(I,J01)=-1
GO TO 210

C
360 DO 370 M=1,MJ
MM=(M+1)SD3
IF (IBJ(MM+1).NE.1) GO TO 370
IF (IBJ(MM+2).NE.J01) GO TO 370
IS=IBJ(MM+3)
GO TO 380
370 CONTINUE

C
380 M1=MM+4
GO TO (390,400,410,420),M1

C
390 IG(K,1)=IL(I,J)
IG(K,2)=IL(I01,J)
IG(K,3)=IS
K=K+1
IG(K,1)=IS
IG(K,2)=IL(I01,J)
IG(K,3)=IL(I01,J01)
K=K+1
IG(K,1)=IL(I01,J01)
IG(K,2)=IS
IG(K,3)=IL(I01,J01)
K=K+1
IG(K,1)=IS
IG(K,2)=IS
IG(K,3)=IL(I01,J02)
GO TO 430
400 IG(K,1)=IL(I,J)
IG(K,2)=IL(I01,J)
IG(K,3)=IS
K=K+1
IG(K,1)=IL(I,J)
IG(K,2)=IS
IG(K,3)=IL(I01,J01)
K=K+1
IG(K,1)=IL(I01,J01)
IG(K,2)=IS
IG(K,3)=IL(I01,J02)
GO TO 430
410 IG(K,1)=IL(I,J)
IG(K,2)=IS
IG(K,3)=IL(I01,J01)
K=K+1
IG(K,1)=IL(I01,J01)
IG(K,2)=IS
IG(K,3)=IL(I01,J02)
K=K+1
IG(K,1)=IL(I01,J02)
IG(K,2)=IS
IG(K,3)=IL(I01,J02)
GO TO 430
420 IG(K,1)=IL(I01,J)
IG(K,2)=IL(I01,J01)
IG(K,3)=IS
K=K+1
IG(K,1)=IS
IG(K,2)=IL(I01,J01)
IG(K,3)=IL(I01,J02)
K=K+1
IG(K,1)=IS
IG(K,2)=IL(I01,J02)
IG(K,3)=IL(I01,J02)
GO TO 430
430 ICK(I,J)=-1
ICK(I,J01)=-1

C
210 CONTINUE
260 CONTINUE
KAM=K-KELOUT
MAXLE=K

C
C
MM=1
IF (MM.EQ.1) GO TO 1302
DO 1301 J=1,JNMMH
JJ=JNMMH+1-J
WRITE(LUN,1350) (ICM(I,J),I=1,INMMH)
CONTINUE
1301 ICASE=1
IF (INMMH.EQ.25) ICASE=2
DO 440 I=1,ICASE
IF (I.EQ.2) GO TO 450
I1=1
I2=INMMH-INMMH+25)
GO TO 440
450 I1=25
I2=INMMH
WRITE(LUN,979)
979 FORMAT(////)
440 DO 470 J=1,JNMMH
JJ=JNMMH+1-J
WRITE(LUN,982) (IL(I,J),I=1,12)
982 FORMAT(2515)
470 CONTINUE

```

```

440 CONTINUE
100 CONTINUE
WRITE(LUN,73) NMAX,NODIN,NODINS
* 1. UNM1: 8 8 OF CELLS IN AN INNERMOST NEST * 15/
1 88 NODINU * 15/ 88 NODINS * 15/
DO 500 J=1,NMSMX
DO 500 J=1,NMSMX
JJ=JCM(I,J)
IF(JJ.EQ.1.OR.JJ.EQ.-4) ICM(I,J)=0
500 CONTINUE
C
CALL EXEC(1,LU,IBUF,64,ITRACS,2,55)
IBUF(26)=NODINO
IBUF(27)=NODINS
IBUF(28)=NODINS-NODINO
CALL EXEC(2,LU,IBUF,64,ITRACS,2,55)
CALL EXEC(8,NAME)
C
STOP
END
END#
FTN#
AENA(AENA1,0)
PROGRAM ASSIN(5,150)
C
C THIS S/P DOES RENUMBERING OF NODES AT THE SURFACE OF OBJECT
C SO THAT LAST "NSURF" NODES ARE ALWAYS CORRESPONDING TO THE
C SURFACE NODES, WHERE "NSURF" IS A TOTAL 8 OF SURFACE NODE.
C
COMMON/AENA1/ID(2560),YD(2560),ID(2560,4),JL(53,53),
IICM(53,53),JCK(52,52)
COMMON/CRESH/IRSHIN,IRSHIN,IRSHMX,IRSHMX,INO,JNO,DX,DIY
COMMON/CNST/RESMAX,MAXNOB,MAXELE,NOBOUT,NODIN,KELOUT,
IAELIN,NODINS
COMMON/IDDAT/LUM,LU,ITRACS
COMMON/OBJ1/NOBJCT,NSEGO(5),ISPACE(64),JSPACE(64),XSBEQ(64),
LYSSE(64),XSESO(64),YESEQ(64),ISLP(64),IVEC(64),BLPSEQ(64),
ZCOO(5),COO(5)
COMMON/OBJ2/YSP(128),YSP(128),XEP(128),YEP(128),NSP(128),
INEP(128),NMP(128),MPAT(5),MAXPAT
COMMON/BLR1/XS(15,6),YS(15,6),XE(15,6),YE(15,6),TY(15,7),
LYN(15,5),YYN(15,5)
COMMON/BLR4/IBUF(128),IBUF(128),NODE(25),IBUF(4,25)
DIMENSION NSURF(128),IBUF(64),NAME(3),IAUX(128)
EQUIVALENCE (ICK,IAUX)
C
DATA NAME/2HSH,2HAD,2HE /
DATA NAME/2HML,2HMT,2NI /
C
IFLG=0
WRITE(LUN,999)
999 FORMAT(/20,' ',5X,'ASSIN STARTS',5X,20,' ')
NABA=0
IF(INER.EQ.0) GO TO 690
ICASE=1
IF(ISHMX.GT.25) ICASE=2
DO 400 I=1,ICASE
IF(I.EQ.2) GO TO 410
I=1
I2=MIN0(ISHMX,25)
GO TO 420
410 I=25
I2=ISHMX
WRITE(LUN,999)
999 FORMAT(/)
420 DO 630 J=1,ISHMX
JI=ISHMX+1-J
WRITE(LUN,992) (IL(I,JI),I=1,I2)
992 FORMAT(25I5)
630 CONTINUE
400 CONTINUE
C
WRITE(LUN,670) ((I0(I,J),J=1,4),I=KELIN,MAXELE)
WRITE(LUN,680) (IX(I),YB(I),I=NODIN,MAXNOB)
670 FORMAT(24I5)
680 FORMAT(8I4,2F6.2)
690 IPAT=0
L=NODINS
LB=MAXNOB
MAXSE=NSEGO(NOBJCT)
DO 1000 N=1,MAXSE
M=0
IS=ISLP(N)
IU=IVEC(N)
MI=XSESO(N)
M2=XSBEQ(N)
MJ=YESEQ(N)
M3=YSBEQ(N)
IF(I,EG,0) GO TO 40
IF(IS,EG,3) GO TO 40
IF(IU,EG,1) GO TO 20
IF(MI,EG,0) GO TO 10
DO 100 L=LA+LB
IF(XG(L),GE,M11.AND,XG(L),LE,M12) GO TO 110
GO TO 100
110 IF(YG(L),GE,MJ1.AND,YG(L),LE,MJ2) GO TO 120
GO TO 100
120 IF(ABS(GB(XG(L)-M11)+MJ1-YG(L)),LE,0.018DY) GO TO 125
GO TO 100
125 M=M+1
NODE(N)=L
CONTINUE
NZ=1
GO TO 400
10 DO 130 L=LA+LB
IF(XG(L),GE,M11.AND,XG(L),LE,M12) GO TO 140
GO TO 130
140 IF(YG(L),GE,MJ1.AND,YG(L),LE,MJ2) GO TO 145
GO TO 130
145 IF(ABS(GB(XG(L)-M11)+MJ1-YG(L)),LE,0.018DY) GO TO 147
GO TO 130
147 M=M+1
NODE(N)=L
CONTINUE
NZ=2
DO 20 IF(IG,GT,0) GO TO 30
DO 150 L=LA+LB
IF(XG(L),GE,M12.AND,XG(L),LE,M11) GO TO 160
GO TO 150
160 IF(YG(L),GE,MJ1.AND,YG(L),LE,MJ2) GO TO 170
GO TO 150
170 IF(ABS(GB(XG(L)-M11)+MJ1-YG(L)),LE,0.018DY) GO TO 175
GO TO 150
175 M=M+1
NODE(N)=L
CONTINUE
NZ=3
GO TO 400
50 DO 180 L=LA+LB
IF(XG(L),GE,M12.AND,XG(L),LE,M11) GO TO 185
GO TO 180
185 IF(YG(L),GE,MJ2.AND,YG(L),LE,MJ1) GO TO 190
GO TO 180
190 IF(ABS(GB(XG(L)-M11)+MJ1-YG(L)),LE,0.018DY) GO TO 195
GO TO 180
195 M=M+1
NODE(N)=L
CONTINUE
NZ=4
GO TO 400
40 IF(IU,EG,1) GO TO 50
DO 200 L=LA+LB
IF(YG(L),GE,MJ1) GO TO 210
GO TO 200
210 IF(XG(L),GE,M11.AND,XG(L),LE,M12) GO TO 220
GO TO 200
220 M=M+1
NODE(N)=L
CONTINUE
NZ=5
GO TO 400
50 DO 250 L=LA+LB
IF(YG(L),GE,MJ1) GO TO 260
GO TO 250
260 IF(XG(L),GE,M12.AND,XG(L),LE,M11) GO TO 270
GO TO 250
270 M=M+1
NODE(N)=L
CONTINUE
NZ=6
GO TO 400
60 IF(IU,EG,1) GO TO 70
DO 300 L=LA+LB
IF(XG(L),GE,M11) GO TO 310
GO TO 300
310 IF(YG(L),GE,MJ1.AND,YG(L),LE,MJ2) GO TO 320
GO TO 300
320 M=M+1
NODE(N)=L
CONTINUE
NZ=7
GO TO 400
70 DO 350 L=LA+LB
IF(XG(L),GE,M11) GO TO 360
GO TO 350
360 IF(YG(L),GE,MJ2.AND,YG(L),LE,MJ1) GO TO 370
GO TO 350
370 M=M+1
NODE(N)=L
CONTINUE
NZ=8
400 NMAX=N
DO 410 M=1,NMAX
IBUF(2)(M)=N
IBUF(4)(M)=NODE(M)
IF(NZ,GE,7) GO TO 420
IBUF(8)(M)=IBUF(4)(M)*81000.0
GO TO 410
420 IBUF(1)(M)=YB(1)(M)*81000.0
410 CONTINUE
C
CALL SORT(NMAX)
C
L=(NMAX+1)*(1-I)/2
DO 430 M=1,NMAX
LL=L+I*VEN
NODE(M)=IBUF(4)(IBUF(2)(LL))
CONTINUE
430 NMAX=NMAX-1
DO 440 M=1,NMAX
IPAT=IPAT+1
NSP(IPAT)=NODE(M)
NEP(IPAT)=NODE(M+1)
440 CONTINUE
IF(IFLG,EG,0) GO TO 1000
NSP(N)=IPAT
DO 450 M=1,NOBJCT
IF(M,NE,NSEGO(M)) GO TO 450
IF(M,EG,1) GO TO 440
MPAT(M)=IPAT-MPAT(N-1)
GO TO 450
450 MPAT(N)=IPAT
450 CONTINUE
1000 CONTINUE
IF(IFLG,EG,1) GO TO 480
IAUX(1)=IPAT
DO 470 I=1,IPAT
IAUX(I+1)=NSP(I)
470 CONTINUE
IFLG=1
CALL NSURF
GO TO 490
480 MAXPAT=IPAT
NSURF=MAXPAT
DO 490 M=1,MAXPAT
L=NSP(M)
LL=NEP(M)
NSURF(M)=L
YSP(M)=XG(L)
YBP(M)=YG(LL)
XEP(M)=XG(LL)
YEP(M)=YB(LL)
490 CONTINUE
NOB=MAXNOB-NSURF
C
CALL EXEC(1,LU,IBUF,64,ITRACS,2,55)
IBUF(9)=NOB
IBUF(10)=MAXELE
IBUF(11)=MAXNOB
IBUF(12)=MAXPAT
IBUF(13)=NSURF
CALL EXEC(2,LU,IBUF,64,ITRACS,2,55)
CALL EXEC(2,LU,XSP,256,ITRACS,3,0)
CALL EXEC(2,LU,YSP,256,ITRACS,3,8)
CALL EXEC(2,LU,NEP,256,ITRACS,3,16)
CALL EXEC(2,LU,YEP,256,ITRACS,3,24)
CALL EXEC(2,LU,NSP,128,ITRACS,3,32)
CALL EXEC(2,LU,NEP,128,ITRACS,3,36)
CALL EXEC(2,LU,NSURF,128,ITRACS,3,40)
DO 510 I=1,32
IBUF(I)=MMP(I)
510 CONTINUE
DI 570 I=1,5
TRM(I)=MPAT(I)
570 CONTINUE
CALL EXEC(1,LU,IBIN,64,ITRACS,3,44)
CALL EXEC(8,NAME)

```



```

NINNK=1-1-1-1-1
NCONA(4)=1-1-1-1-1
100 CONTINUE
M=M+1
NCONA(4)=M+1-1-1-1-1
110 NINNK=1-1-1-1-1
WRITE(LUN,98) (NINNK(I),I=1,N)
98 FORMAT(88 NINNK(2015))
WRITE(LUN,99) (NCONA(I),I=1,N)
99 FORMAT(88 NCONA(2015))

A=0
M=1
IF (ISYN.EQ.1) M=0
DO 200 I=1,INES
  I1=MSHANI-1
  N1=NNI(1)
  N2=NNJ(1)
  IF (ISYN.EQ.1) GO TO 240
  K=K+1
  IG(K,1)=MS
  IG(K,2)=MS+1
  IG(K,3)=MS+(N1+N2)
  IG(K,4)=IG(K,3)-1
240 J1=NEST(1)
  DO 250 J=1,J1
    NN=J
    IF (ISYN.EQ.1) NN=1
    M1=M1-NN
    M2=M2-NN
    IF (I.EQ.INES.AND.J.EQ.J1) GO TO 340
    IF (J.EQ.1) GO TO 270
    JUMP=1
  DO 280
  JUMP=2
280 IF (J.EQ.1) GO TO 290

  A=K+1
  IF (ISYN.EQ.1) GO TO 292
  IG(K,1)=IG(K,1)+1
  IG(K,2)=IG(K,2)+1
  IG(K,3)=IG(K,3)+1
  IG(K,4)=IG(K,3)-1
  GO TO 290
292 IG(K,1)=IG(K,1)+1
  IG(K,2)=IG(K,2)+1
  IG(K,3)=IG(K,2)+1
  IG(K,4)=IG(K,1)+JUMP
  IF (J.ME.J1) GO TO 307
  NCONM(1,2,1)=K
  NCONM(1,2,3)=IG(K,1)+1
  GO TO 307
290 IF (ISYN.EQ.1) GO TO 306
  IF (J.ME.J1) GO TO 295
  NCONM(1,1,1)=K+1
  NCONM(1,1,3)=IG(K,3)+1

  295 DO 300 M=1,M1
    K=K+1
    IG(K,1)=IG(K,1)+1
    IG(K,2)=IG(K,2)+1
    IG(K,3)=IG(K,1,3)+JUMP
    IG(K,4)=IG(K,3)-JUMP
  300 CONTINUE
  IF (J.ME.J1) GO TO 305
  NCONM(1,1,2)=K
  NCONM(1,1,4)=IG(K,4)+1
  305 K=K+1
  IG(K,1)=IG(K,1)+1
  IG(K,2)=IG(K,2)+1
  IG(K,3)=IG(K,2)+1
  IG(K,4)=IG(K,1,3)
  IF (J.ME.J1) GO TO 308
  NCONM(1,2,1)=K+1
  NCONM(1,2,3)=IG(K,4)+1
  GO TO 308
  306 K=K+1
  IG(K,1)=MS+2+M1+N2
  IG(K,2)=MS+1
  IG(K,3)=MS+2
  IG(K,4)=IG(K,1)+JUMP
  IF (J.ME.J1) GO TO 307
  NCONM(1,2,1)=K
  NCONM(1,2,3)=IG(K,1)+1
  307 M2=M2-1

  308 DO 310 M=1,M2
    K=K+1
    IG(K,1)=IG(K,1,4)
    IG(K,2)=IG(K,1,2)+1
    IG(K,3)=IG(K,1,3)+1
    IG(K,4)=IG(K,1,4)+JUMP
  310 CONTINUE
  IF (J.ME.J1) GO TO 315
  NCONM(1,2,2)=K
  NCONM(1,2,4)=IG(K,1)+1
  315 K=K+1
  IG(K,1)=IG(K,1,4)
  IG(K,2)=IG(K,1,2)+1
  IG(K,3)=IG(K,2)+1
  IG(K,4)=IG(K,3)+1
  IF (J.ME.J1) GO TO 318
  NCONM(1,3,1)=K+1
  NCONM(1,3,3)=IG(K,1)+1

  318 DO 320 M=1,M1
    K=K+1
    IG(K,1)=IG(K,1,1)+JUMP
    IG(K,2)=IG(K,1,1)-JUMP
    IG(K,3)=IG(K,1,3)+1
    IG(K,4)=IG(K,3)+1
  320 CONTINUE
  IF (J.ME.J1) GO TO 325
  NCONM(1,1,2)=K
  NCONM(1,1,4)=IG(K,2)+1
  325 IF (ISYN.EQ.1) GO TO 320
  K=K+1
  IG(K,1)=IG(K,1,4)+2
  IG(K,2)=IG(K,1,2)+JUMP
  IG(K,3)=IG(K,1,3)+1
  IG(K,4)=IG(K,3)+1
  IF (J.ME.J1) GO TO 328
  NCONM(1,4,1)=K+1
  NCONM(1,4,3)=IG(K,2)+1

  328 M2=M2-1
  M1=330 M=1,M2
  K=K+1
  IG(K,1)=IG(K,1,1)+1
  IG(K,2)=IG(K,1,2)+JUMP
  IG(K,3)=IG(K,1,3)
  IG(K,4)=IG(K,1,4)

```

```

140 CONTINUE
P=K+1
IG(K,1)=IG(K,1,1)+1
IG(K,2)=IG(K,1,1)
IG(K,3)=IG(K,1,2)
IG(K,4)=IG(K,1,4)+1
IF (J.ME.J1) GO TO 250
NCONM(1,4,2)=K
NCONM(1,4,4)=IG(K,3)+1
250 EDWTIME
MS=IG(K,2)
IF (ISYN.EQ.1) MS=IG(K,4)
200 CONTINUE

340 M=0
DO 630 I=1,4
  DO 630 J=1,40
  M=M+1
  JBUF(M)=NCONA(I,J)
630 CONTINUE

  IF (ISYN.EQ.1) GO TO 352
  MS=IG(K,2)
  K=K+1
  IG(K,1)=MS
  IG(K,2)=MS+1
  IG(K,3)=MINNER(1)
  IG(K,4)=IG(K,3)-1
  NCONM(1,1,1)=K+1
  DO 350 M=1,M1
    K=K+1
    IG(K,1)=IG(K,1,2)
    IG(K,2)=IG(K,1)+1
    IG(K,3)=MINNER(M+1)
    IG(K,4)=IG(K,1,3)
  350 CONTINUE
  NCONM(1,1,2)=K
  K=K+1
  IG(K,1)=IG(K,1,2)
  IG(K,2)=IG(K,1)+1
  IG(K,3)=IG(K,1)+1
  IG(K,4)=IG(K,2)+1
  IG(K,3)=IG(K,1,3)
  NCONM(1,2,1)=K+1

  352 M4=M4+1
  IF (ISYN.EQ.4) GO TO 355
  K=K+1
  IG(K,1)=MINNER(1)
  IG(K,2)=IG(K,1)+1
  IG(K,3)=IG(K,2)+1
  IG(K,4)=MINNER(2)
  NCONM(1,2,1)=K
  M4=2
  M2=M2-1
  355 DO 360 M=1,M2
    K=K+1
    M3=M4+M
    IG(K,1)=IG(K,1,4)
    IG(K,2)=IG(K,1,3)
    IG(K,3)=IG(K,2)+1
    IG(K,4)=MINNER(M3)
  360 CONTINUE
  NCONM(1,2,2)=K
  K=K+1
  IG(K,1)=IG(K,1,4)
  IG(K,2)=IG(K,1,3)
  IG(K,3)=IG(K,2)+1
  IG(K,4)=IG(K,3)+1
  NCONM(1,3,1)=K+1

  C
  M4=M1+M2+1
  IF (ISYN.EQ.1) M4=M2+2
  DO 370 M=1,M1
    K=K+1
    M3=M4+M
    IG(K,1)=MINNER(M3)
    IG(K,2)=IG(K,1,1)
    IG(K,3)=IG(K,1,4)
    IG(K,4)=IG(K,3)+1
  370 CONTINUE
  NCONM(1,3,2)=K
  IF (ISYN.EQ.1) GO TO 382
  K=K+1
  IG(K,1)=IG(K,1,4)+2
  IG(K,2)=IG(K,1,1)
  IG(K,3)=IG(K,1,4)
  IG(K,4)=IG(K,3)+1
  NCONM(1,4,1)=K+1

  C
  M4=M1+2+M2+1
  M2=M2-1
  DO 380 M=1,M2
    K=K+1
    M3=M4+M
    IG(K,1)=IG(K,1,1)+1
    IG(K,2)=MINNER(M3)
    IG(K,3)=IG(K,1,2)
    IG(K,4)=IG(K,1,1)
  380 CONTINUE
  K=K+1
  IG(K,1)=IG(K,1,1)+1
  IG(K,2)=MINNER(1)
  IG(K,3)=IG(K,1,2)
  IG(K,4)=IG(K,1,1)
  NCONM(1,4,2)=K
  382 RELOUT=K
  C
  WRITE(LUN,985) ((IG(K,M),M=1,4),K=1,RELOUT)
  385 FORMAT(2015)
  WRITE(LUN,987) ((I,J,(NCONM(I,J,K),K=1,4),J=1,4),I=2,NEBMAX)
  987 FORMAT('00 NCONM/2X', I J A=1 A=2 A=3 A=4 /
  A(215,416))

  C
  R1=RELOUT+1
  C
  WRITE(LUN,985) ((IG(K,M),M=1,4),K=R1,MAKEL)
  C
  395 FORMAT(2015)
  C
  RETURN
  C
  M=0
  DO 440 I=1,10
  DO 440 J=1,4
  DO 440 A=1,4
  M=M+1
  JBUF(M)=NCONM(I,J,K)
  440 CONTINUE
  CALL EXEC(2,LU,JBUF,256,ITRACS+4,58)
  CALL EXEC(8,MANN)

  C
  STOP
  END
  ENDS

```



```

FTM4
SERIAL AERAZ(0)
PROGRAM AERAZ(1:150)
C THIS S/P WRITES AERAZ PARAMETERS ON DISCS.
COMMON AERAZ(10,2500,10,2500,10,2500,4,1,1,53,53)
1 ICK(1,53),ICK(2,53)
COMMON CRESM(JRSHIN,JRSHIN,JRSHX,JRSHX,INO,JNO,DX,DY)
COMMON IODAT(LUN,LU,ITRACS)
DIMENSION IBUF(1,25),IBUF(2,25),IBUF(1,128),IBUF(2,128)
EQUIVALENCE (IBUF1,IBUF1),(IBUF2,IBUF2)
WRITE(LUN,999)
999 FORMAT(/20,'.5X','AERAZ' STARTS '.5X,20')
NSTOP=3072/128
ISECT=0
DO 100 N=1,NSTOP
DO 110 I=1,128
II=I+128
IBUF1(I)=IG(II)
IBUF2(I)=IG(II)
110 CONTINUE
CALL EXEC(2,LU,IBUF1,25,ITRACS+8,ISECT)
CALL EXEC(2,LU,IBUF2,25,ITRACS+9,ISECT)
ISECT=ISECT+4
ISTART=ISTART+128
100 CONTINUE
C
NSTOP=2560/256
ISECT=0
DO 200 J=1,2
N=J*2
ISTART=0
DO 210 N=1,NSTOP
DO 220 I=1,256
II=I+256
IBUF1(I)=IG(II,J)
IBUF2(I)=IG(II,J)
220 CONTINUE
CALL EXEC(2,LU,IBUF1,256,ITRACS+10,ISECT)
CALL EXEC(2,LU,IBUF2,256,ITRACS+11,ISECT)
ISECT=ISECT+4
ISTART=ISTART+256
210 CONTINUE
200 CONTINUE
C
DO 250 I=1,IRSHX
IBUF1(I)=IL(I,1)
IBUF2(I+64)=IL(I,JRSHX)
250 CONTINUE
DO 260 J=1,JRSHX
IBUF1(J+128)=IL(1,J)
IBUF2(J+192)=IL(IRSHX,J)
260 CONTINUE
CALL EXEC(2,LU,IBUF1,256,ITRACS+12,ISECT)
I=PRO(IRSHX,JRSHX)
II=0
N=0
ISECT=0
DO 300 I=1,IRSHX
DO 310 J=1,JRSHX
II=II+1
N=N+1
IBUF1(N)=IL(II,J)
IBUF2(N)=IG(II,J)
IF(II.EQ.IPRO) GO TO 320
IF(N.LT.256) GO TO 310
320 CALL EXEC(2,LU,IBUF1,256,ITRACS+12,ISECT)
CALL EXEC(2,LU,IBUF2,256,ITRACS+13,ISECT)
ISECT=ISECT+4
N=0
310 CONTINUE
300 CONTINUE
C
WRITE(LUN,781)
781 FORMAT(////)
STOP
END
ENDS

```

```

FTM4
SERIAL AERAZ(0)
PROGRAM GLNAT(1:150)
C THIS IS THE MAIN ROUTINE FOR THE GLOBAL MATRIX SECTION
C OF AETIC
C
COMMON AERAZ(10,4096,10,4096,10,4096,1,1,1,1,2560,1,1,53,53)
1 ICK(1,53),ICK(2,53)
COMMON CRESM(JRSHIN,JRSHIN,JRSHX,JRSHX,INO,JNO,DX,DY)
COMMON IODAT(LUN,LU,ITRACS)
DIMENSION IBUF(1,25),IBUF(2,25),IBUF(1,128),IBUF(2,128)
EQUIVALENCE (IBUF1,IBUF1),(IBUF2,IBUF2)
WRITE(LUN,999)
999 FORMAT(/20,'.5X','GLNAT' STARTS '.5X,20')
CALL EXEC(8,NAME)
STOP
END
BLOCK DATA
COMMON/CNST1/ROUTER(10)
COMMON/CNST2/MESMAX,MAXNOD,MAXELE,NODFS,NODINS
COMMON/CONN/CONU,NCONA(4,48),NCONN(10,4,4)
COMMON/ELER/SXA(10),SYA(10),SMA(10),SXB(10),SYB(10),
1SXB(10),SYC(1,21),SYC(2,1),SXC(1,15),SXC(2,10),
2SXC(10),SXC3(15),SYC3(15),SXC3(15),SYD(10),SYD(10),
3SXD(10),SXE(1,15),SXE(1,15),SME(1,15),SME(2,20),SXE(2,20),
4SME(2,20),SYF(1,36),SYF(1,36),SNF(1,36)
COMMON/IODAT/LUN,LU,ITRACS
COMMON/PSOLV/ISY,IPDIS,IPOT,RDEBY,CPOIS
COMMON/BLK1/ELMAT(9,9)
COMMON/BLK4/IBUF1(25),IBUF2(25),IGA(25),IGG(25)
COMMON/BLK6/A1,A2,A3,DEMOM,AA1,AA2
COMMON/BLK7/NONB,NVAR,JPMA,IBC,A,K1,A2,A3,AA,J,NES,N
COMMON/BLB/NWB,NZ,NZ1,NZ2,NZ3,NCTYP
DIMENSION NAME(3)
DATA NAME/2HNE,2HAT,2H2 /
C
WRITE(LUN,999)
999 FORMAT(/20,'.5X','GLNAT' STARTS '.5X,20')
CALL EXEC(8,NAME)
STOP
END
BLOCK DATA
COMMON/CNST1/ROUTER(10)
COMMON/CNST2/MESMAX,MAXNOD,MAXELE,NODFS,NODINS
COMMON/CONN/CONU,NCONA(4,48),NCONN(10,4,4)
COMMON/ELER/SXA(10),SYA(10),SMA(10),SXB(10),SYB(10),
1SXB(10),SYC(1,21),SYC(2,1),SXC(1,15),SXC(2,10),
2SXC(10),SXC3(15),SYC3(15),SXC3(15),SYD(10),SYD(10),
3SXD(10),SXE(1,15),SXE(1,15),SME(1,15),SME(2,20),SXE(2,20),
4SME(2,20),SYF(1,36),SYF(1,36),SNF(1,36)
COMMON/IODAT/LUN,LU,ITRACS
COMMON/PSOLV/ISY,IPDIS,IPOT,RDEBY,CPOIS
COMMON/BLK1/ELMAT(9,9)
COMMON/BLK4/IBUF1(25),IBUF2(25),IGA(25),IGG(25)
COMMON/BLK6/A1,A2,A3,DEMOM,AA1,AA2
COMMON/BLK7/NONB,NVAR,JPMA,IBC,A,K1,A2,A3,AA,J,NES,N
COMMON/BLB/NWB,NZ,NZ1,NZ2,NZ3,NCTYP
DATA LUN/6,LU/51,ITRACS/0
DATA NVAR/0,JPMA/0,IBC/0
END
SUBROUTINE SORT(N)
COMMON/BLK4/IA(25),IB(25),IBUF3(25),IBUF4(25)
C
N1=N-1
N=1
1 N1=N+1
2 IF(IA(N).LE.IA(N1)) GO TO 3
I1=IA(N)
I2=IB(N)
IA(N)=IA(N1)
IB(N)=IB(N1)
IA(N1)=I1
IB(N1)=I2
3 N1=N1+1
IF(N1.LE.N) GO TO 2
N=N+1
IF(N.LE.N1) GO TO 1
RETURN
END
ENDS

```

```

FTM4
SERIAL AERAZ(0)
PROGRAM GLHT2(1:150)
C THIS S/P FORMS GLOBAL MATRIX FOR POTENTIAL SOLVER AND
C APPLIES BOUNDARY CONDITIONS.
C
COMMON AERAZ(10,4096,10,4096,10,4096,1,1,1,1,2560,1,1,53,53)
1 ICK(1,53),ICK(2,53)
COMMON CRESM(JRSHIN,JRSHIN,JRSHX,JRSHX,INO,JNO,DX,DY)
COMMON IODAT(LUN,LU,ITRACS)
DIMENSION IBUF(1,25),IBUF(2,25),IBUF(1,128),IBUF(2,128)
EQUIVALENCE (IBUF1,IBUF1),(IBUF2,IBUF2)
WRITE(LUN,999)
999 FORMAT(/20,'.5X','GLHT2' STARTS '.5X,20')
NAME=1
IF(NAME.EQ.0) GO TO 333
NES=PARO(NESMAX-1,1)
DO 160 NES=NES1,NESMAX
N1=NESMAX+1-NES
R1=1
IF(RA,NES,NESMAX) R1=NCONN(RA,1,4,2)+1
A2=MAXELE
IF(RA,NES,1) A2=NCONN(RA,1,1,1)
WRITE(LUN,971) NES,RA,R1,A2
971 FORMAT('8 NES=',12,5X,'RA=',12,5X,'R1=',14,5X,'A2=',14)
DO 170 A=A1,A2
IG1=IG(A,1)
IG2=IG(A,2)
IG3=IG(A,3)
IF(IG(A,4).EQ.0) GO TO 220
C
NWB=4
NR=IG(IG2)-IG(IG1)
NY=IG(IG3)-YD(IG2)
A1=NY,NR
A2=NY,NT
A3=NWB,NT,CPOIS
C
IF(RA,NES,1) GO TO 210
IF(NCONU.EQ.0) GO TO 210
DO 190 I=1,NCONU
11 I

```

```

150 CONTINUE
160 GO TO 170
170 AC(1)=NUNV(1)
CALL FELAT
GO TO 170
170 AC(1)=0
CALL FELAT
GO TO 170
170 NND=1
IG(1)=IG1
IG(2)=IG2
IG(3)=IG3
NA=XG(IG1)+YG(IG1)+XG(IG2)+YG(IG2)+
XG(IG3)+YG(IG3)+XG(IG4)+YG(IG4)+XG(IG5)+
YG(IG5)+XG(IG6)+YG(IG6)
N1=YG(IG1)+XG(IG1)
N2=YG(IG2)+XG(IG2)
N3=YG(IG3)+XG(IG3)
A1=XG(IG1)+YG(IG1)
A2=XG(IG2)+YG(IG2)
A3=XG(IG3)+YG(IG3)
C1=HAB2/12.08CFD15
C2=HAB2.0
DEMOH=C2
ELMAT(1,1)=(B1B2+2A1B2-2.08C1)
ELMAT(1,2)=(B2B1+A2B1-C1)
ELMAT(1,3)=(B3B1+A3B1-C1)
ELMAT(2,2)=(B2B2+2A2B2-2.08C1)
ELMAT(2,3)=(B3B2+A3B2-C1)
ELMAT(3,3)=(B3B2+A3B2-2.08C1)
170 CALL FILE
170 CONTINUE
170 CONTINUE
235 CONTINUE
WRITE(LUN,973) KK
973 FORMAT(' KK=',I2)
IF(KK.EQ.1) GO TO 160
DO 240 J=1,4
K1=NCDMM(KK,J,1)
K2=NCDMM(KK,J,2)
NZ=J*2-J/384
IF(KK.NE.2) K3=NCDMM(KK,J,3)
M=0
DO 250 K=K1,K2
M=M+1
IF(KK.NE.2) IG(5)=K3+(M-1)*2
IF(KK.EQ.2) IG(5)=NCDMM(KK,J,M)
NCTYP=1
CALL FELAT
250 CONTINUE
IF(J.EQ.4) GO TO 240
K=N*2+1
NCTYP=0
CALL FELAT
240 CONTINUE
160 CONTINUE
C
IA(NVAR+1)=JPHAX+1
C
DO 270 N=1,NVAR
I1=IA(N)
I2=IA(N+1)-1
NO=MOD(I2+1,4)
DO 280 I=I1,I2
I=I1
IF(JA(I).EQ.NO) GO TO 290
WRITE(LUN,980)
980 FORMAT('ERROR IS DETECTED')
STOP
290 IF(I1.EQ.I1) GO TO 270
M=JA(I1)
A=AN(I1)
I3=I1+1
DO 300 I=I3,I1
I=I3+I-1
JA(I)=JA(I-1)
AN(I)=AN(I-1)
300 CONTINUE
JA(I1)=M
AN(I1)=A
270 CONTINUE
C
*****APPLY THE BOUNDARY CONDITIONS
C
C IMPOT IS THE FLAG INDICATING THE TYPE OF BOUNDARY CONDITIONS
C
C IMPOSED ON THE OUTERMOST EDGES.
C
C IMPOT=1: PHI=0.0
C
C IMPOT=2: PHI=R
C
C IMPOT=3: PHI=KEXP(-R/RDEBY)
C
C IMPOT=4: PHI=KEXP(-R/RDEBY)/R
C
WRITE(LUN,548) K,(AN(IA(I)),I=1,64)
333 IF(IMPOT.EQ.1) GO TO 510
NOHB=0
DEBA=RDEBY*2.0
NND=4
DEMOH=L.0
DO 330 M=1,4
DO 330 N=1,2
K1=HOUTER(N)
K2=HOUTER(N+1)
IF(N.NE.4) K2=K2-1
WRITE(LUN,547) N,K1,K2
547 FORMAT('N=',I3,5X,'K1=',I3,5X,'K2=',I3)
L=0
DO 340 K=K1,K2
L=L+1
NZ=N
DO 350 I=1,4
IGA(I)=IG(A,I)
DO 350 J=1,4
ELMAT(I,J)=0.0
350 CONTINUE
IG1=IGA(1)
IG2=IGA(2)
IG3=IGA(3)
IG4=IGA(4)
NX=XH(IG2)+XG(IG1)
NY=YH(IG3)+YG(IG2)
C
NFD=0
IF(A.EQ.B1.OR.A.EQ.A2) NFD=1
IF(A.EQ.A1) NFD=1
160 GO TO (70,80,90,400),NZ
170 N1=XH(IG1)
N1=AN(YG(IG1))
GO TO 410
410 N1=YG(IG1)
N1=MY
N3=AN(XG(IG2))
GO TO 410
190 N1=XG(IG4)
N1=MX
N3=AN(YG(IG1))
GO TO 410
410 N1=YG(IG1)
IF(IMPOT.EQ.1) GO TO 420
D3=ALOG(1.0+K2*(C1-0.08144))+(1.08144+K2)
P1=(1.08144+K2)*D3+0.08144*(1.08144+K2)
P2=(1.08144+K2)*D3+0.08144*(1.08144+K2)
P3=(1.08144+K2)*D3+0.08144*(1.08144+K2)
IF(IMPOT.EQ.3) GO TO 440
IF(IMPOT.EQ.4) GO TO 430
410 P1=0.0
P2=0.0
P3=0.0
430 B4=SQRT(1.0+(B1B2/B3B2))
B5=SQRT(1.0+(B1/B3B2))
K4=B2/(B4+B5)*(B2+0.08144)
K7=B2B3B4
D3=ALOG(1.0+(B2+B6)/(B1+B5B3))
P1=(1.08144+K7)*D3+0.08144*(1.08144+K7)
P2=(1.08144+K7)*D3+0.08144*(1.08144+K7)
P3=(1.08144+K7)*D3+0.08144*(1.08144+K7)
P1=DEBA
P2=P2*(1.08144+0.08144*B7)/(2.08144*(B1+B2)+B3B2+D3)
P3=P3*(B7-1.08144*B6)/(2.08144+D3)/DEBA
440 P1=P1/E1
P2=P2/E1
P3=P3/E1
C
N1=N2
N2=N2+1-NZ/484
IF(NZ.LE.2) GO TO 450
N1=N2
N2=N2
450 ELMAT(N1,N1)=ELMAT(N1,N1)+P1
ELMAT(N1,N2)=ELMAT(N1,N2)+P2
ELMAT(N2,N2)=ELMAT(N2,N2)+P3
IF(NZ.EQ.3) ELMAT(3,4)=ELMAT(4,3)
WRITE(LUN,888) L,P1,P2,P3
C
888 FORMAT('L=',I3,5X,'P1=',IPE12.5,5X,'P2=',IPE12.5,5X,
'P3=',IPE12.5)
IF(NFD.EQ.0) GO TO 500
NFD=0
IF(N.EQ.K1) NZ=(NZ-1)+(5-NZ)/484
IF(N.EQ.K2) NZ=(NZ+1)-NZ/484
GO TO 340
C
500 CONTINUE
IF(K.NE.K1) BDI(N,L)=BDI(N,L)+ELMAT(N,M)
IF(K.EQ.K1) BDI(N,L)=ELMAT(N,M)
IF(K.NE.K2) BDI(N,L+1)=BDI(N,L+1)+ELMAT(N+1,M+1)
IF(K.EQ.K2) BDI(N,L+1)=ELMAT(N+1,M+1)
BOFF(N,L)=ELMAT(N,M+1)
WRITE(LUN,507) N,(IGA(I),I=1,4)
C
507 FORMAT('N=',I3,5X,'IGA=',I4)
C
WRITE(LUN,509) ((ELMAT(I,J),J=1,4),I=1,4)
C
509 FORMAT('IP4E13.5)
C
CALL FILE
WRITE(LUN,568) K,(AN(IA(I)),I=1,64)
568 FORMAT('K=',I3,'IP10E13.5)
340 CONTINUE
330 CONTINUE
WRITE(LUN,732)
732 FORMAT('88 BDI')
WRITE(LUN,733) ((BDI(N,L),L=1,20),N=1,2)
733 FORMAT('IP10E13.5)
WRITE(LUN,777)
777 FORMAT('88 BOFF')
WRITE(LUN,734) ((BOFF(N,L),L=1,20),N=1,2)
734 FORMAT('IP10E13.5)
DO 1000 I=1,NVAR
I1=IA(I)
I2=IA(I+1)-1
WRITE(LUN,1001) I,(JA(J),J=I1,I2)
1001 FORMAT('I3,3X,I2)
WRITE(LUN,1002) (AN(J),J=I1,I2)
1002 FORMAT('4X,I2F.4)
1000 CONTINUE
CALL EXEC(2,LU,BDI,128,ITRACS+4,B1)
CALL EXEC(2,LU,BOFF,128,ITRACS+4,B3)
STOP
GO TO 800
C
510 NOHB=HOUTER(5)
NA=NOHB+1
DO 600 N=NA,MODFS
IP1=IA(N)
IP2=IA(N+1)-1
DO 610 I=IP1,IP2
JP=JA(I)
IF(JP.GT.NOHB) GO TO 610
JA(I)=I
LAST=N
610 CONTINUE
410 CONTINUE
600 CONTINUE
NC=N
IA(NC)=NUNV+1
450 CONTINUE
NB=IP2+1
NB=LAST+1
NSUB=IA(NB)-IA(NC)
NB=NB+1
DO 700 N=NB,MODFS
NC=NC+1
IA(NC)=IA(N)-NSUB
700 CONTINUE
NVAR=NC
DO 10 N=NB,JPMAX
N1=AN(N)
AN(1)=AN(N)
IA(1)=IA(N)

```

```

10 CONTINUE
11 MAX=NMAX
12 NMAX=NMAX
13 NMAX=NMAX
14 NMAX=NMAX
15 NMAX=NMAX
16 NMAX=NMAX
17 NMAX=NMAX
18 NMAX=NMAX
19 NMAX=NMAX
20 NMAX=NMAX
21 NMAX=NMAX
22 NMAX=NMAX
23 NMAX=NMAX
24 NMAX=NMAX
25 NMAX=NMAX
26 NMAX=NMAX
27 NMAX=NMAX
28 NMAX=NMAX
29 NMAX=NMAX
30 NMAX=NMAX
31 NMAX=NMAX
32 NMAX=NMAX
33 NMAX=NMAX
34 NMAX=NMAX
35 NMAX=NMAX
36 NMAX=NMAX
37 NMAX=NMAX
38 NMAX=NMAX
39 NMAX=NMAX
40 NMAX=NMAX
41 NMAX=NMAX
42 NMAX=NMAX
43 NMAX=NMAX
44 NMAX=NMAX
45 NMAX=NMAX
46 NMAX=NMAX
47 NMAX=NMAX
48 NMAX=NMAX
49 NMAX=NMAX
50 NMAX=NMAX
51 NMAX=NMAX
52 NMAX=NMAX
53 NMAX=NMAX
54 NMAX=NMAX
55 NMAX=NMAX
56 NMAX=NMAX
57 NMAX=NMAX
58 NMAX=NMAX
59 NMAX=NMAX
60 NMAX=NMAX
61 NMAX=NMAX
62 NMAX=NMAX
63 NMAX=NMAX
64 NMAX=NMAX
65 NMAX=NMAX
66 NMAX=NMAX
67 NMAX=NMAX
68 NMAX=NMAX
69 NMAX=NMAX
70 NMAX=NMAX
71 NMAX=NMAX
72 NMAX=NMAX
73 NMAX=NMAX
74 NMAX=NMAX
75 NMAX=NMAX
76 NMAX=NMAX
77 NMAX=NMAX
78 NMAX=NMAX
79 NMAX=NMAX
80 NMAX=NMAX
81 NMAX=NMAX
82 NMAX=NMAX
83 NMAX=NMAX
84 NMAX=NMAX
85 NMAX=NMAX
86 NMAX=NMAX
87 NMAX=NMAX
88 NMAX=NMAX
89 NMAX=NMAX
90 NMAX=NMAX
91 NMAX=NMAX
92 NMAX=NMAX
93 NMAX=NMAX
94 NMAX=NMAX
95 NMAX=NMAX
96 NMAX=NMAX
97 NMAX=NMAX
98 NMAX=NMAX
99 NMAX=NMAX
100 NMAX=NMAX

```

```

100 DENOM=576.0
110 NND=4
120 NND=4
130 NND=4
140 NND=4
150 NND=4
160 NND=4
170 NND=4
180 NND=4
190 NND=4
200 NND=4
210 NND=4
220 NND=4
230 NND=4
240 NND=4
250 NND=4
260 NND=4
270 NND=4
280 NND=4
290 NND=4
300 NND=4
310 NND=4
320 NND=4
330 NND=4
340 NND=4
350 NND=4
360 NND=4
370 NND=4
380 NND=4
390 NND=4
400 NND=4
410 NND=4
420 NND=4
430 NND=4
440 NND=4
450 NND=4
460 NND=4
470 NND=4
480 NND=4
490 NND=4
500 NND=4
510 NND=4
520 NND=4
530 NND=4
540 NND=4
550 NND=4
560 NND=4
570 NND=4
580 NND=4
590 NND=4
600 NND=4
610 NND=4
620 NND=4
630 NND=4
640 NND=4
650 NND=4
660 NND=4
670 NND=4
680 NND=4
690 NND=4
700 NND=4
710 NND=4
720 NND=4
730 NND=4
740 NND=4
750 NND=4
760 NND=4
770 NND=4
780 NND=4
790 NND=4
800 NND=4
810 NND=4
820 NND=4
830 NND=4
840 NND=4
850 NND=4
860 NND=4
870 NND=4
880 NND=4
890 NND=4
900 NND=4
910 NND=4
920 NND=4
930 NND=4
940 NND=4
950 NND=4
960 NND=4
970 NND=4
980 NND=4
990 NND=4
1000 NND=4

```

```

M11 M111
M12 M111
DO 110 M=1,MND
M13 M111
M14 M111
M15 M111
M16 M111
M17 M111
M18 M111
M19 M111
M20 M111
M21 M111
M22 M111
M23 M111
M24 M111
M25 M111
M26 M111
M27 M111
M28 M111
M29 M111
M30 M111
M31 M111
M32 M111
M33 M111
M34 M111
M35 M111
M36 M111
M37 M111
M38 M111
M39 M111
M40 M111
M41 M111
M42 M111
M43 M111
M44 M111
M45 M111
M46 M111
M47 M111
M48 M111
M49 M111
M50 M111
M51 M111
M52 M111
M53 M111
M54 M111
M55 M111
M56 M111
M57 M111
M58 M111
M59 M111
M60 M111
M61 M111
M62 M111
M63 M111
M64 M111
M65 M111
M66 M111
M67 M111
M68 M111
M69 M111
M70 M111
M71 M111
M72 M111
M73 M111
M74 M111
M75 M111
M76 M111
M77 M111
M78 M111
M79 M111
M80 M111
M81 M111
M82 M111
M83 M111
M84 M111
M85 M111
M86 M111
M87 M111
M88 M111
M89 M111
M90 M111
M91 M111
M92 M111
M93 M111
M94 M111
M95 M111
M96 M111
M97 M111
M98 M111
M99 M111
M100 M111
M101 M111
M102 M111
M103 M111
M104 M111
M105 M111
M106 M111
M107 M111
M108 M111
M109 M111
M110 M111
M111 M111
M112 M111
M113 M111
M114 M111
M115 M111
M116 M111
M117 M111
M118 M111
M119 M111
M120 M111
M121 M111
M122 M111
M123 M111
M124 M111
M125 M111
M126 M111
M127 M111
M128 M111
M129 M111
M130 M111
M131 M111
M132 M111
M133 M111
M134 M111
M135 M111
M136 M111
M137 M111
M138 M111
M139 M111
M140 M111
M141 M111
M142 M111
M143 M111
M144 M111
M145 M111
M146 M111
M147 M111
M148 M111
M149 M111
M150 M111
M151 M111
M152 M111
M153 M111
M154 M111
M155 M111
M156 M111
M157 M111
M158 M111
M159 M111
M160 M111
M161 M111
M162 M111
M163 M111
M164 M111
M165 M111
M166 M111
M167 M111
M168 M111
M169 M111
M170 M111
M171 M111
M172 M111
M173 M111
M174 M111
M175 M111
M176 M111
M177 M111
M178 M111
M179 M111
M180 M111
M181 M111
M182 M111
M183 M111
M184 M111
M185 M111
M186 M111
M187 M111
M188 M111
M189 M111
M190 M111
M191 M111
M192 M111
M193 M111
M194 M111
M195 M111
M196 M111
M197 M111
M198 M111
M199 M111
M200 M111
M201 M111
M202 M111
M203 M111
M204 M111
M205 M111
M206 M111
M207 M111
M208 M111
M209 M111
M210 M111
M211 M111
M212 M111
M213 M111
M214 M111
M215 M111
M216 M111
M217 M111
M218 M111
M219 M111
M220 M111
M221 M111
M222 M111
M223 M111
M224 M111
M225 M111
M226 M111
M227 M111
M228 M111
M229 M111
M230 M111
M231 M111
M232 M111
M233 M111
M234 M111
M235 M111
M236 M111
M237 M111
M238 M111
M239 M111
M240 M111
M241 M111
M242 M111
M243 M111
M244 M111
M245 M111
M246 M111
M247 M111
M248 M111
M249 M111
M250 M111
M251 M111
M252 M111
M253 M111
M254 M111
M255 M111
M256 M111
M257 M111
M258 M111
M259 M111
M260 M111
M261 M111
M262 M111
M263 M111
M264 M111
M265 M111
M266 M111
M267 M111
M268 M111
M269 M111
M270 M111
M271 M111
M272 M111
M273 M111
M274 M111
M275 M111
M276 M111
M277 M111
M278 M111
M279 M111
M280 M111
M281 M111
M282 M111
M283 M111
M284 M111
M285 M111
M286 M111
M287 M111
M288 M111
M289 M111
M290 M111
M291 M111
M292 M111
M293 M111
M294 M111
M295 M111
M296 M111
M297 M111
M298 M111
M299 M111
M300 M111
M301 M111
M302 M111
M303 M111
M304 M111
M305 M111
M306 M111
M307 M111
M308 M111
M309 M111
M310 M111
M311 M111
M312 M111
M313 M111
M314 M111
M315 M111
M316 M111
M317 M111
M318 M111
M319 M111
M320 M111
M321 M111
M322 M111
M323 M111
M324 M111
M325 M111
M326 M111
M327 M111
M328 M111
M329 M111
M330 M111
M331 M111
M332 M111
M333 M111
M334 M111
M335 M111
M336 M111
M337 M111
M338 M111
M339 M111
M340 M111
M341 M111
M342 M111
M343 M111
M344 M111
M345 M111
M346 M111
M347 M111
M348 M111
M349 M111
M350 M111
M351 M111
M352 M111
M353 M111
M354 M111
M355 M111
M356 M111
M357 M111
M358 M111
M359 M111
M360 M111
M361 M111
M362 M111
M363 M111
M364 M111
M365 M111
M366 M111
M367 M111
M368 M111
M369 M111
M370 M111
M371 M111
M372 M111
M373 M111
M374 M111
M375 M111
M376 M111
M377 M111
M378 M111
M379 M111
M380 M111
M381 M111
M382 M111
M383 M111
M384 M111
M385 M111
M386 M111
M387 M111
M388 M111
M389 M111
M390 M111
M391 M111
M392 M111
M393 M111
M394 M111
M395 M111
M396 M111
M397 M111
M398 M111
M399 M111
M400 M111
M401 M111
M402 M111
M403 M111
M404 M111
M405 M111
M406 M111
M407 M111
M408 M111
M409 M111
M410 M111
M411 M111
M412 M111
M413 M111
M414 M111
M415 M111
M416 M111
M417 M111
M418 M111
M419 M111
M420 M111
M421 M111
M422 M111
M423 M111
M424 M111
M425 M111
M426 M111
M427 M111
M428 M111
M429 M111
M430 M111
M431 M111
M432 M111
M433 M111
M434 M111
M435 M111
M436 M111
M437 M111
M438 M111
M439 M111
M440 M111
M441 M111
M442 M111
M443 M111
M444 M111
M445 M111
M446 M111
M447 M111
M448 M111
M449 M111
M450 M111
M451 M111
M452 M111
M453 M111
M454 M111
M455 M111
M456 M111
M457 M111
M458 M111
M459 M111
M460 M111
M461 M111
M462 M111
M463 M111
M464 M111
M465 M111
M466 M111
M467 M111
M468 M111
M469 M111
M470 M111
M471 M111
M472 M111
M473 M111
M474 M111
M475 M111
M476 M111
M477 M111
M478 M111
M479 M111
M480 M111
M481 M111
M482 M111
M483 M111
M484 M111
M485 M111
M486 M111
M487 M111
M488 M111
M489 M111
M490 M111
M491 M111
M492 M111
M493 M111
M494 M111
M495 M111
M496 M111
M497 M111
M498 M111
M499 M111
M500 M111
M501 M111
M502 M111
M503 M111
M504 M111
M505 M111
M506 M111
M507 M111
M508 M111
M509 M111
M510 M111
M511 M111
M512 M111
M513 M111
M514 M111
M515 M111
M516 M111
M517 M111
M518 M111
M519 M111
M520 M111
M521 M111
M522 M111
M523 M111
M524 M111
M525 M111
M526 M111
M527 M111
M528 M111
M529 M111
M530 M111
M531 M111
M532 M111
M533 M111
M534 M111
M535 M111
M536 M111
M537 M111
M538 M111
M539 M111
M540 M111
M541 M111
M542 M111
M543 M111
M544 M111
M545 M111
M546 M111
M547 M111
M548 M111
M549 M111
M550 M111
M551 M111
M552 M111
M553 M111
M554 M111
M555 M111
M556 M111
M557 M111
M558 M111
M559 M111
M560 M111
M561 M111
M562 M111
M563 M111
M564 M111
M565 M111
M566 M111
M567 M111
M568 M111
M569 M111
M570 M111
M571 M111
M572 M111
M573 M111
M574 M111
M575 M111
M576 M111
M577 M111
M578 M111
M579 M111
M580 M111
M581 M111
M582 M111
M583 M111
M584 M111
M585 M111
M586 M111
M587 M111
M588 M111
M589 M111
M590 M111
M591 M111
M592 M111
M593 M111
M594 M111
M595 M111
M596 M111
M597 M111
M598 M111
M599 M111
M600 M111
M601 M111
M602 M111
M603 M111
M604 M111
M605 M111
M606 M111
M607 M111
M608 M111
M609 M111
M610 M111
M611 M111
M612 M111
M613 M111
M614 M111
M615 M111
M616 M111
M617 M111
M618 M111
M619 M111
M620 M111
M621 M111
M622 M111
M623 M111
M624 M111
M625 M111
M626 M111
M627 M111
M628 M111
M629 M111
M630 M111
M631 M111
M632 M111
M633 M111
M634 M111
M635 M111
M636 M111
M637 M111
M638 M111
M639 M111
M640 M111
M641 M111
M642 M111
M643 M111
M644 M111
M645 M111
M646 M111
M647 M111
M648 M111
M649 M111
M650 M111
M651 M111
M652 M111
M653 M111
M654 M111
M655 M111
M656 M111
M657 M111
M658 M111
M659 M111
M660 M111
M661 M111
M662 M111
M663 M111
M664 M111
M665 M111
M666 M111
M667 M111
M668 M111
M669 M111
M670 M111
M671 M111
M672 M111
M673 M111
M674 M111
M675 M111
M676 M111
M677 M111
M678 M111
M679 M111
M680 M111
M681 M111
M682 M111
M683 M111
M684 M111
M685 M111
M686 M111
M687 M111
M688 M111
M689 M111
M690 M111
M691 M111
M692 M111
M693 M111
M694 M111
M695 M111
M696 M111
M697 M111
M698 M111
M699 M111
M700 M111
M701 M111
M702 M111
M703 M111
M704 M111
M705 M111
M706 M111
M707 M111
M708 M111
M709 M111
M710 M111
M711 M111
M712 M111
M713 M111
M714 M111
M715 M111
M716 M111
M717 M111
M718 M111
M719 M111
M720 M111
M721 M111
M722 M111
M723 M111
M724 M111
M725 M111
M726 M111
M727 M111
M728 M111
M729 M111
M730 M111
M731 M111
M732 M111
M733 M111
M734 M111
M735 M111
M736 M111
M737 M111
M738 M111
M739 M111
M740 M111
M741 M111
M742 M111
M743 M111
M744 M111
M745 M111
M746 M111
M747 M111
M748 M111
M749 M111
M750 M111
M751 M111
M752 M111
M753 M111
M754 M111
M755 M111
M756 M111
M757 M111
M758 M111
M759 M111
M760 M111
M761 M111
M762 M111
M763 M111
M764 M111
M765 M111
M766 M111
M767 M111
M768 M111
M769 M111
M770 M111
M771 M111
M772 M111
M773 M111
M774 M111
M775 M111
M776 M111
M777 M111
M778 M111
M779 M111
M780 M111
M781 M111
M782 M111
M783 M111
M784 M111
M785 M111
M786 M111
M787 M111
M788 M111
M789 M111
M790 M111
M791 M111
M792 M111
M793 M111
M794 M111
M795 M111
M796 M111
M797 M111
M798 M111
M799 M111
M800 M111
M801 M111
M802 M111
M803 M111
M804 M111
M805 M111
M806 M111
M807 M111
M808 M111
M809 M111
M810 M111
M811 M111
M812 M111
M813 M111
M814 M111
M815 M111
M816 M111
M817 M111
M818 M111
M819 M111
M820 M111
M821 M111
M822 M111
M823 M111
M824 M111
M825 M111
M826 M111
M827 M111
M828 M111
M829 M111
M830 M111
M831 M111
M832 M111
M833 M111
M834 M111
M835 M111
M836 M111
M837 M111
M838 M111
M839 M111
M840 M111
M841 M111
M842 M111
M843 M111
M844 M111
M845 M111
M846 M111
M847 M111
M848 M111
M849 M111
M850 M111
M851 M111
M852 M111
M853 M111
M854 M111
M855 M111
M856 M111
M857 M111
M858 M111
M859 M111
M860 M111
M861 M111
M862 M111
M863 M111
M864 M111
M865 M111
M866 M111
M867 M111
M868 M111
M869 M111
M870 M111
M871 M111
M872 M111
M873 M111
M874 M111
M875 M111
M876 M111
M877 M111
M878 M111
M879 M111
M880 M111
M881 M111
M882 M111
M883 M111
M884 M111
M885 M111
M886 M111
M887 M111
M888 M111
M889 M111
M890 M111
M891 M111
M892 M111
M893 M111
M894 M111
M895 M111
M896 M111
M897 M111
M898 M111
M899 M111
M900 M111
M901 M111
M902 M111
M903 M111
M904 M111
M905 M111
M906 M111
M907 M111
M908 M111
M909 M111
M910 M111
M911 M111
M912 M111
M913 M111
M914 M111
M915 M111
M916 M111
M917 M111
M918 M111
M919 M111
M920 M111
M921 M111
M922 M111
M923 M111
M924 M111
M925 M111
M926 M111
M927 M111
M928 M111
M929 M111
M930 M111
M931 M111
M932 M111
M933 M111
M934 M111
M935 M111
M936 M111
M937 M111
M938 M111
M939 M111
M940 M111
M941 M111
M942 M111
M943 M111
M944 M111
M945 M111
M946 M111
M947 M111
M948 M111
M949 M111
M950 M111
M951 M111
M952 M111
M953 M111
M954 M111
M955 M111
M956 M111
M957 M111
M958 M111
M959 M111
M960 M111
M961 M111
M962 M111
M963 M111
M964 M111
M965 M111
M966 M111
M967 M111
M968 M111
M969 M111
M970 M111
M971 M111
M972 M111
M973 M111
M974 M111
M975 M111
M976 M111
M977 M111
M978 M111
M979 M111
M980 M111
M981 M111
M982 M111
M983 M111
M984 M111
M985 M111
M986 M111
M987 M111
M988 M111
M989 M111
M990 M111
M991 M111
M992 M111
M993 M111
M994 M111
M995 M111
M996 M111
M997 M111
M998 M111
M999 M111
M1000 M111

```

```

THIS S/P WRITES THE VARIABLES ON DISK.
COMMON/ARMAZ/AR(4096), JAC(4096), IAC(1), JBC(1), IBC(1), JAC(1), JBC(1), IAC(1), JBC(1)
COMMON/IDAT/LUM(1), ITRAC(1)
COMMON/PSOLU/ISTR, IPOISS, IPOT, KNE BY LPOIS
COMMON/AL7/NOB, NVAR, JPMAX, NBC, IDS, IDA, ID, IDB, IDV, IDIO,
ID11, ID12
DIMENSION IAC(1), JBC(1), IBC(1), JBC(1), IBC(1), JBC(1), IBC(1), JBC(1)
DIMENSION AYO(256)
FOURVANCE (JBC(1), JBC(1), IBC(1), IBC(1), IBC(1), IBC(1), IBC(1), IBC(1))
DATA NAME/2ND, 2ND, 2ND /
C
WRITE (LUM, 999)
999 FORMAT ('/20 /', 5X, 'MEAS' STARTS', 5X, 20, /)
CALL EXEC(1, LU, JBUF, 44, ITRAC+2, 55)
JBUF(22)=NVAR
JBUF(23)=JPMAX
JBUF(24)=NBC
JBUF(25)=NOB
CALL EXEC(2, LU, JBUF, 44, ITRAC+3, 55)
WRITE (LUM, 971) NVAR, JPMAX, NBC, NOB
971 FORMAT ('8 NVAR=', 14, 5X, 'JPMAX=', 15, 5X, 'NBC=', 14, 5X,
' NOB=', 14)
C
ISECT=0
ISTART=0
ITRACK=ITRAC-30
NSTOP=JPMAX/128+1
DO 150 M=1, NSTOP
IBUF1(I)=JA(ISTART+I)
160 CONTINUE
CALL EXEC(2, LU, IBUF1, 128, ITRACK, ISECT)
ISECT=ISECT+4
ISTART=ISTART+128
IF (NOB(M-48), NE, 0) GO TO 150
ITRACK=ITRACK+1
ISECT=0
150 CONTINUE
C
ISECT=0
ISTART=0
ITRACK=ITRAC+14
DO 170 M=1, NSTOP
DO 180 I=1, 128
IBUF1(I)=JA(ISTART+I)
180 CONTINUE
CALL EXEC(2, LU, IBUF1, 128, ITRACK, ISECT)
ISECT=ISECT+4
ISTART=ISTART+128
IF (NOB(M-24), NE, 0) GO TO 170
ITRACK=ITRACK+1
ISECT=0
170 CONTINUE
C
NSTOP=(NVAR+1)/128+1
ISTART=0
ISECT=0
DO 200 M=1, NSTOP
DO 210 I=1, 128
IBUF1(I)=JA(ISTART+I)
210 CONTINUE
CALL EXEC(2, LU, IBUF1, 128, ITRACK+34, ISECT)
ISECT=ISECT+2
ISTART=ISTART+128
200 CONTINUE
C
NSTOP=NBC/128+1
ISECT=0
ISTART=0
ITRACK=ITRAC+35
DO 250 M=1, NSTOP
DO 260 I=1, 128
IBUF1(I)=IBC(ISTART+I)
IBUF2(I)=JBC(ISTART+I)
IBUF3(I)=YBC(ISTART+I)
260 CONTINUE
CALL EXEC(2, LU, IBUF1, 128, ITRACK, ISECT)
CALL EXEC(2, LU, IBUF2, 128, ITRACK, ISECT+24)
CALL EXEC(2, LU, IBUF3, 128, ITRACK, ISECT+48)
ISECT=ISECT+2
ISTART=ISTART+128
250 CONTINUE
C
WRITE (LUM, 972) (IBC(I), I=1, NBC)
C 972 FORMAT ('IBC' / (251S))
C
WRITE (LUM, 974) (JBC(I), I=1, NBC)
C 974 FORMAT ('JBC' / (251S))
C
NSTOP=NVAR/128+1
ISTART=0
ISECT=0
DO 350 M=1, NSTOP
DO 360 I=1, 128
IBUF1(I)=AYO(ISTART+I)
360 CONTINUE
CALL EXEC(2, LU, IBUF1, 256, ITRAC+34, ISECT)
ISECT=ISECT+4
ISTART=ISTART+128
350 CONTINUE
IF (IPOISS, OT, 0) STOP 0001
IF (IPOT, LT, 0) CALL EXEC(8, NAME)
STOP 0002
END
END

```

1194
SI MAY AF RA, 701
1195 KAR AF RA 119, 1190







```

DO 100 N=1,4
  IMA=I*AMAX(1,N)
  IMA=I*AMAX(1,N)
CONTINUE
  N=INT(AMAX(1,N))
  IF (J.EQ.1) GO TO 250
  NSTART=1
  SUM=A(1)*POT(L1)+POT(L1)+POT(N+1)+POT(N-2)+
  1A(13)*POT(L1)+POT(N)+POT(N+1)+POT(N-1)
  GO TO 250
250 NSTART=3
  L=L+1
  SUM=A(12)*POT(L1)+POT(L1)+POT(N)+POT(L-3)+
  1A(13)*POT(L1)+POT(L-2)+POT(N+1)+POT(N-1)
  RES=SUM-POT(N)
  POT(N)+POT(N)+NEGABRES
  EPS=EPS+ABS(RES)
  N=N+1
  L=L+1
  SUM=A(12)*POT(L1)+POT(L1)+POT(N+1)+POT(N-2)+
  1A(13)*POT(L1)+POT(N)+POT(N+1)+POT(N-1)
  RES=SUM-POT(N)
  POT(N)+POT(N)+NEGABRES
  EPS=EPS+ABS(RES)
  DO 280 N=START,MAX
  N=N+1
  L=L+1
  NS=N+1
  IF (J.EQ.4.AND.K.EQ.AMAX) NS=N+2
  SUM=A(12)*POT(L1)+POT(L1)+POT(L1)+POT(NS)+POT(N-1)+
  1A(13)*POT(L1)+POT(N)+POT(N+1)+POT(N-1)
  RES=SUM-POT(N)
  POT(N)+POT(N)+NEGABRES
  EPS=EPS+ABS(RES)
280 CONTINUE
  N=N+1
  L=L+1
  IF (J.EQ.4) GO TO 285
  SUM=A(12)*POT(L1)+POT(L1)+POT(N+2)+POT(N-1)+
  1A(13)*POT(L1)+POT(N)+POT(N+1)+POT(N-1)
  GO TO 290
285 SUM=A(12)*POT(L1)+POT(L1)+POT(L+3)+POT(N-1)+
  1A(13)*POT(L1)+POT(N+1)+POT(L+2)+POT(N-1)
290 RES=SUM-POT(N)
  POT(N)+POT(N)+NEGABRES
  EPS=EPS+ABS(RES)
250 CONTINUE
  GO TO 230
C
C FOR THE INNER EDGE OF GRID.
C
300 CONTINUE
  IF (I1.EQ.1) GO TO 345
  DO 310 J=1,4
  AMAX=I*AMAX(J)
  N=N+1
  IF (J.EQ.1) GO TO 320
  SUM=A(12)*POT(L1)+POT(L1)+POT(N+1)+POT(N-2)+A(13)*
  1(POT(L1)+POT(N)+POT(N+1)+POT(N-1))
  RES=SUM-POT(N)
  POT(N)+POT(N)+NEGABRES
  EPS=EPS+ABS(RES)
  N=N+1
  L=L+1
  SUM=A(12)*POT(L1)+POT(L1)+POT(N-1)+A(13)*
  1(POT(L1)+POT(N+1)+POT(N-1)+A(14)*POT(N)+A(15)*POT(N+1)+
  2A(16)*POT(N+2)
  GO TO 330
320 L=L+3
  SUM=A(12)*POT(L1)+POT(L1)+POT(N)+POT(L-3)+A(13)*
  1(POT(L1)+POT(L-2)+POT(N+1)+POT(N-1))
  RES=SUM-POT(N)
  POT(N)+POT(N)+NEGABRES
  EPS=EPS+ABS(RES)
  N=N+1
  L=L+1
  SUM=A(12)*POT(L1)+POT(L1)+POT(N-2)+A(13)*
  1(POT(L1)+POT(N+1)+POT(N-1)+A(14)*POT(N)+A(15)*POT(N+1)+
  2A(16)*POT(N+2)
  GO TO 330
330 RES=SUM-POT(N)
  POT(N)+POT(N)+NEGABRES
  EPS=EPS+ABS(RES)
  DO 340 K=3,AMAX
  N=N+1
  NS=N+2
  L=L+1
  IF (J.EQ.4.AND.K.EQ.AMAX) NS=N+2
  SUM=A(12)*POT(L1)+POT(L1)+POT(N-1)+A(13)*
  1(POT(L1)+POT(N+1)+POT(N-1)+A(14)*POT(N)+A(15)*POT(N+1)+
  2(POT(N-1)+A(16)*POT(NS)+POT(N-2))
  RES=SUM-POT(N)
  POT(N)+POT(N)+NEGABRES
  EPS=EPS+ABS(RES)
340 CONTINUE
  N=N+1
  NS=N+2
  L=L+1
  IF (J.EQ.4) GO TO 342
  SUM=A(12)*POT(L1)+POT(L1)+POT(N+2)+A(13)*
  1(POT(L1)+POT(N+1)+POT(N-1)+A(14)*POT(N)+A(15)*POT(N+1)+
  2A(16)*POT(N-2)
  GO TO 344
342 SUM=A(12)*POT(L1)+POT(L1)+POT(L+3)+A(13)*
  1(POT(L1)+POT(L+2)+POT(N-1)+A(14)*POT(N)+A(15)*
  2A(15)*POT(N-1)+A(16)*POT(N-2)
344 RES=SUM-POT(N)
  POT(N)+POT(N)+NEGABRES
  EPS=EPS+ABS(RES)
310 CONTINUE
300 CONTINUE
C
C FOR THE INNERMOST GRID.
C
345 CONTINUE
  MAX=MODIM-1
  DO 350 N=MODIM,MAX
  I=1
  J=1
  K=1
  L=1

```

```

  SUM=A(12)*POT(L1)+POT(L1)+POT(N-1)+
  1A(13)*POT(L1)+POT(L-2)+POT(N+1)+POT(N-1)
  RES=SUM-POT(N)
  POT(N)+POT(N)+NEGABRES
  EPS=EPS+ABS(RES)
CONTINUE
DO 370 N=1,MAX
  I=I+1
  J=J+1
  K=K+1
  L=L+1
  N=MODIM-1+N
  SUM=0.0
  DO 380 I=1,I2
  SUM=SUM+A(1)*POT(I+1)
380 CONTINUE
  SUM=A(I*N)-SUM/A(I)
  RES=SUM-POT(N)
  POT(N)+SUM
  EPS=EPS+ABS(RES)
370 CONTINUE
C
C WRITE(LUM1,99B) ITER,EPS
C 99B FORMAT(ITER,' ',3X,'EPS=',PE13.5)
  IF (ITER.GE.ITMAX) GO TO 510
  IF (EPS.LT.EPS) GO TO 510
  GO TO 2000
C
500 CALL EXEC(8,NAME,10,ITER)
C
510 CONTINUE
  CALL EXEC(8,NAME,20,ITER)
  STOP
  END
  ENDS
FTM4
SEMA(AEM3,0)
PROGRAM MEMA(5,150)
COMMON/EMEA3/IG(256,4),IMOR(256),POT(256),AP(256),
  1EF(256),AR(5840),IMOR(256),CIDW(128),CELE(128),CPRD(128),
  2CPRD(128),CSEC(128),CSEC(128),CSEC(128),CSEC(128),
  3CPNO(128),CPNO(128),PSECT(128),CSECT(128),PENIT(128),
  4XSP(128),YSP(128),XEP(128),YEP(128),XSEG(64),YSEG(64),
  5XSEG(64),YSEG(64),SLPSEG(64),IRDPT(128),IDR(128),
  6SDENT(128),MCONV(128),MCONV(128),MCONV(128),MCONV(128),
  7MERTS(128),MERTS(128),MSECT(128),MCOND(128),MPPAN(64,2),
  8NSUMP(128),ISLP(64),IVEC(64),MPAT(64),MCP(128),MCNA(128),
  9NCNB(384),MCM(128),NSP(128),MEP(128),NSURF(128)
COMMON/CHST2/MSMAX,MAXMOD,MAXELE,MODDUT,MODIN,RELOUT,RELIN
COMMON/IDAT/LUM1,LUM2,LU,ITRACS,NTRACK(32),ITER
COMMON/PSOLV/ISY,IPDIS,IPOT,ROBY,CPOIS,MMAR,JPRA,IBC.
INWB,NODFS,NODINO,NODINS,NODINN
DIMENSION XG(256),YG(256)
DIMENSION BUFR(256),IBUFR(128)
DIMENSION NAME(3),LIST(5)
EQUIVALENCE (AM(1),XG),(AM(256),YG)
DATA NAME/2HDA,2HTA,2H3 /
C
  CALL RMPAR(LIST)
  WRITE(LUM1,999)
  999 FORMAT(20,' ',5X,'MEMA4' STARTS',5X,20,' ')
  ICODE=LIST(1)
  CALL EXEC(1,LU,IBUFR,128,NTRACK(19),16)
  IBUFR(ITER)=LIST(2)
  CALL EXEC(1,LU,IBUFR,128,NTRACK(19),16)
  NSTOP=MAXMOD/256+1
  ISTART=0
  ISECT=0
  NTR=NTRACK(ICODE)
  DO 110 N=1,NSTOP
  DO 110 I=1,256
  BUFR(I)=POT(I+ISTART)
110 CONTINUE
  CALL EXEC(2,LU,IBUFR,512,NTR,ISECT)
  CALL EXEC(1,LU,IBUFR,512,NTRACK(14),ISECT)
  DO 180 I=1,256
  XG(I):TAKT=BUFR(I)
180 CONTINUE
  CALL EXEC(1,LU,IBUFR,512,NTRACK(15),ISECT)
  DO 190 I=1,256
  YG(I):TAKT=BUFR(I)
190 CONTINUE
  ISTART=ISTART+256
  ISECT=ISECT+8
160 CONTINUE
  NSTOP=MAXELE/128+1
  DO 200 J=1,2
  ISTART=0
  ISECT=0
  IF (J.EQ.1) ISECT=40
  DO 210 N=1,NSTOP
  CALL EXEC(1,LU,IBUFR,128,NTRACK(16),ISECT)
  DO 220 I=1,128
  IG(I):TAKT=IBUFR(I)
220 CONTINUE
  ISECT=ISECT+2
  ISTART=ISTART+128
230 CONTINUE
240 CONTINUE
  DO 250 I=1,128
  ISTART=0
  ISECT=0
  IF (J.EQ.2) ISECT=80
  DO 260 N=1,NSTOP
  CALL EXEC(1,LU,IBUFR,128,NTRACK(16),ISECT)
  DO 250 I=1,128
  IG(I):TAKT=IBUFR(I)
250 CONTINUE
  ISTART=ISTART+128
260 CONTINUE
  DO 270 I=1,128

```



```

WRITE(UNIT=11, I=1)
END
* ***** CONTROLMET.MAN HAS BEEN STAMPED AFTER .11.
* *****
* *****
* *****
* *****
* *****
* *****
* *****
* *****
* *****
* *****

```

```

PROGRAM PLUT(5-150)

```

THIS PROGRAM GENERATES POTENTIAL CONTOUR PLOTS. THE SATELLITE POSITION IS ALSO PLOTTED WITH THE CONTOURS.

```

COMMON ALNAA/POT(250),YB(250),YD(250),IG(250,4),
I(50,50),IP(50),YF(50),IHP(50),IL(50,50),
LUNNM/BL1/NN1(10),NNJ(10),PLOUT/IMAX,DX,DY
COMMON BLAS/MDUTER(10),MEST(10),S(4,4),NCONM(10,4,4),
INCUNA(10),IGM(4)
COMMON BLN15,BUF(1,1),IBUF(25),IBUF2(25)
COMMON FILEZ/IMAX,NB,II,MESHAX,MAXMOD,MAXELE,MODOUT
COMMON FLOT1/IFLOT(1),MAX,IMAXI,IMAXI,NS,NA,ISYN,IFLAG
DIMENSION XPP(4),YFP(4),CNP(30)

```

```

IEND=NSMAX-3

```

```

NN=2
NM=1

```

```

ZM=-1.0E+28
SEP=.01
IF(1SYN.EQ.1) GO TO 10
MAX=.5
MAY=.5
SC=1.0
GO TO 20
MAX=2.0
MAY=1.0
SC=0.5
20 SX=SCBDX
SY=SCBDY
SCZ=1.0

```

```

CALL PAPT(MCM,CNP)
IF(NN.EQ.1) GO TO 47
CALL START
CALL SYMBOL(0.0,0.0,0.14,PLEASE MOUNT BLACK LIG-INK PENS;
IBROAD IN POSITION 1 AND EXTRA FINE IN POSITION 2,90.0,80)

```

```

CALL PLOT(0.0,0.0,-3)
CALL NEUPEN(1) GO TO 45
CALL PLOT(IMAX,MAY,-3)
DO 40 I=1,IFLAG
NI=I-1)8NS
NC=NS(I-1)8NS
XI=FLOAT(1)8NS
YI=FLOAT(1)8NS
CALL PLOT(XI,YI,-3)
DO 40 M=M1,M2
XI=FLOAT(1)8NS
YI=FLOAT(1)8NS
CALL PLOT(XI,YI,-2)
40 CONTINUE
CALL PLOT(0.0,0.0,3)
IF(1SYN.EQ.1) GO TO 45
CALL PLOT(10.0,0.0,2)
CALL PLOT(0.0,0.0,3)
CALL PLOT(0.0,10.0,2)
CALL PLOT(0.0,0.0,3)
45 CALL NEUPEN(2)

```

```

47 DO 50 I=1,IEND
II=IEND-I
NI=NI(I)
M=MNI(I)
IF(II.EQ.1) GO TO 70
NM=2
IF(1SYN.EQ.1) NM=1
IMI=NI2
JMI=NI2
IMAX=IMI+1
JMAX=JMI+1
GO TO 80
70 IMAX=NI+1
JMAX=JMI+1
80 DO 90 L=1,IMAX
DO 90 M=1,JMAX
ZP(L,M)=ZM
90 CONTINUE

```

```

IF(1SYN.EQ.1) IP=3
IF(II.EQ.1) GO TO 280
IF(II.EQ.MESHAX) GO TO 100
NI=NCONM(II,I,IP,2)
GO TO 110
100 NI=1
110 A2=NCONM(II,IP,2)
I1=IG(A1,I)
I2=IG(A1,2)
I3=IG(A1,3)
I4=IG(A1,4)
YO=YG(I1)
DDE=(I2-I3)/2.0
DDY=(I4-I3)/2.0
IF(1SYN.EQ.1) GO TO 115
XO=0.0
YO=0.0

```

```

115 DO 120 A=1,42
IF(1SYN.EQ.1) GO TO 124
II=1
JJ=4
GO TO 128
124 II=2
JJ=3
128 DO 130 J=1,II

```

```

I1=J
IF(A,II,NCONM(II,J,1),AND,A,II,NCONM(II,J,2)) GO TO 140
130 CONTINUE
I1=5
I1=8
GO TO 130
140

```

```

140 DO 120 A=1,42
IF(1SYN.EQ.1) GO TO 124
II=1
JJ=4
GO TO 128
124 II=2
JJ=3
128 DO 130 J=1,II

```

```

I1=J
IF(A,II,NCONM(II,J,1),AND,A,II,NCONM(II,J,2)) GO TO 140
130 CONTINUE
I1=5
I1=8
GO TO 130
140

```

```

150 DO 160 L=1,11
IF(1SYN.EQ.1) GO TO 170
N=IG(A,IA)
GO TO 170
170 IF(II.EQ.1) GO TO 174
N=2
174 J1=NCONM(II,J,1)
J2=NCONM(II,J,2)
DO 176 J=1,2
N=M1
IF(A,II,J) GO TO 178
178 CONTINUE
178 N=MCONA(N)
GO TO 180
179 N=NCONM(II,J,1)+NCONM(II,J,2)
180 L=FIX((XG(N)-XO)/DDE)+1.0
M=FIX((YG(N)-YO)/DDY)+1.0
ZP(L,M)=POT(N)

```

```

160 CONTINUE
IF(JJ.EQ.5) GO TO 120
GO TO (190,200,210,220)JJ
190 L1=0
M1=-2
GO TO 230
200 L1=2
M1=0
GO TO 230
210 L1=0
M1=2
GO TO 230
220 L1=-2
M1=0
GO TO 230
230 NI=JJ
N2=JJ+1-JJ/44
N1=IG(N,NI)
N2=IG(N,N2)
L2=L+L1
M2=M+M1
ZP(L2,M2)=(POT(N1)+POT(N2))/2.0
L3=L+L1/2
M3=M+M1/2
ZP(L3,M3)=(ZP(L2,M2)+POT(N))/2.0

```

```

180 CONTINUE
DO 240 L=1,IMAX+2
DO 240 M=1,JMI+2
Z1=ZP(L,M)
Z2=ZP(L,M+1)
Z3=ZP(L,M-1)
IF(Z1.ME.ZM) GO TO 240
IF((Z2.EQ.ZM.OR.Z3.EQ.ZM) GO TO 240
ZP(L,M)=(Z2+Z3)/2.0
240 CONTINUE
DO 250 M=1,JMAX
DO 250 L=2,JMI+2
Z1=ZP(L,M)
Z2=ZP(L+1,M)
Z3=ZP(L-1,M)
IF(Z1.ME.ZM) GO TO 250
IF((Z2.EQ.ZM.OR.Z3.EQ.ZM) GO TO 250
ZP(L,M)=(Z2+Z3)/2.0

```

```

250 CONTINUE
DO 260 L=1,IMAX
YP(L)=XO+DDX*FLOAT(L-1)
260 CONTINUE
DO 270 L=1,JMAX
YF(L)=YO+DDY*FLOAT(L-1)
270 CONTINUE
GO TO 320

```

```

280 DO 290 L=1,IMAX
M=IL(L,JMAX)
XP(L)=XG(M)
290 CONTINUE
DO 300 L=1,JMAX
M=IL(IMAX,L)
YP(L)=YG(M)
300 CONTINUE
DO 310 L=1,IMAX
DO 310 M=1,JMAX
M=IL(L,M)
IF(M.EQ.-1) GO TO 310
IF(MAX.EQ.0) GO TO 306
DO 305 LL=L,IMAX
LI=(LL-1)82+1
IF(M.EQ.IFLOT(LL)) GO TO 310
305 CONTINUE
306 ZP(L,M)=POT(M)
310 CONTINUE

```

```

320 IF(SC.EQ.1.0) GO TO 345
DO 330 L=1,IMAX
XP(L)=XP(L)8SC
330 CONTINUE
DO 340 L=1,JMAX
YF(L)=YF(L)8SC
340 CONTINUE
345 IF(SC.EQ.1.0) GO TO 355
DO 350 L=1,IMAX
DO 350 M=1,JMAX
ZP(L,M)=ZP(L,M)8SCZ
350 CONTINUE
355 IF(NN.EQ.1) GO TO 370
DO 360 L=1,NEN
CN=CNP(L)
CALL CONTOUR(XP,IMAX,YF,JMAX,ZP,IDINK,CN,SEP,CN)
CONTINUE

```

```

370 IF(NN.EQ.1) GO TO 475
WRITE(6,380) (XP(L),L=1,IMAX)
WRITE(6,380) (YF(L),L=1,JMAX)
380 FORMAT(15F9.3)
DO 390 M=1,JMAX
NABA=JMAX+M
WRITE(6,380) (ZP(L,NABA),L=1,IMAX)
390 CONTINUE

```

```

395 NI=0
NI=REOUT(I)
DO 400 A=1,IMAX
IF(IG(A,NI).EQ.0) GO TO 400
M=MNI(I)
IPIFF(A)=A
400 CONTINUE
IF(NI.EQ.0) GO TO 475

```

```

DO 410 M=1,NI

```

```

      N=100000
      DO 430 N=1, N
      DO 430 I=1, N
      CONTINUE
430 CONTINUE
      DO 440 L=1, N
      I=I+1
      N=I+1
      CALL SUBROUTINE
      CONTINUE
440 CONTINUE
      DO 440 L=1, N
      I=I+1
      N=I+1
      CALL SUBROUTINE
      IF (I.EQ.0.0) GO TO 450
      CALL SUBROUTINE
      IF (I.EQ.0.0) GO TO 460
      CALL SUBROUTINE
      GO TO 470
460 CALL SUBROUTINE
470 CALL SUBROUTINE
      YP(I)=C40*(X(I)-XP(I))*XP(I)
      YP(I)=C40*(Y(I)-YP(I))*YP(I)
480 CONTINUE
C
      IF (I.E.1) GO TO 440
      CALL PLOT(XP(1), YP(1), 1)
      CALL PLOT(XP(2), YP(2), 2)
490 CONTINUE
410 CONTINUE
C
475 IF (I.E.ED.0) GO TO 50
      DO 480 M=1, N
      XI=I*PI*(M)
      X2=I*PI*(M+1)
      ZP(1,1)=POT(X1)*BSCZ
      X3=I*PI*(M+2)
      ZP(1,2)=POT(X2)*BSCZ
      X4=I*PI*(M+3)
      ZP(1,3)=POT(X3)*BSCZ
      X5=I*PI*(M+4)
      ZP(1,4)=POT(X4)*BSCZ
      XP(1)=X1*IG(X1,1)*BSC
      XP(2)=X2*IG(X2,2)*BSC
      YP(1)=Y1*IG(X1,1)*BSC
      YP(2)=Y2*IG(X2,2)*BSC
      DO 490 L=1, N
      CN=CN*(L)
      CALL CRYOUR(XP, YP, ZP, IDIRK, CN, SEP, CN)
490 CONTINUE
480 CONTINUE
C
50 CONTINUE
      IF (I.E.ED.1) GO TO 500
      CALL FINISH
500 STOP
      END
      SUBROUTINE PAPLT(NCN, CNP)
      DIMENSION CNP(10)
      DATA CNP/2/
      DATA CNP/50.0, 55.0/
      RETURN
      END
      INDS

```

FILM

7 -